Furniture Fire Dynamics and Smoke Flow in a Two-Story House With Mechanical Ventilation

by

Alexander DiPaola

A thesis
presented to the University of Waterloo
in fulfillment of the
thesis requirement for the degree of
Master of Applied Science
in
Mechanical and Mechatronics Engineering

Waterloo, Ontario, Canada, 2023

Author's Declaration

I hereby declare that I am the sole author of this thesis. This is a true copy of the thesis, including any required final revisions, as accepted by my examiners.

I understand that my thesis may be made electronically available to the public.

Abstract

Synthetic materials in modern furniture, combined with airtight construction practices developed as a response to the call for energy efficient homes, have increased the likelihood of a residential fire becoming ventilation (oxygen) limited. This poses unique risks for occupants and firefighters. There is a fundamental lack of knowledge of the development of modern fire scenarios and how factors such as decreasing compartment oxygen levels or operational mechanical ventilation systems may affect the fire behaviour. In the past, most studies have focused on investigation of ventilation-limited fires at reduced scales or well-ventilated fires at large scale, leaving gaps in both data and understanding when it comes to full-scale, ventilation-limited fires. As part of a larger project, a series of four furniture fire experiments are conducted in a two-storey, multi-compartment burn house, using identical fuel loads under different mechanical ventilation configurations. The burn house is configured with a typical home layout and has been sealed to mimic an energy efficient home. For the experiments, it is equipped with a mechanical ventilation system set to provide typical residential flow rates that might occur during a fire: (1) no ventilation, (2) baseline ventilation, (3) 2x baseline ventilation, and (4) recirculation. Instrumentation is included in all compartments to chart fire growth, smoke flow, and fire induced environment factors such as temperature and gaseous species concentrations. Data from these four experiments is presented to characterize the effects of mechanical ventilation on fire development, smoke flow, and gaseous species distribution throughout the structure and the resulting fire induced room environments. In addition, the data is used to evaluate the effectiveness of existing engineering correlations at predicting certain key parameters that describe development of the fire induced environment. The results discussed throughout this thesis provide spatially and temporally resolved novel data to enhance the current limited understanding of modern furniture fires in multi-storey, multi-compartment structures when a mechanical ventilation system is operational. Specific results allow improved characterization of how modern furniture burns in full-scale ventilation-limited compartments and the impact of mechanical ventilation on these scenarios. The data is critical for improvement of engineering correlations and design guidelines for this category of fires, and over the longer term may be used for validation of more detailed fire models and a foundation for future research.

Acknowledgements

I'd like to thank my supervisor, Dr. Elizabeth Weckman, for her guidance and expertise over the course of my studies. Thank you for teaching me the fundamentals of experimental research and how to think through connecting measurements to physics. I am forever grateful for the opportunities and experiences I have gained while working with you at the fire lab.

To my lab mates, especially Bronwyn, Vusal, Ayaan, and Keon for your help and support through the ups and downs of testing, data analysis, and putting together papers. A special thanks goes to Andy for his help with all the technical challenges that arose throughout various projects.

I'd also like to thank my friends and family for all the love and encouragement over the last two years.

Finally, I'd like to acknowledge funding from the Natural Sciences and Engineering Research Council of Canada (NSERC) through the Canada Graduate Scholarship and from the University of Waterloo Faculty of Engineering through the Engineering Excellence Fellowship.

Table of Contents

List of Figures

List of Tables

List of Abbreviations

ACPH air changes per hour
CO carbon monoxide
CO_2 carbon dioxide
FDS fire dynamics simulator
GER global equivalence ratio
GIS gas instrument station
HFG heat flux gauge
HRR heat release rate
HVAC heating, ventilation, and air conditioning
LES large eddy simulation
LOI limiting oxygen index
MLR mass loss rate
MQH McCaffrey, Quintiere, and Harklroad
N_2 nitrogen
NO_x nitrogen oxide
O_2 oxygen
OA outdoor air
PIV particle image velocimetry
RMS root mean square
THC total unburned hydrocarbons
VOC volatile organic compounds

List of Symbols

A_o	vent opening area, for correlations (m^2)
A_{sample}	surface area of cone calorimetry sample (m^2)
A_T	total compartment wall surface area, for correlations (m^2)
A_z	zone area (m^2)
C_d	orifice/doorway flow coefficient, for correlations
ΔT_g	change in gas temperature, for correlations (K)
D	fire diameter or width used in correlations (m)
$\Delta H_{c,eff}$	effective heat of combustion (MJ/kg)
E	radiative emissive power (kW/m^2)
$F_{1\rightarrow 2}$	view factor from source (1) to target (2)
ΔH_c	total heat of combustion (MJ/kg)
H_o	vent height, for correlations (m)
H	flame height used for correlations (m)
I	velocity fluctuation intensity
k	bidirectional pressure probe calibration constant
L	horizontal distance between the fire centre line and a target (m)
P_{atm}	atmospheric or ambient pressure (Pa)
$\dot{Q}$	heat release rate (MW or kW)
R_{air}	ideal gas constant for air ($287.05\,J/kg\,K$)

R	distance from point source to a target (m)
σ	Stefan-Boltzman constant ($5.67 \times 10^{-8}\,\mathrm{W/m^2\,K^4}$)
THR	total heat release of cone calorimetry sample ($\mathrm{MJ/m^2}$)
T_a	ambient air temperature, for correlations (K)
T_g	gas temperature, for correlations (K)
T	temperature (°C or K)
V	transducer voltage (volts)
Z_D	discontinuity height, for correlations (m)
Z_N	neutral plane height, for correlations (m)
$c_{p,g}$	specific heat of gas/smoke (assumed air), for correlations ($\mathrm{kJ/kg\,K}$)
$c_{p,wall}$	specific heat of compartment wall, for correlations ($\mathrm{kJ/kg\,K}$)
ΔP_{zero}	differential pressure at zero voltage (Pa)
ΔP	differential pressure measured by the bidirectional pressure probes (Pa)
δ_{wall}	thickness of compartment wall, for correlations (m)
Δt	time between samples or time steps (s)
ϵ	radiative emissivity
g	gravitational acceleration constant ($9.81\,\mathrm{m/s^2}$)
h_k	conduction heat transfer coefficient, for correlations ($\mathrm{kW/m^2\,K}$)
k_{wall}	thermal conductivity of compartment wall, for correlations ($\mathrm{kW/m\,K}$)
$\dot{m}_{a,in}$	doorway inflow mass flow rate, for correlations (kg/s)
$\dot{m}_{g,nat}$	total mass flow rate through natural vent, for correlations (kg/s)
$\dot{m}_{g,out}$	doorway outflow mass flow rate, for correlations (kg/s)
$\dot{m}_g$	total ventilation mass flow rate, for correlations (kg/s)
$\dot{m}_z$	zone mass flow rate (kg/s)
$\dot{m}_f$	mass loss rate of fuel (kg/s)
m_f^k	mass of fuel at time step k (kg)
m_{loss}	total mass of cone calorimetry sample consumed during burning (kg)

$\dot{q}''_r$	radiative incident heat flux to a target (kW/m^2)
ρ_a	gas density at ambient temperature, for correlations, assumed air (kg/m^3)
ρ_g	gas density at current gas temperature, for correlations, assumed air (kg/m^3)
ρ_{wall}	density of compartment wall, for correlations (kg/m^3)
ρ_z	zone fluid density, assumed air (kg/m^3)
ρ	fluid density, assumed air (kg/m^3)
θ	angle between normal to a target and the centre line of the fire ($^\circ$)
t_p	thermal penetration time, for correlations (s)
t	exposure time, for correlations (s)
$\bar{u}$	mean velocity (m/s)
u_{rms}	root mean square velocity (m/s)
u_z	zone velocity (m/s)
u	velocity calculated from differential pressure measurements (m/s)
$\dot{V}_z$	zone volume flow rate (kg/s)
w_o	vent width, for correlations (m)
χ_r	radiative fraction

Chapter 1

Introduction

In recent years, firefighters have reported observations of residential fires burning faster and hotter, with some believing this to be a result of the use of petroleum based synthetic materials in modern furniture [1, 2]. These observations of faster fire growth have been confirmed by the Underwriters Laboratory's Fire Safety Research Institute through comparative well-ventilated fire tests fuelled by furniture constructed of modern synthetic materials and legacy furniture constructed of natural materials [3]. These tests found that scenarios with the synthetic materials reached flashover in under five minutes, while scenarios with the natural materials took over 30 minutes to reach flashover[1]. In addition to increased burning rates, firefighters have reported increased smoke production and toxicity in modern fire scenarios [1]. This is significant because smoke accounts for the majority of fire related deaths in residential fires. Statistics Canada has reported that 68% of fire related deaths across Canada can be attributed to smoke inhalation alone, while only 17% are due to burns [4]. The number of fire related deaths is also on the rise in Ontario. In 2022 there were 133 reported deaths from residential fires [2]. This increased from 103 reported in 2021 and only 61 reported in 2017 [5].

In addition to faster fire growth, modern residential fires are also impacted by airtight construction practices, which have become popular due to calls for increased energy efficiency. Airtight construction means that modern homes are designed to have less air exchange with the ambient, and thus less air leakage, compared to older construction. This reduces the amount of ventilation available to fires as they burn which can cause the fire to become ventilation limited and the fire scenario to transition into what is known as an under-ventilated fire. Under-ventilated fires pose significant risks to occupants and

[1]Flashover is a period of rapid fire growth where the fire spreads to all combustibles in the room.

firefighters due to decreased levels of oxygen coupled with increased production of toxic gas and unburned fuel caused by decreased combustion efficiency [6]. The buildup of unburned fuel vapours leaves these fires susceptible to rapid fire growth, and potentially even backdraught, when an influx of air into the structure that may be caused by opening a door leads to a sudden and rapid increase in fire growth that can sometimes be explosive [7].

In response to the significance and increasing occurrence of these scenarios, The University of Waterloo has undertaken an experimental research program aimed at improving current understanding of the behaviour of under-ventilated fires and systematically characterizing the environments created inside a typical residential home during these fires.

1.1 Under-Ventilated Furniture Fire Project

The under-ventilated furniture fire project at the University of Waterloo began when fire investigators reported that it was becoming difficult to explain emerging trends in how, where, and when occupants were dying in residential fires due to a fundamental lack of knowledge about modern fire scenarios. The overbearing research question for the project is to update how much time there is to escape in modern house fires. Additional questions that must be answered to help piece together a comprehensive answer to this larger question include:

1. How does modern furniture burn in ventilation-limited multi-storey structures?
2. What is the impact of ventilation systems on fire development and fire induced environments in structures?
3. What is the impact of added fire retardants in furniture on fire development and fire induced environments in structures?
4. What is the impact of smoke evolution and toxicity on occupant egress from structures during ventilation limited fires?

Answering these questions aims to fill gaps in current knowledge of fire science, in particular related to the complex physics driving development of modern ventilation limited scenarios. Key objectives are aimed toward improved characterization and understanding of ventilation limited fire development and behaviour of ventilation limited fires fuelled by

different sources. The approach to meeting these objectives is to systematically investigate compartment fire development and provide spatially and temporally resolved data, in terms of temperatures, species concentrations, and smoke movement in the two-storey University of Waterloo burn house when burning a range of fuels in scenarios with varying ventilation configurations.

The entire University of Waterloo program involves a long term, multi-year set of research projects that began in 2015 and has followed the timeline depicted in Fig. 1.1. In 2015, a preliminary series of tests was conducted with a total of nine burns. In this series, three different couches with varying levels of fire retardants were burned a total of three times each. The results from these tests provide initial data on the overall development of furniture fires in the burn house, a comparison between fires established on furniture constructed using three different fire retardant strategies [8, 9], and data on repeatability of fire tests in the burn structure [10].

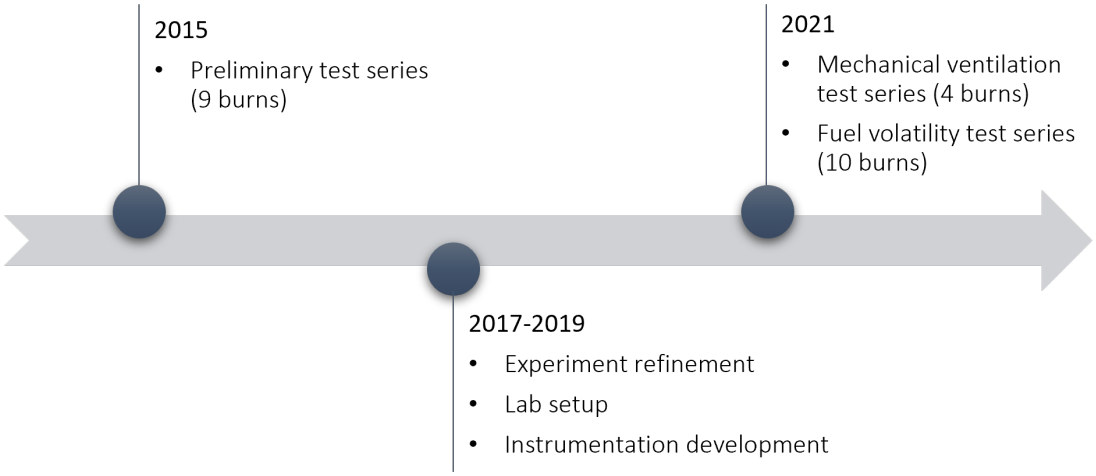

Figure 1.1: Timeline of the under-ventilated fire project.

Following the preliminary test series, the experimental design was refined, and another two series of tests were developed and conducted in 2021. The first test series of 2021 was called the mechanical ventilation test series, which added an heating, ventilation, and air conditioning (HVAC) system to the burn house to study the effects of forced ventilation on fire development and evolution of the fire induced environment. A total of four burns were completed in this series. The second series of 2021 was called the fuel volatility test series, which burned 10 different types of fuels including liquid fuel, wood, and couches with different construction to investigate how different fuel types burned in under-ventilated conditions. Looking into the future, additional test series are planned to further improve

the robustness of the data collected and answer additional questions that arose from results of the previous test series.

1.2 Research Objectives

This thesis presents and discusses results from the mechanical ventilation test series. In these, identical couches are burned under different ventilation configurations to investigate the impact of ventilation on the fire and environmental development in the burn house. Specific objectives of this thesis research are to:

1. Characterize the fire and development of the fire induced environment, by providing spatially and temporally resolved data for the mechanical ventilation test series.
2. Discuss differences between the tests across the different ventilation configurations.
3. Provide data that can be used for fire model validation and to feed future steps of the project, including occupant egress research.
4. Investigate the ability of current engineering correlations to predict the development of the environment in these tests.

This thesis presents the background, methods and results of the research in the following chapters. Chapter 2 presents background necessary to understand compartment fire dynamics and a literature review of previous fire tests that provide insights into fire behaviour and the fire environments that develop inside structures. Chapter 3 details the experimental methods used in the mechanical ventilation tests, including the layout of the burn house structure, the fuel load, ventilation conditions, instrumentation, test procedures, and data analysis methods. Chapter 4 discusses experimental results from the four tests. It first explores the mechanical ventilation supplied to the structure and then discusses the development of the fires with details fuel mass loss rate (MLR), heat flux, compartment temperatures, smoke flow, gaseous species concentrations, and the relationship between these elements. Chapter 5 investigates the application of existing engineering correlations to the present fire scenarios. Specifically, the ability of different correlations to predict transient and steady state values of heat flux, temperature and smoke flow are evaluated. Finally, Chapter 6 presents the conclusions of the research to date with recommendations for further work.

Chapter 2

Background and Literature Review

This chapter provides background information on relevant topics related to compartment fire dynamics, as well as a review of relevant literature. It is organized such that general background on fire behaviour is discussed first and more specific information, pertaining to the present experimental setup and research, is discussed afterwards.

2.1 Fire Development and Heat Release Rate

2.1.1 Defining Heat Release Rate

The amount of heat released by a fire is considered the most important factor in characterizing the fire hazard as it dictates fire size, human survivability, and suppression tactics [11, 12]. This characteristic of a given fire can be provided as a measure of the total heat released over the lifespan of the fire, or as a function of time, termed the heat release rate (HRR). The HRR can also be thought of as the rate at which energy is released from the fuel during the oxidation process in a given fire situation [13]. Other phenomena which affect fire hazard are ignition, flame spread, and smoke/toxic gas production. These other phenomena have all been shown to be related to fire HRR, hence the importance of understanding HRR [11].

The HRR of a fire is determined by two factors: the fuel burning rate ($\dot{m}_f$) and the heat of combustion (ΔH_c) of the fuel, as shown by Eq. 2.1.

$$\dot{Q} = \dot{m}_f \Delta H_c \tag{2.1}$$

The fuel burning rate defines how quickly the mass of the fuel is vaporized and burned. It is often expressed as a mass flux [13]. Burning rate is governed by the balance between the heat of gasification of the fuel, which is the heat input required to gasify a material, and the magnitude of heat imparted to the fuel surface to drive gasification [12]. For a liquid, the heat of gasification is equivalent to the heat of vaporization [13]. Generally, the burning rate is represented by the MLR, a quantity that can be easily measured. However, the MLR is not always equivalent to the burning rate because it is not necessarily true that all of the fuel mass lost is fully oxidized (burned). For example, low combustion efficiency in low O_2 environments leads to a situation where not all the vaporized fuel is burned [13].

The heat of combustion, also referred to as total heat of combustion, is the amount of energy that is released per unit mass of fuel consumed when the fuel is burned completely [12]. Total heat of combustion is typically measured in a bomb calorimeter [14]. This test involves burning a sample of the fuel of interest in a closed chamber under elevated O_2 concentrations and pressure above atmospheric [14]. The conditions inside the chamber ensure that any remaining fuel mass is negligible, providing a measure of the total heat released through oxidation of the fuel, which is coupled with the original mass of the specimen to obtain the total heat of combustion [14]. Heat of combustion depends on the chemical composition of the fuel and, on a molecular level, is governed by the heats of combustion of the individual atoms making up the fuel plus the internal energy relating to the bonds between those atoms [15]. However, heat of combustion in a real situation is also dependent on the concentration of fuel vapour in the air, its ability to mix with oxidizer and the efficiency of the combustion process [12]. Therefore, the heat of combustion in a fire is not an inherent material property of the fuel, but instead depends strongly on the environmental conditions.

A modified heat of combustion, taking into account the conditions under which the combustion process occurs, is referred to as an effective heat of combustion ($\Delta H_{c,eff}$). In compartment fires, conditions change over time as air is consumed, resulting in a decrease in the heat of combustion as the combustion becomes fuel rich [12]. For these reasons, the HRR measured for a particular scenario is only applicable to that specific scenario. For example, the heat release profile of a fuel burned in open air cannot be directly transferred to a situation where that same fuel is burned inside an enclosure [16].

2.1.2 Enclosure Fire Development

Examples of typical HRR development profiles for a compartment fire are shown in Fig. 2.1. The development of a compartment fire can be broken down into four stages: (1) the incubation stage, (2) fire growth, (3) fully developed fire, and (4) the decay period [17].

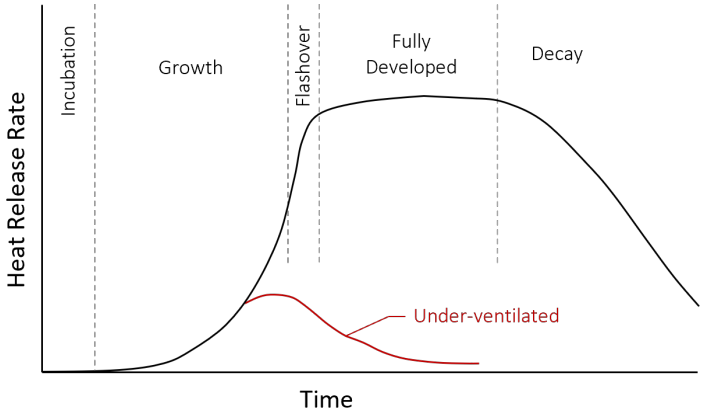

Figure 2.1: Depiction of fire growth curves for well-ventilated and under-ventilated conditions.

The incubation phase occurs from the time of ignition of the fuel to the time of the first noticeable fire growth. The length of this period depends on the definition of when fire growth becomes noticeable. In the case of using HRR to define the fire size, there may be a selected threshold that determines when the fire size noticeable. During the growth phase, the fire develops as it would if it were burning in the open and the conditions inside the compartment remain in the well-ventilated regime [17]. Factors effecting fire growth include the ability of the first material to sustain burning, the ability of other materials to ignite, the distribution of the fuel, the construction of the compartment, and the ventilation conditions [17, 18]. Towards the end of the fire growth phase, one of two events may occur; the fire may reach flashover and proceed into the fully developed phase, or the O_2 concentration in the compartment may reduce to a level low enough that the fire becomes under-ventilated and begins to decay.

Flashover marks the transition from growth to fully developed fire in a well-ventilated compartment [19]. During flashover, there is a sudden, rapid flame spread that can only occur under the right conditions, including sufficient ventilation and sufficient temperature to ignite remote surfaces [19]. In a post-flashover compartment, the fire has extended to involve all combustible surfaces. After the fully developed phase, the fire enters into a decay phase, where the HRR and compartment temperature decrease as the environment in the compartment recovers. In contrast, a fire that enters the under-ventilated regime does not reach flashover and instead burns at a reduced burning rate dependent on the available oxygen, entering directly into the decay phase [17]. Burning is sustained until either all the fuel is consumed or the fire extinguishes due to lack of O_2.

As mentioned previously, the HRR of a material burning in an enclosure differs from

that of the same material burning in an open environment. The effects of an enclosure on fire HRR are generally termed as enclosure effects. Some common enclosure effects are as follows:

- Hot gases collected in the enclosure can increase radiation to the fuel surface and enhance the burning rate by increasing fuel vaporization [13].
- Ventilation may decrease the O_2 available for combustion and reduce the heat of combustion through a less efficient combustion process [13].
- Flame temperatures in the low O_2 environment decrease which reduces heat feedback to the fuel surface hindering vaporization and reducing burning rate in balance with effects noted in 1) above [18].
- Mixing between the smoke produced by the fire and fresher air in the compartment may increase with reduced ventilation further reducing the availability of O_2 than through only 2) above [18].

In general, fires in compartments with large enough openings have increased HRR compared to the same fire under open burning conditions. In contrast, fires in compartments with small openings become under-ventilated, resulting in reduced HRR [13].

2.1.3 Measurement of Fire Heat Release Rate

The measurement of HRR is referred to as calorimetry [14]. In fires, measuring the HRR is not limited to measuring mass loss and multiplying by an effective heat of combustion. In reality, the mass loss method requires the use of another method to determine the HRR independent of mass loss in order to calculate the effective heat of combustion for a given fire situation. Thus, other techniques are commonly used to measure HRR as well. These include the sensible energy rise method and the oxygen consumption method [14].

In sensible energy rise calorimetry, a sample is burned in an apparatus where the volume of air flowing through the test chamber is controlled and the temperature rise of the known air volume is measured [14]. The HRR is then calculated by using thermodynamic relations to determine the energy input into the air required to obtain the measured temperature rise.

Oxygen consumption calorimetry works on the principle that organic materials release a known amount of energy per unit mass of O_2 consumed. In 1980, Huggett determined

that common organic fuels, such as hydrocarbons and polymers, release on average 13.1 kJ ±5% of energy per gram of O_2 consumed in the combustion process [20]. The oxygen consumption method typically works by capturing the combustion products released by a fire through an exhaust duct system and measuring the remaining O_2 concentration [14]. The difference in the O_2 concentration from ambient can then be used to calculate HRR through Huggett's value. The accuracy of the HRR measurement using this method can be improved by measuring the concentration of CO_2 and CO and making appropriate corrections in the calculations [14]. This method can be completed at both large-scale by using a large-scale exhaust duct and gas analysis system and at bench-scale through the use of a standard test apparatus called the cone calorimeter.

In a cone calorimeter test, a sample measuring 10 cm × 10 cm and between 25 mm to 50 mm thick is subjected to a radiant heat flux from a cone-shaped heater [21]. The sample is placed on a load cell to measure the sample mass loss over time. Should the sample ignite, the exhaust gases are drawn through a duct system where a gas sample is captured and pumped through a series of filters and drying columns before being analyzed in a gas analysis system [21]. The heat of combustion can be calculated from cone calorimeter results, since this apparatus measures both HRR and MLR independently. However, the results from the cone calorimeter test are only valid for the tested configuration, which is at bench-scale and is well-ventilated by default [14]. Results from cone calorimeter testing does provide valuable insight into how a material burns, which can be applied to larger-scale, provided that proper care is taken in the scaling of the results [11]. Factors that affect the burning of a material, which can vary significantly between scales, include the fuel size, the amount and configuration of ventilation, the amount of external heating reaching the fuel surface, and the type of ignition [14].

2.2 Smoke Flow in Compartment Fires

In this section, the flow of smoke in fire compartments is discussed. The discussion details the typical behaviour of smoke after it is produced by the fire and discusses possible flow pathways that smoke can take through compartments and structures. Smoke is commonly defined as a suspension of particles in air which is also contaminated by gaseous combustion products [22]. It is often thought of as the visible products from burning materials, however, this does not highlight the fact that smoke contains a relatively large amount of entrained air [23].

2.2.1 Smoke Plumes, Ceiling Jets, and the Smoke Layer

In a fire, hot vapour that is produced through evaporation of the fuel rise upward from the surface of the fuel and are combusted in the flame, producing smoke. The hot smoke produced by the fire continues to rise upwards in a buoyant plume [24]. The rise of smoke in the plume is driven by buoyancy forces, created by density differences between the hot smoke and the cooler surrounding air. Hotter plumes have greater density differences between the smoke and the surrounding air, which causes greater buoyancy forces and results in a faster plume velocity [25]. Fires with higher HRRs tend to release hotter smoke and therefore, have faster moving smoke. The final structure of the fire plume is determined by its interactions with the surrounding air as well as with any physical obstructions such as compartment walls or ceilings [25].

As the plume rises from the fire, shown schematically in Fig. 2.2, the smoke may impinge on the compartment ceiling. When this occurs, the flow of smoke undergoes a right angle turn and begins to flow across the ceiling. This is known as a ceiling jet flow [26]. In a ceiling jet, the flow of smoke propagates radially outward from the point of impingement and continues until the jet impinges onto the compartment walls. As this happens, the upper regions of the compartment begin to fill with smoke and form what is commonly termed a smoke layer [26]. If the smoke remains hot enough that there are sufficient buoyant forces, it will tend to remain in a layer adjacent to the ceiling. The volume of this layer increases, and the interface between the hot smoke layer and the cooler air layer below descends at a rate determined by the smoke production rate [27].

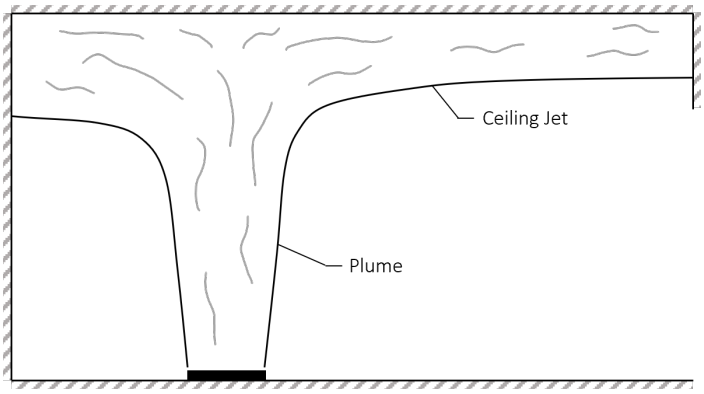

Figure 2.2: Schematic of fire plume and ceiling jet flows in a compartment.

As the smoke plume rises and the ceiling jet flows outwards from the fire, cooler air in the room flows towards the fire plume and is entrained into it. This inflowing air

provides additional O_2 to the fire, critical for continued burning, and also cools the smoke [26]. Compartment surfaces such as walls could restrict entrainment of the air to the open side of the fire if the fire was near one of these surfaces [25]. The volume of entrained air into the plume is significant. Studies have reported that the mass of the plume is almost completely defined by air entrainment, and that any mass generated by the fire is insignificant in comparison [28]. Mixing between the hot smoke and cooler entrained air in the ceiling jet is largely responsible for cooling of the jet. In addition, convective heat transfer between the jet flow and the ceiling results in further cooling of the smoke [26]. As the smoke cools, the velocity of the flow decreases and therefore, the velocity is highest at the fire and decreases as the distance between the smoke and the fire increases [28]. After the smoke interacts with the compartment walls, the heat loss is dominated by convective heat transfer to the ceiling [26]. Cooling of the smoke and subsequent heating of the cooler air, by the fire and by mixing with the smoke, results in a decrease in the temperature gradient in the compartment which decreases the buoyancy forces and results in an increase in the rate of smoke descent [28].

The environment created as smoke builds up inside a compartment can be stratified, where there is a divide between a hot smoke layer near in the upper part of the compartment and a cooler, fresher air layer below. This situation leads to an idealized model of a realistic compartment environment, commonly known as the zone model [29]. In reality, however, there may not be a clear and distinct divide between the two layers (or zones) making up the volume of smoke in a compartment and a volume of fresher air. In the zone model, the smoke comprising the upper layer is assumed to have uniform properties including temperature and density, and the air comprising the lower layer is assumed to have uniform properties equal to that of ambient air [29]. The definition of the two layers implies that there is a boundary between the two layers where there is a sudden change in properties such as temperature and density. The height of this boundary is commonly referred to as the interface height, discontinuity height, or smoke layer height. This model of a stratified environment is most applicable to a pre-flashover compartment and forms the basis for zone computer models [30] and many engineering correlations [13, 29]. In a post-flashover compartment, the environment becomes more well-mixed and can be modelled as a well-stirred reactor with homogenous properties throughout [31].

2.2.2 Vent Flows and Mixing

Once the volume of smoke in the upper layer of a compartment builds up enough for the interface height to descend past the top of any openings, such as door or windows, smoke begins to flow out of the openings. Any openings in the fire compartment that can

be a pathway for the flow of gases out of or into the compartment is called a vent [32]. Flow through vents is caused by pressure differences between the inside and outside of the compartment which arise due to thermal expansion of the gases in the compartment, temperature differences (and resulting buoyancy forces) between the inside and outside of the compartment, and any pressure difference caused by mechanical ventilation [33]. As the smoke begins to flow out, the pressure inside the compartment decreases and as a result ambient air from outside the compartment is drawn into the compartment below the out flowing smoke. This provides a supply of O_2 that is essential for continued burning of the fire [32].

Work by Phral and Emmons studied buoyant flows through vents with the use of a water and kerosene hydraulic model [34]. This work derived theoretical equations and used experiments to validate the theory and conclude that it is possible to calculate vent flow rates in fire scenarios. Building on this work, Rockett in 1976, applied the zone model to a fire compartment and derived correlations to obtain mass flow rates for typical doorway and window vents [35]. Rockett defines the neutral plane height as the height in a vent at which the pressure difference between the inside of the compartment and the outside is zero. This height separates the out flowing smoke from the inflowing air, but does not necessarily occur at the same position as the smoke layer height. In addition, Rockett identifies a ventilation parameter equal to the product of the vent opening area and the square root of the height of the top edge of the vent above the floor ($A_o\sqrt{H_o}$) [35]. Since then, the ventilation parameter has been used extensively to characterize doorway flow rates [31, 32, 36].

Velocity profiles in fire induced vent flows have been studied extensively. A typical vertical flow profile through the centre line of the doorway has zero velocity at the neutral plane height by definition, a maximum inflow velocity near the floor, and a maximum outflow velocity near the ceiling [36, 37, 38]. The shape of the vertical profile is generally smooth but not quite linear, even though theoretical pressure differences predict a linear velocity profile. Magnitudes of the maximum velocities vary depending on the conditions in the compartment, however, they are typically on the order of 1 m/s to 2 m/s for inflow and 3 m/s to 4 m/s for outflow [39]. In the horizontal direction (side to side in the opening), the velocity profile forms a concave shape, where the velocity is slowest on the centre line of the door and is fastest near the door jamb [40]. This concave profile can be explained through potential flow theory, however, in practical terms the horizontal velocity difference is minimal, being only 0.1 m/s to 0.2 m/s when the mean velocity is on the order of 1 m/s to 2 m/s [40].

The precise location of the neutral plane is dependent on the fire scenario, the geometry of the doorway, and the geometry of the fire room [41]. During fire development, the neutral

plane typically starts at a high elevation, near the top of the vent, and descends as the smoke layer descends [32]. It stays at an intermediate height (not necessarily the mid-height of the vent) once the flow develops and reaches a steady state phase. During the decay phase of the fire, the neutral plane rises again as the fire compartment cools and smoke production decreases [32, 38]. Dalziel and Lane-Serff developed a hydraulic model of doorway exchange flows [41]. They indicate that it is incorrect to assume that the NP height should be at the mid-height of the door when there is no net flow. In addition, experiments show that doorway flows are not steady, therefore, it is imperative to use time-resolved measurements for calculating fire induced flow rates through openings, as using time-averaged values could result in underestimations of the true flow [41].

The typical vent flow models used by Rockett have a number of underlying assumptions and neglect some of the more complicated phenomena that occur in compartment fires [35]. More recently, some of these complexities, such as convective and radiative heat loss through vents and mixing between the two layers of the vent flow, have been taken into account for doorway flows [42] and for general vent flow models [43]. The model for mixing between the two flow layers is attributed to Lim [44], and is essentially implemented as a mixing ratio. The mixing ratio is defined as the ratio of the mass flow rate of gas mixing between layers to the mass flow rate of air flowing into the compartment. It is found that the mixing ratio can vary from zero to 1.28 depending on layer temperatures, doorway geometry, and smoke layer height [42, 44].

The studies which derive more complex opening flow models show through the possible values of the mixing ratio, that mixing in doorway flows can be significant. This mixing not only cools the out flowing smoke, reducing the convective heat transferred out of the compartment, but also vitiates the inflowing air, reducing the mass of inflowing O_2. Visualization experiments, conducted in a scaled compartment model connected to a corridor via a doorway, used cotton wads soaked in titanium tetrachloride to produce visible smoke [45]. Observations of the smoke flow through the doorway showed that mixing occurs between the two layers as vortices form and are shed at the interface between the layers.

This flow configuration appears similar to mixing layer flows, which belong to a class of canonical flows called free-shear flows [46]. These types of flows form in the presence of velocity gradients away from walls or other flow boundaries. In the case of two-way vent flows, there is a significant velocity gradient in the vertical direction, which, along with buoyancy effects, produces turbulence. This results in increased mixing compared to when only molecular diffusion is present [47].

Turbulence is a highly three-dimensional phenomenon and consists of multiple-scales from the integral scale (the largest scale), usually on the order of the diameter of the base of

the fire for fire induced flows [48], down to the smallest scale known as the Kolmogorov scale [47]. Turbulent energy is created at the integral scale, which often consists of well-organized structures known as eddies, and the energy is transferred through intermediate scales to the Kolmogorov scale through turbulent energy dissipation [46]. At the smallest scales, viscosity forces dominate to break up the eddies. In free-shear flows such as mixing layers, the eddies are formed by Kelvin-Helmoltz (or shear) instabilities, which form in the presence of strong velocity gradients [47]. High energy flows, with stronger velocity gradients, have increased formation of these instabilities and therefore have increased turbulence, leading to more vigorous large-scale eddies and increased mixing [47].

To characterize the importance of mixing in a fire vent flow, it is imperative to understand the behaviour of the large scale eddies. This is supported by successful use of large eddy simulation (LES) turbulence models in computational fire dynamics models such as fire dynamics simulator (FDS) [49] and FireFOAM [50]. The implementation of LES aims to resolve large scale eddies, while smaller scales are modelled or neglected [48]. Studies comparing computational and experimental results have shown that LES successfully captures important characteristics of turbulence pertaining to mixing in fire compartments, but does lack the fine resolution required for resolving smaller scales which are more important near compartment walls [51].

2.2.3 Measuring Vent Flows

There are several methods to measure the velocity of the gases flowing through a fire compartment vent. Most of these methods involve directly measuring the pressure difference across the opening in at least one location and applying principles of fluid flow to deduce velocity. Typically, the flow profile in a vent is measured with one of three approaches [32]. The first involves measuring the pressure difference, using pressure probes and transducers, across the opening at a sufficient number of locations to provide a resolved profile. The second involves measuring the pressure difference at only one location while measuring the temperature profile throughout the opening. The temperature profile is then used to estimate the pressure profile. The third method is similar to the second, but additional instrumentation is added to photographically determine the neutral plane height instead of relying on temperature measurements to predict it. Most methods have reported accuracies on the order of 10%, however, the accuracy varies largely depending on the situation [32].

The most reliable and accurate method for measuring the velocity profile in a vent is method one, using an array of pressure probes to obtain differential pressure at various

points in the opening [32]. This method also requires the measurement of temperature throughout the opening in order to determine the density of the fluid, which is critical for the conversion of pressure difference to velocity. A common probe used to measure fluid velocity in many applications is the pitot probe. However, the common pitot probe is not ideal for measuring fire induced vent flows for three main reasons: first, the probe may not be sensitive enough to resolve the low speed buoyant vent flows, secondly pitot probes are prone to clogging with soot and finally, pitot probes must be carefully oriented to measure flow as they resolve velocity in only one direction. Pitot probes, therefore, not well suited for fire vent flow applications characterized by low velocity, soot, and unknown flow direction. Instead, a common probe currently used for measuring fire induced vent flows was developed by McCaffrey and Heskestad in 1976 and is known as the bidirectional pressure probe [52]. A schematic of this probe is shown in Fig. 2.3.

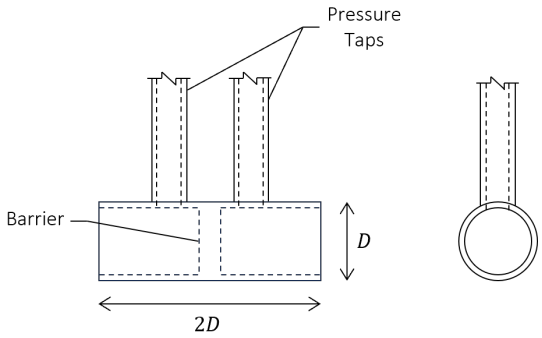

Figure 2.3: Schematic of bidirectional pressure probe.

The bidirectional pressure probe is constructed of a single tube with an outer diameter typically between 19 mm to 25.4 mm (0.75 inches to 1.0 inches) that is open on both ends and has a physical barrier in the centre which separates two sensing ports. Each sensing port leads to a pressure tap that is connected, via tubing, to a differential pressure transducer. The pressure transducer provides a measurement of the pressure difference on either side of the physical barrier [32, 52]. The bidirectional pressure probe operation is similar to that of a double-sided pitot probe. When the probe is situated in a flow, the barrier between the ports causes the flow to stagnate in the port that is facing upstream, thus providing a measure of the stagnation pressure. The downstream side of the probe measures the static pressure of the flow, which is lower than the stagnation pressure. This creates the pressure difference across the probe outlets, which is measured by a differential pressure transducer and then related to velocity through the Bernoulli equation.

Characterization of the probes has found that they are relatively insensitive to the

direction of the incoming flow relative to the centre line of the probe. Typically, the measured velocity varies by a maximum of 10% within an angle of 50° between the main flow velocity direction and the centre line of the probe [52, 53, 54]. This characteristic means that bidirectional pressure probes do not measure a unidirectional velocity, but instead resolve a more spatially averaged velocity over the angular range of the probe which is translated to a single vector that is aligned with the probe centre line. In experiments where the measured velocity from a bidirectional pressure probe is compared to a three-dimensional velocity field, the resulting velocity magnitude has been found to correlate more accurately (within 7%) with a resolved three-dimensional estimate of velocity instead of with the velocity aligned directly perpendicular to the face of the probe (up to 10% error) [55]. Angular sensitivity of the probe is known to be greatest between flow approach angles of 25° to 30°, due to the formation of wakes on the back side of the probe [53].

Bidirectional probes are relatively large bluff bodies so bluff body effects, such as the formation of wakes on the trailing edge of the probe, may affect pressure measurements [56]. Some work has studied the formation of these wakes with sophisticated measurement and modelling techniques and found that the formation of wakes on the back side of the probe may cause the pressure on the back side to fall below the static pressure [56]. This results in an overestimation of the flow velocity and, therefore, a calibration must be performed. Even though bluff body effects have been proven to affect measurements of the static pressure with bidirectional probes, studies have shown that these effects are relatively constant over a wide range of Reynolds number, including the range appropriate for fire induced flows [52, 54].

Calibration of bidirectional pressure probes is completed in a wind tunnel where measurements by the bidirectional pressure probe are compared to measurements from a pitot probe, which has a known calibration factor of one. McCaffrey and Heskestad, who first performed the calibrations, found that an average calibration factor of 1.08 should be applied to the probe to account for the bluff body/Reynolds number effects [52]. This factor was found to be constant over the applicable range of velocities from the calibration. Since then, some studies have confirmed this calibration constant for carefully manufactured probes [53, 54, 57], including calibrations done on the probes used at the University of Waterloo [58]. The largest discrepancies between this average calibration factor exists at very low flow speeds, less than 0.2 m/s [54].

Other factors that introduce uncertainty to measurements of velocity using bidirectional probes include uncertainties in the measurement of fluid density, transducer uncertainties, and uncertainties in the data acquisition circuits [54]. It is recommended that pressure transducers be placed at the same height as the probes to minimize head losses and buoyancy effects in the connecting tubes [52]. Uncertainty in the measurement of fluid density

is affected by the measurement of temperature, as well as the assumption that smoke can be treated as an ideal gas (often represented by properties of air) for the calculation of velocity [58]. This assumption is commonly implemented, including in a series of experiments that used bidirectional probe measurements to calculate enthalpy flow out of a doorway for energy balance calculations on a compartment [59]. Other experiments have proven that assuming smoke behaves as ideal gas (air) only results in minor errors [54].

The application of sophisticated flow measurement techniques, such as particle image velocimetry (PIV) to fire experiments, has allowed for the evaluation of bidirectional pressure effects in large-scale fire environments [60, 61]. Studies that employed both bidirectional pressure probes and PIV to measure doorway flows found that the bidirectional pressure probes agree with PIV measurements of velocity within the error bounds associated with both techniques [55]. The discrepancy between the two techniques varies with height in the opening. Velocities agree best in the faster flow regions near the top and bottom of the doorways away from the neutral plane where the velocities are lowest [62]. This corresponds well with the increased uncertainty in Reynolds number effects on the bidirectional pressure probes seen at slow speeds in the characterization tests described above as well.

2.3 Compartment Temperature and Heat Transfer

This section discusses the development of gas temperatures and the key principles of heat transfer in a fire compartment. All three modes of heat transfer, conduction, convection, and radiation, are important in compartment fires. However, in many situations radiation tends to be the dominating mode.

2.3.1 Temperature Development

During a fire, heat is emitted by the flame through thermal radiation or is carried by the plume and smoke through convection. In a compartment, this heat is transferred to compartment boundaries or convected out of the compartment through openings. Compartment boundaries absorb radiative heat flux directly from the flames and also from hot gases [63]. For example, the hot smoke layer re-radiates heat towards the floor of the compartment. The ceiling and walls of the compartment that are in contact with the flowing smoke are subjected to convective heat transfer as well. Heat that is transferred to the compartment boundaries from the flames or from hot gases is then conducted through

the construction of the boundaries [29, 63]. Additional heat losses occur when thermal radiation escapes through compartment openings and when hot gases are convected out of any openings. The difference in energy between the heat released by the fire and the heat loss from the compartment is transferred to the gases in the compartment, resulting in a temperature increase. Temperatures can become up to 1.3 times higher when a fire is located near a wall, or 1.7 times higher when a fire is near a corner compared to when the fire is in the centre of the compartment, due to the restriction of entrained air into the plume, which is critical for cooling of hot combustion gases [63].

Obtaining temperature measurements in compartment fires is important, since information provided by temperatures can be used to predict the onset of critical phenomenon leading to damage to materials or hazardous conditions. For example, work done to estimate the potential for flashover in a fire room has identified a critical smoke layer temperature between 500 °C to 600 °C [63]. While useful, this threshold is not a perfect estimator as it can vary significantly depending on compartment size, ventilation, fire location, and if the other materials in the compartment are combustible [64]. Temperature measurements are also required to estimate properties of the gases inside the compartment to be implemented in correlations [29, 64]. Further, temperature measurements have been used to identify the interface height between the upper smoke layer and lower air layer in compartments [65]. When a compartment is stratified, a sharp gradient in temperature can be detected at the interface height. When a compartment is more mixed, the gradient diminishes. Overall then, temperature measurements are extremely useful to characterize compartment conditions in fires.

Measuring temperatures in compartments is often done using thermocouples. A thermocouple is a device consisting of two wires made of dissimilar metals with two junctions. When the measurement junction is heated, a voltage is induced across the wires known as the Seebeck voltage [66]. This voltage is proportional to the temperature difference between the junctions, and the temperature on the heated (measurement) end can be calculated if the temperature at the cold end is known [66].

The heated junctions in thermocouples used for measuring temperatures in fires are often left exposed, rather than shielded. This is done to minimize the response time of the thermocouple signal [66] which is critical in rapidly developing fire environments. However, bare-bead thermocouples can be subjected to significant radiation effects if the thermocouple is located near the fire or in other areas subjected to high heat flux [67]. Studies have shown that measurement errors up to 75% could occur if the thermocouple is exposed to high heat fluxes near 25 $\mathrm{kW/m^2}$ [67]. These effects can be mitigated through the use of shielded or aspirated thermocouples. Aspirated thermocouples actively move air around the heated junction to convectively cool the junction, which can reduce radiation

effects by up to 90% while maintaining good response times [67]. However, thermocouples in locations only a few meters away from the flames are subjected to significantly lower radiative flux and therefore, measurements are subject to only minimal radiation effects.

2.3.2 Convective Heat Transfer in Compartment Fires

In open areas, most of the heat generated by a fire is carried away from the fire through the plume [68]. This convective heat transfer is typically in the form of natural turbulent convection caused by buoyancy. Heat fluxes from convection due to fires are typically on the order of $3\,\mathrm{kW/m^2}$ and are much weaker than radiative heat fluxes [69]. Materials typically do not ignite by convection alone without direct flame impingement, therefore, the threat of flame spread is not significantly effected by convective heat transfer [69]. However, the flow of gases away from the fire does pose a significant hazard, mostly due to toxicity, in remote locations where radiant heating is not significant. In compartment energy balances, convection through doorways has been found to account for approximately 16% of the energy loss in the compartment [59]. In contrast, the majority of the heat loss occurs to the compartment walls due to a combination of convection and radiation.

2.3.3 Radiation Heat Transfer in Compartment Fires

Radiation heat transfer is a significant phenomenon in compartment fires, as it contributes heat flux to remote targets and heat feedback to the fuel surface, which as explained previously, is a key factor in determining fuel evaporation and thus, fuel burning rate. At low temperatures convection can dominate, but at high temperatures, such as those reached in flames, radiation dominates [68]. Thermal radiation is also known to be the dominating form of heat transfer in large scale fires [70].

Flames are a significant source of radiation in compartment fires, with emissions from both combustion gases and from particulate matter such as soot [69]. The majority of radiation from a fire, up to 80%, is attributed to radiant emission from particulate matter, while the remaining 20% is emitted by the hot combustion gases [71].

Radiation from flames has been found to be largely dependent on a fuel's propensity to soot. Radiation from the particulate matter is partially in the visible spectrum and is what gives a flame its luminous yellow/orange colour [68]. Soot particles in the flames reach high temperatures and emit radiation as tiny grey bodies, meaning that the emission is not dependent on wavelength, but that the particles are not perfect emitters [68]. Perfect emitters, known as black bodies, are an idealized entity that have an emissivity equal to

one. Emissivity is a property that defines the ratio of radiation emitted from a surface compared to a perfect emitter.

Studies have found that the fraction of the HRR of a fire released by radiation, known as the radiative fraction, increases linearly with sooting propensity [72]. The radiative fraction depends not only on soot production, but also on the size of the fire (pool diameter) which effects non-uniformity of temperatures throughout the flame [68]. In terms of soot production, the amount of soot produced by a flame is closely correlated with a fuel's smoke point, which is defined as the height above the fuel surface at which smoke begins to form. A fuel with a lower smoke point generates more soot as it burns compared to a fuel with a higher smoke point, and as a result has increased radiant emissions [71, 72]. Typically, the radiative fraction of a fire is assumed to be 0.3 for luminous flames, however, this value has been found to vary between 0.18 to 0.43 for common fuels [72].

In terms of hot combustion gases, the main contributing species to thermal radiation in a flame are CO_2 and water vapour, which emit and absorb radiation over specific wavelengths [69, 73]. Therefore, the common assumption that a flame can be treated as homogenous, isothermal, and spectrally grey is best applied only to sooty flames [73]. In addition to contributing radiative emissions, the gases and particulate matter at relatively cooler temperatures near the base of the flame can absorb radiative heat feedback to the fuel surface, effectively blocking this heat from contributing to the burning rate, which could lead to a counterbalancing effect [69].

Depletion of O_2 concentration in compartments has an effect on the radiative properties of flames. The radiative fraction has been found to decrease as the ambient O_2 concentration decreases, consequently the convective fraction increases in lower O_2 environments [74]. In 1981, Santo and Tamanini found that mass loss rate, radiative fraction, and total radiation emissions reduced by nearly 50% when the ambient O_2 concentration was reduced from 20.95% (standard atmospheric concentration) to 18.0% [75]. The results were attributed to a reduction in soot concentration in lower O_2 environments.

The effects of combustion gases on radiation heat transfer in compartments is not limited to emissions from within the flame. The buildup of hot gases in a smoke layer near the ceiling is known to be an important factor in compartment fire radiation and development [68].

Smoke can act as a participating media, meaning that smoke influences the radiative flux emitted from a source that is incident to a target. Both gases and particulate matter within the smoke can absorb, scatter, and emit radiation in a very complex manner that is often simplified as a grey medium with an emissivity of approximately 0.7 [69]. In reality, diatomic gas molecules such as N_2 and O_2 do not participate in radiation as these

species cannot interact with electromagnetic radiation in the thermal region due to a lack of dipole movement in their molecular bonds [68]. Hetero-nuclear molecules such as CO_2, CO, and water vapour, on the other hand, can absorb and emit thermal radiation at discrete wavelengths. This means that in reality, smoke is not a grey medium [68].

Often in fires, the net heat flux to a target is a quantity of interest, as it is used to determine if a remote material may ignite. Remote ignition may occur if the heat flux incident to a material overcomes the critical heat flux needed for ignition [25]. Components of the total incident heat flux to a target include radiative flux from the flames, radiative flux from the hot smoke, and any convective flux from direct interactions between the target and adjacent gases. Often, the contributions of radiation from the flames are considered to makeup the majority of the heat flux to the target and therefore, measurements of flame radiation form the focus of efforts to estimate the incident heat flux to a target.

Radiative flux ($\dot{q}''_r$) from a source to a target is a function of the geometric relationship between the source and the target, expressed as the view factor ($F_{1\rightarrow 2}$), and the emissive power (E), as shown in Eq. 2.2 [76].

$$\dot{q}''_r = F_{1\rightarrow 2}E \tag{2.2}$$

In general radiation heat transfer, the emissive power is calculated as the product of the emissivity of the radiating source (ϵ), the Stefan-Boltzman (σ) constant, and the surface temperature of the source (T) to the fourth power, as shown in Eq. 2.3 [76]. In fires, emissive power is typically estimated from either the HRR and radiative fraction of the fire or by assuming a uniform flame temperature throughout the visible flaming portion of the fire [77].

$$E = \epsilon\sigma T^4 \tag{2.3}$$

The view factor is a quantity, expressed as a fraction, that represents the ratio of the total radiant emissions from the source to that which reaches the target. It is essentially equivalent to the amount of surface area of the source which the target can 'see' from its perspective. Closed form equations for view factors between flames and remote targets have been derived by Mudan [78]. Typically, the fire is assumed to be a vertical rectangle or cylinder and the target is assumed to be a differential area at some distance from the flames [77, 78].

2.4 Combustion Products and Flammability

The main combustion products formed when a common hydrocarbon fuel burns completely are CO_2 and water vapour. In well-ventilated fires, the presence of near atmospheric concentrations of O_2 drives combustion to be nearly complete, resulting in the concentrations of combustion products to be near their stoichiometric values [79]. However, as the combustion process becomes less efficient, which can occur in reduced O_2 environments, the concentrations of CO, soot, and unburned hydrocarbons increase [80]. The formation of combustion products is not only dependent on ventilation, but is also affected by the mode of burning (for example flaming or smouldering), compartment and fuel geometry, compartment temperatures, and the addition of chemicals in the fuels such as flame retardants [6, 79]. It is also possible for many other species to form as well, depending on the chemical makeup of the fuel. Compartment temperatures affect species production in two ways. First, the initial generation of species in the fire changes depending on compartment temperature, and secondly, oxidation of species in the smoke layer changes with temperature. At elevated temperatures, species are more likely to oxidize to form CO_2 and water vapour [6]. Therefore, increased compartment temperatures can result in reduced concentrations of incomplete combustion products. At the same time, in under-ventilated fires, the oxidation of incomplete combustion products is reduced, so there can be many counterbalancing effects in a real compartment fire scenario [6].

The formation of soot occurs in the parts of the flame with reduced O_2 concentrations, such as the interior of the flame, which is also fuel rich [23]. Soot particles tend to form and agglomerate in these regions and will escape the flame if they become large enough. Smaller soot particles, if resident in the combustion zones for long enough, may burn and be destroyed. As discussed previously, smoke is made up of a combination of particulate matter, gaseous combustion products, and entrained air. The combination of visual obscuration and toxicity arising from a developing layer of smoke is what presents the greatest hazard to building occupants during a given fire [23]. Studies of occupant survivability have found that the majority of fire deaths occur due to smoke inhalation, and that 75% of smoke inhalation deaths occur in rooms outside the fire room, while occupants in the fire room are more likely to be overcome by heat [6, 81]. Therefore, understanding both the makeup and the movement of smoke through a structure is critical since they are responsible for the generation and transport of toxic species to these remote locations.

The toxic species that make up smoke can be categorized into two groups: asphyxiants and irritants [23]. Asphyxiants include species such as CO and hydrogen cyanide. Carbon monoxide accounts for approximately half of all fire related deaths and is, therefore, considered the most dangerous killer in fires [6, 82]. When CO is inhaled by an occupant, it

competes with oxygen in the blood and effectively reduces the blood's capacity to carry oxygen. Concentrations as low as 4000 ppm can be fatal in less than one hour. Common chemical irritants that are found in smoke include sulphur dioxide, ammonia, and hydrogen chloride [82]. These species can irritate the airways of an occupant when inhaled, and also irritate parts of the skin and eyes making it more difficult to escape.

The level of ventilation in fires is often characterized by use of an equivalence ratio. An equivalence ratio relates the actual fuel:air ratio in a fire to the stoichiometric fuel:air ratio for the burning fuel [83]. Therefore, a fire with an equivalence ratio of one has complete combustion with no excess air, a fire with an equivalence ratio of less than one has complete combustion with excess air (considered fuel lean), and a fire with an equivalence ratio greater than one has incomplete combustion (considered fuel rich). However, the interactions between vaporized fuel and entrained air are quite complex in fires, and as a result there are many possible definitions of equivalence ratio, which vary depending on the control volume for which they are defined. Throughout the literature, the concept of a global equivalence ratio (GER) is used, which is an equivalence ratio defined considering the entire fire compartment as the control volume [83]. Using this approach, the amount of air entering the compartment through vents is assumed to be equal to the amount of air available for combustion. In reality, this is not the case, as both global and localized mixing can be significant, meaning the equivalence ratio near the fire, which actually dictates combustion, can be very different from that averaged over the full compartment GER [6]. In some cases, the GER has been found to correlate well with trends in the production of CO and other incomplete combustion products from the fire. This may be because even on a global scale the concentration of incomplete combustion products typically increases as ventilation within a compartment is reduced and the GER increases [83, 84].

Assessment of flame extinction is another important consideration in understanding overall fire behaviour as O_2 concentrations decrease in a fire compartment. The minimum O_2 concentration to support the burning of a diffusion flame, such as a fire, is known as the limiting oxygen index (LOI) [85]. The LOI changes with fuel type and a fuel with higher LOI is said to be less flammable than a fuel with a lower LOI. In addition to the need for there to be sufficient oxygen feeding the fire, flame extinction is also related to the Damkohler number, which is the ratio of heat loss to chemical reaction time within the combustion zones [86].

Extinction of flames in compartments has been studied by others, including Quintiere and Rangwala [87]. This work presents a theory for flame extinction in compartment fires based on critical flame temperature, taking into account the effects of O_2 concentration and heat feedback. The theory suggests that at ambient temperature, the minimum O_2

concentration necessary to support burning of a hydrocarbon fuel is 12% by volume [87]. This minimum concentration can drop to as low as 2.5% as the ambient temperature or heat feedback to the fuel surface increases. Other important factors related to extinction include stoichiometry, the heat of gasification of the fuel, and convective heat transfer at the fuel surface [87]. Experiments conducted in the same study found that fires extinguished due to lack of O_2 with small enough vents, while with slightly larger vents the fires extended to a steady state phase characterized by a reduced burning rate compared to open burning [87]. With the slightly larger vents, the fires could grow to a point where the smoke layer temperature became high enough to provide additional heat feedback to the fuel surface to sustain burning at lower O_2 concentrations than for the smaller vent case [87].

Utiskul [88] and Mizukami [89] have also studied extinction of compartment fires using both experiments and theoretical modelling, respectively. The experiments identified four regimes of burning that lead to different modes of extinction depending on the level of ventilation. The regimes are summarized, in order of least to most ventilated, as follows [88]:

1. Extinction due to smoke filling occurs when the compartment has small vents and low O_2 concentrations.

2. Burning at vents occurs when vent flows are significant enough to sustain burning away from the fuel surface. This leads to ghosting and oscillating flames.

3. Burning with oscillations occurs when there is burning at the vents; however, the fire is sustained for a period of time with oscillations in the burning rate and finally extinguishes due to lack of fuel.

4. Steady burning occurs until extinction occurs due to lack of fuel when the fire is well-ventilated.

Theoretical models implemented in the studies, follow the groundwork provided by Quintiere and Rangwala, and identify a flammability limit depending on O_2 concentration and compartment temperature [89]. The flammability limit is linear, starting at 12% O_2 at ambient temperature and decreasing in limiting O_2 concentration with increasing temperature.

2.5 Forced Ventilation Fire Tests

This section presents a review of relevant studies which focus on the influence of mechanical ventilation on fires and/or the environment in compartments throughout a fire scenario as background for interpretation of differences between results observed in the various ventilation configurations studied in this research. Some work has studied the effect of vent position (i.e. high level near the ceiling or low level near the floor) through the use of multiple vent configurations, while others have focused on the effect of ventilation flow rate with the use of only a single configuration. Throughout this section, the term 'configuration' is meant to describe a geometrical change in the ventilation system, such as a change in vent position or size. Changes in ventilation flow rates are not considered a change in configuration.

2.5.1 Studies with Multiple Vent Configurations

Some forced ventilation studies have focused on determining the effects of supply and exhaust vent location on the development of a fire and fire environment inside a compartment. These studies have been completed at reduced scale, in single room-sized compartments, and at multi-compartment scale. Here, ventilation rates are often characterized by how often the total volume of the compartment is exchanged in units of air changes per hour (ACPH).

In 1993, Mizuno *et al.* [90] presented results which showed that vent configuration affected the fire and environment in two ways. First, the quality of air getting to the fire was affected, and secondly, the cooling effect of the supply air varied with ventilation. Mizuno conducted experiments in a 50 cm × 50 cm × 50 cm compartment configured with upper, middle, and lower vents. With low level exhaust, the smoke layer was effectively pulled down over the fire resulting in CO production beginning earlier in the test, however, the max CO concentration was similar for both high level and low level supply at 40 000 ppm (4.0%) [90]. Other tests in a 1.0 m × 0.6 m × 1.0 m reduced-scale compartment studied the effect of vent position on the temperature profile in the compartment [91]. These results showed enhanced mixing of smoke layer and supply air and no thermally stratified layer when the supply was near the ceiling. In contrast, a smoke layer did form when the supply vent was located near the floor and the exhaust was near the ceiling. In addition, lower ventilation flow rates resulted in overall higher compartment temperatures [91].

Similar results have been observed in room-sized single-compartment fire tests. Some studies have reported destruction of the smoke layer at high supply flow rates or when

the supply is located at a high level [90, 92, 93, 94]. An experimental and computational study found that turbulence introduced into the upper smoke layer of a compartment by a ventilation system can cause the smoke layer to breakup [92]. Perturbing the upper layer in a compartment with a supply of fresh air effectively cools the smoke layer and heats the lower layer [94]. Cooling the smoke layer has been found to make the smoke layer more unstable, as the buoyancy forces responsible for the formation of the layer are reduced [90]. In addition to the turbulent momentum and mixing imparted into the smoke layer, the supply of fresher air into the upper layer can also have a cooling effect.

Experiments from a $3.5\,\mathrm{m} \times 2.5\,\mathrm{m} \times 2.5\,\mathrm{m}$ compartment with methane fires between 50 kW to 200 kW had reduced upper layer temperatures, upper layer CO_2, and upper layer CO concentration with high level supply, while, upper layer O_2 concentrations increased with high level air supply [92]. The lower layer O_2 was lowest when both supply and exhaust were at a high level preventing fresh air from circulating to the base of the fire. Another study reported heptane pool fire experiments in a $3.4\,\mathrm{m} \times 3.6\,\mathrm{m} \times 2.05\,\mathrm{m}$ steel compartment with very high flow rates compared to typical residential flow rates, up to $1500\,\mathrm{m}^3/\mathrm{hr}$ (60 ACPH) [93]. The flame was found to tilt towards the incoming supply air as a consequence of the high flow rates. Vent configuration was also found to have a significant effect on the O_2 concentration in the compartment. With one supply vent near the ceiling the minimum O_2 concentration was 17%, while with two vents (one near the floor and one near the ceiling) the fire was able to grow larger and minimum O_2 was 13% [93]. However, the O_2 concentration was higher when there was ventilation compared to when the compartment was sealed. Multi-compartment tests have shown that low level vents that lead to stratified fire compartment environments can also lead to increased fire MLR, due to the increased supply of O_2 to the fire [95]. In fact, the O_2 concentration near the base of the fire was found to be 2% to 3% higher when supply vents were located near the floor versus higher in the compartment. Interestingly, the concentrations of incomplete combustion products, such as CO, remained high, which was attributed to a significant amount of flame being located in the low O_2 environment in the upper layer [95].

Effects of disturbing the upper layer in a compartment with supply air into the layer is more significant at higher flow rates and tends to lead to a more uniform environment in the compartment, further vitiating the supply of air to the fire [92, 93]. The supply of air into a $6.0\,\mathrm{m} \times 4.0\,\mathrm{m} \times 3.0\,\mathrm{m}$ compartment, was varied at rates pertaining to the stoichiometric amount of air needed to supply a range of methane fires between 100 kW to 400 kW [94]. A thermally stratified environment was created in well-ventilated cases (with two to three times stoichiometric air) and in cases where the supply air was fed to the compartment at the low level. It was also found that complete combustion occurred when the supply air was greater than four times the stoichiometric air requirement, but

that flame extinction due to lack of O_2 occurred with less air supply [94]. Environments in compartments that have supply vents at high locations have been predicted well using a mixed-reactor model, consistent with observation that a fire compartment can transition toward well-mixed conditions simply by changing the location of supply air vents [95]. Alternately, when vents are located at a low level and the resulting environment remains stratified, a zone model best represents the environment in the compartment. The effects of stratification become even more significant when fresher air is supplied into the lower layer with a direct flow path to the base of the fire [92, 95].

2.5.2 Studies with a Single Vent Configuration

Some studies have used a single room-size compartment or a multi-compartment structure with only a single vent configuration to investigate the effect of varying ventilation flow rates on development of the fire and the environment created inside the fire compartment. The following discussion presents some of the key findings from these studies as they pertain to the effect of ventilation on burning rate, environmental stratification, and gas specious concentrations in the fires.

Reduced scale pool fire tests, burning hydrogenated tetra-propylene in a $1.88\,m^3$ compartment, found that steady burning could be achieved when the flow rate of supply air was greater than 14 ACPH while extinction occurred due to lack of O_2 with flow rates less than 10 ACPH [96]. Larger scale tests, in a $120\,m^3$ compartment with the same fuel, discovered that varying the ventilation flow rate resulted in three district burning phases. The first was an initial growth phase where the burning rate was the same as the free burning rate of the fuel, the second was unsteady burning caused by a lack of O_2 where the fire HRR would oscillate due to intermittent availability of O_2 to the fire base, and the third was a steady state burning phase at a reduced burning rate [97]. The three burning phases of the fires were only observed to occur when the ventilation flow rate was greater than 2 ACPH. With lower flow rates, the fires would extinguish due to lack of O_2 [96, 97]. This suggests that smaller compartments require more mechanical ventilation than larger compartments to sustain burning, consistent with the idea that the initial compartment volume (and mass of O_2 contained therein) can have a significant effect on the level of ventilation of the fire. In the larger compartment, increases in ventilation flow rate were found to delay the occurrence of the unsteady phase and resulted in increased HRR during the steady phase [97]. The reduced burning rates and the transition to extinction were also shown to be predicted by GER, showing that reduced burning rates are related to reduced the combustion efficiency as the vent flow rate decreases [96].

A study that burned pine wood cribs in a $1.6\,m^3$ compartment found that the fires would extinguish due to lack of O_2 at flow rates less than 5 ACPH [98]. The fire struggled to propagate with flow rates between 5 ACPH to 11 ACPH, and sustained burning was achieved only for flow rates greater than 11 ACPH. Even the tests with sustained burning resulted in high CO production, indicative of low combustion efficiencies. At flow rates above 11 ACPH, the compartment temperature, MLR, and HRR increased linearly with increasing air supply flow rate, while the minimum O_2 concentration in the environment decreased [98]. Other wood tests in a $4.0\,m \times 3.0\,m \times 2.8\,m$ compartment studied the effect of hot gas extraction on a compartment for the purpose of smoke control and used a louvred vent to naturally supply makeup air [99]. Varying the extraction rates between 0 ACPH to 60 ACPH resulted in longer burn durations, lower flame heights, lower CO concentrations, reduced temperature gradients, and increasingly unstable stratified temperature layers [99]. Computational models of the fires were also able to predict these effects [100, 101].

Other large scale tests in a $3.4\,m \times 3.3\,m \times 3.1\,m$ compartment showed similar trends of increasing burning rate and decreasing O_2 concentration with increasing ventilation rates [102]. Temperatures indicated either well-mixed environments or environments stratified into two layers depending on the flow rate. The same compartment was also studied in naturally ventilated cases with varying opening sizes and vent size was also found to have a significant effect on the temperatures and temperature stratification where, due to additional mixing of gases interior to the compartment, more uniform temperatures were present with smaller openings [102]. The behaviour of naturally vented compartments has been found to be similar to mechanically vented ones, showing that the trends found from naturally ventilated tests can be extrapolated to mechanical ventilation [103].

As mentioned previously, the effects of ventilation on combustion processes in the fire cause changes in the combustion efficiency, which in turn can influence the burning rate and change the production of gaseous species in the fire plume. Changes in the species concentrations are tightly coupled to combustion efficiency, creating a feedback loop. Differences in species concentrations caused by ventilation have been shown in fire tests in a $4.5\,m \times 4.0\,m \times 6.0\,m$ compartment. It was observed that the forced ventilation rate have to be twice that of the stoichiometric air amount in order to achieve well-ventilated conditions [104]. In well-ventilated cases, the minimum O_2 concentration was near 14%, the maximum CO_2 concentration was 6%, and the maximum CO concentration was 1000 ppm (0.1%). In under-ventilated cases, the minimum O_2 concentration also decreased to near 14%, but due to differences in the fire development the maximum CO_2 concentration increased to 10%, the maximum CO concentration increased to 17 500 ppm (1.75%), and a significant amount of unburned hydrocarbons were detected as a concentration of methane near 1.0% [104]. In a very large $400\,m^3$ compartment with ($54\,m^2$ of floor area and a ceiling

height of 7.5 m), with low level supply and high level exhaust at a rate of 3 ACPH, the minimum O_2 concentration was 18% when the fire extinguished due to lack of fuel [105]. When the ventilation was turned off shortly after ignition, the minimum O_2 concentration dropped to below 15% and the burning time was reduced as the fire extinguished due to lack of O_2 [105]. Other tests have shown that decreased O_2 concentrations are initially measured at higher elevations due to the buildup of the smoke layer, while concentrations at measurement locations at lower elevations and nearer to the base of the fire decrease later in a test [97].

Experiments in a 4.0 m × 6.0 m × 4.5 m compartment found that extinction occurred when O_2 concentrations were reduced below the LOI for the fuel being burned, and the time to extinction could be modelled as the time needed to reduce the O_2 concentration to below the LOI concentration [106]. Some pool fires in an 8 m^3 compartment extinguished due to lack of O_2 at O_2 concentrations of 8% when the ventilation supply rate was 0.5 ACPH [74]. Additional O_2 supply to the compartment with increased ventilation resulted in shorter fires with increased peak fire MLR and higher peak compartment temperatures.

As explained previously, forced ventilation tests with supply located near the ceiling can result in more well-mixed environments. As a result, O_2 concentrations are more uniform throughout the compartment and are lower near the base of the fire earlier compared to when the environment remains stratified. In addition, lower O_2 concentrations have been found at the base of the fire with decreasing vent size, which has been attributed to increased mixing interior to the compartment [102]. Lower O_2 concentrations near the base of the fire have been shown to result in reduced fire MLR [102]. In some tests, MLR has been shown to vary linearly with O_2 concentration near the base of the fire [107, 108]. Fires in a 5.0 m × 6.0 m × 4.0 m compartment attached to a second compartment of the same size by an open doorway had higher O_2 and higher MLR with increasing flow rates between zero and 4.7 ACPH [107]. Exchange rates higher than this range resulted in significantly different fire burning patterns because of pressure induced convective drafts caused by high flow air supply [107].

Pressures induced by ventilation systems have been shown to affect doorway flows and in some cases, the effects of the ventilation systems cause significant shifts in doorway velocity profiles [109]. Experiments conducted at the multi-compartment scale with a series of three compartments connected together in a continuous line, had supply into the first compartment, the fire located in the middle compartment, and exhaust located in the third compartment [109]. Mechanical ventilation caused the velocity profile in the doorway between the first and second compartment (more upstream in the ventilation flow path) to shift towards increased inflow into the middle compartment, and the neutral plane rose. A similar shift occurred in the other doorway (more downstream of the flow) where the

velocity profile shifted towards increased outflow from the middle compartment, and the neutral plane descended [109]. Other tests have also shown that mechanical ventilation can effect doorway flow rates, and depending on the configuration of the fuel in the room, the convective or 'blowing' effects from doorway flows can enhance MLR [107].

Some studies have measured the time evolution of static pressure variations in compartments with mechanical ventilation. Measurements show that sudden and rapid pressure spikes are generated by the fire at ignition, causing pressurization of the fire room. Similar rapid pressure decreases occur at extinction, causing a sudden depressurization of the fire room [105]. In some cases, the increase in compartment pressure at ignition was 600 Pa to 700 Pa, while the pressure decrease after extinction was approximately 600 Pa, lasting between 30 seconds to 50 seconds each [110]. These pressure variations have been correlated to fluctuations in fire MLR, which may be attributed to local variations in O_2 near the fire caused by the pressure changes [110, 111]. During fire growth, the pressure buildup in the fire room can overcome the static pressure rating of the ventilation fans and cause a flow reversal in the supply ducts, leading to smoke entering the supply side of the ventilation system [103, 110, 112]. The buildup of pressure has also been shown to cause an increase in the exhaust flow rate [105, 112].

In multi-room tests, doorway flows are found to contribute much more flow than is supplied or exhausted through a ventilation system. Entrainment of fresh air entering through the lower parts of a doorway is likely to supply additional air to the fire, enhancing fire MLR and fuel combustion [112]. This suggests that door positions (i.e. open or closed) would have a significant effect on the development of the environment in a room located away from the fire room. In fact, development of both temperatures and species concentrations have been shown to be significantly reduced in rooms adjacent to a fire compartment when the doorway into a room is closed, even when the ventilation system is turned on [112]. Tests in a two-storey house found that the concentration of CO_2 was reduced by nearly 80% in a bedroom when the door was closed, and was only reduced by up to 29% when the HVAC system was on while the door remained open [113]. Similarly, the bedroom experienced 80% less reduction in O_2 concentration with the bedroom door closed and only 23% less reduction with the door open and HVAC system on. Overall, mechanical ventilation was found to increase the speed of species transport to remote compartments, but it also increased dilution of the species [113].

2.6 Other Multi-Storey or Multi-Compartment Tests

In addition to the forced ventilation compartment fire tests discussed above, there are naturally ventilated tests at reduced or single compartment scale [114] and at the multi-compartment, multi-storey scale. This section focuses on the limited number of tests completed at the multi-compartment and/or multi-storey scale, as in the burn house used in the present tests. The intent is to gain insights into the behaviour of fires burning complex fuels and the development of the fire environment in these structures. Some studies provide insights into temperature development, flow paths for smoke and air throughout the structure, and gaseous species concentrations. In addition, some studies aimed to evaluate firefighter tactics and involved intervention and suppression of the fires. In these cases, the focus is on fire growth and environmental development prior to intervention, with only some discussion on flow paths before and after intervention.

2.6.1 Fire Development in Multi-compartment, Single-Storey Structures

Fire tests with complex fuel loads, such as furniture, have been ignited in single-storey, multi-compartment structures in both relatively spacious compartments such as a living room, or in more confined compartments such as a bedroom. In both cases, natural ventilation through doors and windows has been found to affect both fire growth and development of the environment inside the structure. One study, burning a couch in the living room of a single-storey, four compartment structure, found that the fire growth was inhibited and remained in a low burning state for three hours and 25 minutes when all windows were closed [115]. The living room reached a maximum temperature of only 286 °C with species concentrations of 13.6% O_2, 4.5% CO_2, and 4000 ppm (0.4%) CO [115]. When the windows were opened half way, the fire growth was rapid and the environment reached a peak temperature of 630 °C with species concentrations of 3.4% O_2, 14.3% CO_2, and 55 000 ppm (5.5%) CO [115]. Overall, the environment was more hazardous with ventilation than without, due to the accelerated fire growth. In another single-storey house, a living room fire established on furniture was sufficiently ventilated to proceed to flashover [116]. Living room temperatures were stratified prior to flashover and became more uniform after the transition to flashover, while other locations had stratified temperatures throughout the duration of the fire. Gas concentrations in the kitchen, adjacent to the living room, reached peak concentrations of 2.5% O_2, 23.5% CO_2, and 34 000 ppm (3.4%) CO at 0.9 m above the floor [116]. Data from gas sensors at additional heights showed that concentrations increase first at higher elevations and later at lower elevations due to smoke layer descent.

In a single-storey ranch style house, fires were ignited in the bedrooms containing typical bedroom furnishings including a bed, a chair, and nightstands [117]. When the window in the bedroom was closed prior to ignition, the fire reached ventilation-limited conditions in less than six minutes [117]. In this case, gas concentrations reached 14% O_2, 15% CO_2, and 15 000 ppm (1.5%) CO just outside the open bedroom door leading to the hallway. When the bedroom window was open, the fire proceeded to flashover and had lower peak gas concentrations compared to when the windows were closed [117]. In both cases, the peak temperature in the bedroom was over 750 °C. Other single-storey, multi-compartment studies have reported O_2 concentrations as low was 10% with CO_2 concentrations reaching over 10% in more open compartments such as living rooms [118]. Peak concentrations of CO are reported between 7000 ppm to 15 000 ppm (0.7% to 1.5%), depending on proximity to the fire[118].

In 2007, results were published from two fire tests studying fire spread in a single unit of a 23-storey apartment building [119, 120, 121]. In these tests, the fires were initiated in the living room and allowed to spread in two scenarios: (a) the fire growth was unconstrained and (b) the fire growth was controlled with automated venting [119]. In both cases, the fires were well-ventilated in the growth stage and became ventilation-limited leading to a peak burning rate. The unconstrained fire proceeded to flashover, which involved the living room furniture, bookshelves, and surrounding clutter [120]. The smoke layer started to descend as the fire grew then reached a steady height as the fire proceeded to flashover, then continued to descend post-flashover. Compartment temperatures were stratified before flashover and uniform afterwards, reaching over 600 °C [120]. During the automated venting test, the descent of the smoke layer was disturbed which inhibited the positive feedback loop between the buildup of a hot smoke layer and the fire growth rate, effectively reducing the rate of temperature increase in the compartment [121]. The smoke layer height remained higher for a longer duration and the environment remained stratified for longer compared to the unconstrained test [121].

2.6.2 Fire Development in Multi-Storey Structures

A limited number of similar tests with complex fuel loads have been conducted in multi-storey structures. In these studies, a fire is ignited in a compartment on the main floor of the structure and key elements of the environments created by the fire are measured on both the main and upper floors, similar to the scenario in the present research.

The behaviour of complex fuels in large fire studies is not exactly straight forward, but their behaviour is important to understanding the scenario being studied. Therefore, elements of their behaviour are discussed in more detail below. Tests in a single compartment

with a window vent found that a two-seat couch had a higher peak HRR than a three-seat couch because the armrests are closer and this increased heat feedback to the fuel surface [122]. The three-seat sofas, however, did have slower fire growth and prolonged burning, with a peak HRR of 3.2 MW. Other studies have reported the peak HRR of couches to be between 2.5 MW to 4.2 MW [115] with some being as low as 1.2 MW [123]. However, these reported HRRs are from well-ventilated calorimeter tests and may not transfer directly to a compartment scenario due to reduced ventilation. Couches burned in previous under-ventilated compartment fire tests at the University of Waterloo have been reported to reach peak HRRs up to 3.3 MW [8].

Fire tests in a 297 m^2 two-storey colonial style home with floor areas of (3200 ft^2) studied different types of furniture and the impact of having doors or windows open to provide ventilation [124, 125, 126, 127]. Studies focusing on the impact of furniture type found that burning of synthetic materials that make up more modern furniture resulted in faster fire growth and reduced the time to flashover to only four minutes, compared to legacy natural materials, which took 29 minutes or longer to reach flashover [124]. In other cases, where ventilation was more limited, the synthetic modern furniture reached under-ventilated conditions in approximately five minutes, while the natural legacy materials underwent slower growth and continued burning in relatively well-ventilated conditions for up to 15 minutes longer [125].

In the two-storey colonial style house described above, couch fire tests with the front door to the structure closed resulted in the fires reaching under-ventilated conditions prior to flashover, with peak temperatures in the living room that remained below 500 °C [126]. Concentrations of O_2 in the living room and in a main floor bedroom decreased to below 10% prior to venting of the structure [124]. Upper floor temperatures were 200 °C to 300 °C cooler than in the living room and showed less vertical gradient. There was also less gradient in species concentration on the upper floor, however, the open concept of the home still resulted in O_2 concentrations as low as 15%, CO_2 above 6%, and CO above 2000 ppm (0.2%) throughout the upper floor [125]. When the front door to the structure was open prior to ignition, creating a nearby ventilation path to the living room fire, the fire grew to flashover, reaching temperatures over 800 °C in the living room [124]. Venting near the fire resulted in localized combustion and temperature increases, which reduced the change in species concentrations and temperatures in remote compartments on the main floor and on the upper floor [124]. However, localized venting near the base of the fire can further intensify the fire growth [125]. The impact of ignition location was also studied in a similar two-storey colonial style home by igniting fires in the living room, the kitchen, and a bedroom in separate tests [127]. With all vents closed, the fires in the living room and bedroom were ignited, proceeded to flashover, and subsequently extinguished due to

lack of O_2 (near 5%) in under five minutes [127]. The kitchen fire also self-extinguished but did not reach flashover.

An additional series of tests conducted in one unit of an apartment complex, containing 10 apartments which each consisted of three floors, was conducted to study the development of fires and the spread of smoke in these kinds of structures [128]. When the fire was ignited in the living room on the lowest level of the unit, the fire reached flashover, with temperatures over 1000 °C in the living room. In this test, the doorways leading to the floors above the fire were open, and some windows were open, which facilitated the transfer of smoke to other floors and outside the unit [128]. On the lowest level where the fire was ignited, O_2 decreased to 12%, CO_2 increased to 13%, and CO increased to 15 000 ppm (1.5%). On the floor directly above the fire floor, the O_2 concentration decreased to 15%, CO_2 increased to 9%, and CO increased to 10 000 ppm (1.0%) [128].

Previous experiments in the two-storey University of Waterloo burn house burned various types of couches including those containing fire retardants, light fire retardants, and some without any added fire retardants [8]. The most pertinent results to the present tests are those from the non-fire retardant couches. In these tests, concentrations in a compartment adjacent to the fire room on the same floor reached minimum O_2 concentrations of 5% and peak CO between 2200 ppm to 2500 ppm (0.22% to 0.25%) [8]. On the upper floor, O_2 reduced to 12% and peak CO was 1800 ppm (0.18%).

Basement fire scenarios have also been studied since these fires are likely to under ventilate due to a lack of available vents, and can also cause significant structural damage [123]. A study of a couch fire in a basement investigated the effects of having a closed door at the top of the staircase leading to the upper floor of the structure. When the door was open prior to ignition, the basement temperature reached over 700 °C and gas concentrations peaked at O_2 below 10%, 15% CO_2, and 30 000 ppm (3.0%) CO [123]. Smoke was transported to the upper floor resulting in O_2 below 15%, CO_2 up to 8%, and CO 20 000 ppm (2.0%). When the door was closed throughout the test, the fire quickly became ventilation-limited; however, peak temperatures and gas concentrations in the basement were similar to the scenario with the open door, while conditions on the upper floor remained near ambient as the door inhibited transport of smoke between the lower and upper floors [123]. Another study also reported that a closed basement door reduced the rate of fire growth and the transport of smoke to the upper floor, giving occupants nearly twice as much time to escape prior to conditions becoming untenable [129]. In either case, the development of gas concentrations and temperature was slower on the main floor compared to the basement, resulting in a more uniform environment on the upper floor while conditions in the basement remained stratified with height above the floor [123, 129].

2.6.3 Flow Paths for Air and Smoke

Smoke and air flow between compartments in structures is an important factor in the development of the fire and environment. Therefore, flow paths and ventilation both have a critical influence on the temperature and species concentration development in structures during a fire as well. Throughout the studies summarized above, there is some discussion on the important flow paths for smoke transport away from the fire and fresher air transport from more remote compartments towards the fire that is outlined here.

As mentioned in the basement fire tests, the staircase and doorway facilitated the transport of smoke to the upper floor [129]. Tests in the University of Waterloo burn house also identified the staircase as a key area of mixing and smoke transport in ground floor, living room fires [8]. A common theme in tests where the fire is located on a lower level is that the concentration of O_2 reduces first on the same level as the fire and begins to decrease later on the upper levels [8, 127]. This has been explained as the fire first consuming O_2 from the environment nearby and then drawing additional O_2 from more remote locations, such as another floor, once the O_2 concentration nearby becomes reduced [8, 127]. Mixing of smoke with the fresher air also occurs in staircases, which causes vitiation of the air that is being drawn towards the fire [8]. This mixing can result in more uniform or mixed environments on the upper floor, while compartments on the main floor remain stratified with significant vertical gradients [8, 123]. In addition to staircases, other open regions between floors, such as atria in open concept homes, also facilitate the exchange of gases between floors [127].

The opening of vents in various locations of a structure can cause flow paths to shift. Typically, ventilation near the fire focuses flow to the fire compartment, resulting in increased fire room temperatures and lower temperatures throughout the rest of the structure [126]. Far field ventilation, or open vents in more remote locations from the fire, makes the compartments between the vent and the fire part of the flow path, increasing the temperature and species concentrations in these compartments [126]. Some experimental and computational studies have explored the impact of near-field and far-field ventilation during a fire on the ground floor of a four-storey building [130, 131]. The results showed that near-field ventilation increased the fire HRR, while changes in far-field ventilation controlled the flow of smoke throughout the rest of the building [130]. Smoke movement was increased to the upper floors when doorways between the floors were open. Smoke flow in buildings has also been shown to occur through ventilation duct work. An HVAC system was installed but was not running during furniture fire tests in a single-storey home [132]. It was found that without ventilation flow in the duct work, gas transport between compartments increased due to smoke flow through the ducts, which was significant for

rooms with closed doors [132]. Overall, the volume of gases transported by the ductwork without the ventilation system running was still found to be minor compared to the flow of gases through open doorways.

2.7 Large-scale Experimental Repeatability

The final section in this review focuses on the important issue of experimental repeatability, particularly as it pertains to the present large scale fire tests. According to the National Institute of Standards and Technology, there are two methods used to evaluate the uncertainty of a measurement [133]. The first method, referred to as a Type A evaluation, determines uncertainty based on a statistical method. The second method, referred to as Type B, evaluates the uncertainty based on scientific judgment using relevant information such as previous measurement data, manufacturer's specifications, data provided in calibrations, and uncertainties assigned to reference data taken from handbooks [133]. Due to the complex nature of the fire phenomena in compartments and the complexity of measuring these phenomena, the Type B approach is typically used for reporting large-scale fire test uncertainty. In some tests, expanded uncertainties have been reported as 15% for temperature measurements, 14% to 22% for velocity measurements, 8% for heat flux measurements, 12% for gas species concentrations measurements, and 5% for mass measurements [117, 123, 128, 132]. Since the measurements made in this cross-section of fire experiments are similar to those in the present research, these values are deemed representative of the anticipated measurement uncertainties in subsequent results.

Previous experiments have been conducted in the University of Waterloo burn house with the aim of characterizing the repeatability of full-scale experiments in the structure [10]. In total, three distinct sets of experiments were completed, each with three repeats. The results showed the repeatability of measurements within a set of three repeat tests. Measurement of peak HRR varied by 10%, time to peak HRR varied by 5%, and temperature varied between 3% to 10% depending on height and location [10]. Other studies have also reported good repeatability for temperature measurements with less than 3% reported variation [134, 135], while mass loss rate measurements varied between 10% to 30% depending on the time in the test, and species concentration measurements varied up to 40% [134].

In closing, this chapter has discussed key phenomenon which are important to understanding the development of fires, the effects that a compartment has on fire development, and how the environment in the compartment is influenced by fire growth, ventilation configuration, and other compartment effects. Relevant literature of previous compartment fire

tests at scales ranging from reduced compartment scales to full-scale, multi-compartment, multi-storey structures has been reviewed. This literature included tests that study the effects of both forced and natural ventilation. In the next chapter, the methods for conducting the current full-scale furniture fire tests in the University of Waterloo burn house are discussed in detail.

Chapter 3

Experimental Methodology

In this chapter, the methods for conducting the full-scale mechanical ventilated fire rests in the under-ventilated furniture fire project are discussed. First the experimental design is detailed including the layout of the burn house, the fuel load, ventilation configurations, instrumentation, and test procedures. Then, details of data processing and data analysis are discussed.

3.1 Experimental Design

This section outlines details of the experimental design, instrumentation, and test procedures utilized for a series of four full-scale residential fire experiments conducted to study the effect of mechanical ventilation on furniture fires. These allowed characterization of the environment created inside a typical residential house during fires burning the same fuel load under different mechanical ventilation configurations.

3.1.1 University of Waterloo Burn House

All experiments are conducted in the University of Waterloo burn house, shown in Fig. 3.1, located at the Live Fire Research Facility. The burn house is a two-storey, multi-compartment structure designed and built for conducting full-scale residential fire tests. It has a total floor area of approximately 120 m^2 and a total volume of approximately 275 m^3. The structural frame of the house is an assembly of 102 mm steel H studs and I beams, clad with 3.18 mm Corten steel on the exterior.

Figure 3.1: External view of the burn house structure.

Each floor nominally measures 6.9 m by 8 m and is divided into multiple compartments to mimic a typical residential home as shown in Fig. 3.2. The main floor consists of the fire room, the kitchen, and a corridor, each with a ceiling height of 2.4 m. Door 1 (D1) is located on the east wall of the burn house and opens directly into the fire room. Door 2 (D2) is located on the west (opposite) wall at the far end of a corridor running the length of the north wall of the house. Adjacent to Door 2 is an interior doorway that connects the fire room, through the corridor, to the kitchen. Interior walls on the main floor are finished with 15.9 mm thick type-X gypsum board. An additional protective layer of 12.7 mm thick cement board is added on top of the gypsum board in the fire room to further protect the structure from direct fire exposure. The seams between concrete board panels are sealed with Pyromix high temperature mortar. The fire room ceiling also contains 100 mm thick mineral wool batt insulation behind the gypsum board to protect the steel frame from heat exposure. There are three Jeld-Wen Low-E Vinyl-clad windows (0.9 m $\times$ 0.6 m, double pane slider type) on the main floor. Two are located on the east and south wall of the fire room, labelled W1 and W2, and one on the west wall in the kitchen, labelled W3. An open staircase leads to the second floor from the fire room.

The upper floor has an additional two compartments, referred to as the small bedroom and the large bedroom, each with a ceiling height of 2.6 m. At the top of the staircase

there is a landing which connects to a corridor leading to the large bedroom and a door opening into the small bedroom. The interior walls up the staircase and throughout the second floor are not covered in gypsum board, leaving the steel structure exposed.

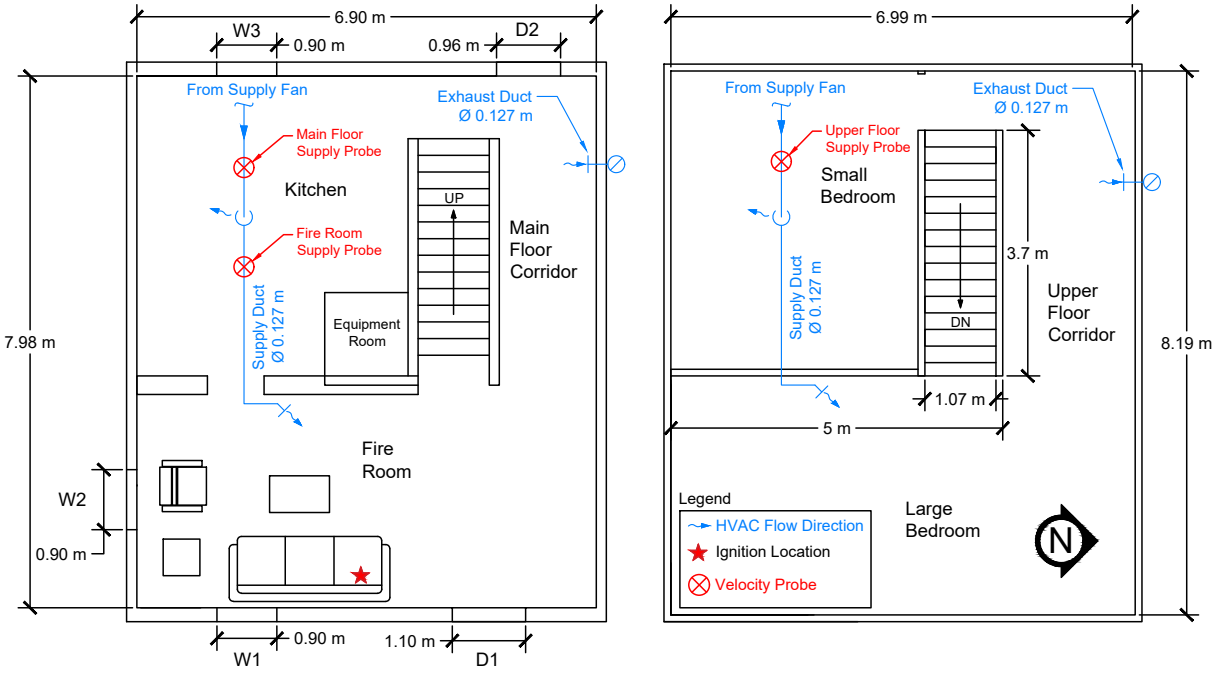

Figure 3.2: Floor plan of the burn house showing overall dimensions, ventilation ductwork, and the fire ignition location.

The burn house is configured as a home constructed with modern airtight practices. All windows and doors are closed after ignition and remain closed for the duration of the tests. To obtain the well-sealed environment, gaps in the structure are sealed with fibrefrax or spray foam insulation. Perfect seals are not entirely possible due to the age and steel construction of the burn house. Therefore, leak testing was completed by RDH Building Science Laboratories prior to the experiments to help identify areas requiring additional sealing. Observations of smoke leakage during calibration tests were also used to further identify leaks. After this, a substantial effort was implemented to eliminate leakage and seal the house as much as practical, however the house was not retested for leaks before these experiments. It is anticipated that the final air leakage rates would be higher than the 2.5 ACH@50Pa specified for a Canadian Energy Star rated home.

3.1.2 Fuel Load

The fuel load consists of primary and secondary fuels to mimic the layout of a typical residential living room. The fire is ignited on the primary fuel and is allowed to spread to the secondary fuels. For consistency, all four tests use the same fuel items, listed below.

Primary fuel:

- IKEA VIMLE couch, purchased from Canada, meeting US California Bureau of Electronic and Appliance Repair, Home Furnishings and Thermal Insulation Technical Bulletin 117-2013 [136], and containing no added flame retardants. The couch measures 2.41 m × 0.98 m × 0.83 m (W × D × H) and weighs approximately 75 kg when fully assembled.

Secondary fuels:

- IKEA VIMLE chair, purchased from Canada, meeting the requirements of [136], and containing no added flame retardants. The chair measures 0.71 m × 0.98 m × 0.83 m and weighs approximately 20 kg when fully assembled.
- IKEA LACK coffee table, measures 0.90 m × 0.55 m × 0.45 m and weighs approximately 8.5 kg when fully assembled.
- IKEA LACK side table, measures 0.55 m × 0.55 m × 0.45 m and weighs approximately 3.5 kg when fully assembled.

Figure 3.3 shows the layout of the fuel in the fire room. The couch is located 0.15 m from the east wall and 1.26 m from the south wall of the fire room. The chair is located 0.25 m from the south wall and 1.5 m from the east wall. The coffee table is located 0.35 m in front of the couch and 2 m from the south wall (roughly centred on the couch). The side table is located 0.2 m from the side of the couch and 0.4 m from the side of the chair.

3.1.3 Ventilation Conditions

Ventilation conditions employed during the tests are designed with flow rates and configurations to mimic typical HVAC systems in modern homes. The supply of outdoor air (OA) and exhaust of gases is facilitated through a system of ductwork, shown schematically in the floor plan of Fig. 3.2. All the ductwork is constructed of 0.127 m (5 inch) diameter

Figure 3.3: Image of the fire room setup prior to a test.

ducts, with balancing dampers located at all supply and exhaust ports. There are two supply ports per floor, located in the fire room, kitchen, small bedroom, and large bedroom. Each floor also has one exhaust port located in the corridor. Images of the supply and exhaust ports are shown in Fig. 3.4.

The ventilation is powered by two Continental MBI150/125 centrifugal in-line fans, one supply and one exhaust, which are located on the exterior of the structure. The fans are capable of producing up to $0.16\,\mathrm{m}^3/\mathrm{s}$ (340 cfm) at 3050 rpm. In these tests, they are fitted with a speed controller to help regulate the flow into the structure. The flows through each supply and exhaust port are balanced immediately before each test by setting the fan to the appropriate speed and adjusting the balancing dampers located near each vent inside the structure. Flow velocities are then measured with a handheld vane anemometer and recorded at each supply and exhaust port prior to each test to verify the fan speed settings, and confirm that proper balancing has been achieved. An acceptable range of flow rates is specified for each test to account for the sensitivity of these adjustments.

Each test is conducted with a different mechanical ventilation configuration. Test 1 is configured for no HVAC, where the fans remain off and the ends of each duct are capped on the exterior of the structure and remain sealed for the duration of the test, ensuring

Figure 3.4: Images of ventilation ports: a) kitchen supply, b) fire room supply, c) small bedroom supply, d) large bedroom supply, and e) upper floor exhaust.

that no OA is introduced to the structure through the ventilation ductwork during the fire. The vents inside the structure remain open to allow for passive air/smoke movement through the ducts. Tests 2 (baseline HVAC) and 3 (2x baseline HVAC) are configured to supply entirely OA into the structure and exhaust a balanced amount of air out of the structure. Test 3 has twice the flow rate of Test 2. For Test 4, the ventilation is configured for recirculation, where there is no supply of OA and instead gases in the structure are recirculated via the exhaust ductwork. In this configuration, only one fan is used and any duct sections that are not in use are capped to close off the open ends. The suction side of the fan is connected to the exhaust ducts and the discharge side of the fan is connected to the supply ducts to recirculate exhaust gases directly back into the structure. The velocity and corresponding flow rates at each supply port for all tests and the resulting number of ACPH are listed in Table 3.1.

3.1.4 Instrumentation and Data Collection

The burn house is instrumented with various sensor types for continuous measurement and recording of the evolving fire environments. This includes gas temperature, heat flux, fuel mass, gas flow velocity, and concentrations of various gases. O_2, CO_2, and CO form

Table 3.1: Ventilation configurations and flow rate specifications for each test.

Test	Configuration	Supply Port Velocity (m/s)	Supply Port Flow Rate (m^3/s)	ACPH
1	No HVAC	0	0	0
2	Baseline HVAC	0.85 - 1.0	0.011 - 0.013	0.56 - 0.66
3	2x Baseline HVAC	1.70 - 2.0	0.022 - 0.025	1.13 - 1.33
4	Recirculation	0.85 - 1.0	0.011 - 0.013	N/A

the basic suite of species concentration measurements used primarily in the present work. Other concentration measurements include total unburned hydrocarbons (THC), nitrogen oxide (NO_x), and a selection of other toxins. The structure is monitored by video for the full test, facilitating video recording of the fire and smoke development from multiple angles. Reference ambient conditions such as external air temperature, barometric pressure, wind, and relative humidity are recorded for each test via a Cole-Parmer weather station.

Thermocouples

Gas temperatures are measured using 24 AWG type-K (chromel-alumel) thermocouples with a bead diameter of approximately 1 mm, made by twisting together the ends of the exposed wires. The wires are individually insulated with Nextel ceramic fiber and sheathed with an Inconel overbraid to provide abrasion resistance, as well as protection from moisture and continuous high temperature exposures. These thermocouples are rated for 980 °C continuous and 1090 °C short-term service [137].

Type-K thermocouples are known to have a standard manufacturer's uncertainty of 2 °C and an expanded uncertainty of 4 °C when including the complete data acquisition system. The response time for a 24 gauge exposed bead thermocouple is less than 1 second in air moving at about 20 m/s, so the potential delay in thermocouple response will be on the order of 1–2 seconds in these experiments [137].

The location of the thermocouples and thermocouple rakes are shown by green '×' symbols in Fig. 3.5. On the main floor, there are three rakes located above the couch and one above the chair, with each rake containing four thermocouples. These are centred over each of the cushions on the couch and chair. One rake containing two thermocouples is located in the doorway between the kitchen and the fire room, another containing eight thermocouples is located to the more open side in the fire room, one containing four thermocouples is located in the corridor, and one containing six thermocouples is located

centrally in the kitchen. On the second floor, there are three rakes, each containing four thermocouples. These are located in the small bedroom, large bedroom, and the upper floor corridor.

Prior to testing, each thermocouple is checked to ensure connectivity and response, using a hand-held lighter. Any thermocouples which are found to be faulty are repaired accordingly.

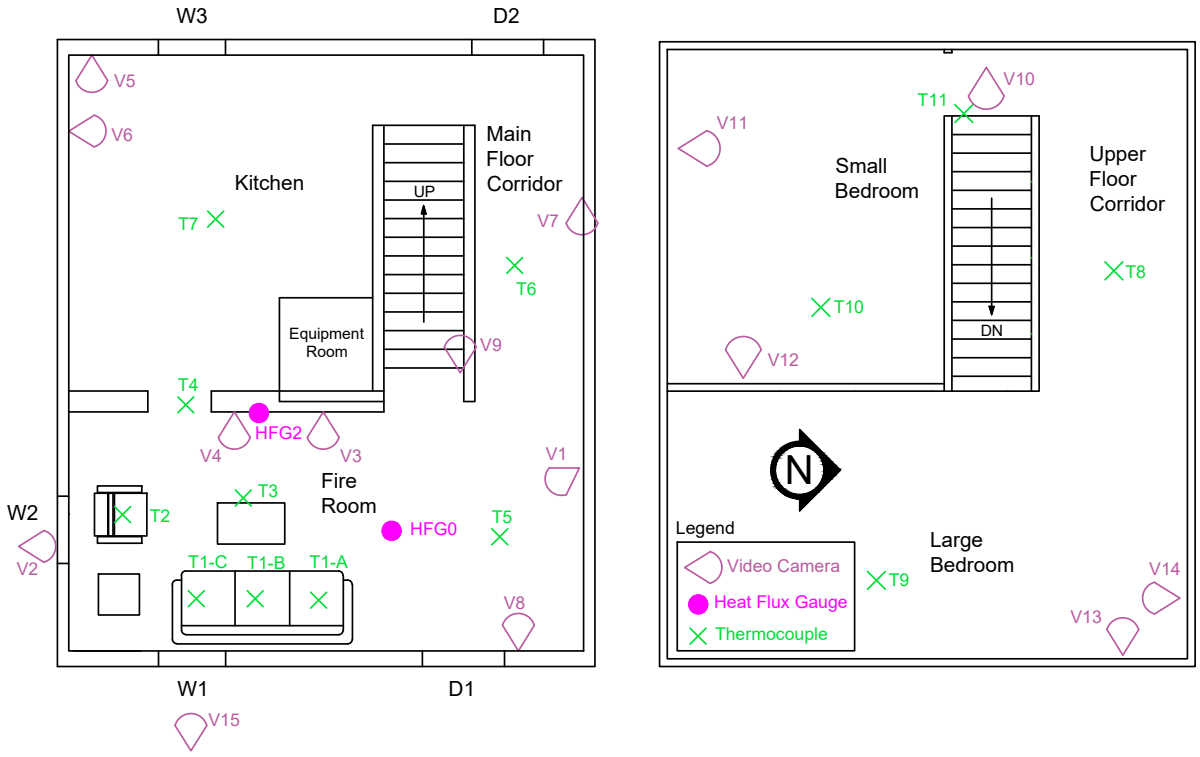

Figure 3.5: Floor plan of the burn house showing the positions of thermocouple rakes, heat flux gauges, and video cameras.

Heat Flux Gauges

Two water-cooled Vatell TG1000-1 Gardon heat flux gauges (HFGs) are placed in the fire room, as shown by the pink dots in Fig. 3.5. One gauge, denoted HF2, is positioned on the wall approximately 2 m across from the couch, 2.55 m from the south wall, and 0.79 m above the floor (roughly in line with the centre couch cushion). The other, denoted HF0,

is located on the floor of the fire room, 4.33 m from the south wall and 1.61 m from the east wall. This HFG is facing the ceiling to measure the radiation emitted by the fire plume. Both gauges are provided with a voltage-heat flux calibration curve from the manufacturer and have a typical accuracy of 3% FS [138].

Prior to testing, each HFG is checked to ensure connectivity and response, using a hand-held lighter.

Load Cells

The mass of the couch is measured with four MARS MSB-60 load cells, each measuring 0.45 m × 0.45 m with a maximum capacity of 60 kg (for a total combined capacity of 240 kg). The load cells have a resolution of ±0.01 kg and a manufacturer's specified total error of 0.05% of applied load [139]. The four load cells are positioned under the corners of the couch to split the load between them, and they are configured so that the measured mass output is the sum of the four individual readings. Each load cell is individually protected with a layer of fiberfrax insulation, installed carefully to ensure proper movement of the scales throughout a test. A 1.2 m × 2.4 m sheet of 15.9 mm type-X gypsum board that has been wrapped with aluminum foil is placed across all four load cells on top of the individual insulation layers. This acts as a platform to hold the couch and contain any falling debris from the couch as it burns during the fire. The gypsum board also provides protection to the load cells from heat and burning debris.

The chair is placed on a single MARS MSB-120 load cell, measuring 0.61 m × 0.76 m with a maximum capacity of 120 kg. This load cell also has a manufacturer's specified total error of 0.05% of applied load [139]. This load cell is protected with the same layers of insulation and gypsum board as used under the couch.

The load cells for the couch and chair are calibrated before each test using known calibration masses verified on a calibrated lab scale. The span mass of the cells is first set at a value 50% higher than the anticipated sample weight, and then the maximum output value is set to 25% higher than the sample weight. Load cell signals are recorded by the data logger as analogue signals and are converted to mass using a linear fit to the calibration points determined before each test using the known masses.

Bidirectional Pressure Probes

Gas velocities are measured throughout the structure using bidirectional differential pressure probes, whose operation is explained in detail in Sec. 2.2.3. A rake of probes is located

in each doorway of the structure as shown in Fig. 3.6 and marked by the red crossed circle symbol. Probe rakes A4 and A8 (at the bottom and top of the stairs, respectively) each have eight pressure probes installed at approximate heights of 0.4 m, 0.65 m, 0.9 m, 1.15 m, 1.4 m, 1.6 m, 1.8 m, and 2.0 m above the floor. Rake A9 located at the entrance to the upper floor SW room has four pressure probes installed approximately 0.4 m, 0.9 m, 1.15 m, and 1.6 m above the floor. The remainder have two probes, each positioned at approximately 0.4 m and 1.6 m above the floor, except for A1 and A7 which are positioned at one third and two thirds of the height of the windows. All pressure probes protrude roughly 15 cm into the opening of each doorway. The response of each probe is tested prior to every burn using a small handheld fan.

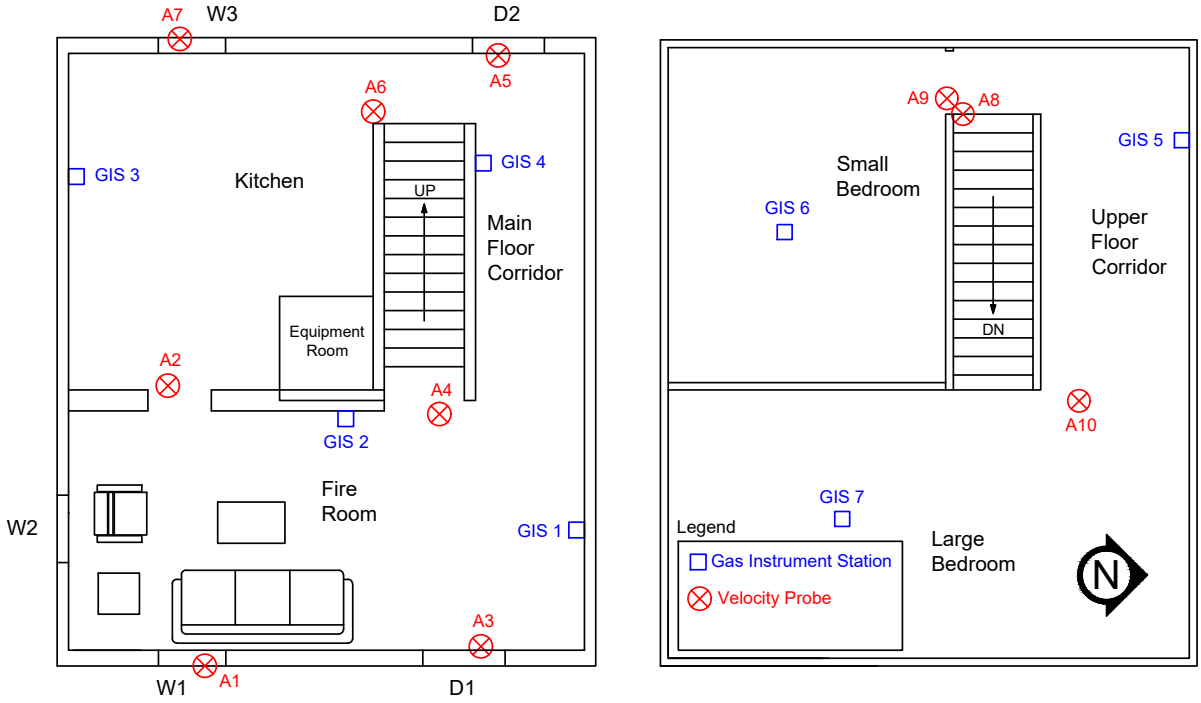

Figure 3.6: Floor plan of the burn house showing the positions of velocity probes and gas instrument stations.

Additional probes are positioned in the ventilation ducts to measure supply and exhaust velocities. The positions of the supply duct probes are shown in Fig. 3.2. On the main floor, one probe is located in the main supply duct upstream of the kitchen supply vent and one is located between the kitchen and fire room supply vents. On the upper floor, there is only one probe located in the main supply duct upstream of the small bedroom

supply vent. The exhaust ducts are fitted with velocity probes, one for each floor, in the vertical section of duct located on the exterior of the structure.

Each bidirectional pressure probe is connected to an individually calibrated Setra 267 differential pressure transducer with a range of ±25 kPa and 0.5% FS accuracy. Calibration procedures are explained in Sec. 2.2.3. Each probe is also paired with a thermocouple to measure the gas temperature necessary to correct for gas density in the velocity calculations. Typical errors in the calculation of velocity, including the measurement of pressure, are on the order of 10% [52].

Gas Concentrations Sensors

Concentrations of oxygen (O_2), nitrogen oxides (NO_x), hydrogen chlorides (HCl), hydrogen cyanide (HCN), carbon monoxide (CO), ammonia (NH_3), carbon dioxide (CO_2), methane (CH_4), and VOCs are measured using custom-built gas sampling units manufactured by Fire & Risk Alliance, LLC. These units, shown in Fig. 3.7, contain a variety of different sensor technologies including electrochemical sensors, metal oxide sensors, and other environmental sensors to measure humidity and temperature.

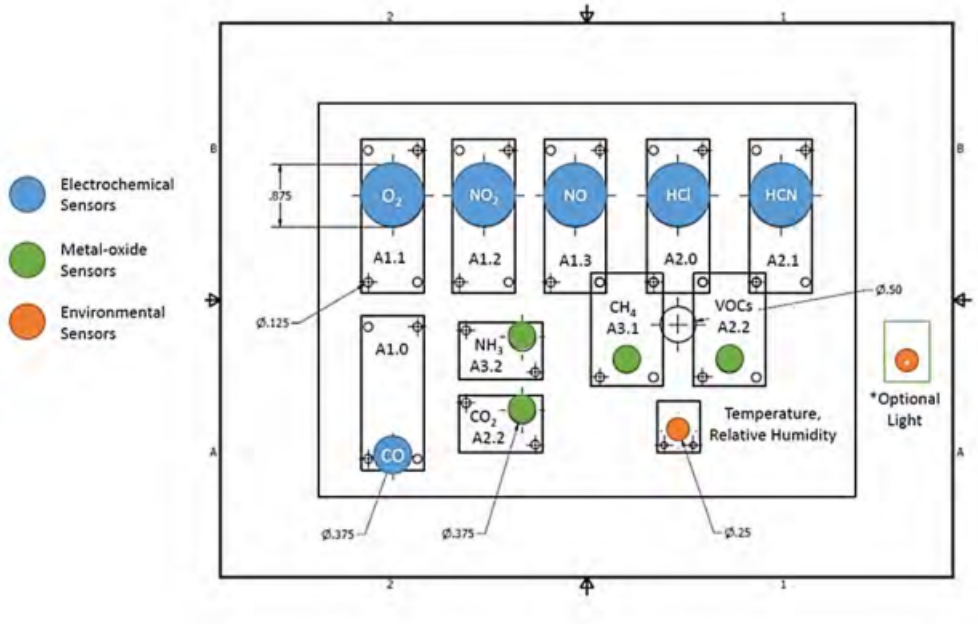

Figure 3.7: Schematic of custom-built gas sensor unit.

In the burn house, there are seven gas instrument stations (GISs) (shown by the blue squares in Fig. 3.6), each containing up to three of these gas sensor boxes at heights of 0.3 m, 0.9 m, and 1.5 m above the floor. Stations 1 and 2 in the fire room have only two units at the 0.3 m and 0.9 m heights due to the extremely harsh environment that develops at higher elevations. All other stations have three units. Station 3 in the main floor SW room is shown in Fig. 3.8 as an example. The use of multiple units at each station allows for building a spatially resolved picture of gas concentrations throughout the structure in a relatively budget friendly manner.

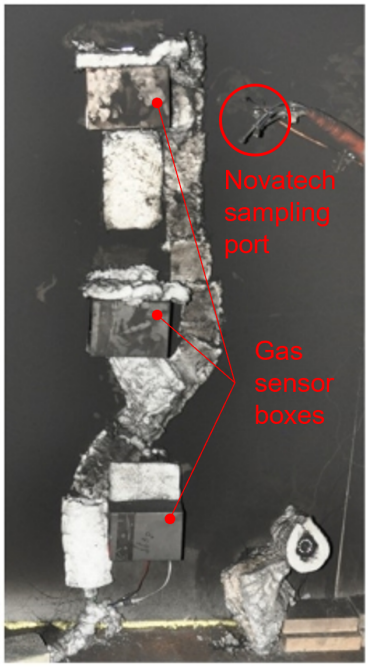

Figure 3.8: Photograph of GIS 3 in the main floor SW room, showing three gas sensor units and the Novatech sampling port.

Each unit operates with an on-board Arduino microcontroller, which simultaneously stores and outputs signals at a rate of four samples/second. The output data is sent directly via Ethernet to a stand-alone laptop that runs a LabView program to retrieve and convert the raw output to a voltage from each sensor. These raw voltages are then converted into concentrations using calibration curves provided by the manufacturer [140]. Each gas sensor unit is tested prior to each burn to ensure that each individual gas sensor is operational.

Additional gas concentration measurements are taken with a Novatech P-695 gas anal-

ysis system complete with Servomex Servopro 4900 paramagnetic and infrared analyzers to measure concentrations of O_2, CO_2 and CO, a Baseline 8800H to measure THC, and TML-41H chemiluminescence analyzers to determine NO_x concentrations. For the no HVAC test, the baseline HVAC test, and the recirculation test, the Novatech sampling port is located at the 0.9 m height in the kitchen adjacent to the custom gas unit at this location. The sampling port is moved to the 1.5 m height in the same location for the 2x baseline HVAC test, see Fig. 3.8. These measurements are complementary and serve as a comparison to the measurements from the custom units. The Novatech system is calibrated according to operating procedures on the day of each test, which provides a linear voltage to concentration calibration curve for each gas using a zero value based on sampling of pure nitrogen and a span value obtained using a mixture containing known concentrations of the gases of interest [141].

Typical errors for concentration data are on the order of 12% depending on the analyzers used and measurement conditions in a specific test [118]. More detailed assessment of the accuracy of the novel gas sensor units used in the present work remains under investigation.

Video Collection

A QSee high definition analog video recorder is used to record simultaneous inputs from 16 Lorex LBV2531-1080p, hybrid colour-night vision security cameras. These have proven to be effective cameras to employ during fire testing due to their low cost and relatively good image resolution in both well-lit and unlit heated environments. Camera locations and angles are represented by the magenta coloured cone symbols in Fig. 3.5. The cameras record at 30 frames per second and are used to visually track the development of the fire, the spread of flames, smoke layer progression, and smoke flow during each test.

Data Acquisition

Signals from the thermocouples, load cells, differential pressure transducers, heat flux gauges, and Novatech gas analysers are recorded using a National Instruments Compact FieldPoint distributed data logging system that allows remote placement of the analogue to digital signal conversion hardware. Four modular backplanes (NI cFP-1808), in conjunction with a sufficient number of Compact FieldPoint modules, are utilized to facilitate the required temperature (NI cFP-TC-125) and analog voltage or current (NI cFP-AI-110) measurements. The backplanes communicate with a local network switch using gigabit Ethernet to transfer the digitized signals back to a central computer running a custom

LabVIEW program. Data is collected from all channels simultaneously at 1.125 second increments (0.89 Hz) and saved to Comma Separated Value (CSV) files.

The video recorder, gas sensor, data acquisition, and LabView computers are all located in a control room inside the main Fire Research Facility building, at a safe distance from the burn house. This provides one weather-safe, central location from which to monitor the tests and operate all instrumentation.

3.1.5 Test Procedures

The test procedures are broken down into a series of steps organized into three phases: pre-ignition, ignition, and after extinction. The progress of procedure completion, as well as any necessary information, is recorded on a test day checklist to ensure consistency.

In the pre-ignition procedure, all daily calibrations and checks are performed as outlined in the previous instrumentation section. The fuels are vacuumed to clean off any dust collected during storage, and then weighed individually. After weighing, the fuels are placed into position on the load cells. Finally, the mechanical ventilation system is turned on to the appropriate setting for the test configuration and flow rates are measured and recorded.

The test starts by recording at least five minutes of baseline data from all instrumentation, immediately prior to ignition and with the burn house evacuated of any occupants and the doors closed. Starting times for each recording system and the start of data collection are recorded relative to a master clock. Once the baseline data is collected, the ignition crew makes entrance to the fire room through D2 and places a Type 4 ignition wood crib [142], weighing approximately 10 g, in position on the couch. The wood crib is placed at the back of the first couch cushion 0.32 m from the arm rest, as shown in Fig. 3.9. Ignition is then performed according to the BS 5852 Furniture Flammability Standard [142]. First, 1.4 ml of isopropanol is dispensed on the cotton wick at the base of the wood crib, a countdown is initiated, and the crib is ignited using a hand-held butane lighter and the ignition time is recorded. Once the crib is ignited, D2 is left open for 30 seconds to allow for evacuation of the ignition crew.

The door is then closed and the fire burns uninterrupted until either a) the flammable components of the entire fuel load are burned out, b) flashover of the burn room occurs, or c) the fire self-extinguishes. During this time, an observer records all key events that take place, such as cracks forming in any of the windows or flame out of the fire.

After extinction (or suppression), the fire service ventilates the structure by opening D1, then a window on the second floor directly above D2, and then D2 itself. A positive

Figure 3.9: Image of the Type 4 igniter wood crib in position on the first couch cushion.

pressure ventilation fan is placed in front of D2 and is turned on to aid in evacuation of smoke and hot gases from the structure. Once clear, the fire service makes entrance into the fire room to remove any remaining unburnt fuel. Any remaining flames or smouldering areas are extinguished or cooled with water.

Data logging systems and instrumentation are run for an additional 30 minutes after extinction to capture the cooldown period and baseline measurements post-fire. After 30 minutes, the equipment is shut down and those times are again recorded. Any remaining fuel is allowed to dry (if water is used) and then weighed on the calibrated lab scale as a cross-check of the load cells to determine the total amount of fuel burnt.

3.2 Analysis of Data

3.2.1 Signal Processing and Data Smoothing

As described previously, the National Instruments system records the data at a rate of 0.89 samples/second, while gas sensor data from the custom-built units are recorded at a

rate of four samples/second. Raw data signals are converted to their respective measurements through the use of manufacturer's calibration curves (gas sensor boxes and heat flux gauges), calibrations performed prior to each test (load cells and Novatech gas sensors), previous wind tunnel calibrations (bidirectional pressure probes) [58], or directly by the data acquisition system (thermocouples).

Some of the recorded data is smoothed, to remove excess noise, while some is simply maintained as recorded raw values for use in calculations and/or presentation. Mass measurements from the load cells are smoothed with an 11-point centred moving average prior to any calculations such as MLR or HRR. Velocity calculations are performed using raw measurements of differential pressure and temperature, however, the resulting velocity is smoothed with an 11-point centred moving average for plotting and flow rate calculations. All other measurements, including gas concentrations, heat flux, and temperatures, remain as raw data (not smoothed) for use in calculations and presentation. A summary of the data smoothing methods is in Table 3.2.

Table 3.2: Summary of data smoothing methods.

Data Type	Smoothing Method
Fuel mass	11-point centred moving average
Fuel mass loss rate	Uses smoothed mass
Temperature	Raw
Heat flux	Raw
Gas concentrations	Raw
Velocity	11-point centred moving average
Volume/mass flow rate	Uses smoothed velocity
Velocity Fluctuations	Uses raw velocity

Throughout the results in Chapter 4, values of temperature, heat flux, MLR, and gas concentrations are often given at a specified time. These values are determined as the instantaneous measurement from the data at the time closest to the specified time. Maximum or minimum values of these quantities are also discussed and are instantaneous maximum/minimum values from the measurements. The data used for these instantaneous values is either raw or smoothed depending on the data type, as listed in Table 3.2. Snapshot images from the video recordings are also presented at specified times. These snapshots are a single frame of the video extracted at the time in the test that is closest to the specified time. Since the start of the test is considered to be at ignition, the times for all events are specified as the time of occurrence after ignition. Further, more in

depth methods for calculating HRR from MLR data, velocity from bidirectional pressure measurements, and velocity fluctuations from the velocity data follow in the next sections.

3.2.2 Heat Release Rate Calculations

The heat release rate of the couch is calculated using the mass loss method, Eq. 3.1, where $\dot{Q}$ (MW) is the HRR, $\Delta H_{c,eff}$ (MJ/kg) is the effective heat of combustion of the fuel, and $\dot{m}_f$ (kg/s) is the mass loss rate of the fuel.

$$\dot{Q} = \Delta H_{c,eff} \dot{m}_f \tag{3.1}$$

The mass loss rate is calculated using a central difference approximation as shown in Eq. 3.2, where m_f^k (kg) is the smoothed mass of the couch at the current time step k, and Δt is the time difference between time steps (1.125 seconds in this case).

$$\dot{m}_f = \frac{m_f^{k+1} - m_f^{k-1}}{2 \cdot \Delta t} \tag{3.2}$$

To estimate the effective heat of combustion of the couch, cone calorimetry testing of an assembly of cushion materials cut from one of the identical couches is competed according to ISO 5660-1 [143]. The assembly consists of 50 mm thick foam, liner, and fabric, as shown in Fig. 3.10. The assembly is placed into a steel sample holder, leaving only the top surface of the fabric exposed. Two repeat tests are conducted at three incident heat fluxes of 25 kW/m^2, 35 kW/m^2, and 50 kW/m^2 with the use of a spark igniter. An example of the remnants after a sample is burned is shown in Fig. 3.10.

The effective heat of combustion is calculated from the calorimetry results using Eq. 3.3, where THR (MJ/m^2) is the total heat released during burning of the sample, A_{sample} (0.008 84 m^2) is the exposed surface area of the sample, and m_{loss} (kg) is the mass of the sample that is consumed during burning. Total heat released is calculated as the integral of the heat release rate curve between the times of ignition and flame out of the sample.

$$\Delta H_{c,eff} = \frac{THR \times A_{sample}}{m_{loss}} \tag{3.3}$$

The heat of combustion of the couch is taken to be the average of values measured over six cone calorimeter tests. The value of 20.86 MJ/kg is comparable to other non-fire retardant foam and fabric couches used in previous work [8].

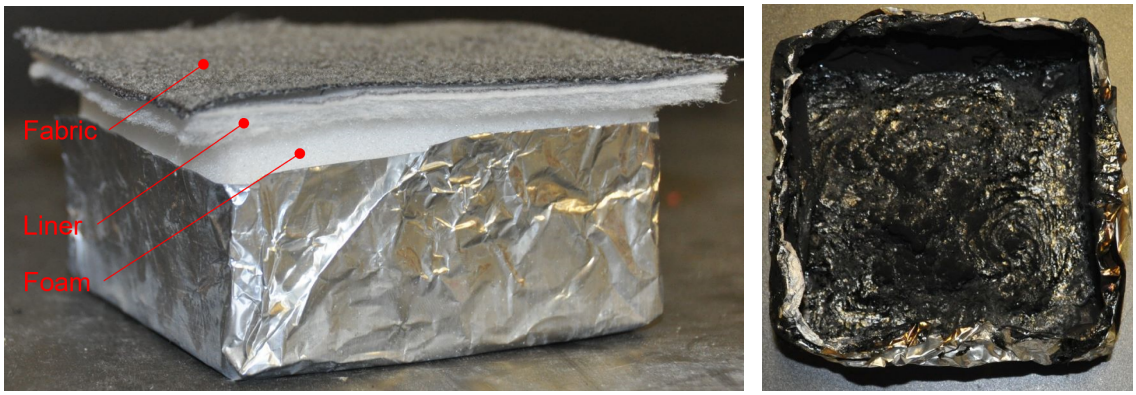

(a) Sample assembly prior to testing. **(b)** Sample after testing.

Figure 3.10: Images of a cone calorimetry sample before and after testing at $35\,\mathrm{kW/m^2}$

Using the mass loss method in this manner assumes a constant heat of combustion for the couch, and therefore ignores decreased combustion efficiency caused by the under-ventilated nature of the fires in these experiments. Further investigation is necessary to create a method for correcting the HRR calculated with the mass loss method in an under-ventilated scenario. Reported values of HRR are determined under well ventilated burning conditions and therefore are not accurate to the scenario on hand, and should only be used for comparison between the tests presented here and not to values reported elsewhere in the literature.

3.2.3 Velocity Calculations

Doorway and ventilation ductwork velocities are calculated using measurements of differential pressure from the bidirectional pressure probes using the Bernoulli equation, shown in Eq. 3.4, where u (m/s) is the calculated velocity, k is the probe calibration constant, ΔP (Pa) is the differential pressure, and ρ ($\mathrm{kg/m^3}$) is the density of the fluid (assumed to be air). Assuming the fluid to be air is typical of velocity calculations in fire scenarios and results in negligible errors due to the high nitrogen concentration in air and the relatively low concentrations of combustion products [54]. A 'sign' correction must be added to the end of the equation to account for the direction of flow due to the absolute value used under the square root.

$$u = \frac{1}{k}\sqrt{\frac{2|\Delta P - \Delta P_{zero}|}{\rho}} \times \begin{cases} 1, & \text{if } \Delta P > \Delta P_{zero} \\ -1, & \text{if } \Delta P < \Delta P_{zero} \end{cases} \tag{3.4}$$

The differential pressure is calculated using Eq. 3.5, where V (volts) is the measured voltage, and DPT_{slope} and $DPT_{intercept}$ are the slope and intercept of the linear calibration curve of each probe determined during wind tunnel calibrations.

$$\Delta P = DPT_{slope} \cdot V + DPT_{intercept} \tag{3.5}$$

The doorway velocity calculations are corrected for drift or daily fluctuations in the output of the pressure transducers using a value of ΔP_{zero}, which is the differential pressure corresponding to the zero voltage of the probes on the day of the test. The zero voltage is found as the average of the first 60 data points collected during the baseline measurement prior to each test. Using this method effectively zeros out any natural flows that occur due to ambient buoyancy within the house due to uneven heating by the sun or residual flow at a given probe rake due to the mechanical ventilation system. Therefore, the calculated velocities represent those characteristic of flows induced only by the fire. For the probes in the ductwork, the ΔP_{zero} found during wind tunnel calibrations is used, since the ventilation system is turned on prior to the baseline measurements and thus the velocity in the ducts during the baseline trace is not zero.

The density of air is calculated using the ideal gas law, Eq. 3.6, where P_{atm} (Pa) is the atmospheric pressure during the test, $R_{air} = 287.05\,\mathrm{J/kg\,K}$ is the gas constant for air, and T (K) is the instantaneous temperature of the fluid measured by the thermocouple adjacent to the probe. Atmospheric pressure is recorded from a nearby weather station during the tests.

$$\rho = \frac{P_{atm}}{R_{air} \cdot T} \tag{3.6}$$

3.2.4 Volume and Mass Flow Calculations

In order to calculate the doorway volumetric and mass flow rates, the doorway velocities are numerically integrated over the area of the doorway opening. For this, the doorway area must first be discretized. Each doorway is divided into 'zones' using the location of the velocity probes to divide the height of the doorway as shown in Fig. 3.11. Each zone has

a height equal to the distance between two adjacent velocity probes, or between the probe and the top or bottom of the doorway for the top and bottom zones, respectively. The width is taken equal to the width of the doorway. This results in three zones in doorways that have two probes, five zones in the doorway with four probes, and nine zones in the doorways that have eight probes.

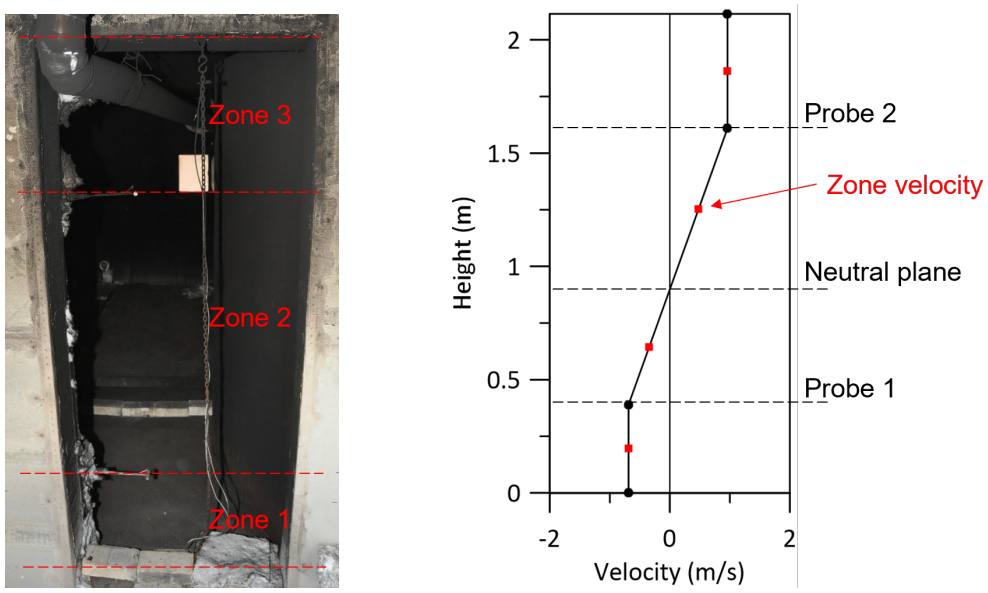

(a) Doorway zones. **(b)** Example velocity profile.

Figure 3.11: Diagram showing example doorway zones divided by velocity probes and an example velocity profile with neutral plane and zone velocities.

An example velocity profile is shown in Fig. 3.11, where velocity is plotted on the x-axis and height on the y-axis. Velocities within a zone are assumed to change linearly. Therefore, calculating the velocity at any given height is done by linear interpolation of the measured velocities at the top and bottom of that zone. Zones at the top or bottom of the doorway are assumed to have a constant velocity equal to that measured by the nearest probe.

The next step is to calculate the height of any neutral planes in the doorway. A neutral plane is defined as any height where the velocity through the doorway passes through zero (changes from direction). Neutral plane heights are important on their own, as they provide insight into the flow patterns established across openings during a fire. It is also necessary to identify their heights within a doorway in order to calculate the total doorway inflow and outflow rates independently. In some cases, more than one neutral plane appears to be

present in a given doorway at any one time due to changing flow patterns between sections of the opening. Therefore, each zone is evaluated for a neutral plane at each point in time using the following steps:

1. Check if a neutral plane exists in each zone in the doorway. If the direction of the probe velocity at the top and bottom of a zone are opposite, then it assumed that there is a neutral plane within the zone.

2. When a neutral plane is found, the height of the neutral plane is estimated through linear interpolation of the heights and velocities of the probes at the top and bottom of that zone.

Each zone that is found to contain a neutral plane is then divided into an additional two zones using the height of the neutral plane as the border (refer to Fig. 3.11) between zones of negative and positive velocity (inflow and outflow across the opening). This is done so that each zone has flow in only one direction, simplifying the volume flow rate calculations.

With the velocity profile of the doorway known, and the doorway discretized into zones, the volume flow rate is then calculated using the following steps:

1. The area of each zone (A_z) is found using the height (or thickness) of the zone equal to the distance between the probes at the top and bottom of the zone, and the width of the doorway.

2. Assuming the velocity profile across a zone is linear, the representative velocity in each zone (u_z) is calculated as the average of the velocities at the borders of the zone (either the measured probe velocity or zero if one border is a neutral plane).

3. Finally, the zone volumetric flow rate is calculated as $\dot{V}_z(\mathrm{m}^3/\mathrm{s}) = u_z(\mathrm{m/s}) \cdot A_z(\mathrm{m}^2)$.

The mass flow rate of each zone is calculated as $\dot{m}_z(\mathrm{kg/s}) = \rho_z \cdot \dot{V}_z$, where the zone density (ρ_z) is calculated using the ideal gas law with a temperature equal to the average temperature measured by the thermocouples adjacent to the velocity probes at the top and bottom of the zone. Once the zone mass flow rates are calculated, the total mass flow in each direction is found by taking the sum of the mass flow rates in their respective directions (*i.e.* the sum of all positive flows is taken as the total inflow through the opening while the sum of all negative flows is taken as the total outflow).

3.2.5 Quantification of Velocity Fluctuations

Velocity fluctuations are quantified for the purpose of characterizing large-scale velocity fluctuations throughout the structure. Understanding the large-scale fluctuations allows for discussion of the mixing of gases throughout the structure, since the large-scales of turbulence are responsible for the majority of mixing in these flows. More in-depth discussion on turbulence and complete turbulence statistics are not possible due to the relatively slow sampling rate and the localized, spatially-averaged characteristics of the velocity measurements.

Velocity fluctuations are quantified by calculating the root mean square (RMS) of the velocity fluctuations (also referred to as RMS velocity) and the corresponding fluctuation intensity as determined from measured velocities collected during the period of peak velocity at each velocity probe throughout the structure. The velocity during this period can be approximated as quasi-steady, simplifying the calculation of mean velocity. Expanding the calculations beyond this period would greatly increase the complexity of extracting velocity statistics from the measurements due to the rapidly changing mean flow velocities observed during the growth and decay phases of the fires. An example plot of velocity versus time is shown in Fig. 3.12 and the selected time period of quasi-steady flow is highlighted to provide context for the fluctuating values reported in the results section.

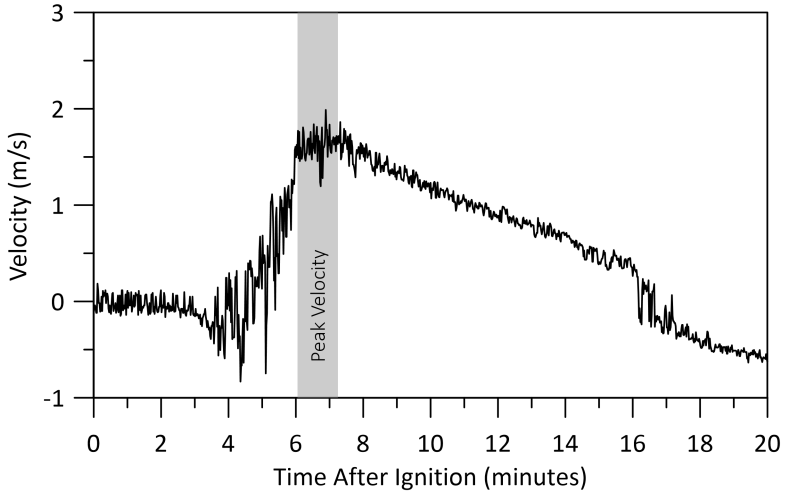

Figure 3.12: Example plot of raw velocity measured at the 1.41 m probe at the bottom of the stairs, showing the period of peak velocity.

The RMS of velocity is based on the RMS value of the discrete velocity measurements during the period of peak velocity, calculated using Eq. 3.7, where u_{rms} (m/s) is the RMS

velocity, u (m/s) is the raw velocity, $\bar{u}$ (m/s) is the mean velocity, and N is the total number of discrete measurements collected during the period. The mean velocity is calculated as the arithmetic average of all discrete velocities during the time period.

$$u_{rms} = \sqrt{\frac{1}{N}\sum_{i=1}^{N}(u_i - \bar{u}_i)^2} \tag{3.7}$$

Fluctuation intensity (I) is then calculated as $I = u_{rms}/\bar{u}$. This allows for a direct comparison of the intensity of velocity fluctuations between locations.

This chapter has outlined the methods for conducting the current full-scale furniture fire tests in the University of Waterloo burn house. Details including the layout of the burn house structure, fuel load, ventilation conditions, instrumentation, test procedures, and data analysis have been presented. The next chapter presents results from the experimental study. It begins with presenting data pertaining to the HVAC system to understand the supply of air into the fire room, then progresses into discussion on the fire development, compartment temperatures, smoke flow, species concentrations, and the details of extinction. Throughout the results, the impact of the ventilation configuration on the fire and environmental development in the structure is discussed.

Chapter 4

Experimental Results

Results from the mechanical ventilation experiments are presented throughout this chapter. First, ventilation duct flow measurements are presented to examine the supply of ventilation into the burn house for all the tests. Then the development of the fires is compared between ventilation configurations and details of MLR and heat flux are discussed. To characterize the fire induced environment, details of compartment temperature, smoke flow, and species concentrations are presented along with the relationship between MLR, heat flux, and O_2 concentrations in the fire room. Finally, details of fire room O_2 concentrations and temperature at extinction are discussed.

4.1 Ventilation Duct Flow

The size and growth of fires in general is controlled either by the supply of fuel to the combustion reaction or the supply of oxygen. In the present work, the base fuel materials remain the same and the supply of air to the fire room is varied from test to test. It will be shown in Sec. 4.2 that the fires become ventilation limited, meaning that fire growth is limited by the amount of oxygen available and not by the amount of fuel. In this situation, the supply of air through the HVAC system can potentially have a significant impact on the growth of the fire and thus the development of the environment inside the house. In rooms located away from the fire room or on the upper floor, (*i.e.* the far field), momentum differences between the supplied air and hot fire gases may promote mixing of the gases inside those rooms such that the supply of fresh air dilutes the concentrations of toxic gases being transported from the fire room. As a basis for interpretation of later

results, therefore, this section characterizes how the supply of OA through the HVAC system changes over the course of the tests.

As outlined in Sec. 3.1.3 each test has a nominal supply flow rate of incoming 'air' and an exhaust flow rate set to balance the supply. Test 1 has no mechanical ventilation, and thus no set supply or exhaust flow rate, however the ducts inside the structure remain open, so smoke can flow between compartments through the duct system. Tests 2 and 3 have supply flow rates set to a baseline level of a residential HVAC system and 2x the baseline HVAC which translates to nominal flow rates between $0.011\,\mathrm{m}^3/\mathrm{s}$ to $0.013\,\mathrm{m}^3/\mathrm{s}$ and $0.022\,\mathrm{m}^3/\mathrm{s}$ to $0.025\,\mathrm{m}^3/\mathrm{s}$, respectively. Test 4 is set for 100% recirculation of gases in the structure with the same supply and exhaust flow rates as in Test 2.

Figure 4.1 shows a plot of the time varying supply duct flow rates into the fire room and corresponding gas temperatures in the HVAC ducts for the four tests. Flow rates are calculated from the velocity measured by the velocity probe located inside the duct immediately upstream of the fire room supply vent. A positive flow rate indicates supply into the fire room and a negative flow rate indicates a backflow into the duct. In the test with no HVAC, a backflow of heated smoke into the duct begins as the fire is ignited and persists to the end of the test. This is expected since pressures in the fire room would be higher than in any other room so, with the ventilation fan off, there is nothing to resist the flow of hot smoke back into the HVAC duct. Consistent with this, backflow is delayed in the baseline HVAC test, beginning at 4:40 (m:ss) after ignition and persisting to 16:23 after ignition. The recirculation test shows similar trends with backflow and duct gas temperature beginning slightly later, at 5:37, and continuing until 12:44 after ignition. This is again expected since these two tests have the same nominal supply flow rates. When the supply flow rates are doubled for the 2x baseline HVAC test, the pressure created by the fire is no longer sufficient to overcome the force of the HVAC supply and no evidence of backflow of heated gases into the supply duct is observed, although a brief decrease in flow rate and a small increase in duct gas temperature is measured shortly after five minutes into the test.

Figure 4.2 shows a similar plot for the flow rates in the main floor supply ducts across the four tests. The velocity probe used to calculate these flow rates is located in the duct upstream of the kitchen supply vent and therefore best measures the total supply to the main floor (kitchen plus fire room). This plot shows backflow past the kitchen supply vent occurs only in the no HVAC test. Since there is no forced HVAC to resist backflow from the fire into the ductwork and past the vent, the backflow again begins at the time of ignition of the fire. In this case, it persists until 6:14 after ignition, following which it transitions to a supply flow into the kitchen, due to continued backflow past the fire room vent for the remainder of the test. In the tests with baseline HVAC and recirculation, the

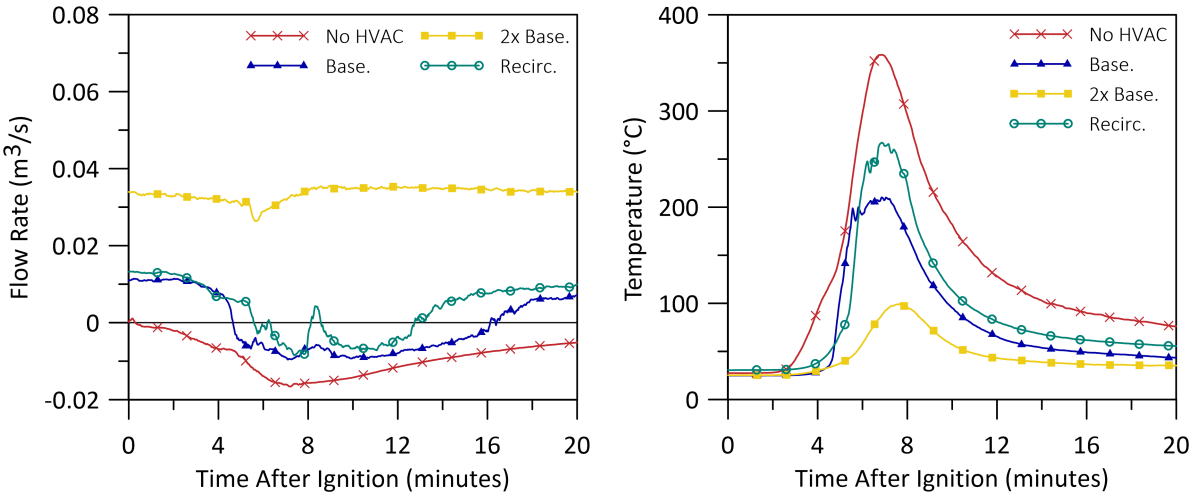

(a) Volumetric flow rate

(b) Supply gas temperature

Figure 4.1: Fire room ventilation supply volumetric flow rate and gas temperature in the duct measured upstream of the fire room supply vent for all four tests.

smoke that is flowing back into the fire room duct and vent must be then flowing into the kitchen through the kitchen supply vent, since no backflow past the kitchen vent and only small duct gas temperature increases are observed in either of these two tests. Again, the test with 2x baseline HVAC shows a minor decrease in flow rate and very small increase in duct gas temperature shortly after five minutes into the test.

Supply flow rates to the upper floor and corresponding temperatures are plotted as a function of time in Fig. 4.3. These flow rates are measured upstream of the small bedroom and therefore represent the total supply to the upper floor (small bedroom plus large bedroom). At this location, backflow into the upper floor duct occurs between 2:44 to 7:06 after ignition and again at 12:22 after ignition to the end of the test for the case with no HVAC. Backflow is also observed in the test with baseline HVAC at times between 5:00 to 5:45 after ignition. No backflow into the supply duct is measured for the 2x baseline HVAC test and the recirculation test, although in the recirculation test a significant decrease in flow rate does occur shortly after five minutes into the test and persists for approximately two minutes.

Duct temperatures shown in Figs. 4.1 through 4.3 were measured at the same location as the velocity probes. They show the same trends for each location across all tests. The highest peak temperatures are seen in the test with no HVAC because there is no supply of cooler OA flowing through the duct and hot smoke is flowing back into the duct. As a

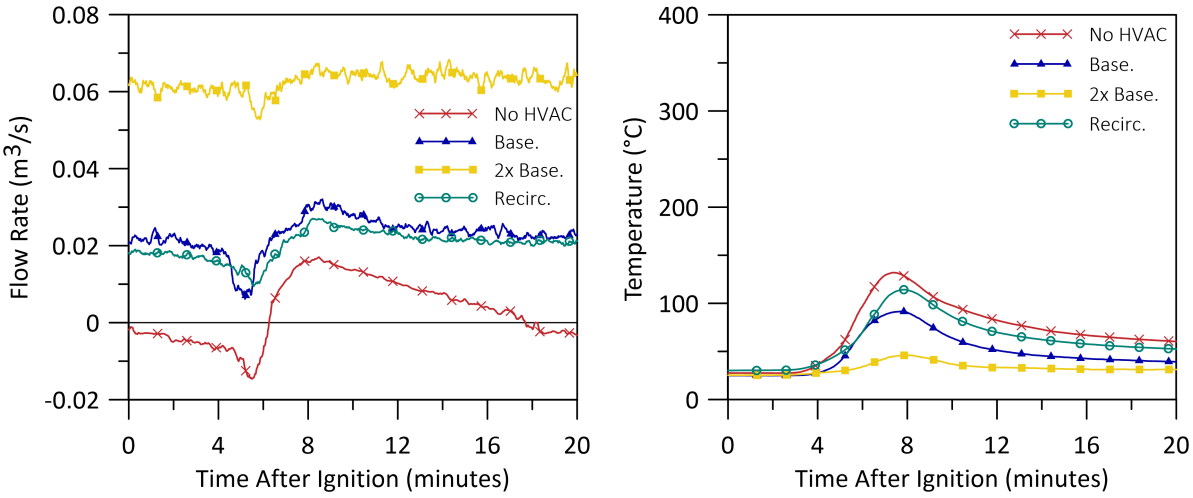

(a) Volumetric flow rate **(b)** Supply gas temperature

Figure 4.2: Main floor total (kitchen plus fire room) ventilation supply volumetric flow rate and gas temperature in the duct measured upstream of the kitchen supply vent for all four tests.

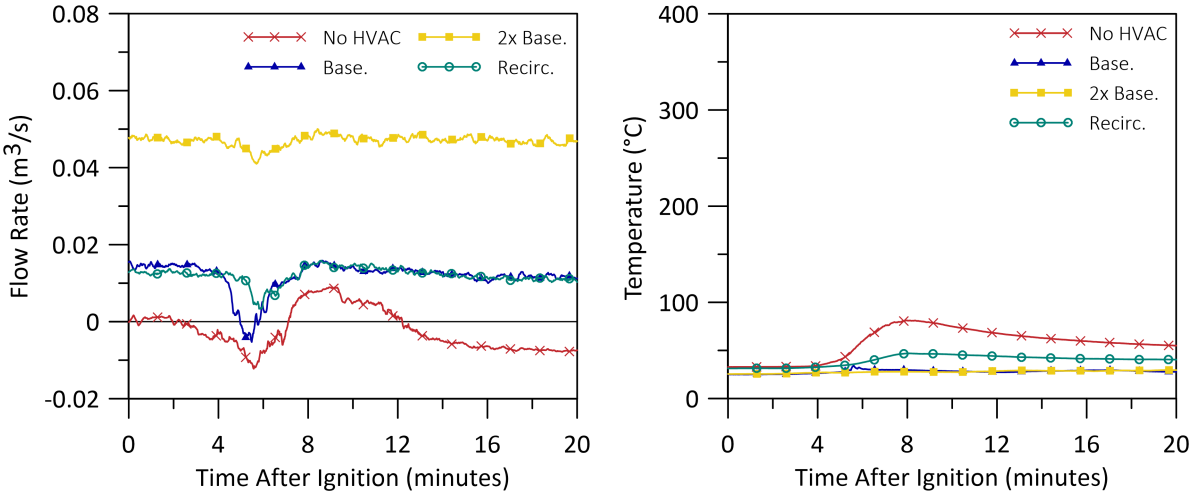

(a) Volumetric flow rate **(b)** Supply gas temperature

Figure 4.3: Upper floor total (small plus large bedrooms) ventilation supply volumetric flow rate and gas temperature in the duct measured upstream of the small bedroom supply vent for all four tests.

result, temperatures in the ducts reach over 350 °C at the fire room supply probe, 130 °C at the main floor supply probe, and 80 °C at the upper floor supply probe. Again, due to the lack of cool OA supply into the ducts, the second-highest peak temperatures are seen for the test with recirculation. Due to the difference in the backflow of hot smoke in these tests, temperatures are 100 °C cooler than in the no HVAC test at the fire room supply probe, 17 °C cooler than the no HVAC test at the main floor supply probe, and 34 °C cooler than the no HVAC test at the upper floor supply probe. With a continual supply of cooler OA in the ducts, duct gas temperatures in the baseline HVAC test are cooler than those in the recirculation test; 57 °C cooler at the fire room supply probe, 22 °C cooler at the main floor supply probe, and 13 °C cooler at the upper floor supply probe. As expected, the coolest peak temperatures are recorded in the test with 2x baseline HVAC; below 100 °C at the fire room probe, below 46 °C at the main floor probe, and below 30 °C at the upper floor probe. In this situation, there is no backflow of hot smoke into the ducts to mix with the cool supply air, so it can only be heated via heat transfer from hot ambient gases through the HVAC duct walls.

Test 1, with no HVAC, exhibits an interesting development of flows through the duct work. Given that there is no mechanical ventilation in this test, the flows observed are a result of buoyancy (*i.e.* density differences between the hotter smoke and cooler air in the rooms). It is interesting, then, that at times there appears to be supply flow to both the main floor and the upper floor, although there is no vent in between. In an attempt to explain these interesting flow developments, Fig. 4.4 presents a timeline of flow in the vents for this test.

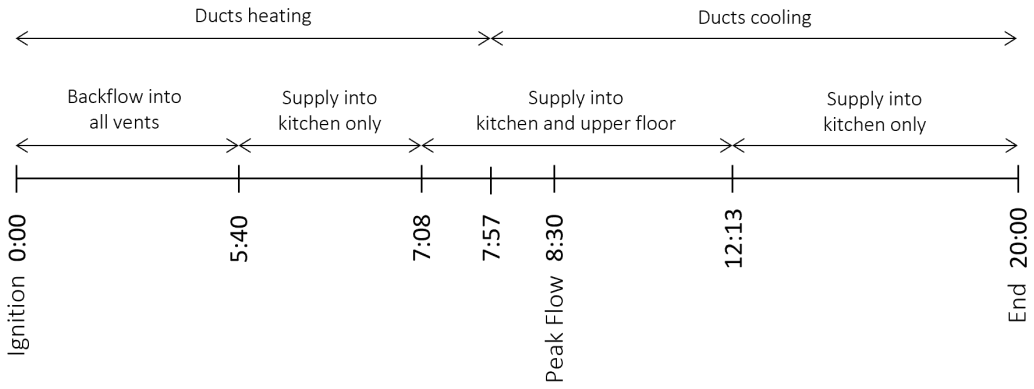

Figure 4.4: Timeline of duct flow phases for the no HVAC test.

From ignition to 5:40 after ignition, there is a backflow of hot gas into all the vents (the fire room, the kitchen, and the upper floor duct). This results in pressurization of the

vertical section of duct connecting the two floors on the exterior of the structure. From 5:40 to 7:08 after ignition, a supply of air into the kitchen is seen, while backflow in the vents persists in the other locations. This indicates that the pressure in the section of duct between the main and upper floors has increased sufficiently to overcome the pressure from the backflow of smoke into the fire room supply vent, such that the kitchen receives supply. During this time, the total inflow of smoke into the ducts remains greater than the outflow into the kitchen, meaning that the ducts are still pressurizing. Heating of the gases in the ducts likely also plays a role in the pressurization of the ducts, since the duct gases expand as they heat. The main floor duct heats up until 7:23 and the upper floor duct heats up until 7:57. It is shortly after this, at 8:30 when the supply flow rate into the kitchen peaks. From 7:08 to 12:23 after ignition, measurements show that both the kitchen and the upper floor are being supplied with flow from the ducts. This suggests that the pressure in the section of duct between the two floors has risen enough to overcome both the backflow from the fire room and the backflow from the two bedrooms. The pressure in this section of duct should now be decreasing. After 12:23 into the test, the flow from the upper floor duct reverses so that there is again backflow into the upper floor duct from the two bedrooms. On the main floor, there is still backflow into the duct from the fire room and supply into the kitchen, although the flow rates are decreasing. This makes sense from a conservation of mass perspective, since backflow into the upper floor duct and the fire room are supplied into the kitchen similarly to the times between 5:40 and 7:08 after ignition. The difference is that now the gases in the ducts are simultaneously cooling, contributing to an overall decrease in pressure as well.

The backflow observed in these experiments is consistent with what is expected in full scale fire progression. During a fire, the fire compartment, and potentially entire structure, pressurizes due to increases in temperature and volume expansion of gases and production of smoke due to combustion. Previous research has shown that there are significant pressure spikes in a compartment immediately after ignition of the fire and also immediately after the fire burns out [110]. Pressure variations throughout the structure have been shown to cause smoke to backflow into ducts, as was seen in these experiments as well.

The interesting observations seen across these tests point to the importance of understanding the configurations of, and potential flows through, both passive and active air supply and exhaust ducts in multi-compartment, multi-storey residential structures in different fire situations. Backflow into the HVAC ducts during a fire is an important phenomenon because it can provide additional, and potentially unanticipated, paths for toxic gas transport to compartments adjacent to a fire room. When backflows occur there is also a period of time when there may be a reduced, or no, supply of fresh OA to the fire room. When this occurs, the supply of O_2 to the fire will also be restricted to that

available through doorway flows. A decrease in the supply of OA to the fire room could further restrict the amount of O_2 available for combustion, thereby impacting overall fire growth and spread, as well as smoke and toxic gas evolution, in real situations as well.

4.2 Fire Progression

The progression of each of the four fires is presented and discussed in detail in this section. Key indicators of fire size, namely the MLR and fire heat flux as measured at the wall of the burn room (HFG 2), are first used to compare the fires that developed under each of the ventilation conditions. Then, interesting phenomenon related to the MLR and heat flux for each test are discussed separately. Finally, similarities between the MLR and heat flux are discussed, showing that both measurements are good indicators of fire growth patterns.

4.2.1 Timeline of Fire Events

Figure 4.5 shows a plot of the MLR from the no HVAC test, which is used as a reference or representative test throughout this chapter. While there are some notable differences between tests, the overall trends in development of the fires, and thus the MLR results, are very similar. The plot in Fig. 4.5 is broken down into four main phases of fire development: 1) incubation, 2) growth, 3) decay, and 4) extinction. The first is the incubation phase, which begins at ignition of the small wood ignition crib and ends once MLR begins to increase. As the MLR begins to increase, the fire transitions into the growth phase, where the fire establishes on the couch and the flames spread. Based on the data, the beginning of the growth phase is the time at which the sustained value of MLR is greater than 3 g/s. During this phase, the fire is considered well ventilated since the concentration of O_2 remains high as the fire grows. As the peak MLR or peak fire size is reached, the fire growth becomes limited by ventilation (availability of O_2). After this, the fire enters the decay phase, where it no longer has the O_2 required for continued growth and decreases in size. At this point, the fire is under-ventilated, and it continues to decay until flame out occurs. This signals the beginning of the extinction phase, where there is no longer any flaming combustion. For these tests, a flame out time is difficult to obtain through visual observation due to buildup of smoke in the fire room, which obscures the camera views. Instead, flame out time is defined based on measured MLR data as the point at which the MLR has a sustained value less than 3 g/s. The value of 3 g/s is selected to indicate flame out because fluctuations in the MLR measurements of up to 3 g/s continue until the end

of data collection. This is consistent with an extinction phase in which there may continue to be a small amount of mass loss as a result of smouldering combustion.

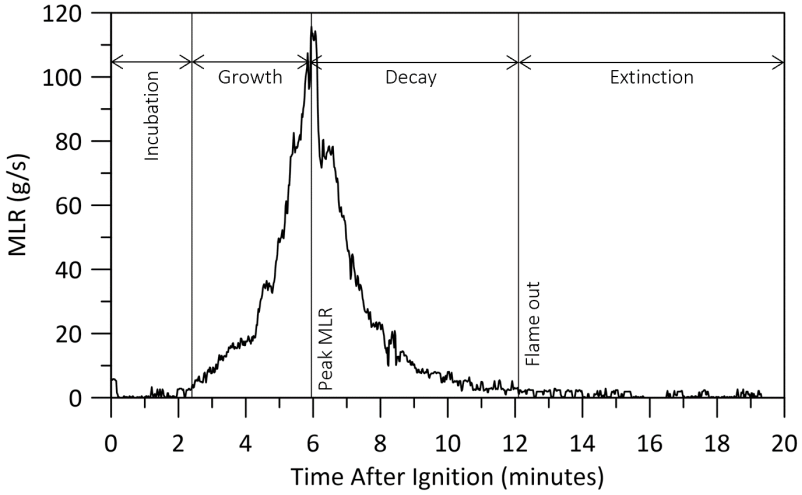

Figure 4.5: Representative MLR plot from the no HVAC test depicting the phases of fire development from incubation, fire growth, fire decay, and extinction.

Four key events, and their corresponding times after ignition, are selected for comparison of the overall development of the fires through each test. These indicate progression through early fire growth, peak fire size, and decay. The four events are: (1) when smoke descends to the top of the window behind the couch (W1) which is indicative of the time it takes for a smoke layer to form near the ceiling and begin its descent, (2) ignition of the second couch cushion which is indicative of a well established and rapidly spreading flame, (3) peak MLR which is indicative of the peak fire size, and (4) when the O_2 concentration measured at the 0.9 m height in the small bedroom (GIS 6) decreases to 15%. This latter point is chosen since an O_2 concentration of 15% is an indicator of significant ambient environmental degradation on the upper floor, and is an event that occurs during the decay phase of these fires.

Figure 4.6 shows images of the fire from the no HVAC test at these key times to provide a visual illustration of the fire and progression of the environment in the fire room throughout the test. When the smoke layer builds up enough to reach the top of the window at 2:50 after ignition (Fig. 4.6a), the fire has grown to establish itself on the first couch cushion. The heat from the fire has caused the fabric on the nearest armrest to rip, exposing the liner underneath. Shortly after, the liner melts and exposes the foam underneath, which then off gases and ignites. This series of events characterizing ignition

of the armrest is also observed in cone calorimeter testing of the composite assembly of foam, liner, and fabric taken from an identical couch. After this time, the fire continues to spread, eventually consuming most of the first cushion and igniting the second at 4:10 into the test (Fig. 4.6b). At this point, the smoke layer in the room has developed further and is now filling in a large volume from the ceiling to a depth that nears the bottom of the window. The fire reaches its peak size, at 5:57 into the test (Fig. 4.6c). The fire room is now nearly completely filled with smoke, obstructing the view from the camera to a small area illuminated by the flames. In the decay phase, depicted by the image in Fig. 4.6d at 7:30 after ignition when 15% O_2 is reached on the upper floor, the buildup of smoke has become so great that there is almost nothing except smoke visible in the camera view.

(a) Smoke reaches the top of the window

(b) Second cushion ignites

(c) Peak MLR

(d) 15% O_2 on the upper floor

Figure 4.6: Images from the no HVAC test showing the fire development.

The times it takes the fire in each test to reach these key stages are summarized in Table 4.1. Comparing the tabulated times shows that the early fire development is very similar regardless of the ventilation configuration, with only a 10-second variation between the time it takes for smoke to descend to the top of the window across all four tests. The time taken for ignition of the second cushion is also very consistent across tests, occurring at 4:10

after ignition for each of the no HVAC, the 2x baseline HVAC, and the recirculation tests. The time differs slightly for the baseline HVAC test, with the time taken for ignition of the second cushion being delayed by about 16 seconds. Examination of the video recordings of this fire indicates that the difference is because the flaming region of the fire has a different flame shape than seen in the other tests. In the baseline HVAC test, the flames spread up the back cushion of the couch instead of spreading horizontally across the couch. The second cushion then begins to off-gas and subsequently ignites due to radiant heating (the mode of ignition also observed in the cone calorimeter) instead of igniting as a result of more continuous flame spread across the surface of couch cushions that is observed in the other three tests.

Table 4.1: Timeline of fire milestones for each test.

	Time After Ignition (m:ss)			
Event	No HVAC	Base.	2x Base.	Recirc.
Smoke reaches top of window	2:50	3:00	2:55	2:55
Second cushion ignites	4:10	4:26	4:10	4:10
Peak HRR	5:57	5:44	6:30	6:36
15% O_2 on upper floor	7:30	8:16	9:13	7:35

More distinct differences in the fire timelines between the different HVAC configurations begin to appear between ignition of the second couch cushion and peak MLR. These become even more significant in the later stages of development of the environment during the decay phase of the fire. There is a 51-second difference between the earliest peak MLR (baseline HVAC test) and the latest peak (recirculation test). The time taken to reach peak MLR in the recirculation test, however, is an anomaly because one of the checker boards used to track smoke density in the fire compartment fell during the test, causing intense mixing and likely an increase of O_2 locally at the fire. This resulted in a double peak in the MLR with an inherent delay in the timing of the second, higher peak. The 2x baseline HVAC test also appears to have a delayed time to peak MLR which is reached at a time similar to the second peak in the recirculation test. Reasons for the differences are discussed later when further details of the MLR curves are presented. The largest difference in the fire timelines across the four tests is observed in the time taken for the O_2 concentration to decrease to 15% at the 0.9 m height above the floor in the small bedroom. For this, there is a one-minute and 43-second difference between the shortest (no HVAC) and the longest (2x baseline) times. Both tests with no supply of OA take comparable times to reach this threshold. There is also a clear and not unexpected trend that tests with increased supply

of OA into the structure took longer to reach lower O_2 concentrations. This confirms the importance of understanding the significant effects that HVAC systems can have on both fire development and on the resultant fire induced environment. In a multi-compartment multi-story structure, this impacts the fire room, but is also extremely important to smoke and toxic gas distributions even in far field locations.

A visual comparison of the fires is shown in Figs. 4.7 and 4.8 at times when the second cushion ignites and at the time when peak MLR is reached, respectively. The images in Fig. 4.7 clearly show that the baseline HVAC flame is taller and narrower compared to the flames in the other tests. As mentioned previously, the difference in flame shape and smoke layer height is likely due to the different flame spread process in this test, with the flame spreading vertically up the back cushion of the couch instead of horizontally across the cushion. Repeat tests would be necessary to determine if the different flame behaviour is due to the ventilation configuration or other factors in that particular experiment. Either way, the anomaly does point out that the nature of early flame spread is another factor that has a large effect on development of the fire and therefore the evolution of the fire induced environment throughout the house.

At peak MLR (Fig. 4.8), a thick layer of smoke has filled the fire room and there is nearly zero visibility except in those regions in which illumination by the flames is sufficiently intense to penetrate the smoke directly between the camera and the fire. The images show that the optical density of the smoke is different in the different tests. The purple hue in the 2x baseline HVAC test (Fig. 4.8c) indicates that the smoke in that test is thick enough that the camera has transitioned to night mode due to a lack of ambient illumination. The different coloration in the three other tests likely indicates less smoke buildup, possibly due to slower smoke layer descent in those scenarios.

4.2.2 Comparison of Mass Loss Rates

The measured MLRs are plotted for all four tests in Fig. 4.9 from the time of ignition to 12 minutes after ignition. This allows examination of differences in the test to test fire sizes and growth/decay patterns. Overall, fuel MLRs-time curves exhibit similar slopes across all tests in the early growth stages of the fires and reach comparable peak values although there are some minor yet notable differences across the entire burn times. To highlight these, Table 4.2 lists important values related to the MLR of fuel in each fire, including instantaneous peak values of fuel MLR, total burn time of the fire, fire decay time, total fuel mass lost before peak MLR is reached, and total fuel mass loss at flame out.

The test with no HVAC reached the highest peak value of MLR at 116 g/s, followed

by the test with recirculation at 103 g/s, the baseline HVAC test at 98 g/s, and lastly the 2x baseline HVAC test with the lowest peak value of 96 g/s. It is interesting that having increased supply of OA in these tests does not appear to correlate with an increase in fuel burning rate as might be expected. In fact, tests with supply of OA have comparably lower peak MLR values. The time taken to reach a peak value of MLR varies as well, as listed in Table 4.1. There does not appear to be a clear relationship between the value of peak MLR and the time taken to reach the peak value. The baseline HVAC test reaches lower values of peak MLR than either the no HVAC or recirculation tests, but the peak is reached the earliest compared to any of the other tests, at 5:44 after ignition. In contrast, the 2x baseline HVAC test takes longer to reach the peak value of MLR, at 6:30 after ignition, and burns with the lowest peak MLR value, albeit a value quite close to that measured in the baseline HVAC test as well.

An explanation for the reduced peak burning rates with increased OA supply may, at least in part, be attributed to the location of the supply air vents in the burn structure. Air is supplied at a location high above the floor within the compartment such that, once the

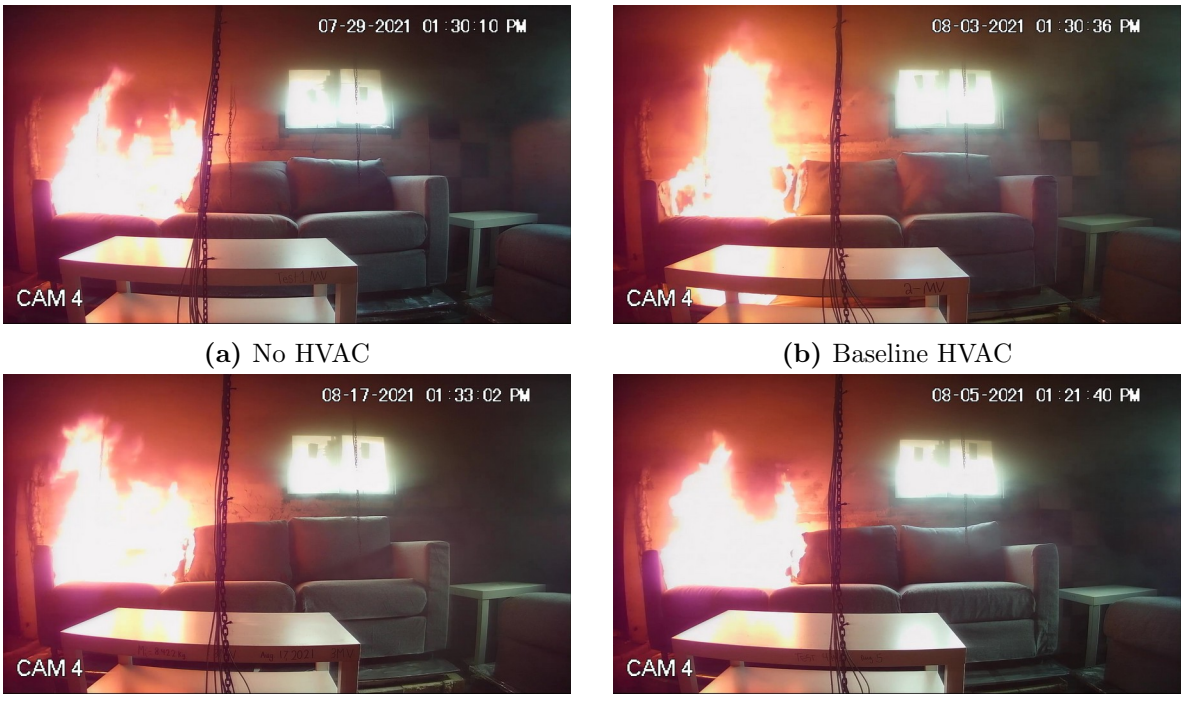

(a) No HVAC

(b) Baseline HVAC

(c) 2x Baseline HVAC

(d) Recirculation

Figure 4.7: Images comparing the four tests at the time when the second cushion ignites.

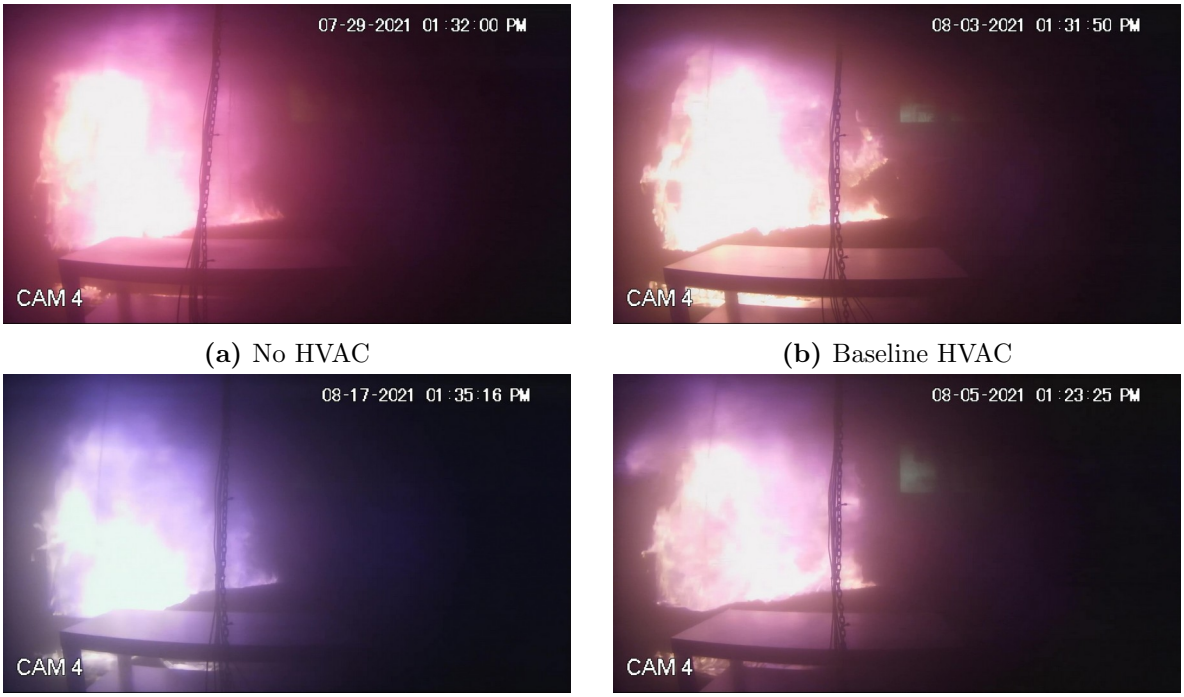

(a) No HVAC **(b)** Baseline HVAC

(c) 2x Baseline HVAC **(d)** Recirculation

Figure 4.8: Images comparing the four tests at the time of peak MLR.

fire is ignited and hot gases migrate towards the ceiling, the fresh air supply is forced into the upper regions of the compartment, which contain the hot smoke produced by the fire. Instead of feeding fresh air directly to the fire as might be the case with supply located nearer to the floor, the high supply configuration used in these tests effectively pushes smoke down over the fire, resulting in a faster increase in smoke layer depth and thus earlier, and more pronounced, interactions between the smoke layer and the combustion zones within the flames. Since the smoke contains mostly combustion products and very low levels of O_2 (see Sec. 4.5), the decreasing smoke layer height would tend to choke the fire and result in a decreased burning rate. A faster rate of smoke layer descent is evident in the 2x baseline HVAC test, as can be seen with the lower smoke layer height when the second cushion ignites and with the thicker smoke layer at peak MLR, shown in Fig. 4.7. Reduced burning rates as a result of ventilation supply into the upper layers of fire compartments have also been shown in studies by [93] and [95]. This effect is more evident in the 2x baseline HVAC test than it is in the baseline HVAC test or the recirculation test, since the increased ventilation flow rate in the 2x baseline configuration results in more

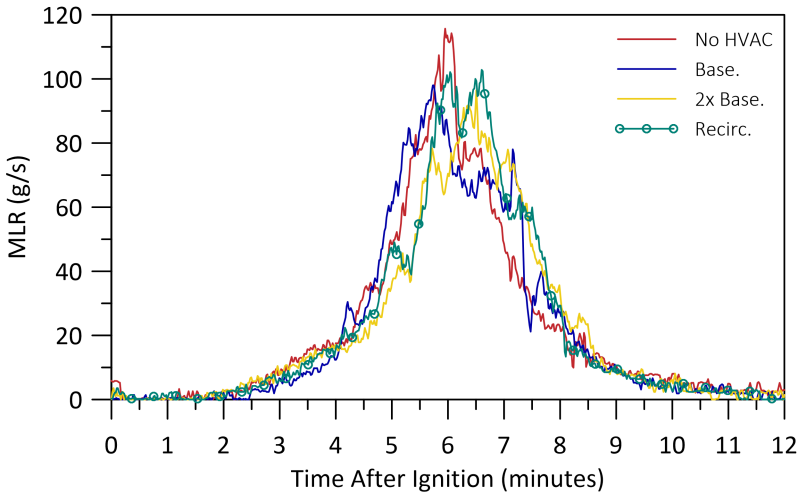

Figure 4.9: Comparison of measured MLR for all tests from ignition to 12 minutes after ignition.

Table 4.2: List of important mass related values for each test.

	Unit	No HVAC	Base.	2x Base.	Recirc.
Peak MLR	g/s	116	98	96	103
Total burn time	mm:ss	12:06	11:03	10:31	10:48
Decay time	m:ss	6:09	5:19	4:01	4:12
Total mass loss to peak	kg	7.3	6.3	8.3	9.8
Total mass loss to flame out	kg	15.8	15.8	15.7	16.3

mixing and imparts significantly more momentum to force the smoke layer downwards. The impact is further enhanced in this test as well, since there is also a continual supply of air into the upper layer in the fire room, as there is no backflow into the ducts with the higher ventilation flow rates.

Total burn time, from ignition to flame out, also varies between tests. As noted previously, flame out time is defined as the time when the MLR decreases to a sustained value below 3 g/s. As listed in Table 4.2, the 2x baseline HVAC test has the shortest total burn time of 10:31, followed by the recirculation test with a burn time of 10:48, the baseline HVAC test with a burn time of 11:03, and the no HVAC test having the longest burn time of 12:06. Interestingly, the 2x baseline HVAC test reaches peak MLR latest but has the earliest flame out time, hence it also has the shortest decay phase of the all the tests. Although driven by a series of complex interactions between fire size, air availability and

fire HRR, the reduction in total burn time might be explained by the faster rate of smoke layer descent caused by the ventilation supply, which reduces the local supply of oxygen to, and thus smothers, the fire earlier in this test. Reduction in supply of oxygen to the fire due to configuration and composition of ambient gases local to the fire would also be consistent with results seen for the recirculation test and the baseline HVAC test, which have the second and third-shortest burn times and also the second and third-shortest decay phases[1], respectively.

Results in Table 4.2 also show that tests which take longer to reach peak MLR correspond to those with higher values of overall fuel mass loss at the time peak values are reached. The baseline HVAC test has the earliest time to peak with the least fuel mass consumed to that time, 6.3 kg, followed by the no HVAC test with a mass consumed of 7.3 kg. The 2x baseline HVAC and recirculation tests, with delayed peak MLR have the most mass loss of 8.3 kg and 9.8 kg, respectively. Since the growth phases of the fires are so similar, tests with delayed peaks would be expected to have higher overall mass consumption when they reach peak values of MLR since they have had additional time to burn at similar rates.

Interestingly, despite differences in the details of burning in the different stages of the fire, all the tests show very similar total mass of fuel burned by the time flame out occurs. The no HVAC and baseline HVAC tests both burn measured values of 15.8 kg, the 2x baseline HVAC test burns slightly less at 15.7 kg, and the recirculation test burns the most at 16.3 kg. This can be explained through further examination of the ventilation flow rates, which are in line with typical residential supply flow rates, used in the experiments. The mass of O_2 introduced into the structure by the ventilation system (1.26 ACPH) over the 10 to 12 minute burn time of the fires is negligible compared to the mass of O_2 contained in the original volume of air (275 m^3) inside the structure. Hence, the amount of fuel that can be consumed in any of the fires is limited by the original volume of available air, resulting in a consistent amount of fuel burned over the duration of the fires. On the other hand, the presence and configuration of the ventilation system do affect the details of the fuel burning rates. The location of the supply vents high in the compartments, affect the burning rate of the fires since the smoke layer is pushed down over the flames as noted above. At some points in the fire, this likely results in local deficiencies in O_2 near the fire, but overall will depend more on the flow rate of the supply than the detailed composition of the supply air (*e.g.* outdoor or recirculated air). The increased mass of fuel consumed in the recirculation test is coupled to the double peak in fuel MLR (more burning at a higher rate) and thus increased temperatures experienced in this test, as explored in more

[1]The shorter time seen in the recirculation test over the baseline test is also consistent with the combination of supply location and recirculation of smoke back from exhaust to supply.

detail in Sec. 4.3. For the same fuel-air mixtures, elevated temperatures heat the fire environment and may prolong and enhance pyrolysis, allowing the fire to continue burning at lower O_2 concentrations [87].

4.2.3 Details of Individual MLR Curves

Once the overall features of fire development were assessed, it was of interest to examine differences in the details of fire growth and spread through a more in depth analysis of time-variations in MLR as connected to visual observations of the fire plume and the environment in the fire room at key times during the fire for each test. To this end, the following four figures show plots of the MLR curves of each test individually, with markings to highlight key phenomenon that occur during the fires. Each phenomenon or event is accompanied by an image or a series of images to show how the fire or smoke is behaving as the event occurs. Images are selected from camera 4, viewing the front of the couch, and camera 1, viewing the side of the couch.

Figure 4.10 shows a plot of MLR versus time after ignition from the no HVAC test, with accompanying images from that test. Two events which occur before peak MLR are of interest and are discussed further here. The first is a notable increase in the slope of the MLR curve at 4:18 after ignition, and the second is a period of apparent constant mass loss with time between 4:33-4:47 after ignition. Comparison of fire video images with the MLR versus time curve indicates that the increase in slope occurs eight seconds after the second couch cushion ignites and five seconds prior to there being visible burning on the underside of the couch (burn through), which is visible in the view from camera 1 in Fig. 4.10. The increased burning rate can be attributed to the combination of burn through and flame spread beyond the first cushion. Visible off-gassing from the parts of the couch not already burning begins after the initial spread of flames to the second cushion and resultant increase in slope of the MLR-time curve. This also corresponds to the time when the MLR appears to flatten out for a period of time. This could correspond to a buildup of pressure inside the couch cushions as their temperatures rise high enough to begin pyrolysis of the inner cushion materials[2]. Such buildup of pressure would manifest as an increase in mass happening at the same time as the fire continuing to burn and consume fuel with possible cancellation of the two effects, resulting in the period of apparently constant MLR. During the period of constant mass loss, off-gassing is observed from the second and third

[2]Slight increases in the measured mass of the chairs, which never ignite, are also observed and are thought to be caused by a similar buildup of pressure within the cushions due to rising temperatures and off-gassing of interior couch materials underneath the still intact cushion covers.

cushions of the couch. These off-gases are not observed to ignite, as further ignition and flame spread appears to be hindered by smoke filling in the fire room. It is interesting that the direction of smoke movement also visually appears to change during this period of approximately constant mass loss. As the period begins, the smoke layer is descending and filling the room. Near the end of the period, the layer transforms from having an approximately horizontal interface across the room to having a lower smoke layer interface visible on the right-hand side of the image (away from the fire) and a higher smoke layer interface closer to the fire. Shortly after this happens, the MLR begins to increase again and the smoke closest to the interface appears to change direction and move from right to left across the image towards the flames of the fire. This may be due in part to the natural draw of air into the lower regions of the fire, as well as the side of the room between the couch and the exterior south wall filling with smoke so that as more smoke is produced and fills towards the middle of the room, it appears as though the smoke layer is moving toward the flames.

A plot of the MLR curve with accompanying images for the baseline HVAC test is shown in Fig. 4.11. Two events before peak MLR in this test are again of interest. There is an increase in slope of MLR similar to that described above, as well as a local peak and valley in the time-varying MLR. In this test, these events occur sequentially in time, such that they will be described as a single event. There is a sharp increase in slope of MLR at 4:00 after ignition leading into a local peak in MLR. This corresponds to the time when burn through is observed and flames become visible on the underside of the couch in video traces of the fire. It occurs at nearly the same time in this test as it does in the no HVAC test, suggesting that burn through of the couch is fairly consistent between these two tests as well. Off-gassing from the second cushion is observed to begin during the period of increased MLR, but prior to burn through. The off-gassing continues and can be seen from both the second and third cushions during the period of decreasing MLR that follows. At 4:26, corresponding with the bottom of the valley in MLR, the second cushion is observed to ignite by radiant (remote) ignition of the off-gases from the left-hand side of the second cushion closest to the flames. The local peak and valley is therefore likely a characteristic of this sudden ignition of the cushion. Following this, the fire begins to grow again at a faster rate as the second cushion becomes involved. Off-gasses from areas of the cushions further away from the flames are not observed to ignite, as was observed in the no HVAC test as well. It should be noted that remote ignition of off-gases from the second cushion is different than the ignition mode of the second cushion in the other tests where ignition occurs due to horizontal flame spread across the surface of the cushions. This is supported in video recordings of this fire which indicate that flame spread in this test is preferentially vertical compared to the other tests. Due to the differences in flame spread, ignition of the

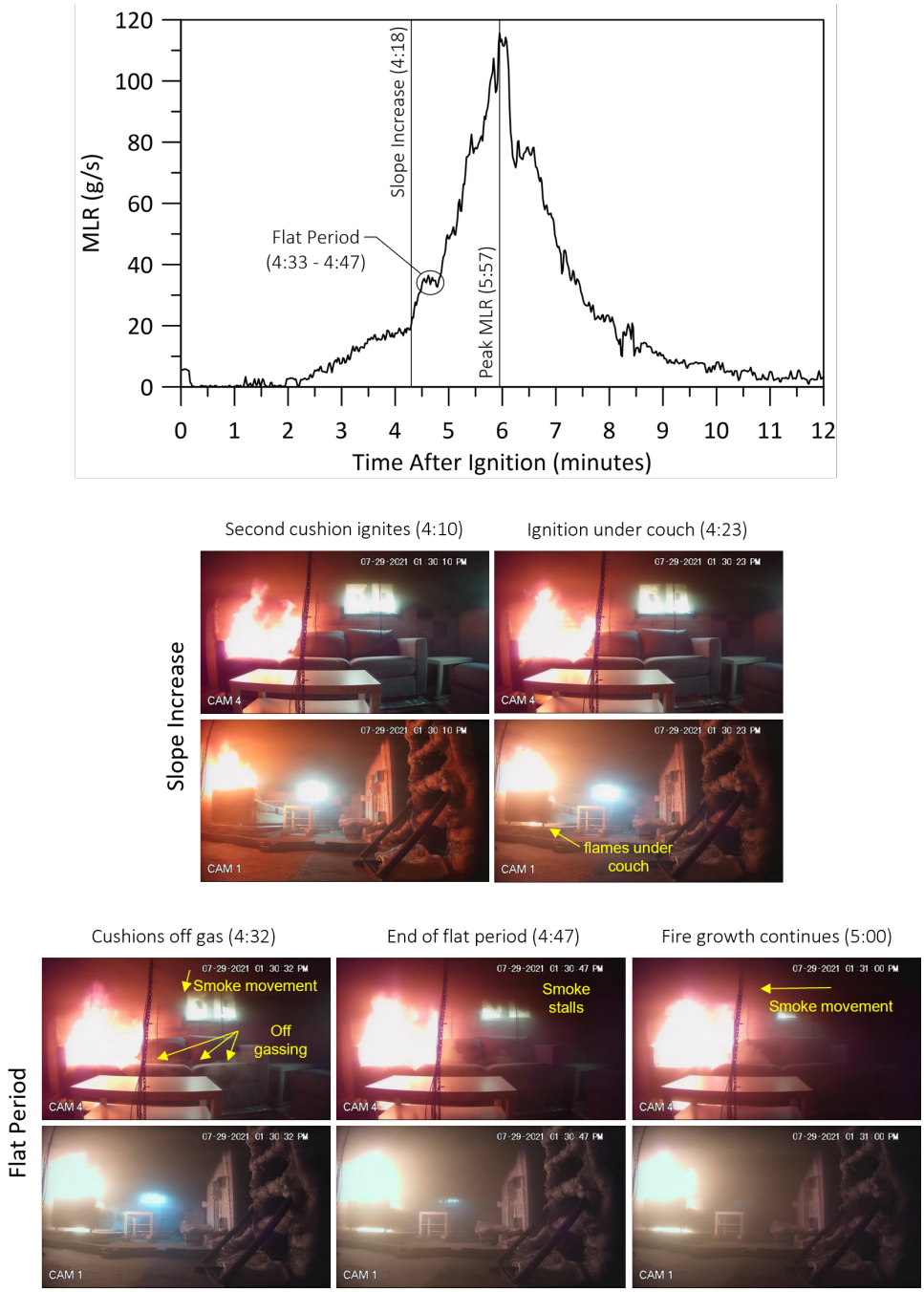

Figure 4.10: Plot of MLR from the no HVAC test with images of the fire during the slope increase and flat period.

second cushion is also delayed in this test in comparison to any of the others.

The same plot and images for the 2x baseline HVAC test are shown in Fig. 4.12. In this test, there are also two events before peak MLR that merit discussion. The first is the increase in slope of the MLR-time curve that occurs at 4:43 after ignition, and the second is a local peak at 5:11 followed by a valley at 5:19 after ignition. The increase in slope occurs as the flame spreads horizontally across the couch cushions and the fire becomes established on the second cushion of the couch, following a very similar pattern as in the no HVAC test. Again following trends seen in the no HVAC test, burn through of the first cushion occurs seven seconds after the initial increase in the MLR-time curve and is linked to ignition and flame spread beyond the first cushion of the couch. Observations of off-gassing from the couch cushions are difficult to obtain in this test because of the increased smoke filling and mixing of the smoke layer as a result of the ventilation, which pushes smoke into the view of the camera. Nonetheless, there is no noticeable off-gassing from the couch cushions prior to the increase in MLR. The peak and valley in values of MLR seen in this test correspond to a change in the nature of the smoke layer descent, similar to what is observed during the period of constant mass loss rate in the no HVAC test. Before the local peak in MLR, the smoke layer in the video images is moving from right to left away from the exterior south wall of the fire room and towards the fire. This suggests that the right-hand side of the room is filled with smoke, and smoke is now flowing towards the centre of the room. After the peak occurs and the MLR begins to decrease towards the valley, the smoke is seen moving downwards in a diagonal direction over top of the flames. Then, once the fire starts to grow again, the smoke flow changes direction toward an upwards diagonal direction. These observations are illustrated by arrows superimposed on the last three series of images in Fig. 4.12 and point to the strong relationship between smoke movement and fire growth. In this case, the coupling between smoke/air movement and fire growth indicate a period in which decreasing fire size correlates with increased smoke accumulation and layering in the fire room. Subsequent fire growth is then accompanied by changes in smoke flow patterns, such that smoke/air are drawn back up and inwards towards the growing flame plume. The MLR-time curve in this test has three distinct peaks, instead of one individual peak as seen in the two previous tests. While the three peaks may be explained through additional interactions between the smoke and flames, the buildup of smoke in the fire room by this time is enough that the cameras have transitioned into night mode. This makes it very difficult to relate any visual observations of smoke movement to later peaks in the MLR since night mode reduces the colour and contrast of the images so that the smoke layer is no longer distinct but instead blends into other dark regions of the image.

Finally, Fig. 4.13 shows the MLR versus time plot and accompanying images from

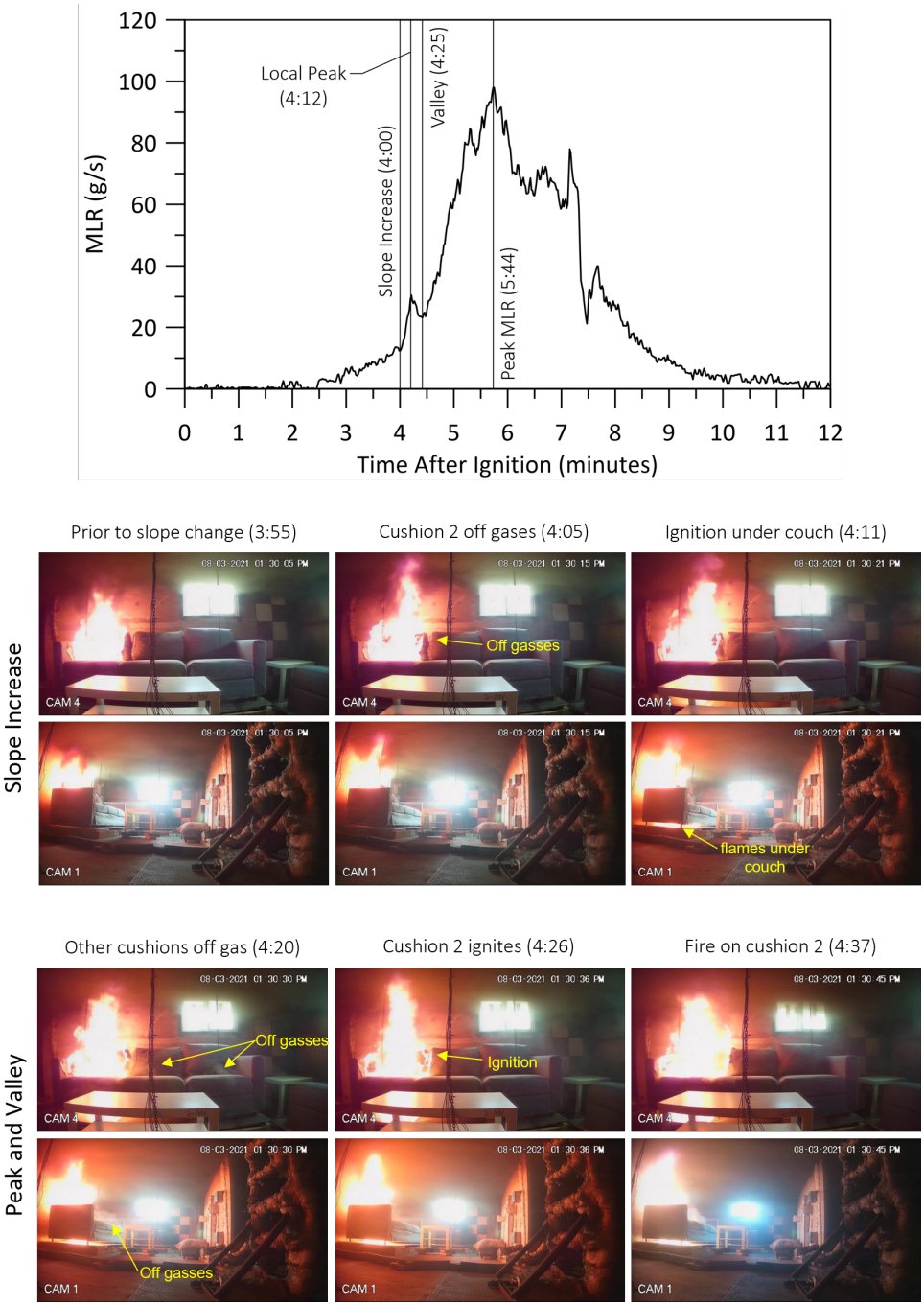

Figure 4.11: Plot of MLR from the baseline HVAC test with images of the fire during the slope increase and the local peak and valley.

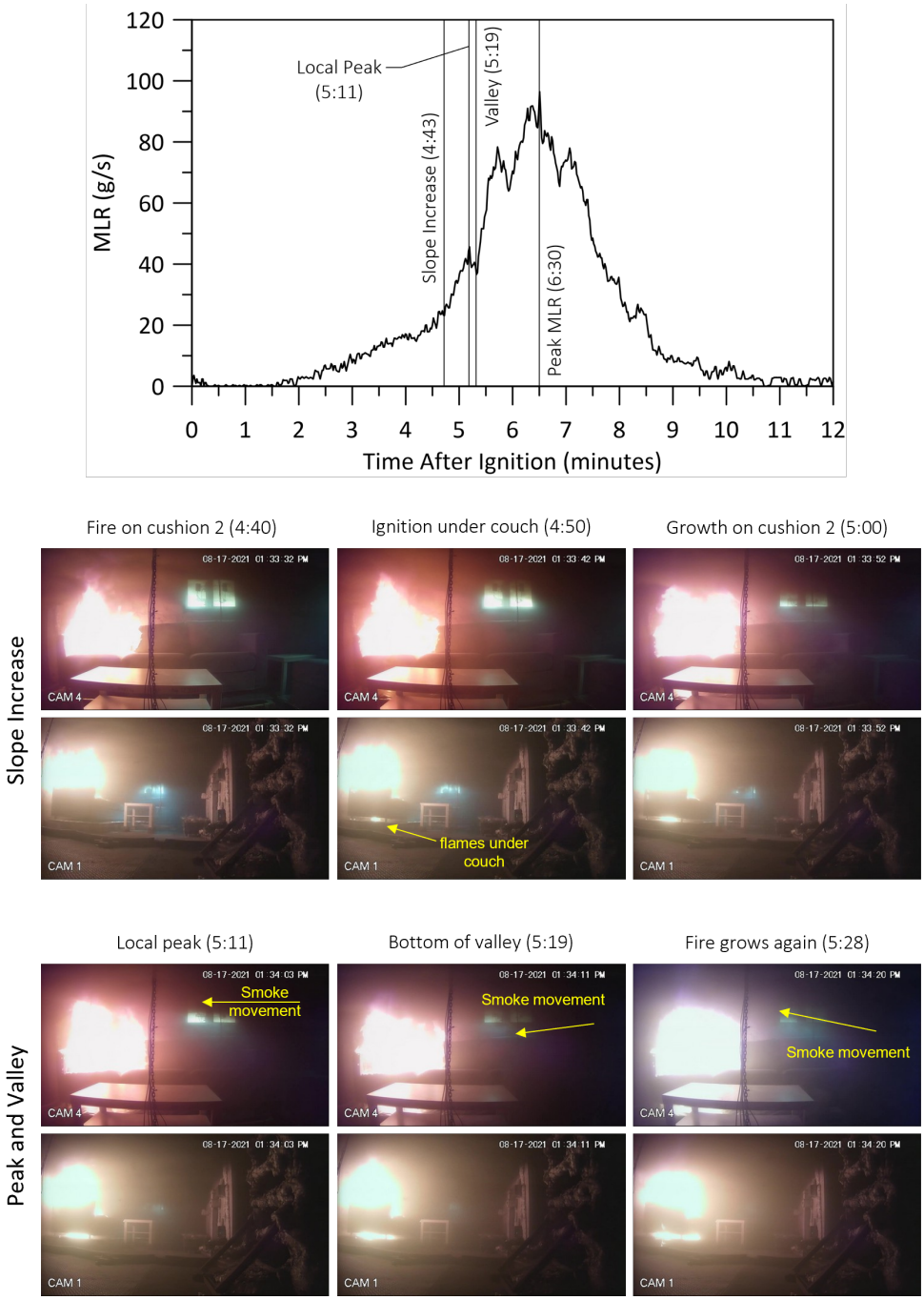

Figure 4.12: Plot of MLR from the 2x baseline HVAC test with images of the fire during the slope increase and the local peak and valley.

the recirculation test. Similar to the other tests, there is an increase in the slope of MLR at 4:42 after ignition, which corresponds to ignition of the second cushion and occurs 9 seconds prior to burn through of the first couch cushion. Also similar to the other tests is a local peak in MLR at 5:06 and valley at 5:20 after ignition. Interestingly, off-gassing from the couch cushions is not observed in this test. Instead, the local peak and valley correspond to changes in smoke movement from a downwards direction while the MLR is decreasing to an upwards direction once the fire starts to grow again, following similar patterns as discussed for the 2x baseline HVAC test. A unique aspect of the measured MLR versus time in this test is the distinct double peaks that occur at 6:02 and 6:37 after ignition. These can be attributed to an unanticipated experimental anomaly. One of the checker boards fell from the wall of the compartment into the fire room 10 seconds prior to the first peak in MLR. The series of images surrounding these peaks illustrate a change in flow and flame patterns as the checker board falls. Specifically, the falling board creates a period of intense mixing in the fire room, effectively pulling smoke from the hot upper layer downwards towards the floor and pushing cooler, fresher air containing higher O_2 concentrations from the floor upwards into the compartment as the board hits the floor. The influx of fresher air to higher elevations, and thus towards the fire base, causes the flame height to increase, which can be seen in the video images of the fire around the time that the first peak in MLR is recorded. As the flame extension recedes, the fire size and burning rate reduce again until the valley in MLR occurs. Following this, the MLR increases again, reaching the second peak of MLR before the fire begins to run out of O_2 and decay. The visual observations of events taking place in the fire room suggest that the first peak in MLR may be a false peak caused by disruption of the evolving fire room environment by the falling checker board, whereas the second peak of fire MLR is more likely representative of the actual peak burning rate that occurs at a time when the fire becomes ventilation limited.

It is clear that increases in the slope of the MLR with time curve are linked to ignition and flame spread on the couch. Results across tests indicate that it takes approximately four minutes for the fire to burn through the first cushion, after which it can begin to spread on the underside of the couch, while flames also spread horizontally across to the second cushion. Fire growth accelerates as more surface area of fuel, from both the top and underside of the cushions, becomes involved in the fire. In contrast to the horizontal flame spread in the other three tests, flames spread vertically up the back cushion in the baseline HVAC test indicating the inherent variability that can occur in large scale fire experiments. Local peaks and valleys in the MLR curves during fire growth, when examined together with video observation of smoke flow patterns in fire room, demonstrate the expected tight coupling between changes in fire size and air/smoke moment though it is not clear which

is the driving force. An exception is the baseline HVAC test where there is less smoke buildup and video images are clearer. In this test, there is more visible evidence of off gassing of couch materials but changes in the smoke movement are not observed speaking to challenges in interpretation of the coupled physical effects that characterize full scale fire development in multi-compartment, multi-storey structures.

4.2.4 Comparison of Heat Flux

Measured values of heat flux emitted by the fires as recorded by HFG 2 on the interior wall across from the couch are plotted in Fig. 4.14 versus time over the period from ignition to 12 minutes after ignition. Values of heat flux in all four tests begin to increase at approximately 2:30 after ignition, with some variation depending on the test. These times

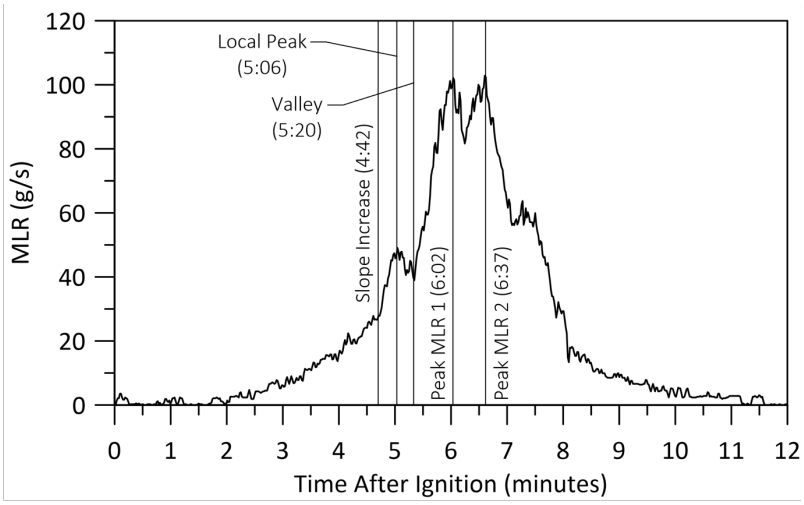

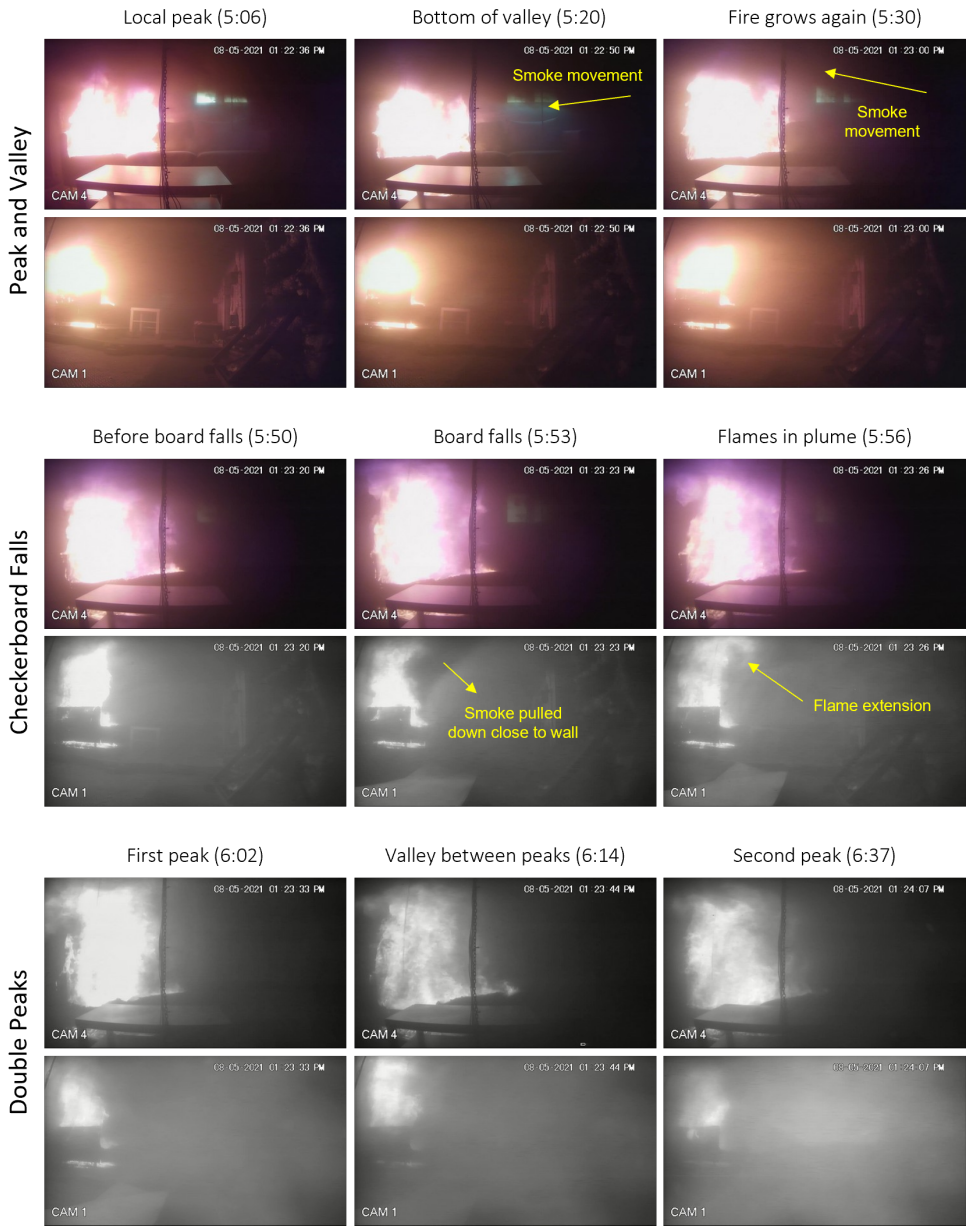

Figure 4.13: Plot of MLR from the recirculation test with images of the fire during the slope increase, the local peak and valley, when the checker board falls, and during the double peaks.

are similar to the incubation periods observed in the MLR measurements as well. Following this initial delay, measured heat flux increases linearly for a period of time before there is a sharper increase in slope between 4:25 to 5:22 after ignition. These times are consistent with, though occur shortly after, the increase in slope of the MLR-time curves. After this, the heat flux measurements reach peak values and then decay until the end of the test. Values of instantaneous peak heat flux and the time to peak heat flux are listed in Table 4.3. The highest values of peak heat flux, 12.4 kW/m^2, are measured in the recirculation test, followed by the baseline HVAC test with 12.1 kW/m^2, and the no HVAC test with 10.9 kW/m^2. Notably, the 2x baseline HVAC test has a significantly lower peak heat flux of 9.0 kW/m^2 and spends a longer period of time at peak heat flux compared to the other tests. The peak value is also reached later than in any other test, at 6:43 after ignition, compared to the other tests which peak between 40 seconds and 55 seconds earlier (5:48 to 6:03 after ignition).

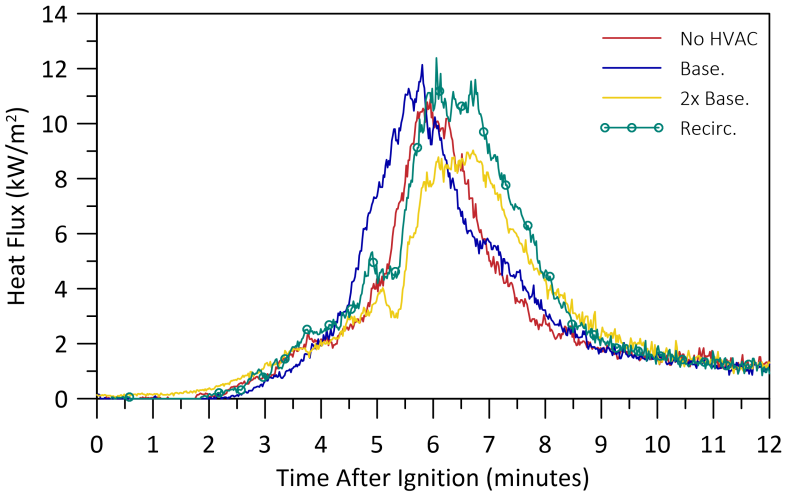

Figure 4.14: Comparison of measured heat flux for all tests from ignition to 12 minutes after ignition.

Table 4.3: Values of measured instantaneous peak heat flux and time to peak heat flux for each test.

	Unit	No HVAC	Base.	2x Base.	Recirc.
Peak heat flux	kW/m^2	10.9	12.1	9.0	12.4
Time to peak heat flux	m:ss	5:57	5:48	6:43	6:03

The lower and longer duration of peak heat flux observed during the 2x baseline HVAC test provide further evidence to support the notion that increased rates of smoke layer descent with time are connected to observed reductions in fire heat release rate. In addition, the increase in buildup of smoke within the environment during this test may obscure the direct line of sight between the HFG and the flames which could also result in a lower measured value of heat flux. Either way, the results indicate that the HVAC supply and its role in pushing the smoke layer downwards into a fire compartment can have a significant effect on heat flux exposure to the compartment walls, with important implications from a fire safety standpoint. Increased levels or prolonged times of exposure to radiative heat flux to the walls would result in higher material surface temperatures and/or larger depths of thermal penetration into the wall materials, increasing the risk for remote ignition, thermal degradation and loss of structural integrity.

To further examine the similarities and differences between the MLR and heat flux profiles, the following figures show the heat flux and MLR measurements over plotted for each individual test. The heat flux profiles are scaled so that the peak of the heat flux profile lines up with the peak of the MLR profile for ease of comparison of the plots. Figure 4.15 shows the profiles with time for the no HVAC test. It can be seen that there is good agreement between the MLR and the heat flux during all phases of the fire. Both heat flux and MLR begin to increase at the same time and are steady from 3:40 to 4:18 after ignition. Immediately after this, the slopes of both MLR and heat flux curves increase and reach peak values at the same time. The progression of the heat flux profile through the rest of the fire growth and into the decay phase also agrees well with the MLR profile. The heat flux profile is noticeably smoother than the MLR, especially at around 6:00 after ignition when there is a sudden drop in measured MLR. This is in part due to differences in the response times of the two measurement devices but also due to specific fire event. Large instabilities in measured MLR are relatively common, normally due to pieces of the couch/fuel falling down as they burn or other material falling onto the load cells as the fuel collapses. Due to smoke buildup in the fire room, it is difficult to visualize such phenomenon, particularly as the fire reaches peak size and then decays. Once in the decay phase, at 7:02 after ignition, trends of heat flux with time clearly start to deviate from those for the MLRs, with heat flux values remaining higher than anticipated. At this point, there is a fairly dense layer of smoke in front of the HFG. Radiative and convective heat transfer from the smoke layer, as well as from the flames, reach the surface of the gauge such that the heat flux measurement is no longer dominated by heat flux from the fire alone beyond this time.

Comparison of time varying profiles of MLR and heat flux for the baseline HVAC test are shown in Fig. 4.16. Similar to the previous test, MLR and heat flux follow similar

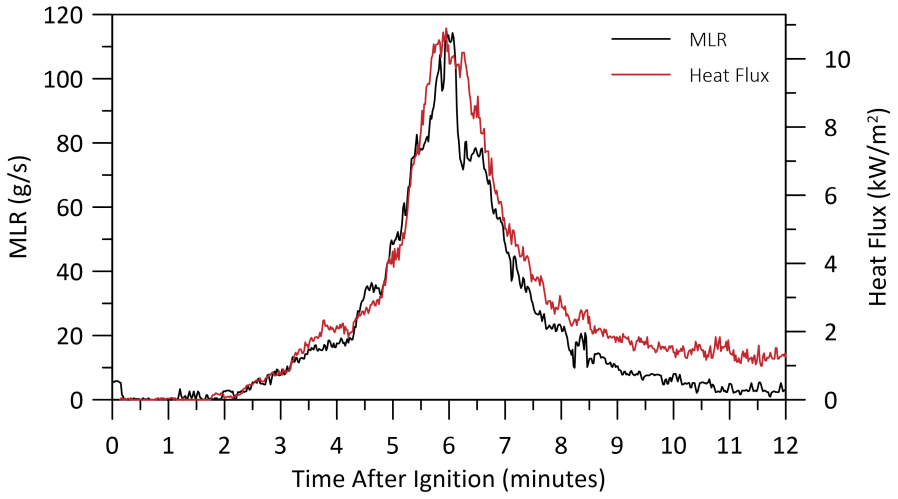

Figure 4.15: Comparison of MLR and heat flux profiles for the no HVAC test.

trends through the growth phase, at peak values, and into the decay phase of the fire. The heat flux curve is again smoother with time than the MLR curve, resulting in some differences in shape between 4:12 to 4:25 after ignition where there is a peak and valley in the MLR and between 6:20 to 7:46 after ignition as the value of MLR levels out for a period of time. This is followed by a large sudden drop in MLR at 7:46 most likely due to a portion of the fuel collapsing and falling from the scale. Consistent with results for the no HVAC test, at 8:20 after ignition, the heat flux profile deviates from that of MLR for the remainder of the test due to the influence of smoke on the measurement.

The comparison between the MLR and heat flux profiles for the 2x baseline HVAC test is shown in Fig. 4.17. There is generally good agreement between the profiles of both measured quantities during the growth phase of the fire. From 2:33 after ignition, the fire heat flux appears to grow slightly faster than MLR with time; however, both support that there are peaks and valleys in fire size between 5:06 to 5:20 after ignition. While the profiles are significantly different near the peak values, with the heat flux appearing more steady while the MLR profile shows three distinct peaks, both reach maximum values at around the same times. Differences may again relate to bits of fuel collapsing on the load cell, or alternately may result from increased smoke-flame interactions in this test due to increased ventilation flow rates. As in the previous two cases, the impact of additional heat transfer to the HFG from the accumulated hot smoke is evident after 7:31 past ignition and through the decay and extinction phases of the fire.

Figure 4.18 shows the comparison between fire MLR and heat flux profiles for the

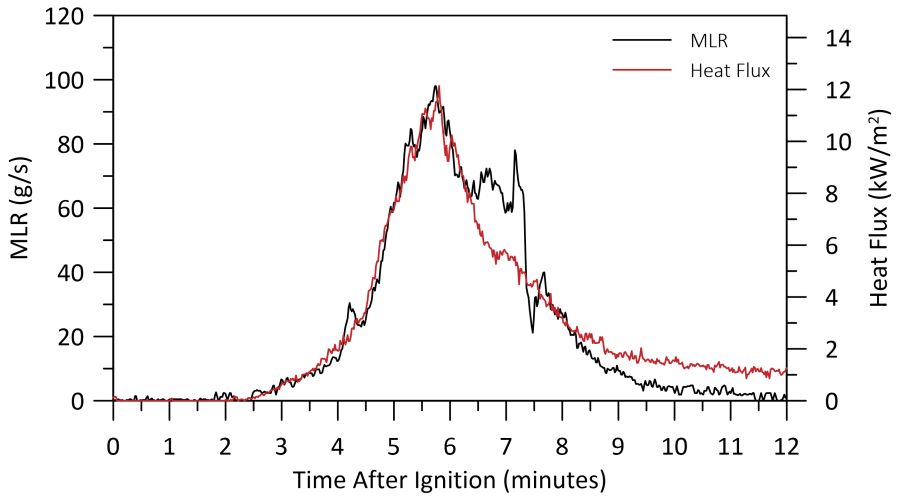

Figure 4.16: Comparison of MLR and heat flux profiles for the baseline HVAC test.

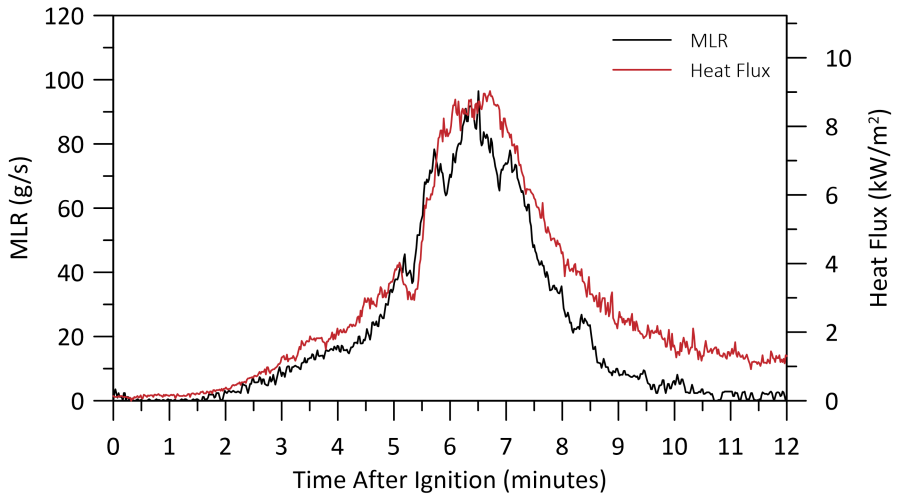

Figure 4.17: Comparison of MLR and heat flux profiles for the 2x baseline HVAC test.

recirculation test. There is good agreement between the two profiles during the fire growth phase with some deviation from 3:20 to 4:10 after ignition where the heat flux profile is above the MLR profile. During peak burning, both profiles follow the peak and valley from 5:06 to 5:20, as well as exhibiting similar double peaks shortly after 6:00 past ignition. The first peak occurs at 6:02 in both profiles, while the time of the second peak differs by about eight seconds. The profiles deviate from one another over most of the decay and extinction phases, with the heat flux profile above the MLR profile, as in the previous tests.

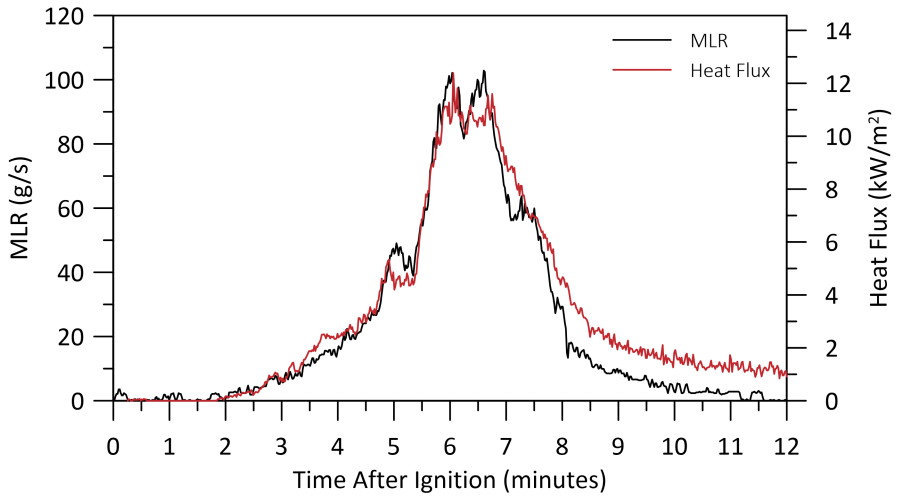

Figure 4.18: Comparison of MLR and heat flux profiles for the recirculation test.

Overall, heat flux and MLR profiles are good indicators of fire size, agreeing well during the growth phases of all the fires as well as around the peak fire sizes. For the most part, they follow changes in rate of fire growth and illustrate comparable peaks/valleys in value during more steady burning periods, particularly in the no HVAC test, the 2x baseline HVAC test, and the recirculation test. However, the heat flux profile for the baseline HVAC test does not appear to follow the peak/valley seen in the MLR curve for the same test. In this case, the flame spread vertically up the couch back instead of across the top of the first cushion may have promoted burning on the backside of the couch, which would be hidden from the view of the HFG, thus preventing the gauge from following more subtle changes in fire size. Differences between heat flux and MLR profiles during fire decay are consistent with enhanced heat transfer from hot smoke in the fire room and seem to occur across all tests.

4.3 Compartment Temperatures

Previous sections have detailed the overall fire mass loss rates and heat flux. This section details the temporal development and spatial distribution of temperature in the fire room and adjacent compartments for the four tests. Fire room temperature distributions and flame temperature data are first presented to provide another measure of fire growth patterns. Following this, measurements of gas velocity are presented to provide the link between fire growth and environment development throughout the structure, then detailed species concentrations are presented for both near field and far field locations.

Figure 4.19a shows time resolved temperature measurements from T1a (0.93 m) for the no HVAC test. Temperatures at this location are a good indication of the temperatures in the flaming zones of the fire, as the thermocouple is located inside the flame throughout most of the test. The flame temperature in the no HVAC test is seen to follow the same overall development in time as the fire MLR, reaching a peak value of 1000 °C between 5:25 and 6:00 after ignition, corresponding to the period during which the fire MLR also reached its maximum value.

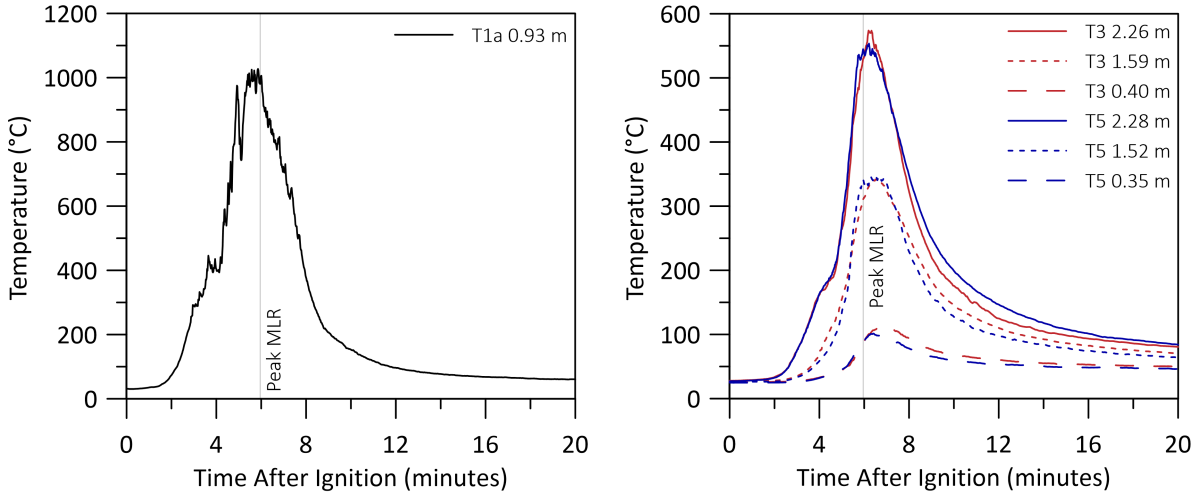

(a) Flame Temperature **(b)** Fire Room Temperatures

Figure 4.19: Plots of fire room and flame temperatures over time for the no HVAC test.

Temperature measurements for the no HVAC test collected at thermocouple rakes T3 (0.40 m, 1.59 m, and 2.26 m) and T5 (0.35 m, 1.52 m, and 2.28 m), in the fire room, are plotted versus time in Fig. 4.19b. Temperatures measured at T3 and T5, which are located in the centre of the fire room and on the corridor side of the fire room, respectively,

are similar throughout the entire test for each of the heights shown. This indicates that there is no significant horizontal gradient in temperature at a given height in the fire room with respect to the north-south or east-west directions. There are, however, large vertical gradients in temperature, as marked by the peak temperatures at T3 2.26 m and T3 0.40 m reaching 573 °C and 111 °C, respectively. Compartment temperatures measured near the ceiling at T3 and T5 again follow the fire growth and decay with time, as was also charted in previous discussions on the flame temperature and fire MLR. Interestingly, a period of relatively constant compartment temperature is measured by T3 at 2.26 m, T5 at 2.28 m, and the flame temperature thermocouple between 3:40 to 4:20 after ignition. This is a similar time period to the periods when fire MLR and heat flux profiles (Fig. 4.15) flatten out in the same test, providing further evidence that the fire did undergo a period of more constant burning before it grew to its peak size.

Figure 4.20 shows time resolved temperature measurements for the baseline HVAC test at the same locations as for the no HVAC test above. The flame temperature in the baseline HVAC test, shown in Fig 4.20a, grows linearly to a peak value of 1043 °C at 5:31 after ignition. The shape of the flame temperature plot is fairly smooth, similar to the trends with time observed in the heat flux measurements from this test. It does not show the same peak and valley during the growth period that is seen in the MLR plot (see Fig. 4.16), but is consistent with the smoother heat flux profile. The peak temperature is reached 13 seconds prior to the peak in fire MLR at which time, the flame temperature has decreased to 924 °C. In comparison to the no HVAC test, the maximum flame temperature is slightly higher while the measured flame temperature at peak fire MLR is slightly lower consistent with the short time during which the fire burned near peak values.

Temperatures measured at T3 2.26 m (Fig. 4.20b) increase through the early growth period of the fire to values of 495 °C at their peak. The slope of the temperature curve increases at 4:22 after ignition, approximately 20 seconds after the increase in slope is observed in the MLR plot shown in Fig. 4.11 for the same test. The overall temperature profile with time measured at T5 2.28 m is similar, although the peak temperature reached at this location is approximately 40 °C higher than the temperature at the similar height (2.26 m) at T3. This difference is also seen at intermediate heights and is likely due to the impact of the HVAC system which supplies cooler OA into the upper hot regions of the fire room closer to T3, resulting in a lower upper layer temperature at that location. At the same time, the hot smoke produced by the fire is directly pulled towards the HVAC exhaust port in the corridor closer to T5. Measured temperatures are similar between the two locations near the floor where there is much less influence of the HVAC system on conditions in the compartment.

Flame temperatures from the 2x baseline HVAC test measured from T1a at 0.93 m

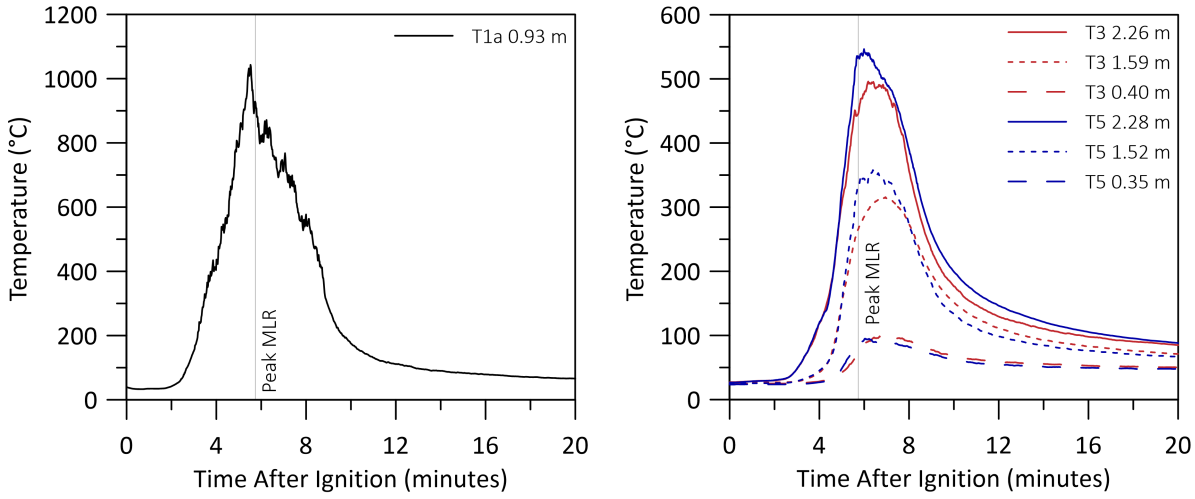

(a) Flame Temperature

(b) Fire Room Temperatures

Figure 4.20: Plots of fire room and flame temperatures over time for the baseline HVAC test.

above the fire room floor over time are shown in Figure 4.21a. These show similar trends as in the previous tests; however, the instantaneous maximum flame temperature in the 2x baseline HVAC test is 933 °C and the flame temperature at peak fire MLR is also lower at 891 °C. These temperatures are over 65 °C cooler than in the previous two tests, a somewhat unexpected result given that increased supply of air into the structure during this test.

Select fire room temperatures at T3 and T5 in the 2x baseline HVAC test are shown in Fig. 4.21b. Temperatures measured by the top thermocouples, T3 2.26 m and T5 2.28 m, are similar for the entire duration of the test, reaching temperatures up to 531 °C with essentially no horizontal temperature gradients (north-south or east-west) evident at this height. Temperatures grow linearly in time until 5:30 after ignition. Following this, the temperature increases more rapidly, consistent with increases in both the fire MLR and heat flux at the same time (see Fig. 4.17). Some differences in peak measured temperatures are evident between T3 and T5 at lower heights. For instance, comparison of peak temperature measured at T3 1.59 m and T5 1.52 m shows that the peak temperature at T3 is 325 °C, which is approximately 25 °C cooler than the peak temperature reached at a similar height on rake T5. On the other hand, comparison of temperatures measured at the lowest heights, T3 0.40 m and T5 0.35 m, indicates slightly higher peak temperatures at T3 than the similar height at T5, opposite to the measured values at the intermediate height. Temperature differences at intermediate and lower positions in this test may be driven by

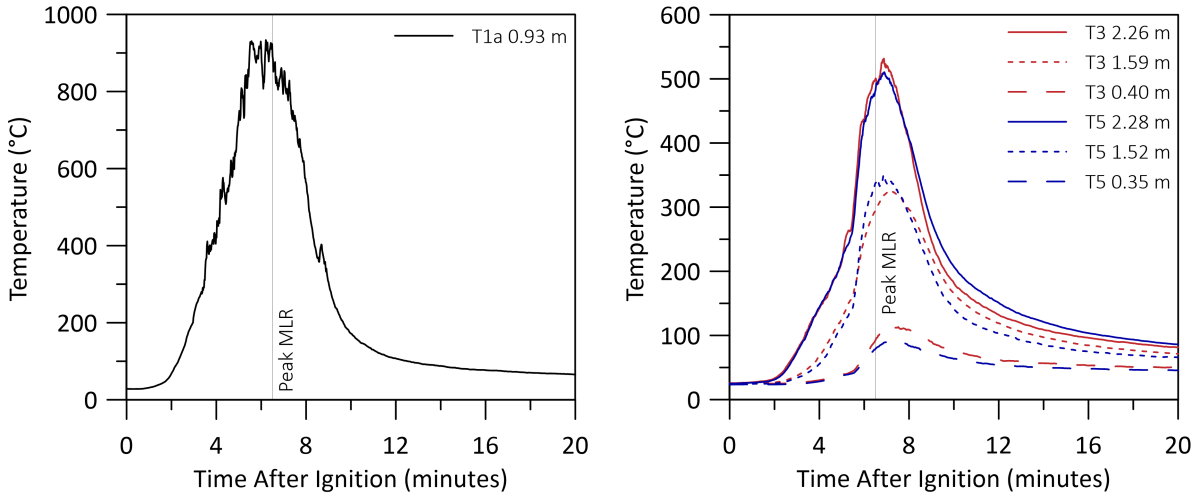

(a) Flame Temperature

(b) Fire Room Temperatures

Figure 4.21: Plots of fire room and flame temperatures over time for the 2x baseline HVAC test.

the higher volumes of cooler OA supplied through the elevated HVAC system impacting the smoke layer in the middle and lower regions of the compartment. For thermocouple locations in closer proximity to the supply vent, the higher flow of supply air in this test will force hotter smoke further down than in previous tests, resulting in cooling of temperatures at intermediate heights and increased temperatures closer to the floor of the compartment. These observations, coupled with the reduced flame temperatures observed in this test with the increased supply of OA to the upper layer of the compartment, is further evidence of the importance of flame-air flow-smoke interactions in under-ventilated compartment fires.

Flame temperature, measured by T1a, is plotted with time in Fig. 4.22a for the re-circulation test. The temperature increases linearly until 3:31 after ignition when there is a sudden increase in the temperature followed by a slow decrease. This occurs approximately one minute prior to similar trends in the fire MLR and fire heat flux with time shown in Fig. 4.18. Measured flame temperature peaks at 950 °C, which is hotter than in the 2x baseline HVAC test but cooler than in the other tests. After the peak, the flame temperature decreases to approximately 800 °C and remains at this temperature for several minutes. This corresponds to the period of time over which double peaks in fire MLR are measured and therefore may also be attributed to the falling of the checker board in the fire room.

Figure 4.22b, shows fire room temperatures plotted over time at T3 and T5, for the

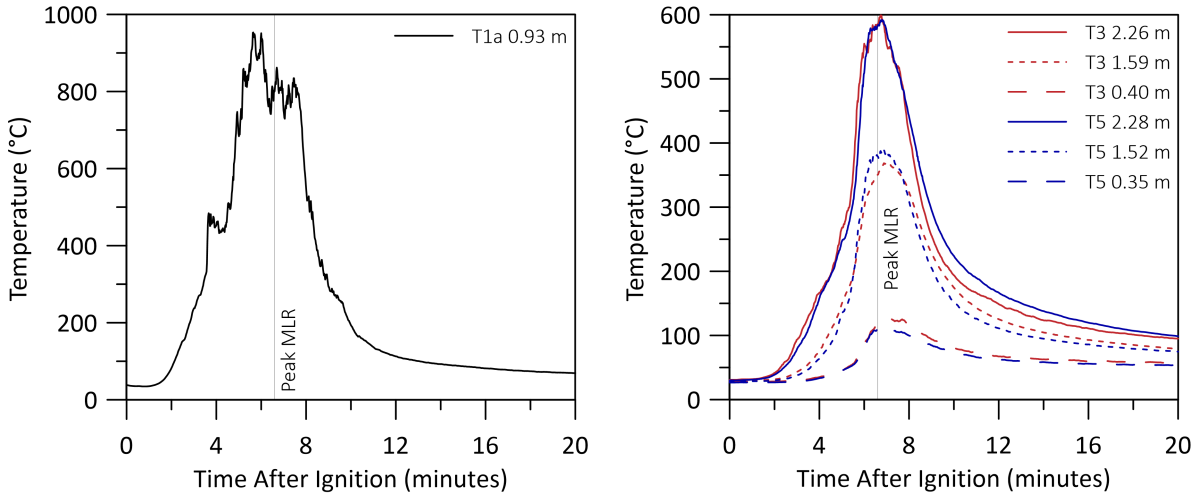

(a) Flame Temperature

(b) Fire Room Temperatures

Figure 4.22: Plots of fire room and flame temperatures over time for the recirculation test.

recirculation test. Temperatures at both thermocouple rake locations are similar throughout the entire test, at each of the three heights shown. Fire room temperatures at the higher heights initially increase linearly as with the flame temperatures in the fire. They increase more rapidly at 5:20 after ignition, the same time as the fire MLR increases after the peak and valley during fire growth in Fig. 4.13. Temperatures near the ceiling reach up to 599 °C at peak, which is approximately 30 °C hotter than in any of the other tests. Peak temperatures near the floor of the compartment increase to 125 °C. This is also hotter, by up to 10 °C, than in any of the other tests. The hotter temperatures throughout the compartment are consistent with the recirculation of heated smoke through the HVAC system.

In summary, temperatures measured by thermocouples placed above the couch cushions in the flames of the fire provide a complementary indication of fire growth patterns to both MLR and heat flux data. Peak flame temperatures are cooler when higher flow rates of OA are supplied in the 2x baseline HVAC test and when the hot flame gases are recirculated in the recirculation test, as compared to flame temperatures in the no HVAC and baseline HVAC tests. In both situations, it could be due to greater under ventilation of the fire: in the first case due to increased volumes of cooler OA driving hot smokey gases toward the fire plume; in the latter, due to recirculation of fire gases back into the fire environment.

The temperatures at thermocouple rakes T3 and T5 in the fire room are similar throughout all the tests. Comparison of temperatures at the same heights above the floor indicates

that there are only very small horizontal temperature gradients between the two locations depending on details of the ventilation configurations. At the same time, there are large temperature gradients with height from floor to ceiling. Fire room temperatures develop linearly with time during the early slower growth phase of all the fires and then increase more rapidly shortly after the fire growth rate (MLR) increases. When OA is supplied in the baseline HVAC configuration, temperatures at T3 in the centre of the fire room are cooler than at T5 closer to the main floor corridor. This is because the outside supply air mixes with hot fire gases leading to cooler temperatures in the vicinity of the supply, at the same time as hot fire gases are preferentially pulled towards the exhaust port. In contrast, when the supply of OA is doubled in the 2x baseline HVAC configuration, temperatures become more spatially uniform. This may be attributed to further increases in mixing between the hot fire gases and supply air, leading to destruction of the smoke layer with the increased flow rates.

Figure 4.23 compares compartment temperatures across all four tests in the centre of the fire room (T3), at the top of the stairs (T11), and in the centre of the small bedroom (T10). These locations represent positions near the fire as well as in far field locations, for the purpose of describing the difference in environmental development throughout the structure. The figure shows profiles of temperature versus height at three selected key times: at ignition of the second cushion, at peak MLR, and when 15% O_2 is reached on the upper floor as measured at GIS 6 0.9 m in the small bedroom. These times are the same as used in previous discussions of fire development. They correspond to early fire growth during well ventilated conditions, developed temperatures near the peak, and temperatures after flame out of the fire, respectively.

In the centre of the fire room at ignition of the second cushion, temperatures near the ceiling have increased to 180 °C in all four tests . Temperature profiles are similar across tests, with temperatures within 25 °C at each height. At the higher elevations, temperatures measured in the recirculation test are the hottest while those in the 2x baseline HVAC test are the coolest. At peak MLR, temperatures in the centre of the fire room have increased to 550 °C near the ceiling and 60 °C near the floor, with a fairly linear temperature gradient with height. At this time, the recirculation test remains the hottest, followed by the no HVAC test, the 2x baseline HVAC test, and the baseline HVAC test has the coolest temperatures. Peak temperatures are measured in the fire room shortly after peak fire MLR is recorded in all four tests. Even taking into account the thermal inertia of the ambient gases and two second response time for the thermocouples, this suggests that the fires continue to produce enough heat to increase hot gas temperatures for a short period even after the fires begin to decay. By the time O_2 concentrations have decreased to 15% on the upper floor, the fire has passed peak MLR and temperatures in the fire room

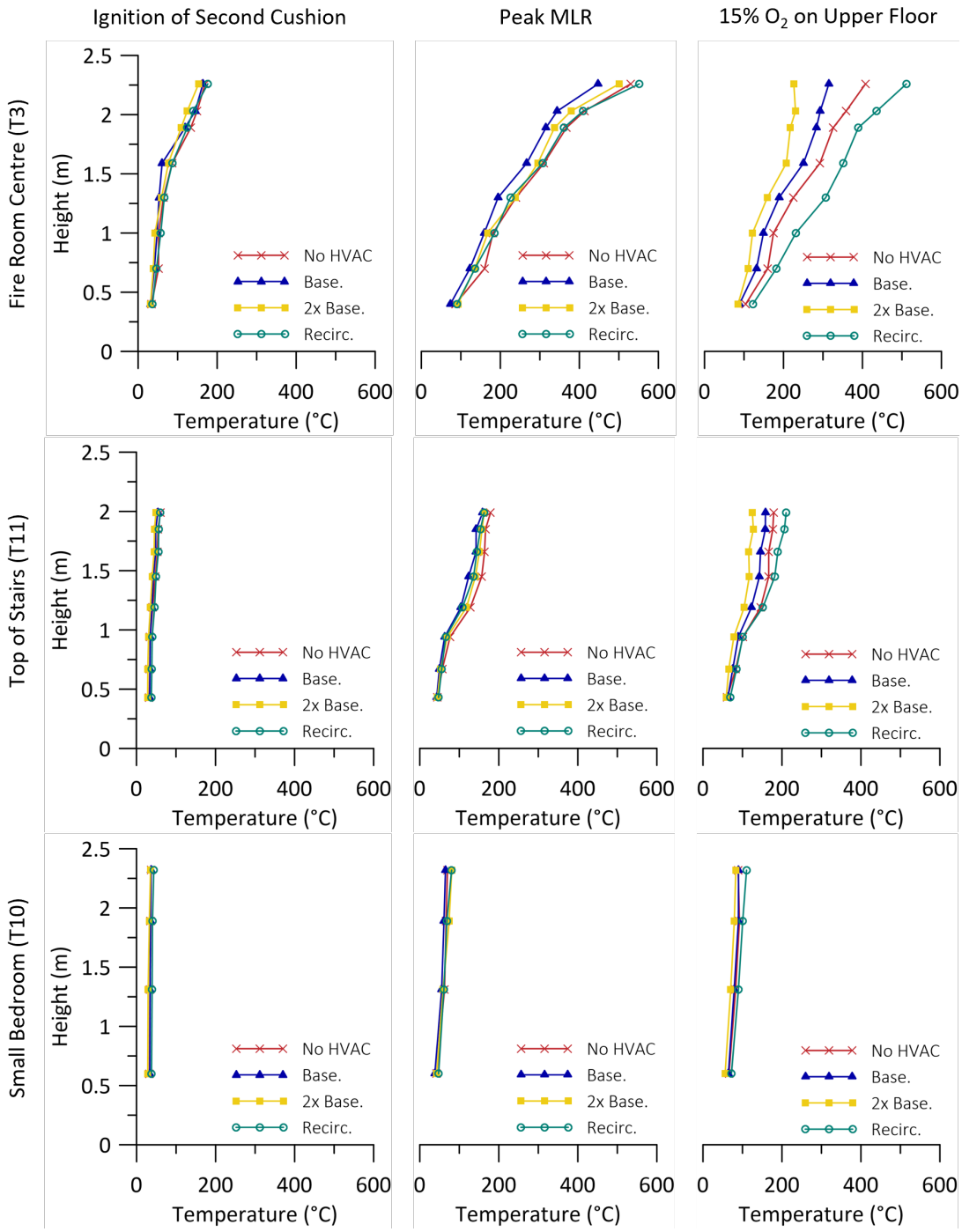

Figure 4.23: Plots of temperature versus height profiles as measured in the fire room (T3), at the top of the stairs (T11), and in the small bedroom (T10) at selected key times.

have begun to cool. The greatest differences between measured temperatures across tests are seen at this time, with maximum differences of up to 285 °C between the recirculation and 2x baseline HVAC tests near the ceiling. The hottest temperatures are recorded at all heights in the recirculation test, followed by the no HVAC test, the baseline HVAC test, and the 2x baseline HVAC test has the coolest temperatures. The impact of recirculating hot fire gases back into the fire environments are evidenced in the temperatures measured during recirculation test which only cool by 40 °C between peak fire MLR and the time O_2 concentrations reach 15% on the upper floor. The opposite effect is seen in the baseline HVAC and 2x baseline HVAC tests in which the supply of cooler OA results in increased cooling of the compartment environments once the fire has decayed. This is enhanced by an increased time of cooling in the baseline HVAC and 2x baseline HVAC tests. The no HVAC and recirculation tests both have one minute and 33 seconds for the fire environment to cool between the time of peak fire MLR and time when 15% O_2 is measured on the upper floor. In contrast, the baseline and 2X HVAC tests have two minutes and 32 seconds and two minutes and 43 seconds, respectively, for cooling because the supply of fresh OA into the small bedroom prolongs the time required for the oxygen concentration to reduce to 15%.

Temperatures at the top of the stairs increase at most by 30 °C between the start of the test and ignition of the second cushion. When the second cushion ignites, temperature profiles with height are fairly uniform and are similar between all four tests, with a maximum temperature difference of only 11 °C at the top thermocouple. By the time of peak fire MLR, the temperature profiles in all tests have developed into a more classic two-zone profile. In this case, the temperatures below 1.0 m above the floor are uniform and the temperatures above approximately 1.5 m off the floor are also fairly uniform, but are hotter than the temperatures at the lower heights. Temperatures near the top of the doorways reach 180 °C while those near the bottom of the doorway are near 47 °C. These profiles illustrate the layering of the hot smoke flowing up the staircase on top of the cooler, fresher air flowing down the staircase. The temperature profiles are similar between all four tests, with a maximum difference of 33 °C occurring at 1.45 m above the floor. The hottest temperatures are measured in the no HVAC test, while the coolest are in the baseline HVAC test. The largest differences in temperatures at the top of the stairs between tests are seen at the time that 15% O_2 is reached on the upper floor, after the fire has extinguished. Between the time of peak fire MLR and 15% O_2, temperatures have increased by approximately 20 °C near the bottom of the doorway for all tests. During the same time period, temperatures near the top of the doorway remain nearly constant in the no HVAC and baseline HVAC tests, have begun to cool in the 2x baseline HVAC test, and have continued to increase in the recirculation test. There is an 85 °C difference in temperature at the top

of the doorway between the tests, with the hottest temperature of 210 °C measured in the recirculation test and the coolest of 179 °C in the 2x baseline HVAC test. This pattern is the same as seen in the centre of the fire room, and is consistent with recirculation of gases leading to hotter temperatures and increased supply of OA producing cooler temperatures.

At the centre of the small bedroom, the temperatures throughout the tests remain much cooler compared to the other locations presented. This is expected due to the increased distance from the fire to the small bedroom. As it travels, the hot smoke cools through mixing with cooler, fresher air and additional heat losses to the compartment walls. When the second cushion ignites, the temperatures in all four tests at the centre of the small bedroom are uniform in height, with only a 7 °C difference between floor and ceiling, and all remain within 10 °C of ambient. By the time of peak fire MLR, temperatures approach 80 °C near the ceiling and 48 °C near the floor due to flow of hot smoke into this region. Temperatures between tests vary at most by 16 °C, with the recirculation test having the hottest temperatures and the baseline HVAC test having the coolest. Temperatures in the small bedroom continue to rise from the time of peak fire MLR until 15% O_2 concentration is reached on the upper floor. Temperatures are still quite low, ranging between 90 °C to 110 °C near the ceiling and between 55 °C to 72 °C near the floor at the time when 15% O_2 is reached on the upper floor. Again, the recirculation test has the hottest temperatures, while the 2x baseline HVAC test has the coolest, and the no HVAC and baseline HVAC tests have intermediate temperatures within a few degrees of each other.

In general, differences between the tests are minor during early stages of fire growth up until peak fire size, especially near the floor of the compartments. The largest differences are observed in the upper layer of the compartments during later stages of the tests after flame out and when the environment is recovering back to ambient conditions. Supplying OA through the HVAC system results in cooler compartment temperatures, while recirculating smoke through the HVAC system effectively traps in heat and results in higher compartment temperatures, particularly in the later stages of the tests. The effects of the HVAC system are most marked in temperatures measured in the fire room, but can be observed at far field locations as well. In general, temperature profiles in the far field are more uniform with height, suggesting a well-mixed thermal environment on the upper floor.

4.4 Smoke Flow

Buoyant flow through the doorways of a structure is typically responsible for the majority of the smoke and air transport in a fire induced environment. The flow of hot smoke away

from the fire room to adjoining compartments is responsible for the transport of toxic gases to far field locations, and the flow of fresher air into the fire room is the main supply of fresher air to the fire. In this section, details of smoke and gas flow throughout the burn house for the current tests are characterized using time resolved measurements of velocity at multiple points in each doorway of the structure. Comparisons between the four tests are made for profiles of velocity versus height, velocity fluctuations, and mass flow rates through the openings.

4.4.1 Doorway Velocity Profiles

The following figures and surrounding discussion characterize the development of gas velocity at each doorway in the structure for the no HVAC test as a reference case. Comparisons between the tests are also made at each doorway using velocity versus height profiles at three key times: (1) ignition of the second couch cushion, (2) peak MLR, and (3) after the flow reversal occurs. These key times are selected for similar reasons as the key times for the fire development discussed in the previous section. They provide a point for comparison during fire growth, at the fire peak, and during fire decay. Specific to (3), a flow reversal occurs in each test as the temperatures in the compartments cool and pressures rebalance throughout the structure[3]. The flow reversal times selected for the plots are shortly after the net mass flow of smoke/air changes from out of the fire room to into the fire room. Therefore, point (3) occurs at slightly different times in each test, but the times chosen are representative of the same phenomenon for comparison. In the no HVAC test the flow reversal time used for the plots is therefore 17:40 after ignition, for the baseline HVAC test it is 17:20, for the 2x baseline test it is 18:25, and for the recirculation test it is 15:40. The times for the other two events are found in Table 4.1.

One path for smoke flow is from the fire room to the kitchen, and vice versa for air from the kitchen into the fire room. There are two doorways in this path: the fire room/kitchen doorway directly connects the two compartments, and the corridor/kitchen doorway connects the compartments via the main floor corridor. Figure 4.24 shows plots of velocity over time as measured by the bidirectional pressure probes in these two doorways, for the no HVAC test. Each of these doorways is instrumented with two velocity probes located 0.39 m and 1.63 m above the floor in the fire room/kitchen door and 0.44 m and 1.61 m in the corridor/kitchen door as listed in the legends for the two plots in Fig. 4.24. A positive velocity represents a flow from the fire room or corridor into the kitchen, and a negative velocity represents a flow from the kitchen back into the fire room or corridor.

[3]This phenomenon is discussed further in the velocity results.

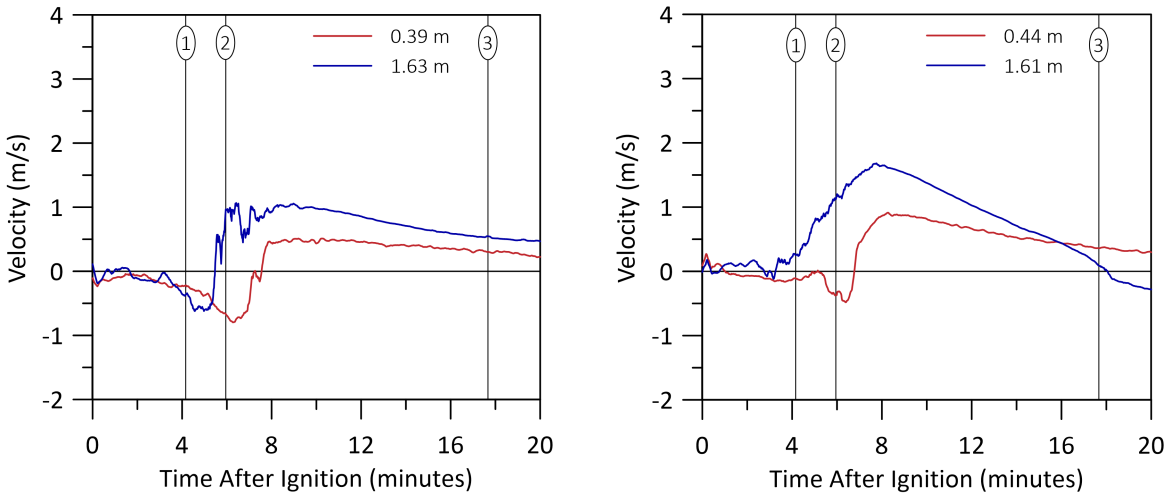

(a) Fire room/kitchen door

(b) Main floor corridor/kitchen door

Figure 4.24: Plots of velocity versus time as measured by the bidirectional pressure probes in the kitchen doorways with vertical timelines at (1) ignition of the second cushion, (2) peak MLR, and (3) after the flow reversal.

In the early growth stages of the fire, prior to ignition of the second cushion, negative values of measured velocity in the doorway between the fire room and the kitchen slowly increase due to a flow of air from the kitchen towards the fire through this opening. Following this, the direction of velocity changes as the ceiling smoke layer in the fire room becomes established and higher temperature smoke in the fire room begins to flow through the doorway to the adjoining compartment. This transition occurs first at the upper probe, between ignition of the second cushion and peak MLR, and later, after the peak MLR, at the lower doorway probe due to the time it takes for the smoke layer to descend and flow from the fire room to the kitchen at the lower heights. Positive measured velocities at both probes indicate flow of smoke from the fire room to the kitchen for the remainder of the test, decreasing in value gradually over time.

The velocity-time profiles measured in the corridor/kitchen doorway follow similar trends. Measured velocity at both probe locations is very small until after ignition of the second cushion. The velocity at the upper probe then begins to increase in the positive direction and the velocity at the lower probe increases in the negative direction. The contrast between velocity values measured at the kitchen-fire room door and the low measured velocities at the corridor/kitchen doorway during the early stages of the fire suggest that the fire draws more air through the kitchen/fire room doorway than from the far end of

the corridor. At the same time, little smoke is accumulating at the ceiling and flowing down the corridor and into the kitchen until the fire has grown and spread to the second couch cushion. After the fire reaches its peak, the direction of velocity at the lower probe changes, similar to the fire room/kitchen doorway, and indicates flow of smoke from the fire room down the corridor for the remainder of the test. Interestingly, the velocity measured at the upper probe in this doorway decreases at a faster rate over time than at the lower probe as the fire decays. Measured velocities at the upper probe also subsequently change direction suggesting a flow of hotter gases back toward the fire room after the flow reversal.

Figure 4.25 compares the velocity versus height profiles at the fire room/kitchen doorway for all four tests at the three times described above[4]. Common across all four tests, the velocity at both probes at ignition of the second cushion (Fig. 4.25a) indicates flow from kitchen to fire room. The magnitudes of the velocities at each probe are also very similar across all tests. At the lower probe (0.39 m), velocities range from −0.20 m/s to −0.29 m/s, with the slowest velocity for the 2x baseline HVAC test and the fastest for the recirculation test. At the upper probe (1.63 m) measured velocities are higher in magnitude, ranging from −0.32 m/s to −0.36 m/s, with the baseline HVAC test having the slowest velocity and the no HVAC test having the fastest. In this case, the difference is only 0.04 m/s or approximately 12% across tests suggesting very similar flow of air toward the fire in all cases.

At the time of peak MLR of the fire, (Fig. 4.25b), velocities indicate that a two-way flow across the doorway has developed in all tests. Smoke is flowing from the fire room into the kitchen, and air from the kitchen is flowing into the fire room. Velocities at the lower probe are between −0.62 m/s and −0.84 m/s, with the slowest measured velocity for the 2x baseline HVAC test and the fastest for the recirculation test consistent with differences seen when the second cushion ignites. The velocities at the upper probe are between 0.34 m/s and 0.97 m/s, with the 2x baseline HVAC test having the slowest velocity and the no HVAC test having the fastest. More significant differences in doorway velocity profiles are seen at this time, now that the fire induced flow has developed. Trends in the velocity profiles suggest that increasing HVAC flow rates reduces the flow velocities through the fire room/kitchen doorway. Increased supply of OA into the kitchen may increase the pressure in the kitchen and, therefore, provide additional resistance to any flow of smoke into the kitchen.

After the flow reversal (Fig. 4.25c), measured velocities at the upper probe have decreased in magnitude and the velocities at the lower probe have changed direction sug-

[4]There are only two probe locations in the doorway, therefore linear fit profiles are used to illustrate the results.

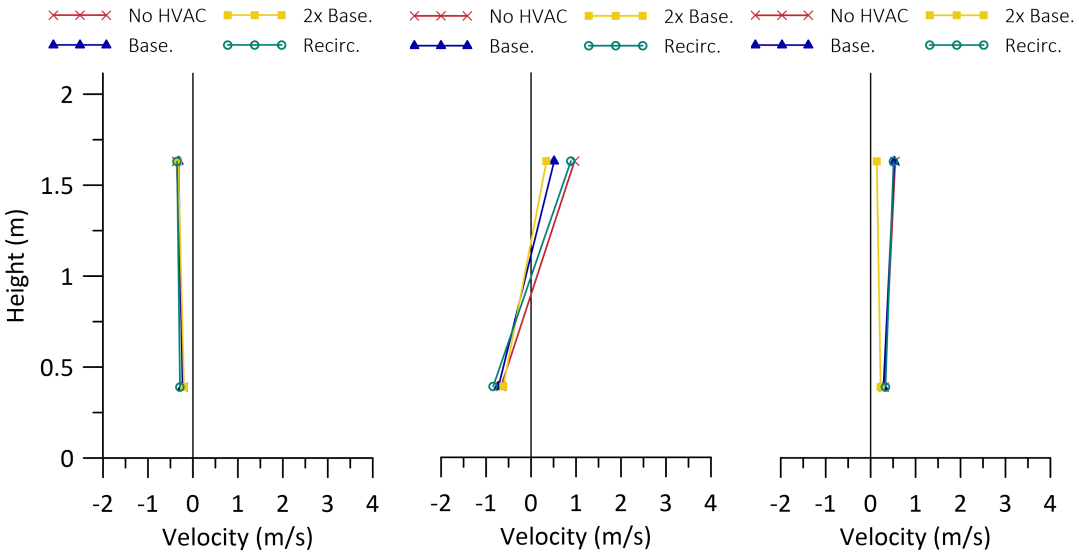

(a) Ignition of second cushion **(b)** Peak MLR **(c)** After flow reversal

Figure 4.25: Plots of velocity versus height as measured in the fire room/kitchen doorway at selected key times.

gesting a one way flow of smoke from the fire room into the kitchen in all tests. Velocities at the lower probe range from 0.22 m/s to 0.33 m/s, with the 2x baseline HVAC test having the slowest velocity and the recirculation test having the fastest, consistent with values measured at previous times. Velocities at the upper probe range from 0.14 m/s to 0.55 m/s, with the 2x baseline HVAC test having the slowest velocity and the no HVAC test having the fastest. At both locations, the velocity of the 2x baseline HVAC test is clearly slower compared to the other tests, which are all within 0.04 m/s at both the upper and lower probes. The significantly slower velocities in the 2x baseline HVAC test after the flow reversal may also be affected by the continued supply of additional OA to the kitchen.

The velocity versus height profiles at the key times for the corridor/kitchen doorway are shown in Fig. 4.26. At the time of ignition of the second cushion (Fig. 4.26a), a two-way flow profile across the door has developed, although the flow velocities are very slow. At the lower probe, the velocities range from −0.05 m/s to −0.16 m/s, with the slowest velocity for the 2x baseline HVAC test and the fastest for the baseline HVAC and recirculation tests, comparable to test to test variations noted for the kitchen-fire room doorway. Velocities at the upper probe range from 0.16 m/s to 0.30 m/s, with the slowest velocities measured in the recirculation test and the fastest in the 2x baseline HVAC test. Velocities measured at both probe locations are lower compared to those measured at the

fire room/kitchen doorway, consistent with the longer travel distances down the corridor resulting in greater cooling of the hot gases and loss of flow momentum.

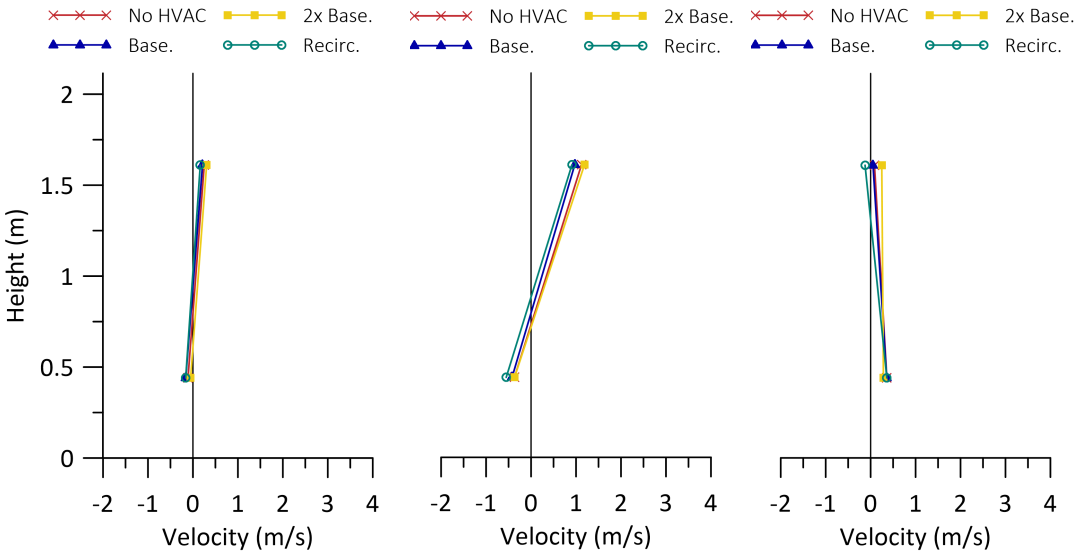

(a) Ignition of second cushion **(b)** Peak MLR **(c)** After flow reversal

Figure 4.26: Plots of velocity versus height as measured in the main floor corridor/kitchen doorway at selected key times.

At peak MLR of the fire, (Fig. 4.26b), the two-way flow profile has developed further in all four tests, with velocities at the lower probe between −0.37 m/s and −0.55 m/s. Velocities measured in the 2x baseline and the no HVAC tests are slowest and those in the recirculation test are fastest. Velocities at the upper probe are between 0.91 m/s and 1.19 m/s, with the slowest velocity in the recirculation test and the fastest in the 2x baseline HVAC test.

After the flow reversal, measured velocities at the lower probe change direction in all four tests. At the upper probe, the velocities for the no HVAC test, baseline HVAC, and 2x baseline HVAC decrease in magnitude and remain positive, while the velocity in the recirculation test changes direction. Velocities at the lower probe range from 0.28 m/s to 0.36 m/s, slowest for the 2x HVAC test and fastest in all the other tests. Velocities at the upper probe range from −0.12 m/s to 0.25 m/s, with the negative velocity in the recirculation test, the fastest positive velocity in the 2x baseline HVAC test, and slower positive velocities of less than 0.1 m/s in the other two tests.

Another major path for smoke and air flow is from the fire room up the staircase to the

upper floor. The smoke enters the staircase from the doorway at the bottom of the stairs and flows towards the upper floor through the doorway at the top of the stairs. Figure 4.27 shows velocity plotted over time as measured by the eight bidirectional pressure probes in each of these two doorways for the no HVAC test as a reference case. The probes are installed at heights between 0.39 m to 1.99 m at the bottom of the stairs, and between 0.42 m to 1.97 m at the top of the stairs, as listed in the legends of the plots. Only seven probes are shown in the plot for the bottom of the stairs because the probe at 0.90 m malfunctions during the test and is therefore removed from the data. For both doorways, a positive velocity represents flow from the fire room up the stairs and into the upper floor, and a negative velocity represents flow from the upper floor down the stairs and into the fire room.

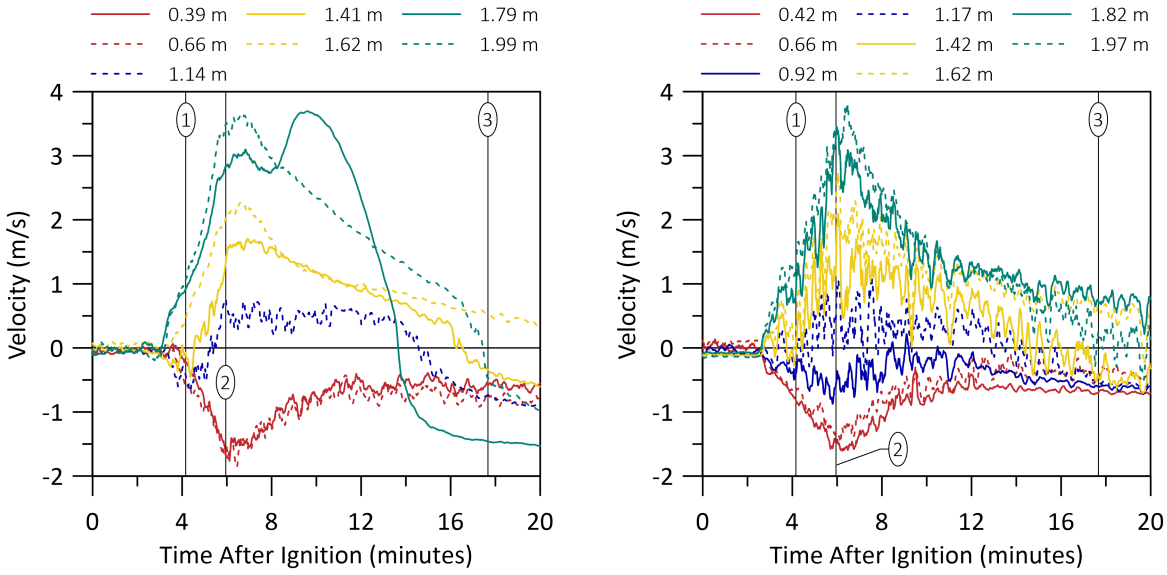

(a) Bottom of staircase

(b) Top of staircase

Figure 4.27: Plots of velocity versus time as measured by the bidirectional pressure probes in the staircase doorways with vertical timelines at (1) ignition of the second cushion, (2) peak MLR, and (3) after the flow reversal.

The plots show that the velocities at the bottom and top of the stairs develop in a similar fashion over the course of the test as expected since flow into one of these doorways should be matched at the other to conserve mass. In the early stages of fire growth, the velocity at all probes is close to zero. At approximately 3:00 after ignition, the velocities at lowest four probes at the bottom of the stairs increase in a negative direction, while

velocities at the other probes increase in the positive direction. After ignition of the second cushion, velocities at the 1.14 m and 1.41 m probes begin to decelerate and ultimately change direction. Peak velocities of up to 3.5 m/s in the positive direction and −1.7 m/s in the negative direction are reached at or shortly after the time of peak MLR of the fire for all probes except the 1.79 m probe. The velocities at the probes that do peak, gradually decrease throughout the decay phase of the fire until closer to the flow reversal. The velocity measured by the probe at 1.79 m appears anomalous since it increases velocity at approximately 8:00 and peaks at around 9:30 after ignition . The same velocity pattern occurs in all tests suggesting that it may be an actual flow event; however, there is no clear explanation for the observed trend. By the time of flow reversal, measured velocities at most probes are negative, indicating that most of the flow at the bottom of the stairs is into the fire room. At the top of the stairs, the velocities develop in a similar manner, with peaks of up to 3.4 m/s for flow from the fire room to −1.4 m/s for flow to the fire room. Velocity measurements at these locations have larger and more frequent fluctuations than observed in those at the bottom of the stairs. This indicates that there is increased mixing at the top of the stairs, which has important implications in terms of the development of the environment on the upper floor, as discussed previously for temperatures in Sec. 4.3 and will be discussed for species concentrations in Sec. 4.5. Further discussion on velocity fluctuations and mixing throughout the house is presented later in Sec. 4.4.3.

Velocity versus height profiles at the bottom of the stairs are compared between the four tests at the three key times in Fig. 4.28. In general, the profiles at all three times are similar across tests. At ignition of the second cushion (Fig. 4.28a), the velocity profile indicates development of two-way flow through the opening, with smoke leaving the fire room above approximately 1.5 m above the floor and air entering the fire room at heights below this level. The development of two-way flow occurs earlier at this location compared to the kitchen doorways because the doorway opening at the bottom of the stairs extends to the ceiling, higher than at the kitchen doors. Therefore, less smoke needs to accumulate at the ceiling before smoke begins flowing through this doorway. Velocity differences between the tests range between 0.04 m/s and 0.35 m/s with the largest differences occurring at the bottom probe (0.39 m) and the middle probes (1.41 m and 1.62 m). There is no consistency between which test exhibits the fastest or slowest velocity.

Two-way flow through the doorway at the bottom of the stairs has further developed by the time of peak fire MLR (Fig. 4.28b), marked by fairly linear profiles of velocity between 0.66 m to 1.99 m above the floor. Velocity at the bottom probe (0.39 m) is nearly the same as the probe directly above it in all four tests. Velocity differences between the tests vary from 0.10 m/s to 1.08 m/s, although most locations show less than 0.28 m/s difference, except for the 1.14 m probe. The largest differences in measured velocities between tests

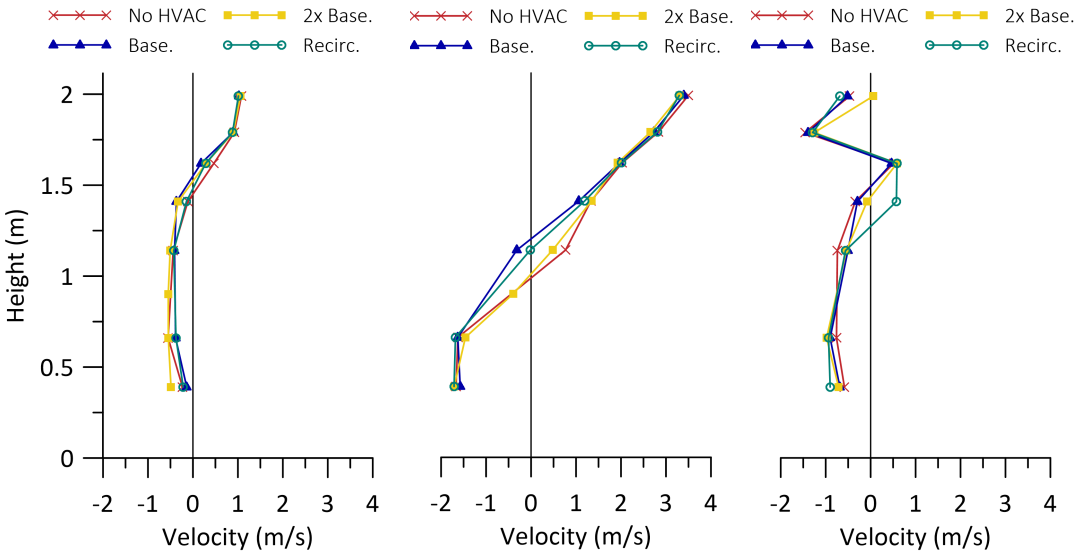

(a) Ignition of second cushion **(b)** Peak MLR **(c)** After flow reversal

Figure 4.28: Plots of velocity versus height as measured in the doorway at the bottom of the staircase at selected key times.

occur around the middle of the doorway between 0.9 m to 1.5 m above the floor. From the middle of the doorway to the top of the doorway, the no HVAC test consistently has the fastest measured velocity. This is opposite to the kitchen doorways, in which the 2x baseline HVAC test is consistently the slowest and the recirculation test the fastest.

After the flow reversal (Fig. 4.28c), the velocity profiles clearly favour the negative direction suggesting flow into the fire room. The anomaly of measured values of velocity at the probe 1.79 m above the floor is observed in the profiles of all tests. It appears as though there is a region of recirculating flow near the top of the doorway, where velocities below that height are in the opposite direction and the velocity above is significantly slower. Again, the cause of this is unclear, however it is consistent across all four tests. Differences between the velocities of the four tests range from 0.12 m/s to 0.92 m/s and there is no test that consistently has the fastest or slowest velocities. The largest differences are seen in the upper portion of the doorway above 1.4 m. Differences at the probes below this height are all within 0.3 m/s.

Figure 4.29 shows velocity versus height profiles at the top of the staircase for all four tests. The profiles show similar trends across all four tests at each of the three key times. At ignition of the second cushion (Fig. 4.29a), a two-way flow has developed with

velocity profiles similar to the profiles at the bottom of the stairs. Below 1.0 m above the landing, the velocities for all tests are slower than −0.82 m/s, with the fastest velocities occurring at the bottom probe. Velocities at these locations are similar between the four tests, with differences less than 0.22 m/s. Above the 1.0 m height, the velocities vary more significantly between tests. In the recirculation test, positive velocities are measured at 1.7 m and above, while in the no HVAC and the 2x baseline HVAC test positive velocities are measured above 1.62 m, and for the baseline HVAC test velocity is not positive until 1.82 m above the landing. At the middle heights, between 1.17 m and 1.82 m, the velocity differences are between 0.44 m/s to 0.56 m/s, larger than at lower locations. The velocity differences at the top probe are more similar to those of the lower probe, with the largest difference being 0.32 m/s. The fastest velocities are measured at the top and bottom probes in the no HVAC tests, while the 2x baseline HVAC test has the slowest measured velocity. This is similar to the trends seen in the kitchen doorways, but differs from trends in velocity measured at the bottom of the stairs.

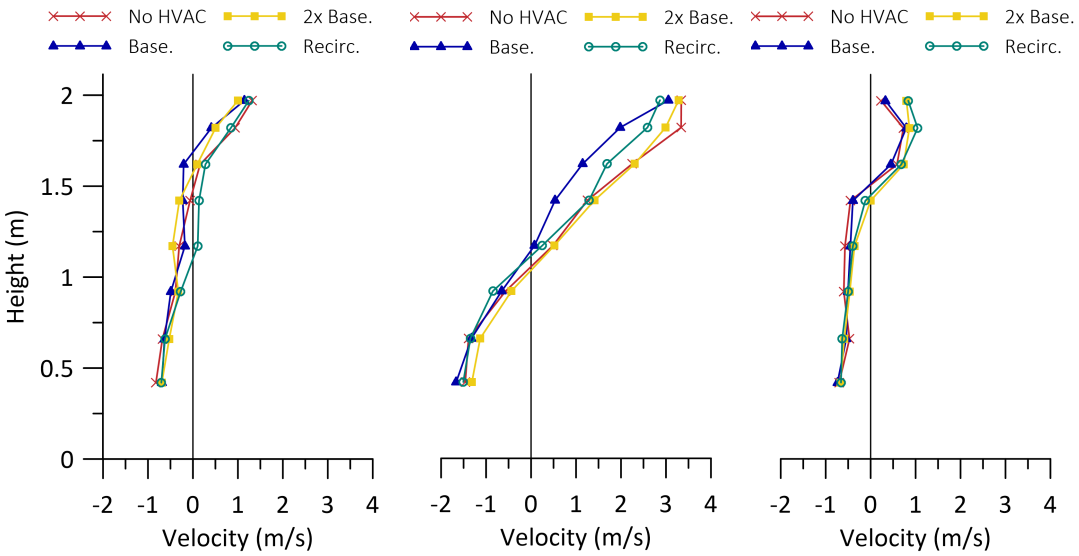

(a) Ignition of second cushion **(b)** Peak MLR **(c)** After flow reversal

Figure 4.29: Plots of velocity versus height as measured in the doorway at the top of the staircase at selected key times.

At peak MLR of the fire, (Fig. 4.29b), profiles of velocity with height indicate further development of two-way flow across the doorway at the top of the stairs. The fastest positive velocities of up to 3.34 m/s are measured at the top probe, and the fastest negative velocities of up to −1.66 m/s at the bottom probe. In this case, measured velocities at the

probes below the 1.0 m height are negative and above this height are positive for all tests. The lower probes show the most consistent velocity measurements across tests, with a maximum difference of 0.44 m/s. The locations with the largest velocity differences are those probes between 1.42 m and 1.82 m, with differences between 0.88 m/s and 1.35 m/s, respectively. This is consistent with measurements at the bottom of the stairs, where the largest differences between tests are found in the middle to upper part of the door. The no HVAC and the 2x baseline HVAC tests result in the fastest velocities of smoke flow from the fire room up the stairs and through the doorway at the top of the stairs, while the baseline HVAC test has the slowest. On the other hand, the fastest negative velocities are measured in the baseline HVAC test, while the slowest are measured in the 2x baseline HVAC test.

After the flow reversal (Fig. 4.29c), velocities have decreased at all probes for all tests. The velocity of the flow at 1.17 m and 1.42 m above the landing has changed direction, indicating flow down the stairs back into the fire room at all probes below 1.42 m above the landing. Further, profiles below this height show very little change in velocity with height. The smallest differences in velocity between the tests, less than 0.16 m/s, occur at the bottom three probes, while the largest differences, between 0.21 m/s and up to 0.6 m/s are seen at the upper probes. Positive velocities are measured at probes positioned at 1.62 m and higher leading to a fairly unique profile, where measured velocity is slower at the top probe than at the one below it. This suggests some similarity to the flow profile at the bottom of the stairs after flow reversal, where there is evidence of a recirculation zone; however, the difference in velocity between the upper probes is not as significant at the top of the stairs as it is at the bottom of the stairs.

Smoke flowing up the staircase carries its momentum into the landing at the top of the stairs and impinges against the back wall of the landing. From there, the smoke must turn 90° to either flow into the small bedroom, through the small bedroom doorway, or into the upper floor corridor and ultimately into the large bedroom, through the large bedroom doorway. Figure 4.30, shows velocity plotted against time as measured by the bidirectional pressure probes in these two doorways for the no HVAC test as a reference case. The small bedroom doorway is equipped with four probes at heights of 0.38 m, 0.89 m, 1.14 m, and 1.59 m. They are installed such that a positive velocity represents a flow from the landing into the bedroom and a negative velocity represents a flow from the bedroom into the landing. The large bedroom doorway has two probes, similar to the kitchen doorways, installed at heights of 0.38 m and 1.59 m. A positive velocity in the large bedroom doorway represents a flow from the upper floor corridor into the bedroom, and a negative velocity represents a flow from the bedroom into the corridor.

As seen in the plots, the peak velocities at both of the bedroom doorways are lower than

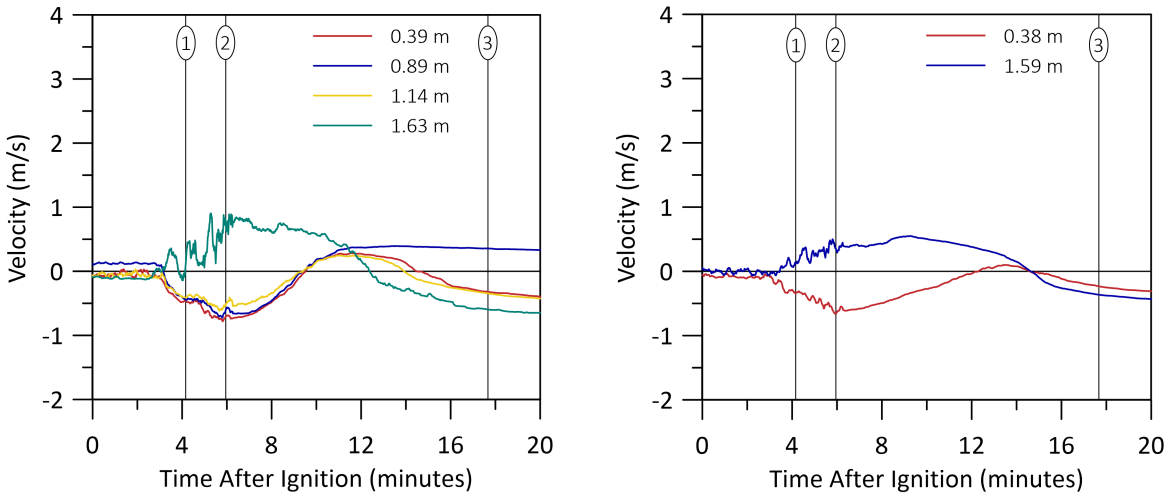

(a) Bottom of staircase **(b)** Top of staircase

Figure 4.30: Plots of velocity versus time as measured by the bidirectional pressure probes in the bedroom doorways with vertical timelines at (1) ignition of the second cushion, (2) peak MLR, and (3) after the flow reversal.

velocities measured at other doorways in the house. This is expected since the bedroom doorways are the furthest points downstream for the smoke flow. There would also be relatively large flow losses in the landing due to the presence of the back wall and required change in flow direction. Peak velocities in the small bedroom doorway are less than 0.87 m/s in either direction. Further losses are experienced in the second 90° corner and longer corridor before smoke enters the large bedroom. Peak velocities at the large bedroom door are therefore the slowest at less than 0.66 m/s in either direction.

Development of the velocities in the small bedroom doorway is consistent with the trends seen in the other doorways throughout the house. In the early growth stages, the velocities are very low and, in general, favour the direction of out of the bedroom. Velocities begin to increase around 3:30 after ignition, comparable to profiles of velocity at the top of the stairs. Probes at and below 1.14 m above the floor measure negative values of velocity, while positive velocities are measured at the probe at 1.63 m height. After the peak MLR of the fire, velocities decrease until approximately 9:25 after ignition when measured velocities at all of the lower probes change direction, indicating that flow is now into the bedroom through the entire doorway. There may be flow in the opposite direction (out of the bedroom) either above the top probe or below the bottom probe, as these heights are missed in the measurements. At 12:25 after ignition the velocity measured at

the top probe changes direction again indicating that a two-way flow is re-established in the doorway. Between 13:00 and 13:30 after ignition, the bottom probe and the probe at the 1.14 m height change direction such that flow is predominantly out of the bedroom. This corresponds to the onset of the flow reversal. The only outlet for smoke from the small bedroom is through the small bedroom door, so after some time a buildup of smoke in the bedroom creates enough pressure to overcome the force of the smoke flowing into the room from the landing and hence creates a flow reversal. Given the time at which this occurs, the effect is assisted by the decreasing pressure in the fire room caused by reduced generation and cooling of smoke/gases as the fire decays.

Velocities in the large bedroom doorway follow a similar development with time as in the small bedroom doorway. Initially, velocities are low and favour flow into the upper floor corridor. As the smoke flow develops, velocity measured at the bottom probe is negative (smoke into the corridor), while it is positive at the upper probe (smoke into the large bedroom). Similar to profiles in the small bedroom doorway, at 12:15 after ignition, the velocity measured by the bottom probe changes direction indicating one-way flow into the bedroom. Velocity at both probes changes direction again at 14:40 after ignition as one-way flow out of the bedroom is established. The slight delay in these changes, as compared to the small bedroom, is consistent with the large bedroom being further downstream.

Velocity versus height profiles at the small bedroom door for all tests at the key times are shown in Fig. 4.31. The similar profiles indicate that flows on the upper floor develop similarly in each test. At the time of ignition of the second cushion (Fig. 4.31a), the velocity profile is fairly uniform below 1.14 m with negative velocities, while a slow positive velocity is measured at the top probe in all four tests. The velocities at all heights are similar across all four tests, with a maximum difference of 0.12 m/s at the top probe. This follows the trend seen at the other locations where the probes around the 1.0 m to 1.5 m heights have the most variation. There is no consistent ranking in terms of which tests have the fastest or slowest velocities at each height.

At peak fire MLR (Fig. 4.31b), the velocity profiles indicate development of two-way flow across the opening. The profile below 1.14 m suggests fairly uniform negative velocities with height, higher in magnitude than earlier in the fire. Positive velocities at the top probes have also increased in magnitude with time. Again, the largest differences in velocity values between tests occur at the top probe, with a difference of up to 0.76 m/s. The bottom three probes all show similar velocities between the tests, with differences below 0.15 m/s. At this time, the recirculation test has the slowest measured velocities at both the top and bottom probes.

After the flow reversal (Fig. 4.31c), velocity measurements show there is flow out of

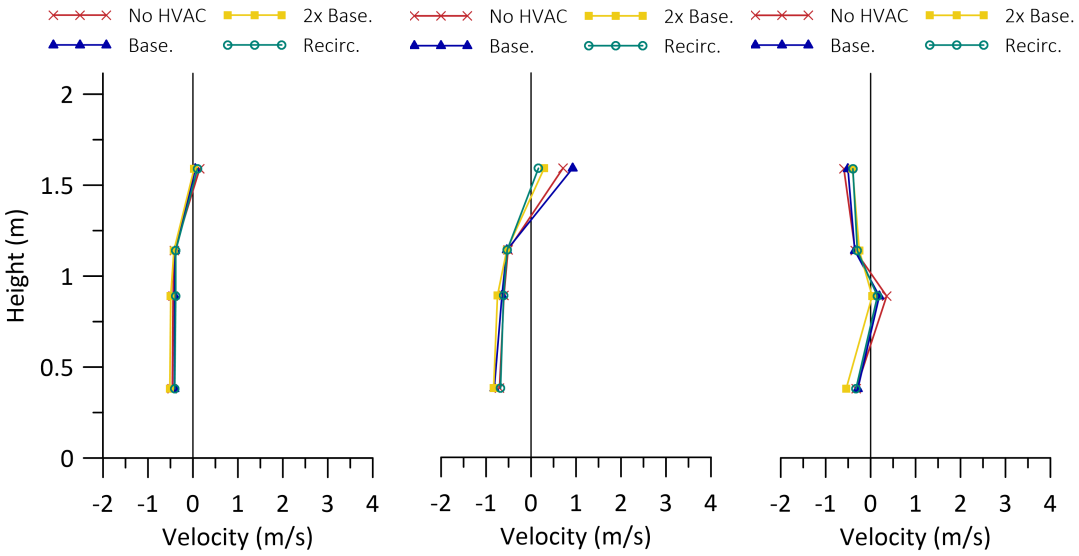

(a) Ignition of second cushion **(b)** Peak MLR **(c)** After flow reversal

Figure 4.31: Plots of velocity versus height as measured in the small bedroom doorway at selected key times.

the bedroom below the bottom probe, then flow into the bedroom around the location of the 0.89 m probe, and flow out of the bedroom above the 1.14 m probe to the top of the door. This illustrates the complexities of flows that occur during the flow reversal and are likely more extreme at the small bedroom doorway because of the proximity of that doorway to the landing. There is increased variation in measured velocity at the lower two probes across tests, which now have differences of 0.26 m/s and 0.32 m/s at 0.38 m and 0.89 m, respectively. Lower differences in velocity, 0.10 m/s and 0.20 m/s, are observed at the 1.14 m and the 1.59 m probes, respectively. There is no consistent ranking for which tests have the fastest or slowest velocities at each height.

Figure 4.32 shows velocity versus height profiles in the large bedroom door for all four tests at the three key times. At ignition of the second cushion (Fig. 4.32a), the velocity profiles for all tests except the 2x baseline HVAC test show two-way flow across the opening. Velocities at the bottom probe (0.38 m) are between −0.22 m/s and −0.34 m/s. At this height, the baseline HVAC test has the slowest velocity and the no HVAC test has the fastest. At the top probe (1.59 m), velocities for the three tests with positive velocities are between 0.12 m/s to 0.19 m/s of one another. The 2x baseline HVAC test has a velocity of −0.07 m/s, and the maximum difference in velocity including all four tests is 0.26 m/s. At this height, the recirculation test has the fastest velocity and the 2x baseline HVAC test

has the slowest (regardless of direction).

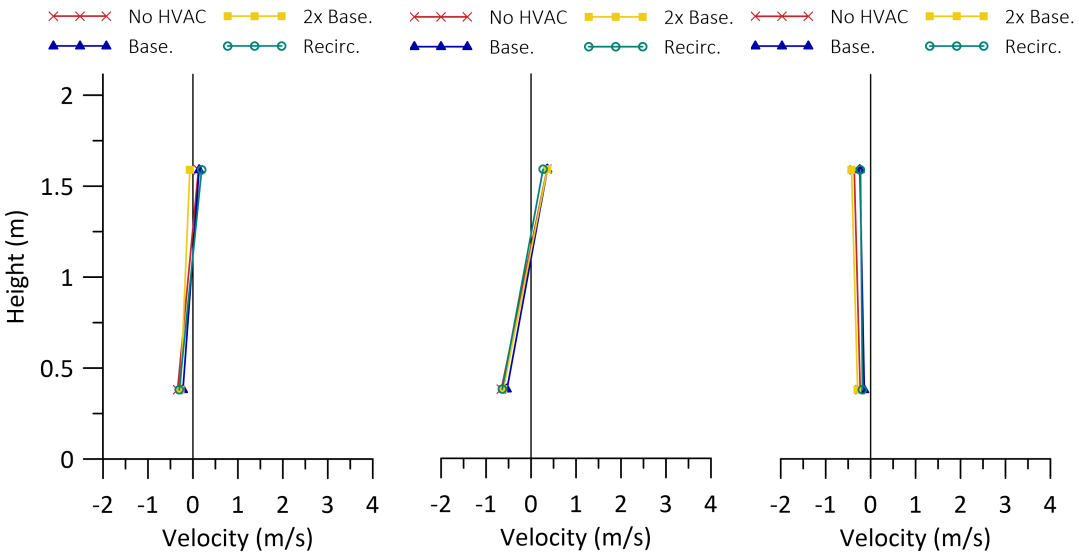

(a) Ignition of second cushion **(b)** Peak MLR **(c)** After flow reversal

Figure 4.32: Plots of velocity versus height as measured in the large bedroom doorway at selected key times.

At peak MLR of the fire, (Fig. 4.32b), measured velocities indicate further development of two-way flow across the opening, with smoke flowing into the large bedroom in the top part of the doorway and air flowing out of the bedroom into the corridor in the bottom part of the doorway. Negative velocity is measured at the bottom probe and positive velocity at the upper probe for all four tests. Velocities at the bottom probe are between $-0.54\,\mathrm{m/s}$ to $-0.66\,\mathrm{m/s}$, with the no HVAC test having the fastest velocity and the baseline HVAC test having the slowest. Velocities at the top probe range from $0.27\,\mathrm{m/s}$ to $0.36\,\mathrm{m/s}$, with the recirculation test having the slowest velocity and the other tests all having the same faster velocity. Slower velocities, coupled with the relatively small differences between tests, further shows the effects of losses on smoke flow rates as number of turns and distance downstream of the fire increases.

After the flow reversal (Fig. 4.32c), the velocities have slowed and the velocities measured at the top probe have changed direction, showing one-way flow out of the bedroom into the upper floor corridor. This suggests that an increase in pressure in the large bedroom relative to the pressure outside the bedroom causes the flow to reverse. Comparing values across tests, velocities are between $-0.14\,\mathrm{m/s}$ to $-0.29\,\mathrm{m/s}$ at the bottom probe and

between −0.23 m/s to −0.43 m/s at the top probe. At this time, the 2x baseline HVAC test has the fastest velocity at both probes, while the recirculation test has the slowest.

4.4.2 Doorway Mass Flow Rates

In this section, detailed flow rates across each doorway in the structure are presented for the no HVAC test as a reference case, then the mass flow rates into and out of the fire room are compared between the four tests. Comparisons of the flow rates into and out of the fire room are important for additional understanding of the fire dynamics, and also serve as a consistency check on the velocity measurements discussed above. Smoke originating from the fire will first collect along the ceiling of the fire room but as it accumulates, it must flow out of the fire room to the other compartments in the house. These flows are important to better understand tenability of compartments throughout the structure. At the same time, flows of fresher air from other compartments to the fire room are important ventilation for combustion.

Figure 4.33 shows plots of mass flow rates over time for the fire room/kitchen door and the main floor corridor/kitchen door for the no HVAC test. Each plot shows two profiles, one of flow from the fire room to the kitchen, and one of flow from the kitchen into the fire room. At the fire room/kitchen door (Fig. 4.33a), there is initially some flow into the fire room with nearly no flow into the kitchen[5]. As the fire begins to grow, the flow into the fire room increases and eventually peaks at 5:00 after ignition, with a flow rate of 0.88 kg/s. Shortly after this peak, the flow rate into the fire room rapidly decreases, while the flow rate into the kitchen begins to increase. At 7:43, the flow rate into the fire room through the doorway reduces to 0 kg/s and the flow rate into the kitchen rapidly increases. There is now a one-way flow of smoke into the kitchen for the remainder of the test. The maximum flow rate into the kitchen occurs at 10:24 with a flow rate of 1.23 kg/s. After the peak, the flow rate into the kitchen decays linearly until the end of the test.

There is almost no flow through the main floor corridor/kitchen door (Fig. 4.33b) until 4:00 after ignition, when the flow rate of smoke down the corridor and into the kitchen begins to increase. There is a small amount of flow into the corridor between 2:44 to 3:34 and 5:25 to 6:44 after ignition with maximum flow rates of 0.27 kg/s and 0.24 kg/s, respectively. After 6:44 after ignition, the flow rate into the corridor reduces to 0 kg/s while the flow rate into the kitchen rapidly increases. The flow rate into the kitchen then peaks at 9:11 after ignition reaching a maximum flow rate of 2.08 kg/s. After the peak, the flow

[5]Mass flow towards the fire room is shown as a negative value in the plots for better visualization of mass balance. Direction and magnitude of the flows are also provided in the discussion.

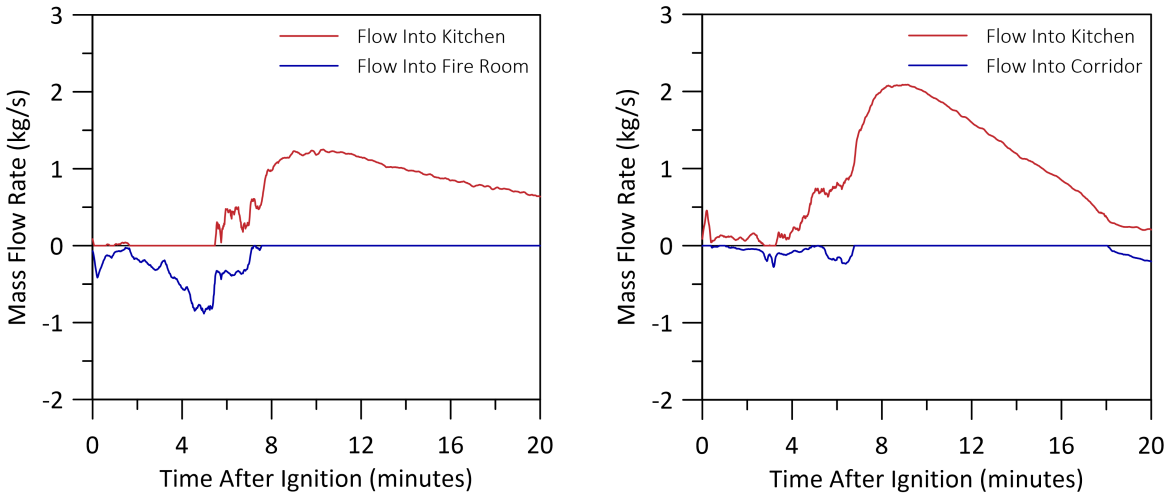

(a) Fire room/kitchen door **(b)** Main floor corridor/kitchen door

Figure 4.33: Plots of total mass flow rate into the kitchen and into the fire room or main floor corridor through the kitchen doorways.

rate into the kitchen decreases linearly until 18:14 after ignition, when the flow rate into the corridor re-establishes and there is again two-way flow in the doorway.

Figure 4.34 shows plots of mass flow rates over time for the no HVAC test for the doorways at the bottom and top of the stairs. Flows at the bottom of the stairs are between the fire room and the staircase, and at the top of the stairs flow is between the upper floor landing and the stairs. At the bottom of the stairs (Fig. 4.34a), there is only a small flow rate into the fire room until 3:25 after ignition when the flow rates in both directions begin to increase. The flow rates are then fairly well-balanced until 6:04 after ignition when the flow rate into the fire room begins to decrease. At this point, the flow into the stairs levels off until 8:10 after ignition, when it increases slightly. Peak flow into the fire room occurs at 6:04 after ignition with a maximum flow rate of 1.37 kg/s, and peak flow into the staircase occurs at 9:32 after ignition with a maximum flow rate of 1.44 kg/s. After the period of peak flow, the flow rate into the staircase decreases for the remainder of the test. The flow rate into the fire room first decreases after the peak and then increases again at 12:00 after ignition until the end of the test, where a flow rate of 1.53 kg/s is reached. This trend of increasing flow into the fire room towards the end of the test is a result of the flow reversal.

At the top of the stairs (Fig. 4.34b), the flow slightly favours flow into the stairs (towards the fire room) at the beginning of the test until 2:45 after ignition. After 2:45

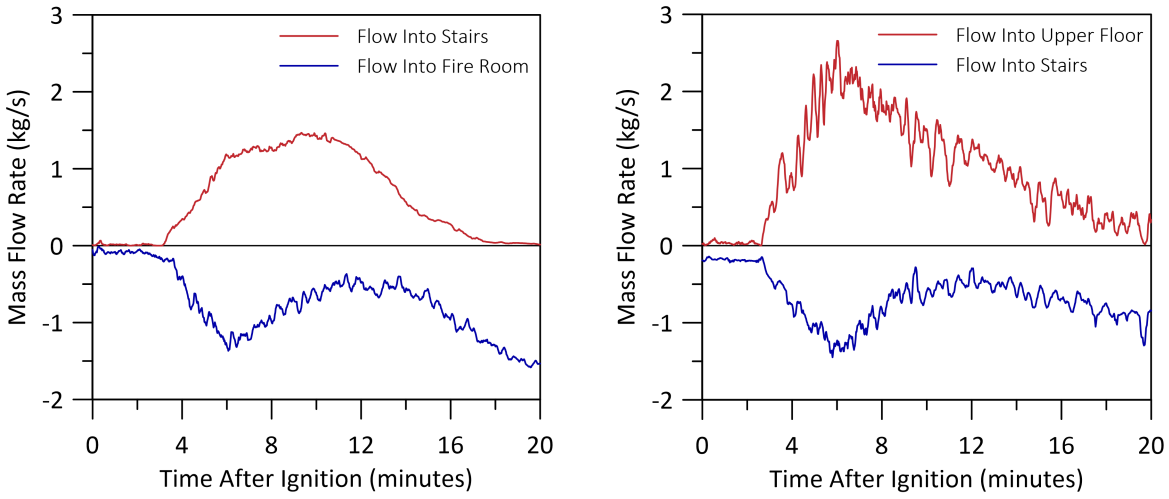

(a) Bottom of Staircase **(b)** Top of staircase

Figure 4.34: Plots of total mass flow rate into the staircase and into the fire room or upper floor landing through the staircase doorways.

into the fire, flow rates in both directions start to increase, with the flow rate into the upper floor developing faster than the flow rate into the stairs. Peak flow into the upper floor occurs at 6:04 after ignition with a maximum flow rate of 2.63 kg/s, and peak flow into the staircase and back toward the fire room occurs at 5:48 after ignition with a maximum flow rate of 1.45 kg/s. After the peak, the flow rate into the upper floor decreases linearly until the end of the test. The flow rate into the stairs decreases until approximately 12:00 after ignition, and then increases again, eventually reaching a flow rate of 0.96 kg/s at the end of the test. Again, this pattern of increasing flow towards the fire room near the end of the test is a result of the flow reversal.

The mass flow rates into and out of the small and large bedrooms are shown plotted over time in Fig. 4.35 for the no HVAC test. At the small bedroom doorway (Fig. 4.35a), flow slightly favours the direction into the upper floor landing until 3:10 after ignition, when flow in both directions begins to increase. The flow rate into the landing develops at a faster rate and is more stable than the flow into the bedroom. Peak flow into the landing occurs at 5:48 after ignition reaching a maximum flow rate of 0.86 kg/s, then begins to decrease to 0 kg/s at 9:26 into the test. The flow rate into the small bedroom peaks and remains constant at a flow rate of 0.61 kg/s between 10:11 to 11:22 after ignition. Since the flow rate into the landing is 0 kg/s across these times, it appears that there is a one-way flow of smoke into the bedroom during this period. The flow rate into the bedroom

decreases from the peak until the end of the test. The flow rate into the landing increases again at 12:29 after ignition and reaches a flow rate of 0.78 kg/s at the end of the test.

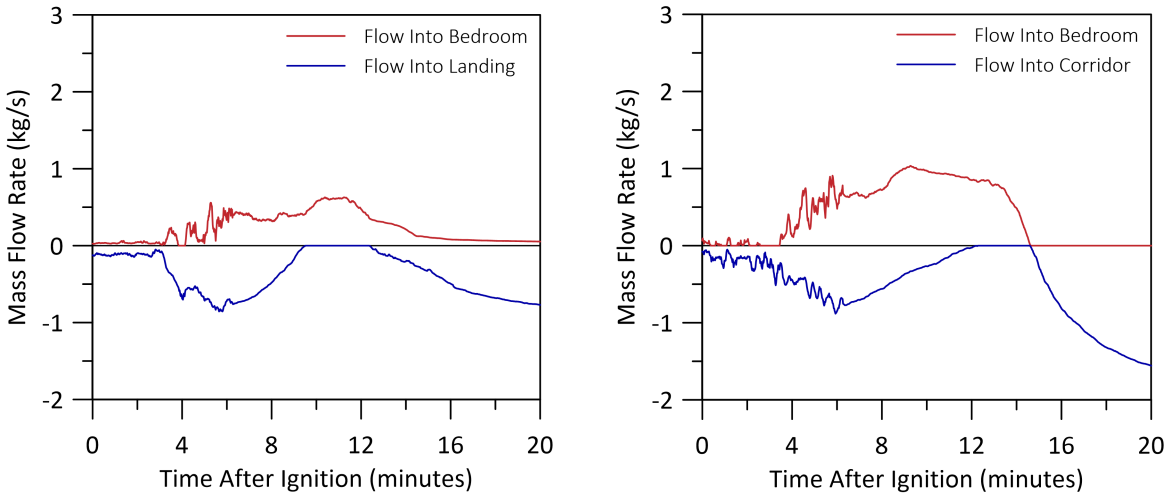

(a) Small bedroom **(b)** Large Bedroom

Figure 4.35: Plots of total mass flow rate into the bedroom and into the upper floor landing or upper floor corridor through the bedroom doorways.

At the large bedroom doorway (Fig. 4.35b), the flow rate into the upper floor corridor increases slowly from the beginning of the test and peaks at 6:00 after ignition reaching a maximum flow rate of 0.87 kg/s. It then decreases to 0 kg/s by 12:16 into the test. Flow into the large bedroom begins to increase at 3:26 after ignition reaching peak values at 9:25 into the test with a maximum flow rate of 1.01 kg/s. The flow rate into the bedroom then decreases slowly until 12:49 after ignition when it decreases more rapidly to 0 kg/s at 14:40 into the test. At this time, the flow rate into the corridor suddenly increases and reaches 1.58 kg/s by the end of the test. This sudden change in flow direction is also noted in the velocity profiles, as discussed previously.

The following three figures compare calculated mass flow rates into and out of the fire room across the four different tests. First, a comparison is made between the total mass flow rate into and out of the fire room, then the flow rates are compared for two main paths: between the fire room and kitchen and between the fire room and stairs, separately.

The total mass flow rates into and out of the fire room are plotted over time in Fig. 4.36, for all four tests. The total mass flow rate into the fire room is the sum of the flow rates from the fire room/kitchen door, the main floor corridor/kitchen door, and the doorway at the bottom of the staircase. Comparison between the mass flow rates between the fire

room and the other compartments is important for understanding potential differences in the flows and thus the environment that may develop in adjacent compartments, with implications for tenability as well as combustion of the fuel. For all four tests, the inflow of fresher air into the fire room (Fig. 4.36a) increases until about 5:00 after ignition and then becomes constant for approximately two minutes before decreasing. This pattern is consistent with the development of the fire, where the peak and decrease in inflow rates align with the times when the fire MLR reaches a peak value and subsequently begins to decay. The decrease in mass inflow to the fire room also supports the notion that the fire becomes under ventilated after reaching its peak MLR. Peak mass flow rates into fire room are between 1.88 kg/s to 2.29 kg/s, with the no HVAC test having the lowest maximum flow rate and the 2x baseline HVAC test having the highest. After the peak, the mass inflow rates decrease until approximately 11:30 to 13:00 after ignition, depending on the test, and then begin to increase again as the fire room cools and the pressures throughout the structure rebalance. By the end of the test, the flow rate has increased to rates near that of the peak mass inflow rates. This increase in flow rate begins earliest in the recirculation test and latest in the 2x baseline test. The mass outflow rates from the fire room (Fig. 4.36b) for each test develop linearly to peak values that occur between 8:57 to 10:34 after ignition depending on the test. Maximum outflow rates from the room are between 3.90 kg/s to 4.74 kg/s, which are significantly higher than the peak mass inflow rates and occur comparably later in the tests. In the case of outflow, the recirculation test has the lowest maximum flow rate and the no HVAC test has the highest. In addition, the recirculation test reaches the peak outflow rate most quickly while the 2x baseline HVAC test takes the longest, which is consistent with the pattern seen in the times when the inflow rate begins to increase during decay of the fire. After the peak, the mass outflow rates in each test decrease until the end of the tests.

Figure 4.37 shows plots of the total mass flow rates between the fire room and the kitchen over time for all four tests. These flow rates are the sum of the flow rates between the fire room/kitchen door and the main floor corridor/kitchen door. Flow from the kitchen to the fire room (Fig. 4.37a) increases during the first five minutes of the tests, showing similar trends as the total mass inflow rate into the fire room. After approximately 5:00, the mass flow rates from the kitchen to the fire room for all tests rapidly decrease to 0 kg/s by 8:00 after ignition. During the growth phase, up to 5:00 after ignition, the flow from the kitchen to the fire room makes up approximately half of the total mass inflow rate into the fire room. Since the inflow rate from the kitchen to the fire room is reduced to zero after 8:00, flow down the staircase is responsible for the supply of fresher air into the fire room during the later stages of fire growth and into fire decay. The flow rate from the kitchen to the fire room begins to increase again 15:00 after ignition as the fire room

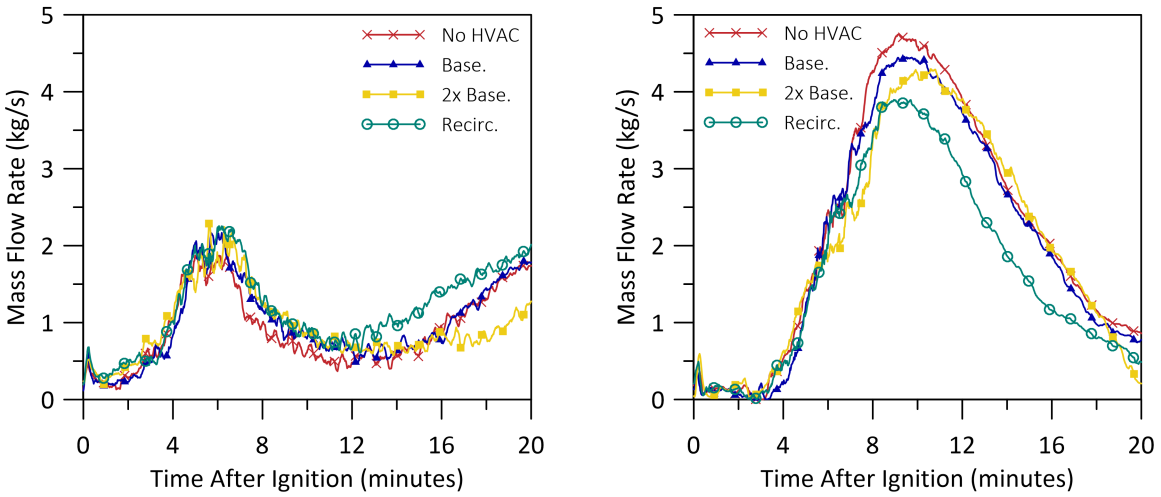

(a) Fire room total inflow

(b) Fire room total outflow

Figure 4.36: Plots of total mass flow into and out of the fire room through the fire room/kitchen door, the main floor corridor/kitchen door, and the doorway at the bottom of the staircase for all four tests.

cools and pressures rebalance throughout the structure. The mass flow rate from the fire room into the kitchen (Fig. 4.37b) follows the same trends with time as the total flow rate out of the fire room. Flow from the room first grows linearly from the start of the test until it reaches peak values at approximately the same times as for the flows into the room. The recirculation test has the lowest maximum flow rate and the no HVAC test has the highest. Peak mass outflow rates from the fire room into the kitchen make up approximately three quarters of the total outflow from the fire room, suggesting there is much more smoke transported into the kitchen than is being transported to the upper floor through the staircase.

Figure 4.38 shows plots of the mass flow rates over time between the fire room and the staircase for all four tests. The flow rates from the stairs into the fire room (Fig. 4.38a) develop in a similar fashion in all four tests from the initial fire growth stage, through to reaching peak flow rates, and subsequently decreasing for a period of time until later in the fire when the flow rates begin to increase again. This is the same as the trend shown for the total mass flow rate into the fire room in Fig. 4.36a. During the growth phase, up until 8:00 after ignition, the flow rate from the stairs into the fire room makes up approximately half of the total flow into the fire room for all tests. From 8:00 until 15:00 after ignition, the flow from the stairs to the fire room makes up all of the flow of fresher air into the

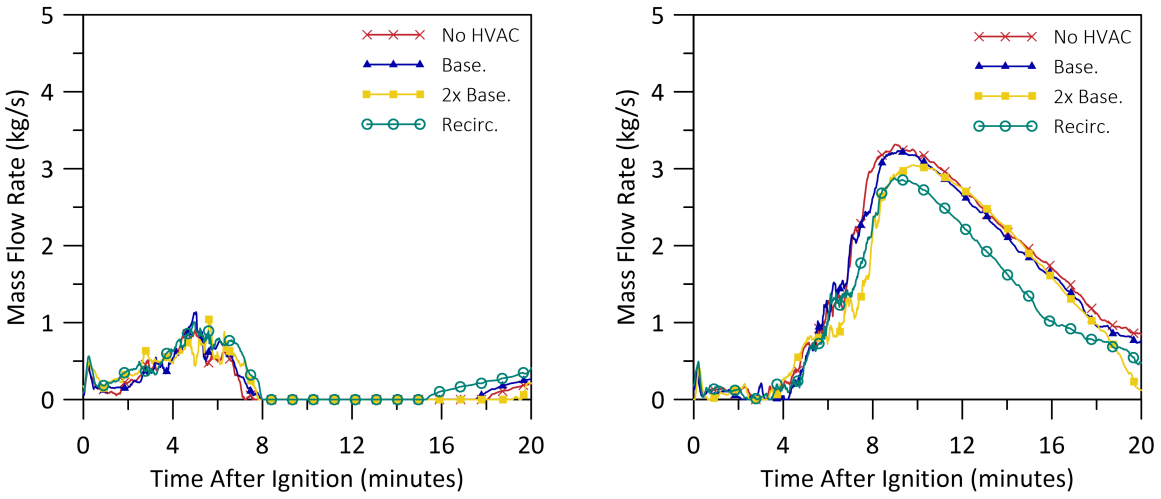

(a) Kitchen into fire room

(b) Fire room into kitchen

Figure 4.37: Plots of total mass flow between the fire room and kitchen through the fire room/kitchen door and the main floor corridor/kitchen door for all four tests.

fire room for all tests, as this is the period when flow rates from the kitchen into the fire room have decreased to 0 kg/s. The flow rates from the fire room to the stairs (Fig. 4.38b) develop in a similar fashion for all tests until shortly after 8:00 into the fire. At this time, flow rates from the fire room to the stairs account for approximately one quarter of the total flow rate into the fire room. Shortly afterwards, the flow rates from the fire room into the stairs begin to differ across the four tests. In the no HVAC test, the flow rate increases again to the highest values amongst the four tests, while the baseline HVAC and 2x baseline HVAC test increase only slightly, and the recirculation test does not increase but instead decreases for the remainder of the test. This trend is a result of a recirculation region that occurs near the top of the doorway (measured by the top three probes) at the bottom of the stairs during later stages of the tests. It is reflected in the mass flow rates beginning at 8:18 after ignition for the no HVAC test, 9:00 into the fire for the baseline HVAC test and 8:36 after ignition for the 2x baseline HVAC test, but does not occur in the recirculation test even though the anomaly appears to be present in the velocity profile for the recirculation test (see Fig. 4.28).

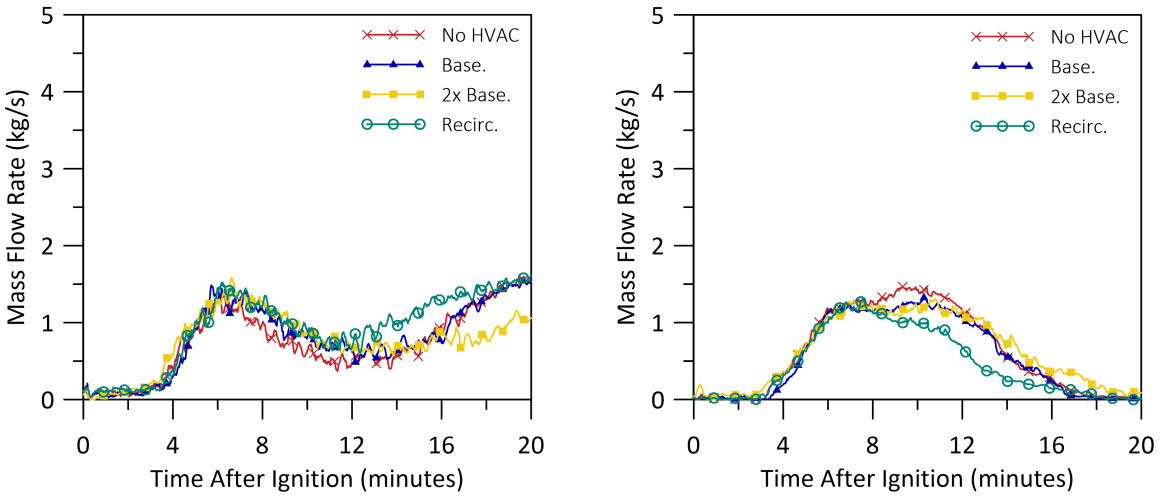

(a) Stairs into fire room **(b)** Fire room into stairs

Figure 4.38: Plots of mass flow between the fire room and staircase through the doorway at the bottom of the stairs for all four tests.

4.4.3 Doorway Velocity Fluctuations

In this section, doorway velocity fluctuations are compared between the four tests using RMS velocity to better quantify the large-scale fluctuations in the flow at various locations throughout the structure. These drive the mixing of smoke with fresher air and thus their magnitudes and distribution have important implications with respect to the development of the environment inside each compartment. The following plots show vertical profiles of mean velocity, RMS velocity, and fluctuation intensity (RMS velocity normalized by mean flow velocity) at each velocity probe location. The mean flow velocity and associated RMS velocity values are determined over the time period corresponding to maximum measured velocity at each probe, as discussed in Sec. 3.2.5. During this period, the baseline velocity is approximately steady, allowing a time-averaged velocity to represent the mean flow with fluctuation around that value.

Profiles of mean velocity, RMS velocity, and fluctuation intensity with height at the fire room/kitchen door are shown in Fig. 4.39. Mean velocity profiles (Fig. 4.39a) are similar for the no HVAC test, the baseline HVAC test, and the recirculation tests, with mean velocities near 0.5 m/s at the bottom probe and increasing to 1.0 m/s at the top probe. The 2x baseline HVAC test has a more uniform velocity profile with height, with measured mean velocities of 0.63 m/s and 0.64 m/s at the top and bottom probes, respectively. At

the bottom probe of the fire room/kitchen doorway, the RMS velocities (Fig. 4.39b) are similar across all tests, varying between 0.03 m/s to 0.05 m/s. At the top probe, the recirculation test has the highest RMS velocity of 0.36 m/s, the baseline HVAC test has the second-highest of 0.25 m/s, while the no HVAC and 2x baseline HVAC tests have significantly lower RMS velocities of 0.05 m/s and 0.03 m/s, respectively. As expected, the normalized velocity fluctuation intensity profiles (Fig. 4.39c) follow the same trends as the RMS velocity profiles. At the bottom probe, all four tests show similar fluctuation intensities between 6% and 9%. At the top probe, high fluctuation intensities of 35% are measured during the recirculation test, with lower values of 26% for the baseline HVAC test, and much lower intensities of 3% to 5% for the 2x baseline and no HVAC tests, respectively. These distributions indicate increased large-scale turbulence and mixing at the upper probe position for the baseline and recirculation tests, while the no HVAC and 2x baseline HVAC tests have comparably lower turbulence and mixing at this location. The one way flow profile seen in Fig. 4.39a indicates that mixing in this doorway occurs within the hot smoke layer.

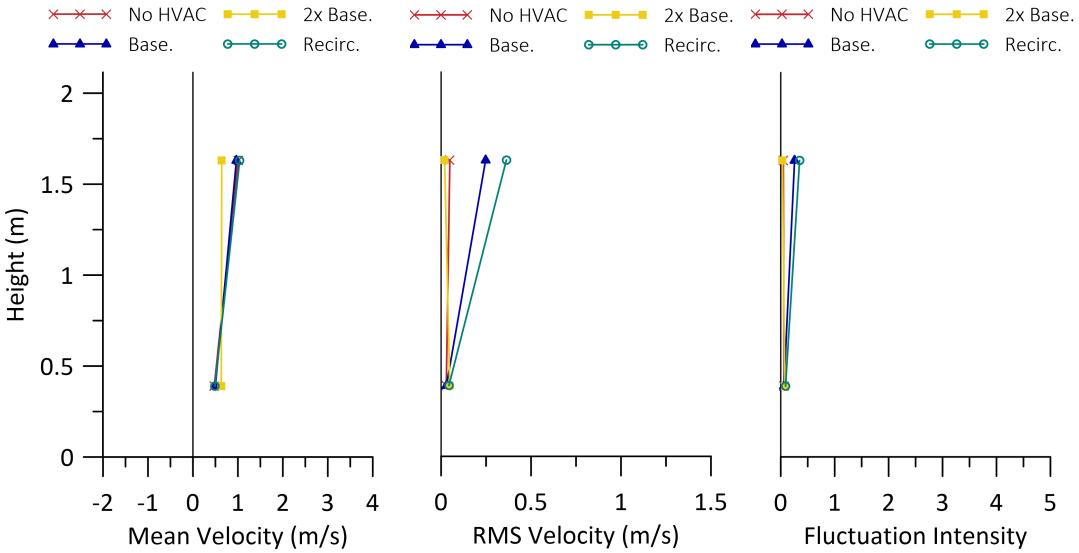

(a) Mean velocity **(b)** RMS velocity **(c)** Fluctuation intensity

Figure 4.39: Plots of mean velocity, RMS velocity, and fluctuation intensity versus height as measured in the fire room/kitchen doorway at peak velocity.

Figure 4.40 shows height profiles of mean velocity, RMS velocity, and fluctuation intensity for the doorway between the main floor corridor and the kitchen. In this doorway, mean velocity profiles (Fig. 4.40a) are similar for all four tests. At the bottom probe,

values of mean velocity are near 0.8 m/s which are approximately 0.3 m/s faster than peak velocities measured at the fire room/kitchen door. At the top probe, mean velocities are near 1.5 m/s, approximately 0.5 m/s faster than for the fire room/kitchen door. The RMS velocities (Fig. 4.40b) are also similar for each test, with RMS velocities at the bottom probe ranging from 0.02 m/s to 0.04 m/s and RMS velocities at the top probe ranging between 0.05 m/s to 0.07 m/s. Therefore, velocity fluctuation intensities at the main floor corridor/kitchen door (Fig. 4.40c) range from 3% to 5% at both the bottom and top probes. At the bottom probe, the recirculation test has the highest RMS velocity and fluctuation intensity, followed by the 2x baseline HVAC test, the no HVAC test, and the baseline HVAC test with the lowest values. At the top probe, the recirculation test again has the highest RMS velocity and fluctuation intensity, followed by the no HVAC test, the 2x baseline HVAC test, and again, the baseline HVAC test with the lowest values. In general, there are greater fluctuation intensities measured at the top probes in the doorway, again suggesting enhanced mixing at these positions. An exception is in the 2x baseline HVAC test, which has a greater fluctuation intensity at the bottom probe.

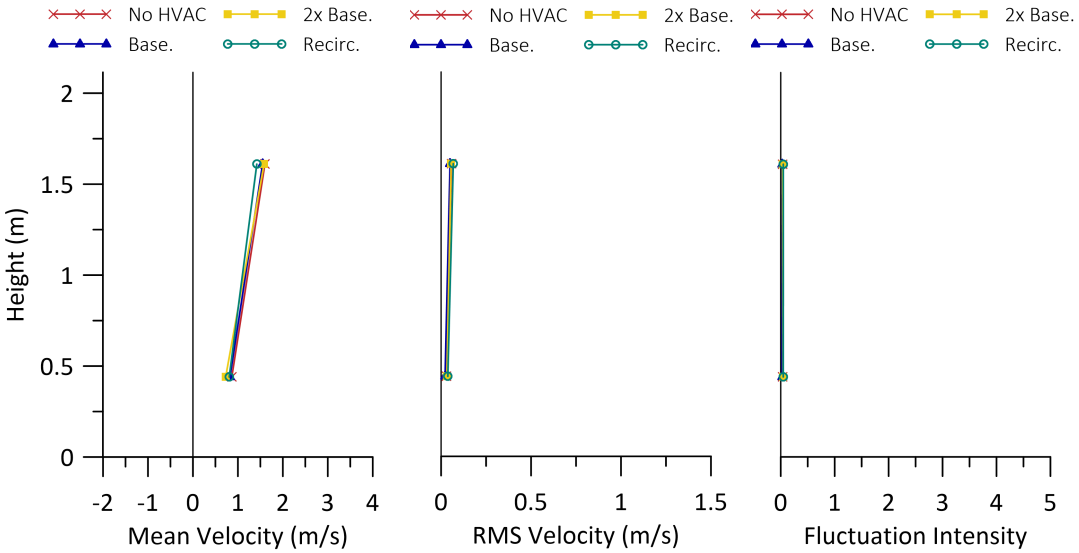

(a) Mean velocity **(b)** RMS velocity **(c)** Fluctuation intensity

Figure 4.40: Plots of mean velocity, RMS velocity, and fluctuation intensity versus height as measured in the main floor corridor/kitchen doorway at peak velocity.

The doorways at the bottom and top of the stairs are fitted with eight velocity probes, which provides more resolved details of RMS velocity, and fluctuation intensity with height, allowing for a more detailed analysis of the velocity gradients that occur during periods

of peak flow through the openings, as well as the corresponding intensity of the velocity fluctuations. Profiles of mean velocity, RMS velocity, and fluctuation intensity are shown in Fig. 4.41 for the doorway at the bottom of the stairs. The mean velocity profiles (Fig. 4.41a) for all tests indicate similar mean velocities of near $-1.5\,\mathrm{m/s}$ at the bottom of the doorway and velocities at the top of the doorway near $3.5\,\mathrm{m/s}$. The largest difference in velocity between tests occurs toward the middle of the profile, at the 1.14 m probe, where the measured mean velocities for the baseline HVAC and recirculation tests are approximately $-0.55\,\mathrm{m/s}$, while those for the no HVAC and 2x baseline HVAC tests are approximately $0.50\,\mathrm{m/s}$, of similar magnitude but opposite in direction. Profiles of RMS velocity versus height, (Fig. 4.41b), are similar across all four tests. The RMS velocity increases with height from the bottom probe to the probe approximately 1.0 m above the floor, then decreases with height between 1.0 m to approximately 1.5 m, and increases slightly with height above 1.5 m. In the no HVAC test, the baseline HVAC test, and the recirculation test, the highest RMS velocities are present at 1.14 m above the floor, which is immediately above the neutral plane height. At this height, the 2x baseline HVAC test has the highest RMS velocity of $0.47\,\mathrm{m/s}$, followed by the no HVAC test with an RMS velocity of $0.42\,\mathrm{m/s}$, the recirculation test with an RMS velocity of $0.36\,\mathrm{m/s}$, and the baseline HVAC test has the lowest RMS velocity of $0.29\,\mathrm{m/s}$. For the 2x baseline HVAC test, however, the highest RMS velocity is actually $0.61\,\mathrm{m/s}$, measured at0.90 m above the floor. This indicates that in the doorway at the bottom of the stairs, the highest fluctuations in velocity occur immediately below the neutral plane. Unfortunately, this cannot be correlated to measurements from other tests, since the data from this height is omitted due to a faulty velocity probe. The fluctuation intensity profiles at the bottom of the stairs (Fig. 4.41c) follow similar patterns as the RMS velocities, with similar velocity fluctuation intensities at the bottom two heights and the four probes above 1.41 m. The largest differences between tests are seen at 1.14 m above the floor, which is the height with the greatest fluctuation intensities for the no HVAC, the baseline HVAC, and the recirculation tests. At this height, the 2x baseline HAVC test has the greatest fluctuation intensity of 112%, followed by the no HVAC test with 80%, the recirculation test with 57%, and the baseline HVAC test with the lowest at 54%. As with RMS velocity, a higher fluctuation intensity of 128% is actually measured at 0.9 m above the floor in the 2x baseline HVAC test. The very high values of velocity fluctuation intensity measured at heights near the neutral plane confirm the intense mixing that takes place along the interface between the faster moving upper hot smoke layer and slower layer of cooler air closer to the floor.

Profiles of mean velocity, RMS velocity, and fluctuation intensity with height above the landing are shown for the doorway at the top of the stairs in Fig. 4.42. The mean velocities (Fig. 4.42a) are similar between each test and show an approximately linear profile from

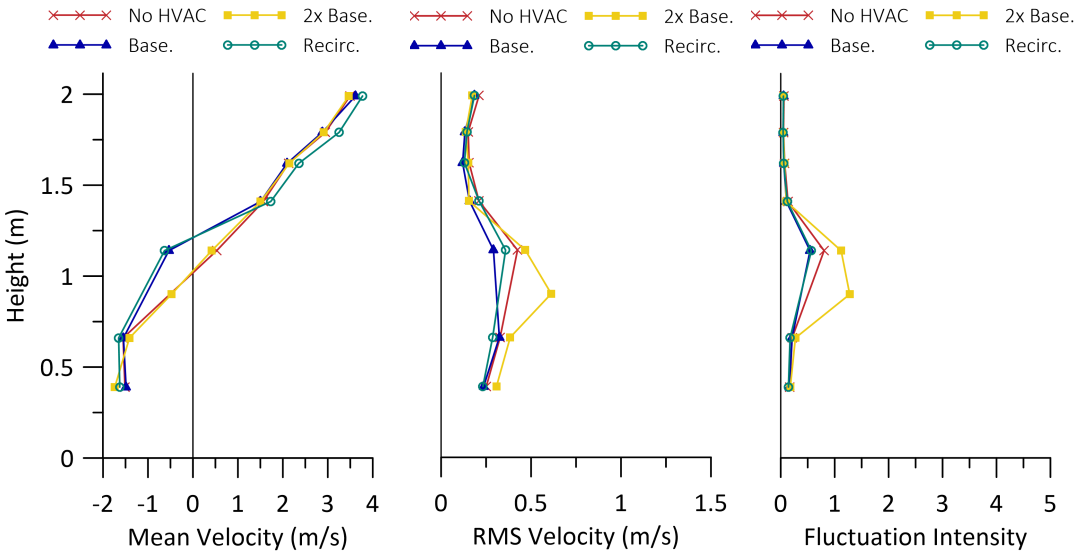

(a) Mean velocity **(b)** RMS velocity **(c)** Fluctuation intensity

Figure 4.41: Plots of mean velocity, RMS velocity, and fluctuation intensity versus height as measured in the doorway at the bottom of the stairs at peak velocity.

the landing to the ceiling, with velocities ranging from approximately −1.5 m/s at the bottom probe up to 3.0 m/s at the top probe. Comparing values of RMS velocity between tests (Fig. 4.42b) indicates that values are similar between tests for the probes below 0.92 m with more variation in RMS velocity at positions above this height. From the bottom of the doorway to 0.92 m above the landing, RMS velocities in all tests increase from approximately 0.2 m/s up to 0.6 m/s. The highest RMS velocities in the no HVAC, baseline HVAC, 2x baseline HVAC tests occur at the three probes located between 1.17 m to 1.62 m above the landing. At these heights, the highest RMS velocities, up to 1.34 m/s, are measured in the no HVAC and the 2x baseline HVAC tests, while comparable RMS velocities up to 1.20 m/s are measured in the baseline HVAC test, and comparably lower RMS velocities, near 0.91 m/s, are measured in the recirculation test. Above 1.62 m, the RMS velocities decrease with height in all tests except for the recirculation test, which has a more uniform RMS profile with height in the upper part of the doorway. The fluctuation intensity profiles between tests (Fig. 4.42c), follow similar trends as seen at the bottom of the stairs. The magnitude of the fluctuation intensities are similar at the bottom two probes and the top three probes in the doorway. More variation in velocity fluctuation intensity between the tests is seen with proximity to the neutral plane height. The highest fluctuation intensity for all tests occurs at 1.17 m above the landing, which is the probe

immediately above the neutral plane during the period of peak flow through the opening. At this height, the 2x baseline HVAC test has the highest fluctuation intensity of 403%, followed by the no HVAC test with 298%, and the recirculation and baseline HVAC tests with similar intensities of 221% and 202%, respectively. The highest through the lowest fluctuation intensities are seen in the same tests as at the bottom of the stairs; however, the fluctuation intensities at 1.62 m above the landing are more than 3.6 times greater at the top of the stairs than they are at the bottom of the stairs for every test. Increased velocity fluctuation intensities are also measured at the four probes above this height at the top of the stairs, while similar values of velocity intensity are measured at the lower three probe positions in both doorways. The increased fluctuation intensities at the top of the stairs indicates that significant large-scale turbulence and mixing is generated at this location, which has important implications on the development of the environment on the upper floor.

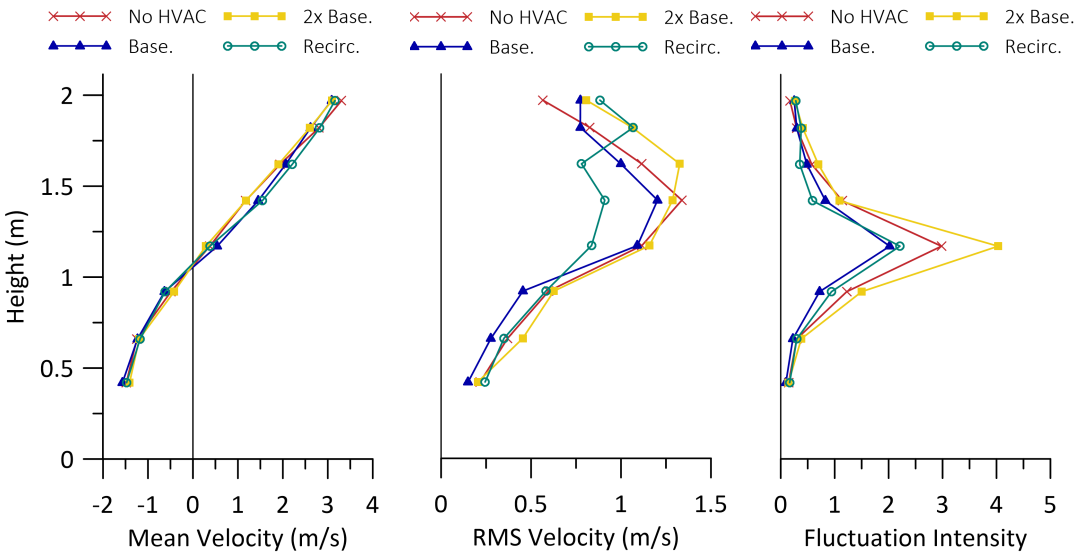

(a) Mean velocity **(b)** RMS velocity **(c)** Fluctuation intensity

Figure 4.42: Plots of mean velocity, RMS velocity, and fluctuation intensity versus height as measured in the doorway at the top of the stairs at peak velocity.

The distribution and comparison of values between the lower and upper staircase openings illustrate the large-scale fluctuations that are generated in the staircase. The fluctuation intensity profiles at both the bottom and top of the stairs indicate that the heights with the highest fluctuation intensities are at the probes immediately above or below the neutral plane height, and all other heights have relatively low fluctuation intensities in

comparison. This is expected since, near the neutral plane, the mean velocities are low due to the velocity gradient and the definition of the neutral plane, while the RMS velocity is relatively high due to proximity to the shear interface between the layer of smoke flowing out of the fire room and the fresher air flowing into the fire room. Thus, the flow evolves into a mixing layer type of flow, in which mixing is generated by large-scale fluctuations caused by the shearing action between the two layers of flow in opposite directions [47]. This promotes mixing between the flow of smoke up the stairs and the flow of fresher air down the stairs, an important consideration in both understanding and modelling of fire induced environment development in multi-compartment and multi-storey structures.

Profiles of mean velocity, RMS velocity, and fluctuation intensity with height at the four probes installed in the small bedroom door are shown in Fig. 4.43. The mean velocity profiles show that the bottom three probes are positioned below the neutral plane height, whereas the top probe is positioned above the neutral plane. The mean velocity profiles (Fig. 4.43a) of all four tests are similar and show a fairly uniform profile in height from the bottom of the doorway up to 1.14 m above the floor, with velocities between −0.5 m/s to −0.8 m/s. Above this height, the mean velocity changes direction and reaches magnitudes between 0.5 m/s and 0.8 m/s, depending on the test. Both the RMS velocity (Fig. 4.43b) and fluctuation intensity profiles (Fig. 4.43c) have similar shapes as the mean velocity profiles with similar values of RMS velocity at each height. At the bottom three probes, the RMS velocities range from 0.08 m/s to 0.20 m/s, while the highest RMS velocities for all tests are measured at the top probe, with magnitudes between 0.68 m/s to 0.75 m/s, depending on test. Fluctuation intensities at the bottom three probes are similar for all tests. Intensity magnitudes at these locations are between 11% and 33%, with the higher values measured at the probe 1.14 m above the floor. More variation between tests is seen in values measured at the top probe position (1.59 m), where the highest fluctuation intensities also occur. Here, the 2x baseline HVAC test has the highest intensity of 151%, the recirculation and baseline HVAC tests have similar intensities of 132% and 129%, respectively, and the no HVAC test has the lowest intensity of 86%.

Figure 4.44 shows profiles of mean velocity, RMS velocity, and fluctuation intensity with height for the large bedroom door. Profiles in this doorway are similar to those at the kitchen doors, as there were only two velocity probes installed. The mean velocity profiles for all four tests at the large bedroom door (Fig. 4.44a) show two-way flow, with flow out of the large bedroom at the bottom probe and flow into the bedroom above. Velocities at the lower probe vary from approximately −0.60 m/s for the baseline HVAC, 2x baseline HVAC, and recirculation tests to a lower value of −0.35 m/s in the no HVAC test. At the top probe, all four tests have a similar mean velocity between 0.36 m/s to 0.47 m/s. Comparison of the RMS velocities between tests (Fig. 4.44b) shows that all four tests

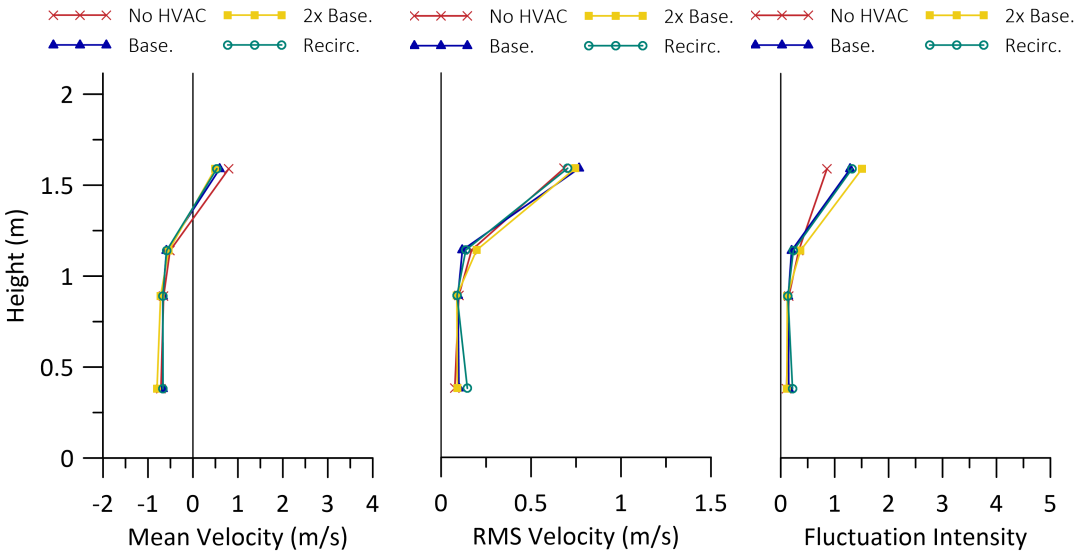

(a) Mean velocity **(b)** RMS velocity **(c)** Fluctuation intensity

Figure 4.43: Plots of mean velocity, RMS velocity, and fluctuation intensity versus height as measured in the small bedroom doorway at peak velocity.

have similar RMS velocities of between 0.05 m/s to 0.08 m/s at the lower probe. At the top probe, the recirculation test has the highest RMS velocity of 0.21 m/s, followed by the baseline HVAC test with an RMS velocity of 0.19 m/s, and the no HVAC test with an RMS velocity of 0.16 m/s. The 2x baseline test has a lower RMS velocity at the top probe compared to the other tests of 0.07 m/s. In fact, the 2x baseline HVAC test is the only test to have a lower RMS velocity at the top probe compared to the bottom probe. Fluctuation intensities (Fig. 4.44c) between the four tests are similar at the bottom probe, with values between 11% and 16%. There is more variation at the top probe, with the recirculation test having the highest intensity of 56%, the no HVAC and baseline HVAC tests having the same intensity of 40%, and the 2x baseline HVAC test having the lowest intensity of 20%.

The top probe in the large bedroom doorway measures a higher velocity fluctuation intensity than the bottom probe in all four tests. This is consistent with the general trends seen at the fire room/kitchen door and the main floor corridor/kitchen door as well. In all cases, these doorways lack the spatial resolution that would be needed to measure higher fluctuation intensities near the neutral plane height. Nonetheless, the more detailed distributions with height at the other locations are still consistent with the general patterns seen in the doorways with only two probes. It is expected that increasing

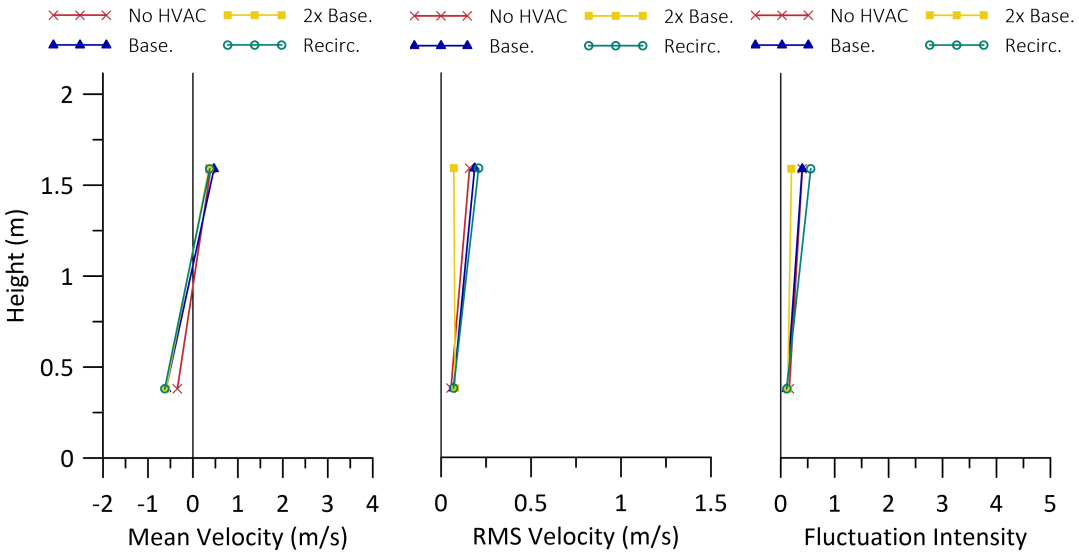

(a) Mean velocity **(b)** RMS velocity **(c)** Fluctuation intensity

Figure 4.44: Plots of mean velocity, RMS velocity, and fluctuation intensity versus height as measured in the large bedroom doorway at peak velocity.

the spatial resolution of velocity measurements through installation of additional probes in the doorways with a lower number of probes would also show that the highest velocity fluctuation intensities are measured near the neutral plane height as this is consistent with mixing layer flows which would be expected to occur even with the smaller overall velocity gradients present at far field locations, such as the large bedroom door.

4.5 Species Concentrations

Development of gaseous species concentrations, specifically O_2, CO_2, CO, and VOC throughout the burn house for the four tests are presented in this section. Characterizing species distributions through the structure is imperative to better understanding the nature of combustion of the couches and the combustion efficiency, as well as to the understanding the gaseous environments to which an occupant may be exposed during these fire scenarios.

Figure 4.45, shows a plot of the fire MLR from the no HVAC test along with measurements of O_2, CO_2, and CO concentrations at GIS 1 0.9 m in the fire room from the same test. All four tests follow a very similar development of species concentration in the fire room. It can be seen that the concentrations of each species remain at ambient conditions

during the incubation and early growth phases of the fires. As the fire grows toward peak MLR, the concentration of O_2 begins to rapidly decrease, while the concentration of CO_2 simultaneously begins to rapidly increase. After the peak MLR of the fire, the concentration of O_2 reaches a minimum value, remains at this minimum until after the fire flames out, and then quickly recovers to a steady state value, which is maintained for the remainder of the test. The concentration of CO_2, is seen to rapidly increase up to 10 000 ppm, at which point the sensor saturates. Unfortunately, measurements of CO_2 become unreliable after the sensor saturates and therefore, the remaining data is omitted from this plot and concentrations of CO_2 are not compared between the tests. As expected, an increase in CO concentration follows shortly after the decrease in O_2 and increase in CO_2 since CO production is favoured once the concentration of O_2 decreases. The concentration of CO peaks shortly after peak fire MLR is reached, and then reduces to a steady state value that is maintained until the end of the test.

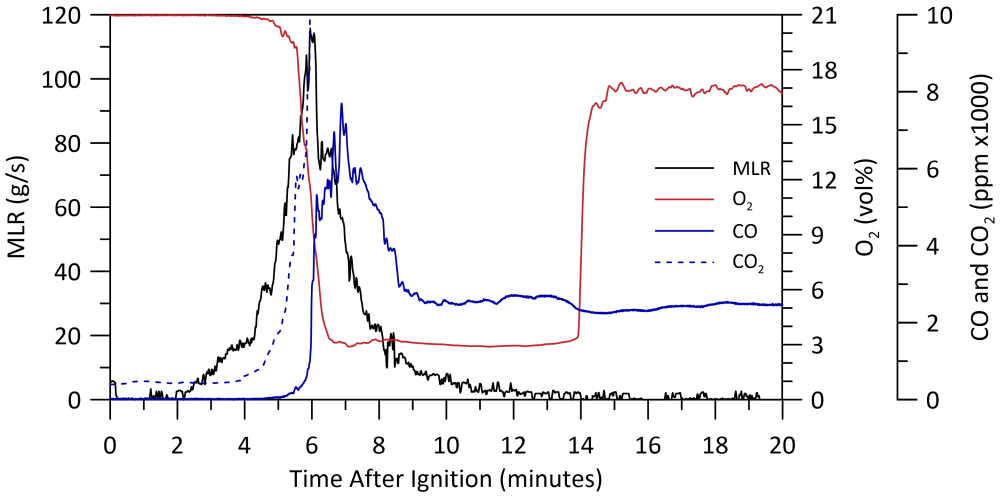

Figure 4.45: Plot of MLR with O_2, CO_2, and CO measurements from the no HVAC test at GIS 1 0.9 m in the fire room.

The following subsections present the evolution of O_2, CO, and VOC concentrations in detail for the no HVAC test, showing the development of the concentrations at various locations throughout the main and upper floors of the burn house. This test is used as a reference case, since all four tests show similar trends in the evolution of the species throughout the structure during the tests. Species concentrations are then compared between the four tests at key locations in the fire room and in the small bedroom on the upper floor. The implications of the similarities or differences in species distributions are discussed.

4.5.1 Oxygen Concentration

This section discusses the depletion of O_2 throughout the burn house during the tests. First, the O_2 concentrations throughout the main floor and upper floor are presented in detail for the no HVAC test as a reference case. Then, comparisons are made between the four tests in the fire room, to compare the O_2 available to the fire and the O_2 concentration in the smoke/combustion products, and in the small bedroom, to compare the concentrations in a far field location.

Figure 4.46 shows measurements of O_2 concentration throughout the main and upper floors for the no HVAC test. Main floor locations include GIS 1 (0.3 m and 0.9 m) in the fire room, GIS 3 (0.3 m, 0.9 m, and 1.5 m) in the kitchen, and GIS 4 (0.9 m) in the main floor corridor. Upper floor locations include GIS 5 (0.3 m, 0.9 m, and 1.5 m) in the upper floor corridor, GIS 6 (0.3 m and 0.9 m) in the small bedroom, and GIS 7 (0.3 m and 0.9 m) in the large bedroom. Certain species concentration measurements are omitted from the presented data; these sensors experienced a malfunction during the test. Oxygen concentrations on the main floor are stratified with height, where concentrations of O_2 near the floor are higher than concentrations near the ceiling throughout the test. As was observed with temperature measurements, horizontal gradients in concentration at a given height above the floor are much lower (north-south and east-west directions). On the main floor, the O_2 begins to decrease first at GIS 3 1.5 m. They sequentially decrease at the lower heights at this location as the smoke layer descends into this region of the compartment, linking the decrease in O_2 to smoke layer descent. Concentration of O_2 at the 1.5 m height decreases to the lowest minimum concentration of less than 3%, compared to 9.1% and 10.6% at the 0.9 m and 0.3 m heights, respectively. After minimum values are measured, the O_2 concentration at GIS 3 recovers gradually over the remainder of the test. Measured O_2 concentrations at GIS 4 0.9 m follow closely with measurements at the same height at GIS 3, decreasing to slightly lower minimum concentrations of 7.5% at approximately the same time. Recovery of O_2 concentration at this location also matches closely with trends seen at GIS 3. Concentrations of O_2 in the fire room (GIS 1) decrease at a later time than those at other locations on the main floor, indicating O_2 continues to be drawn towards the fire room as the fire develops. Measured concentrations at 0.3 m and 0.9 m heights begin to decrease at approximately the same time. The concentration at the higher height decreases rapidly and reaches a minimum concentration of less than 3%, comparable to that measured at1.5 m height at GIS 3, at approximately the same time. As at GIS 3, this minimum concentration is maintained for a period of time before it sharply increases to 16.0% in less than one minute. At GIS 1 0.3 m, concentrations of O_2 decrease much more slowly than at any other location. It first reduces to a concentration of approximately 17%

and remains at that concentration for the remainder of the test. There appears to be more fluctuations in the O_2 concentration at this location, but the cause of these fluctuations is unclear.

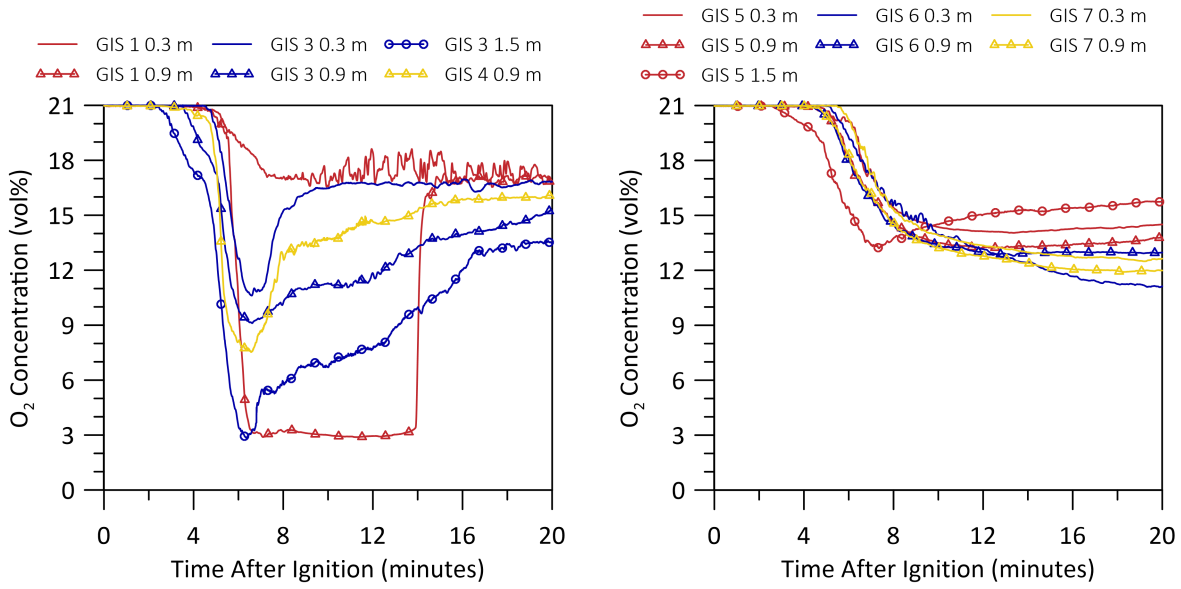

(a) Main floor **(b)** Upper floor

Figure 4.46: Plots of main and upper floor O_2 concentrations over time for the no HVAC test.

On the upper floor, decreases in O_2 concentration at GIS 5 1.5 m are measured first, and reach a minimum concentration of 13.2% before recovering slightly to a steady state for the remainder of the test. Concentrations at 0.9 m heights at all locations on the upper floor begin to decrease at approximately the same time, but after those at the 1.5 m height. Finally, concentrations at the lowest height (0.3 m) begin to decrease after those at the 0.9 m height, again consistent with smoke layer descent in the compartments on the upper floor. Measured O_2 concentrations at the 0.9 m and 0.3 m heights on the upper floor decrease gradually to steady-state concentrations, in contrast to the more rapid decrease and recovery seen at most locations on the main floor. Most prominent at GIS 6 0.3 m, there is sometimes a continuous, slow reduction in O_2 concentration throughout the decay phase of the fire as well. Minimum O_2 concentrations at all heights and all locations on the upper floor are between 11.1% and 14.0%, with the lowest concentration measured at GIS 6 0.3 m and the highest at GIS 5 0.3 m. Differences in concentrations between heights is much less than on the main floor, indicating a more uniform (less stratified) environment on the upper floor as a result of the increased mixing in the flows of smoke up/down the

staircase, through the landing and into the upper floor compartments.

The trends discussed above for the no HVAC test are observed in all four tests with slight differences in the values of minimum oxygen concentration across tests, as well as in the slope of the decreasing concentration trace over time. The most interesting of these differences occurs at GIS 1 in the fire room and at GIS 6 in the small bedroom, and will be discussed here.

Measurements of O_2 concentration at GIS 1 0.3 m provide the best indication of the concentration of O_2 available to the fire. Figure 4.47, shows plots of the O_2 measurements at this location from ignition to 20 minutes after ignition for all four tests. For approximately the first five minutes of all tests, the O_2 concentrations remain near ambient and then decrease linearly as the fires enter the rapid growth phase. The recirculation and no HVAC test have similar slopes of decrease in concentration, $-0.025\,\%/s$ and $-0.024\,\%/s$, respectively, while the baseline HVAC and 2x baseline HVAC tests have shallower slopes of $-0.021\,\%/s$ and $-0.022\,\%/s$, respectively [6]. As expected, supplying OA into the house reduces the rate at which O_2 is decreased within the structure. Eventually, the O_2 concentrations in each test reach minimum values and remain near this value for the remainder of the test. The lowest minimum concentration of 15.5% is measured in the recirculation test, followed by the baseline HVAC test with a minimum concentration of 15.8%, the 2x baseline HVAC test with a minimum concentration of 16.2%, and the no HVAC test has the highest minimum concentration of 16.6%. It is interesting that O_2 concentrations in the no HVAC test decreases to the minimum concentrations one minute and 32 seconds earlier than any of the other tests. This minimum concentration is higher than in the other tests even though the O_2 concentration decreases at a faster rate and there is no mechanical ventilation to feed fresh air into the structure. In contrast, the 2x baseline HVAC test reaches a minimum O_2 concentration last, which is consistent with the additional supply of OA.

Oxygen concentrations are compared between the four tests at GIS 1 0.9 m in Fig. 4.48. This location best represents the species concentrations in the smoke produced by the fire because it is located near the fire and is not greatly influenced by the flow through doorways, as at GIS 2. At this height on GIS 1 the development of O_2 concentration with time is quite different than seen at the 0.3 m height. The O_2 concentrations remain near ambient during the early stages of fire growth, then initially decrease in a linear fashion, with slopes slightly steeper, but comparable to those calculated 0.3 m height but later transition to very rapid decrease in concentration. During the initial decrease, the

[6] Slopes of O_2 decrease are calculated from a line of best fit through the measurements during the period of decreasing concentration.

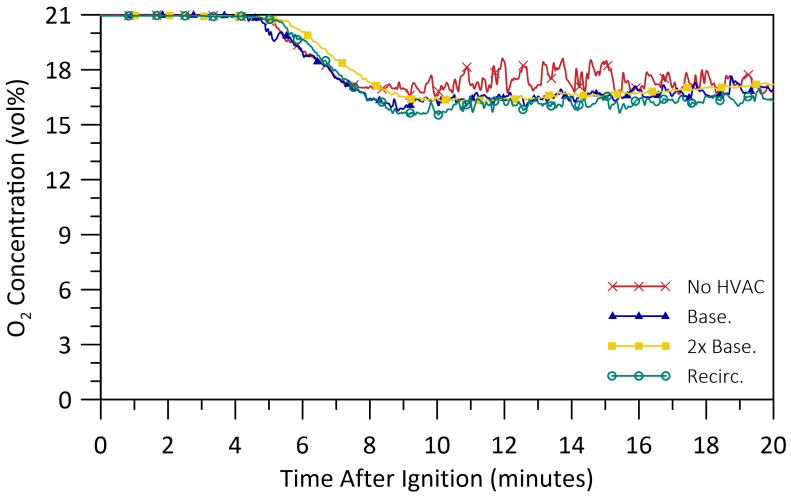

Figure 4.47: Plot comparing O_2 measurements from the four tests at GIS 1 0.3 m in the fire room.

recirculation test has the steepest slope of −0.070 %/s, followed by the 2x baseline HVAC test with a slope of −0.037 %/s, the no HVAC test with a slope of −0.029 %/s, and the baseline HVAC test has the shallowest slope of −0.020 %/s. This does not follow the same ranking as for the 0.3 m height, although the recirculation test has the steepest slope in O_2 concentration at both heights. During the second (rapid) phase of concentration decrease, the no HVAC, baseline HVAC, and recirculation concentrations decrease linearly. The no HVAC test has the steepest slope of −0.309 %/s, and the baseline HVAC and recirculation tests have similar, more shallow slopes of −0.240 %/s and −0.237 %/s, respectively. The decay in O_2 concentration in the 2x baseline HVAC test during this phase is the shallowest and also closer to quadratic with time, likely due to the increased supply of OA to the fire room in this test.

Minimum O_2 concentrations are reached after the period of rapid decrease in concentration and stay near these low values for some time prior to recovery. The minimum concentrations, all below 3%, are similar in all tests with the lowest, 2.5% O_2, measured in the recirculation test, followed by the baseline HVAC and 2x baseline HVAC tests with 2.7% O_2, and the no HVAC test with the highest minimum concentration of 2.9% O_2. There are significant differences in the length of time that the O_2 concentrations remain at minimum values in each test. Minimum concentrations are reached first in the no HVAC test, at 6:36 after ignition, and remain at these concentrations for the longest time, seven minutes and 12 seconds. In the baseline HVAC test, minimum concentrations are measured

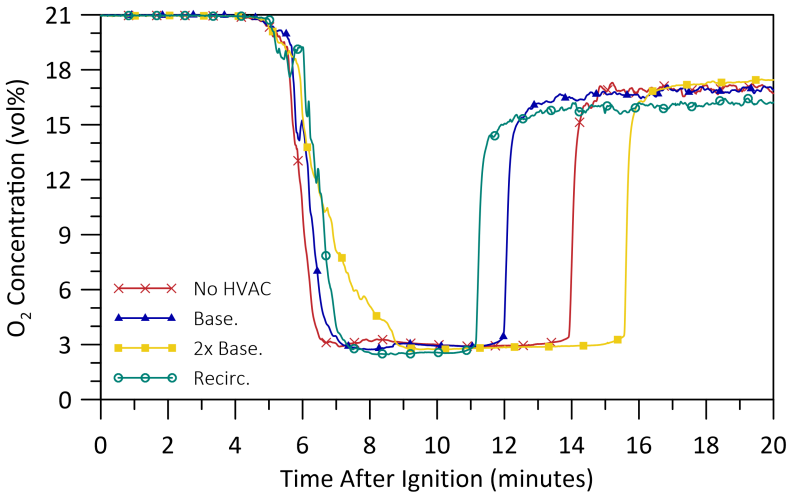

Figure 4.48: Plot comparing O_2 measurements from the four tests at GIS 1 0.9 m in the fire room.

beginning at 7:12 after ignition and remain at these levels for four minutes and 36 seconds. Concentrations in the recirculation test reach minimum values at 7:32 after ignition and remain low for three minutes and 35 seconds. Finally, the 2x baseline HVAC test takes the longest to reach the minimum O_2 concentration at 9:00 after ignition, but concentrations remain low for the second-longest lengths of time, six minutes and 30 seconds. Overall, increasing HVAC flow rates increase the length of time taken for O_2 concentrations to reach their minimum values, consistent with the expected trend of delayed reduction of O_2 with increased supply of OA. In the 2x baseline HVAC test, the longer time taken to reach the minimum O_2 concentrations is also consistent with this test having the most delay before peak fire MLR, which is observed as well. There is less consistency in the length of time over which concentrations remain at their lowest values across tests. As expected, the no HVAC test remains at minimum concentration levels for the longest length of time, as there is no supply of additional ventilation to the fire room other than through natural doorway flows. Interestingly, however, the 2x baseline HVAC test, with the highest flow rates and a continuous supply of OA into the fire room, exhibits the second-longest length of time at minimum O_2 concentrations, a seemingly contradictory result. Further, the recirculation test appears to remain at minimum concentrations for the shortest length time and is the earliest to recover of all tests, which is also not expected since this test does not have any supply of fresher OA. Although no apparent link can be found between the recovery of O_2 in the fire room and the mechanical ventilation configuration, further investigation does identify a link between the O_2 concentration, the MLR, and the exchange of smoke and

air through the doorways of the fire room, which is discussed in Sec. 4.6.

Recovery of O_2 concentrations at GIS 1 0.9 m is rapid for all four tests, with recovery from minimum concentrations to 15% O_2 occurring in less than one minute. After this rapid recovery, the concentrations reach a steady state value until the exterior doors of the structure are opened at the end of the tests. The 2x baseline HVAC test has the highest steady state O_2 concentration of 17.3%, followed by the no HVAC and baseline HVAC tests with similar concentrations of 16.9% and 16.8%, respectively, and the recirculation test has the lowest steady state concentration of 16.1%. This trend matches expectations and is also consistent with the trend of measurements taken at the 0.3 m height at GIS 1 where the recirculation test has the lowest concentration and the 2x baseline HVAC test has the highest.

On the upper floor, the development of the O_2 concentrations follows a slower sigmoid shaped response in time, similar to that seen at GIS 1 0.3 m. The four tests are compared at GIS 6 0.9 m in the centre of the small bedroom in Fig. 4.49. Again, the concentrations of O_2 remain near ambient during the incubation and early growth states of the fire. Following this, concentrations decrease with the fastest decrease in concentrations during the no HVAC and recirculation tests, while slower rates of decrease are measured during the baseline HVAC and 2x baseline HVAC tests. This is consistent both with the patterns seen at the other locations and with higher supply rates of fresher OA reducing the overall rate of decrease of O_2 in a test. A characteristic slope of the decrease in concentration was not well-defined due to the curvature of the measured data with time at this location. Minimum measured O_2 concentrations are similar between the baseline HVAC (14.5%), the 2x baseline HVAC (14.7%), and the recirculation (13.9%) tests, while a comparably lower minimum concentration of 12.8% was measured in the no HVAC test. Once again, the ranking of the minimum concentrations from lowest to highest is consistent with the ventilation configuration, where increased supply of OA results in higher overall O_2 concentrations. The other quantity of interest at GIS 6 0.9 m is the time it takes for the O_2 concentration to reduce to 15%. This is both a key threshold for occupant tenability [144] and is also used throughout the presented results as a key time representative of conditions throughout the structure during environmental recovery after flame-out. This 15% O_2 threshold on the upper floor is reached first in the no HVAC test, at 7:30 after ignition, followed closely in the recirculation test at 7:35 after ignition, the baseline HVAC test at 8:16 after ignition, and the 2x baseline HVAC test at 9:13 after ignition (as presented also in Table 4.1). The times to reach 15% O_2 at GIS 6 0.9 m are consistent with the ventilation configuration, where increased supply of OA sustains the O_2 concentration at higher values for prolonged periods.

The mechanical ventilation configuration has discernible effects on the distribution

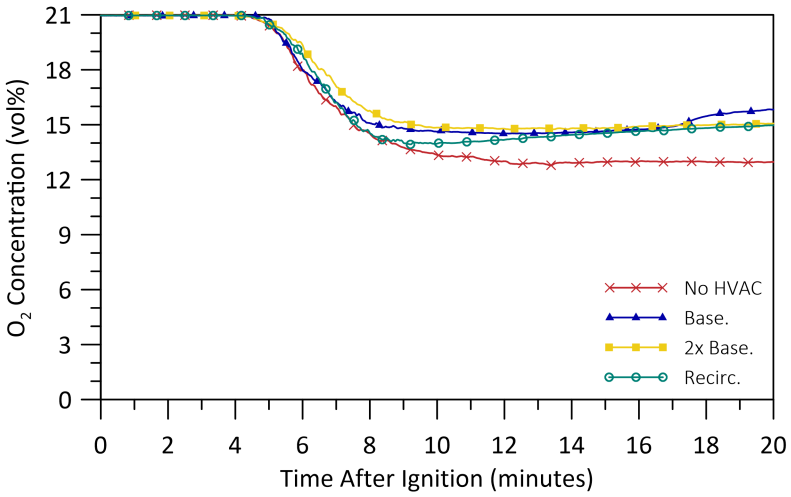

Figure 4.49: Plot comparing O_2 measurements from the four tests at GIS 6 0.9 m in the small bedroom.

and rates of reduction of O_2 concentration throughout the house. The no HVAC and recirculation mechanical ventilation configurations result in the fastest rates of decrease of O_2 in both near-field and far-field locations. Minor differences between the steady-state O_2 concentrations are measured in the fire room and in the minimum concentrations in the small bedroom. Trends are also consistent with the supply of OA, where increased supply generally results in higher O_2 concentrations. On the other hand, HVAC is seen to have little effect on the minimum O_2 concentrations in the fire room. This may be due to the location of the supply ports, which are near the ceiling. Therefore, the supply air enters into the hot layer of the compartment, rather than into the lower layer, from which the fire likely draws the major portion of its ventilation. Overall, similarities between the minimum and steady state concentrations of O_2 throughout the house across tests are consistent with similarities between the total amount of fuel mass burned in each of the tests, and indicate that the HVAC system may not be supplying large enough quantities of air compared to the initial volume of the house to noticeably prolong burning.

4.5.2 Carbon Monoxide

Concentrations of CO throughout the burn house are presented in this section. First, the CO concentrations throughout the main floor and upper floor are presented in detail for the no HVAC test as a reference case. Then, comparisons are made between the four tests in

the fire room, to compare the CO produced by the fire and gain insight into the efficiency of the combustion, and in the small bedroom, to compare the conditions and toxic CO distributions in a far field location.

Figure 4.50 shows measurements of CO concentration throughout the main and upper floors for the no HVAC test. Main floor locations include GIS 1 (0.3 m and 0.9 m) in the fire room, GIS 3 (0.3 m and 1.5 m) in the kitchen, and GIS 4 (0.3 m, 0.9 m, and 1.5 m) in the main floor corridor. Upper floor locations include GIS 5 (0.3 m, 0.9 m, and 1.5 m) in the upper floor corridor, GIS 6 (0.3 m, 0.9 m, and 1.5 m) in the small bedroom, and GIS 7 (0.3 m, 0.9 m, and 1.5 m) in the large bedroom. Data omitted from the presented locations were from sensors which experienced a malfunction during the test. On the main floor, increases in CO concentration occur first at 1.5 m height above the floor, at 3:00 after ignition. Concentrations first increase linearly until 4:00 after ignition, at which time the concentration levels out at approximately 1000 ppm until after 5:00 into the test. Concentrations at the 1.5 m heights then rapidly increase until peak values of concentration are reached. At the other two heights at all locations on the main floor, measured increases in CO concentration are rapid and occur at the same time as the rapid increase in the concentrations measured at the height of 1.5 m above the floor. At a height of 1.5 m at GIS 3 in the kitchen, the highest peak CO concentrations of 8800 ppm are reached, followed by peak concentrations of 7700 ppm at the 0.9 m height at GIS 1 in the fire room. Similar peak CO concentrations of 5630 ppm and 5470 ppm, respectively, are measured at 0.3 m above the floor at both GIS 3 in the kitchen and GIS 4 in the main floor corridor. At most locations, peak concentrations of CO are reached and then the concentrations decrease to near steady state lower values until the end of the test. The locations that do not follow this development are GIS 1 0.3 m, GIS 4 0.9 m, and GIS 4 1.5 m. At GIS 1 0.3 m the CO concentration begins to increase rapidly then very quickly reaches 1000 ppm after which further increases are much slower but continue throughout the test, eventually reaching a peak value of 2470 ppm. This matches the temporal evolution of the O_2 concentration at the same location. At GIS 4 0.9 m and 1.5 m, the concentration of CO rapidly increases to a value greater than 10 000 ppm, values at which the sensors saturate. Following this, the response of the sensors is unreliable and subsequent measurements are omitted from the plots. Therefore, concentrations during the recovery of the environment cannot be investigated at these locations.

On the upper floor, the sensor on GIS 5 at a height of 1.5 m above the floor in the corridor is the first location to measure an increase in CO concentrations. Concentrations at 1.5 m heights at the other two locations on the upper floor follow approximately two minutes later, and concentrations at the 0.9 m heights at all three locations on the upper floor begin to increase at this latter time as well. Increases in concentrations at the 0.3 m

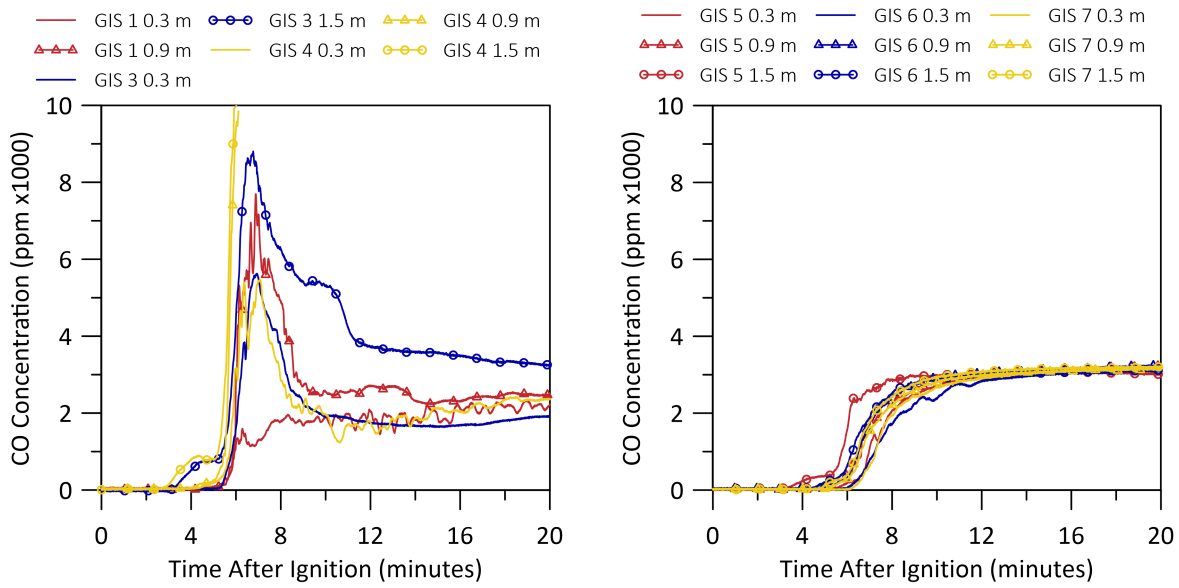

(a) Main floor **(b)** Upper floor

Figure 4.50: Plots of main and upper floor CO concentrations over time for the no HVAC test.

heights at all three locations are also measured shortly thereafter. This is consistent with the trends seen in the O_2 concentrations on the upper floor, and with the time it would take for descent of the smoke layer at the measurement locations. The development of CO concentrations on the upper floor is slower than on the main floor, and follows a sigmoid shaped curve, similar to the decrease in O_2 concentrations. All locations on the upper floor have comparable maximum/steady state CO concentrations between 3100 ppm and 3290 ppm.

The development of CO concentrations is similar for all four tests, however, there are some key differences in peak concentrations and in steady state concentrations, both in the fire room and on the upper floor. The following discussion highlights these differences as measured at GIS 1 in the fire room and GIS 6 in the small bedroom on the upper floor.

Figure 4.51 shows measurements of CO concentration for all four tests plotted over time at GIS 1, 0.3 m above the floor. At this location, the development of CO is characterized by a continuous increase over time for the duration of the test. The most rapid increase in CO concentration is seen between 5:00 to 10:00 after ignition for all tests. This is consistent with, and slightly delayed from, the decrease in O_2 concentration at the same location, as would be expected since the formation of CO is favoured once the O_2 concentration is reduced. The rate of increase of CO is significantly slower after 10:00 into all tests with

peak concentrations achieved late in the tests, between 19:00 to 20:00 after ignition. The no HVAC and baseline HVAC tests show the highest measured concentrations of CO, with instantaneous maximum values reaching 2470 ppm and 2230 ppm, respectively, and the 2x baseline HVAC test has the lowest maximum concentration of 1290 ppm. Somewhat unexpectedly, the recirculation test has a maximum concentration of only 1840 ppm. As seen in the O_2 concentration distribution throughout the house, the ranking of tests from highest to lowest measured concentrations is somewhat consistent with the ventilation configuration. The no HVAC test has the highest concentrations and the least ventilation, and the 2x baseline HVAC test has the lowest concentrations with the most OA supplied to the fire room.

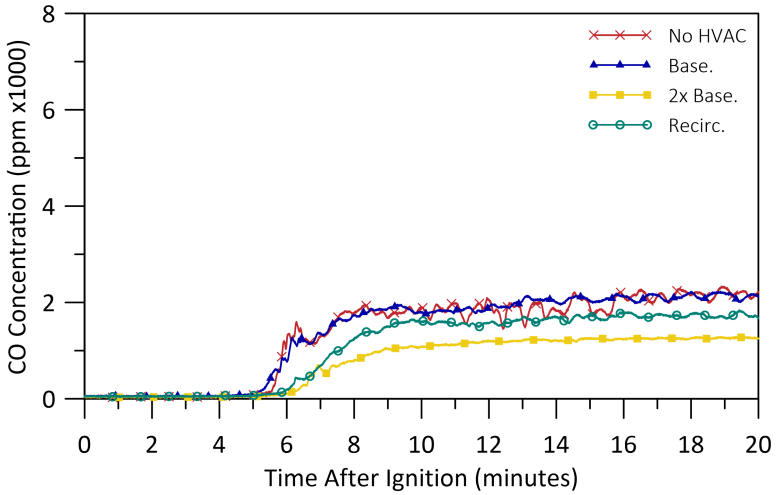

Figure 4.51: Plot comparing CO measurements from the four tests at GIS 1 0.3 m in the fire room.

Concentrations of CO measured at GIS 1 0.9 m are compared between the four tests in Fig. 4.52. At this location, the increase in CO is characterized by two phases, first a slow increase with time which later transitions into a phase of rapid increase. The same trends with time are seen in the decreasing O_2 concentrations at the same location during the growth of the fire. This is expected, since the production of CO should follow, but be slightly delayed from, the decrease in O_2 in the environment. Peak concentrations at GIS 1 0.9 m occur at approximately 7:00 after ignition in all tests. The no HVAC test has the highest measured peak concentration of 7700 ppm, followed by the recirculation test with a peak concentration of 6850 ppm, the baseline HVAC test with a peak concentration of 5600 ppm, and the 2x baseline HVAC test has the lowest peak concentration of 3700 ppm. This ranking is consistent with the expected effect of the HVAC configuration,

where increased supply of OA reduces the concentration of CO. After peak concentrations are reached, CO concentrations at GIS 1 0.9 m decrease to a steady state value after 10:00 into the test and remain at those levels until the end of the tests. The no HVAC test has the highest steady state concentration of CO at 2470 ppm, followed by the baseline HVAC test with a concentration of 2140 ppm, the recirculation test with a concentration of 1700 ppm, and the 2x baseline HVAC test has the lowest steady state concentration of 1290 ppm[7]. The ranking of steady state concentrations from highest to lowest across tests does not follow the order of the peak concentrations at this location, but does match the ordering of concentrations seen at GIS 1 0.3 m. Again, it is unexpected for the concentrations in the recirculation test to be lower than in both the no HVAC and baseline HVAC tests. This anomaly may result because there are higher temperatures experienced in later stages of the recirculation test which may create favourable conditions for the oxidation of CO to CO_2. Unfortunately, this cannot be confirmed since the concentrations of CO_2 saturated as they exceeded the measurement range of the sensors. Since this location best represents the species concentrations in the smoke/combustion products amongst measurement locations in these tests, the concentrations of CO measured at this location should provide an indication of overall combustion efficiency of the fire. In general, combustion efficiency would be anticipated to decrease, and therefore production of CO increase, in fires with less ventilation. The present data broadly supports this theory when peak concentrations of CO are considered. By this indicator, the highest concentrations of CO (least efficient fire) and, therefore, most under-ventilated test are in the no HVAC test, while the lowest concentrations (most efficient fire) and, therefore, most well-ventilated test is the 2x baseline HVAC test.

Figure 4.53 shows a plot comparing the concentrations of CO as measured at GIS 6 0.9 m in the small bedroom on the upper floor. At this location, CO concentrations are characterized by a continual increase over time, with a sigmoid shaped response similar to that seen in the O_2 decrease at the same location and the increase of CO at GIS 1 0.3 m. The most rapid increase in concentration of CO is between 5:00 to 10:00 after ignition in all tests. Peak concentrations occur late in all tests, except for the 2x baseline HVAC test, which shows a slow decrease in concentration after 13:05 into the test compared to the slow increase in concentration seen in the other tests. The no HVAC test has the highest peak concentration of 3290 ppm, followed by the baseline HVAC test with a peak concentration of 2640 ppm, the recirculation test with a peak concentration of 2220 ppm, and the 2x baseline HVAC test has the lowest peak concentration of 1530 ppm. The ranking of tests from the highest peak concentration to lowest is consistent with the ordering of peak concentration values at GIS 1 0.3 m and with the steady state concentrations at GIS

[7]Steady state concentrations are calculated as the average concentration after 10:00 into the test.

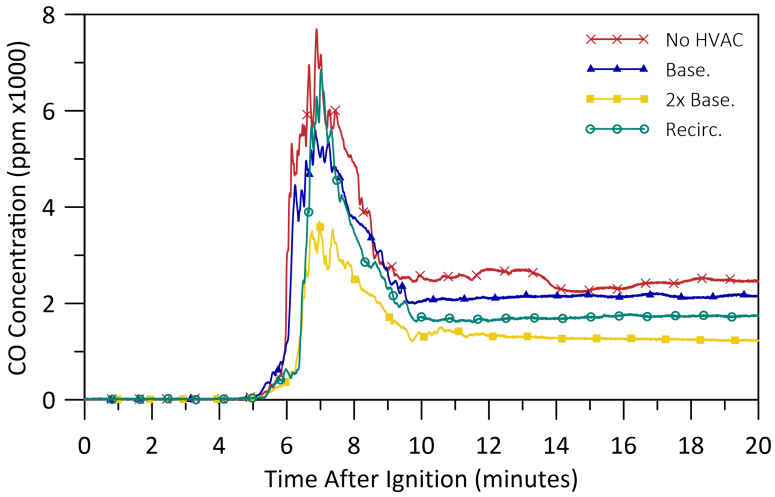

Figure 4.52: Plot comparing CO measurements from the four tests at GIS 1 0.9 m in the fire room.

1 0.9 m. At GIS 6 in the small bedroom, the supply of OA or recirculated gases through the HVAC system in all but the no HVAC test could dilute the concentration of CO. The additional OA supplied in the 2X baseline HVAC test could also explain the slow decrease in concentration seen in that test after the peak value is reached.

Overall, the production of CO is highest in the tests that have the least amount of ventilation. In the 2x baseline HVAC test, which supplies the most OA to the fire room and other compartments, the peak concentrations of CO and steady state concentrations of CO during later stages of the tests, are lowest. General trends of increasing CO concentration throughout the house match closely with patterns seen in the decrease of O_2 concentration with time, which is a good indication of reliable and consistent readings from both sensors. Interestingly, the steady state concentrations of CO are higher in the baseline HVAC test than they are in the recirculation test, even though there is no new OA supplied into the structure during the recirculation test. At the same time, the peak concentration of CO in the upper layer of the fire room is higher in the recirculation test than in the baseline HVAC test. While the latter observation is consistent with the baseline HVAC test having a higher combustion efficiency than the recirculation test, it is not clear why the concentrations in later stages of the recirculation test decrease to lower levels than measured for the baseline HVAC test.

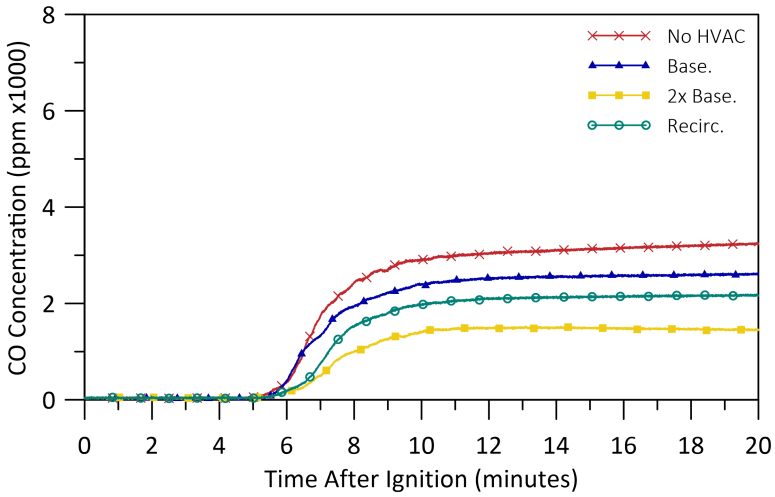

Figure 4.53: Plot comparing CO measurements from the four tests at GIS 6 0.9 m in the small bedroom.

4.5.3 Volatile Organic Compounds

In this section, concentrations of VOC throughout the burn house are presented. First, the VOC concentrations through the main floor and upper floor are presented in detail for the no HVAC test as a reference case. Then, comparisons are made between the four tests in the fire room, to compare the VOC produced by the fires and to provide an additional comparison on the combustion efficiency, and in the small bedroom, to compare the conditions in a far field location.

Figure 4.54 shows measurements of VOC concentration throughout the main and upper floors for the no HVAC test. Main floor locations include GIS 1 (0.3 m and 0.9 m) in the fire room, GIS 3 (0.3 m, 0.9 m, and 1.5 m) in the kitchen, and GIS 4 (0.3 m, 0.9 m, and 1.5 m) in the main floor corridor. Upper floor locations include GIS 5 (0.3 m, 0.9 m, and 1.5 m) in the upper floor corridor, GIS 6 (0.3 m, 0.9 m, and 1.5 m) in the small bedroom, and GIS 7 (0.3 m, 0.9 m, and 1.5 m) in the large bedroom. Concentrations of VOC begin to increase at GIS 1 in the fire room immediately after ignition. The initial increase is slow, but then transitions to grow more rapidly, at a similar time to increasing VOC concentrations at GIS 3 0.9 m and shortly after the increase at GIS 4. VOC concentrations at both heights at GIS 1 in the fire room follow similar trends with time in the initial phase until peak concentrations are reached. The VOC concentration at 0.3 m then levels to a steady state concentration immediately after the peak, while concentrations at the 0.9 m height first peak and then reduce to a steady state concentration for the remainder of the test.

Concentrations of VOC at the other main floor locations, GIS 3 and GIS 4, both increase first at the 1.5 m heights, followed by the 0.9 m and 0.3 m heights sequentially afterwards. The increase in concentration at GIS 3 in the kitchen takes place later than measured at GIS 4 in the main floor corridor at all three heights; however, concentrations increase more rapidly and smoothly with time at GIS 3. Peak VOC concentrations on the main floor are between 1450 ppm and 1650 ppm, with GIS 1 0.3 m and GIS 4 0.3 m having the lowest peak concentrations compared to the others. All locations reach peak concentrations between 6:00 to 7:00 after ignition, comparable to the times when peak CO concentrations are reached at the same measurement locations. After the peak, the concentrations of VOC reduce to steady state concentrations between 1070 ppm to 1450 ppm. Interestingly, GIS 1 0.3 m has the highest steady state concentration of all locations on the main floor.

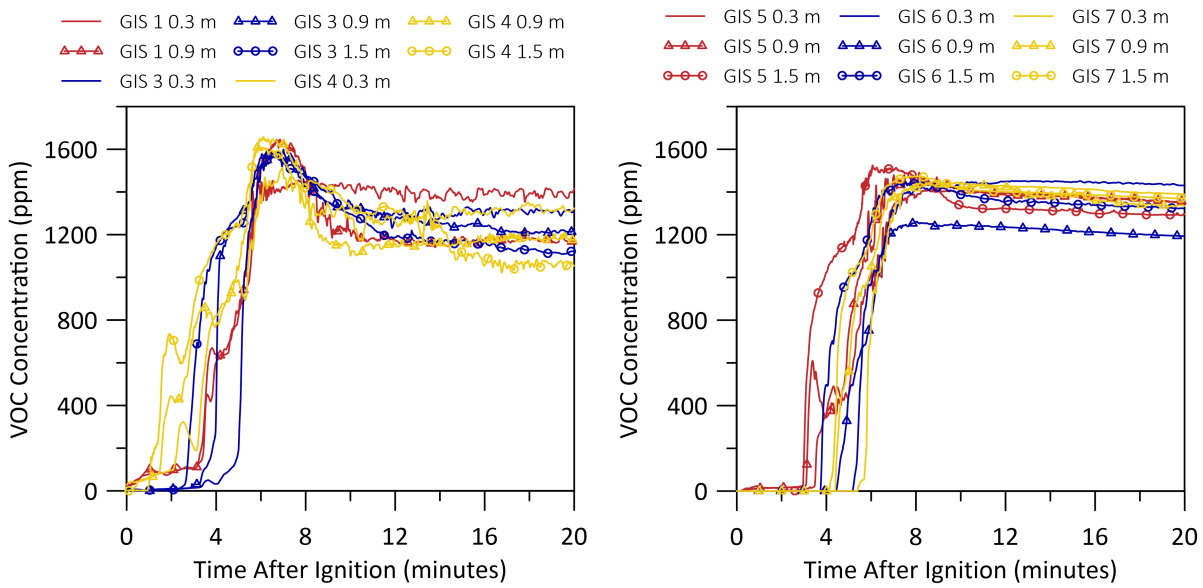

(a) Main floor **(b)** Upper floor

Figure 4.54: Plots of main and upper floor VOC concentrations over time for the no HVAC test.

On the upper floor, concentrations of VOC begin to increase two to three minutes later than on the lower floor, as is expected due to the time required for smoke to flow from the main floor to the upper floor. Similar to the main floor, all locations on the upper floor show concentrations of VOC increase first at the 1.5 m height, followed by the 0.9 m and 0.3 m heights sequentially afterwards. Measurements at all locations increase rapidly to peak concentration, which is reached approximately one minute later than on the main

floor. Concentrations at most locations on the upper floor increase to a peak value and then decrease to a steady state concentration, similar to the response seen on the main floor, although there are lower decreases between peak and steady state than are measured on the main floor. One location, GIS 6 0.9 m in the small bedroom, decreases only very slightly after the peak value and instead reaches a fairly steady concentration with only a slight decrease over the remainder of the test. This location has a comparably lower peak concentration of 1260 ppm, while all other locations have peak concentrations between 1410 ppm to 1520 ppm, comparable to the steady state concentrations on the main floor.

The development of VOC concentrations is similar for all four tests. There are some key differences in peak concentrations and in steady state concentrations, both in the fire room and on the upper floor. The following discussion highlights these differences at GIS 1 in the fire room and GIS 6 in the small bedroom on the upper floor.

Figure 4.51 shows measurements of VOC concentrations for all four tests plotted over time at GIS 1 0.3 m. At this location, the VOC concentrations with time are characterized by an increase in concentration from the time of ignition to approximately 7:00 after ignition. After this, concentrations reach a steady state value which is maintained for the remainder of the tests. Concentrations in all tests, except for the recirculation test, begin to increase immediately after ignition, earlier than initial increases and decreases are observed in CO and O_2 respectively. In the recirculation test, concentration of VOC begin to increase later, at 2:45 after ignition. In the 2x baseline HVAC test, concentrations increase to 700 ppm early in the test, then decrease to values similar to those measured in other tests and remain at similar concentrations for the remainder of the test. Peak values of VOC concentration at GIS 1 0.3 m are similar between all four tests, varying by less than 120 ppm. The highest peak concentration of 1450 ppm is measured in the no HVAC test, followed by the baseline HVAC test with a peak concentration of 1410 ppm, the recirculation test with a peak concentration of 1340 ppm, and the 2x baseline HVAC test with the lowest peak concentration of 1330 ppm. Steady state concentrations are within 90 ppm of the respective peak concentration values, and also similar, within 80 ppm of each other, between all four tests.

Concentrations of VOC are compared between the four tests at GIS 1 0.9 m in Fig. 4.52. In the no HVAC and 2x baseline HVAC tests, the VOC concentrations increase slowly immediately after ignition. This initial growth phase transitions to a more rapid increase in concentration, at 3:00 and 5:00 after ignition for the no HVAC and recirculation tests, respectively. In the baseline HVAC and recirculation tests, the concentration of VOC begins to increase at 3:40 after ignition with similar fast rates of increase as compared to the no HVAC and 2x baseline HVAC tests. After reaching peak concentrations, VOC concentrations decrease in each of the four tests and eventually reach steady state concentration

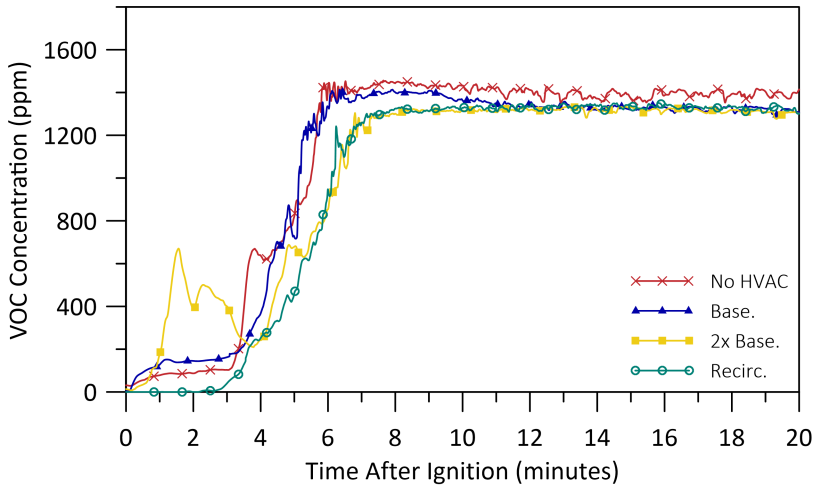

Figure 4.55: Plot comparing VOC measurements from the four tests at GIS 1 0.3 m in the fire room.

values at approximately 10:00 after ignition. This is the same trend as seen with the CO concentration at this same location. The highest peak concentration of VOC, 1650 ppm, is measured at GIS 1 0.9 m in the no HVAC test, followed by the baseline HVAC test with a concentration of 1600 ppm, the recirculation test with a concentration of 1540 ppm, and the 2x baseline HVAC test with the lowest peak concentration of 1470 ppm. The highest concentrations in no HVAC and lowest in the 2x baseline HVAC test is consistent with values of CO concentration measured in the tests as well. For the baseline HVAC and recirculation tests, however, the values of peak VOC concentration are not consistent compared to concentrations of CO as the baseline HVAC test has a higher concentration of VOC than the recirculation test, indicating that combustion in the baseline HVAC test produces more unburned fuel than for the recirculation test. Steady state concentrations at GIS 1 0.9 m are similar between all four tests, with all concentrations being within 100 ppm of each other. The no HVAC test has the highest steady state concentration of 1170 ppm, followed by the recirculation test with a concentration of 1100 ppm, the baseline HVAC test with a concentration of 1090 ppm, and the 2x baseline HVAC test has the lowest steady state concentration of 1070 ppm. The ranking of tests from the highest to lowest steady state concentrations of VOC is as expected based on the ventilation configurations in the different tests. Interestingly, the ranking does not match that based on steady state concentrations of CO at this location. With respect to VOC, the recirculation test has higher steady state concentrations of VOC compared to the baseline HVAC test, possibly since higher temperatures in the later states of the recirculation test lead to prolonged

generation of VOC after flame out. In addition, steady state concentrations of VOC at the 0.9 m height of GIS 1 in all tests are lower than the concentrations at 0.3 m above the floor at the same location. This is consistent with VOC oxidizing to CO in the hotter temperatures of the upper layer. It may also explain the continuing slow increase of CO throughout the tests as well.

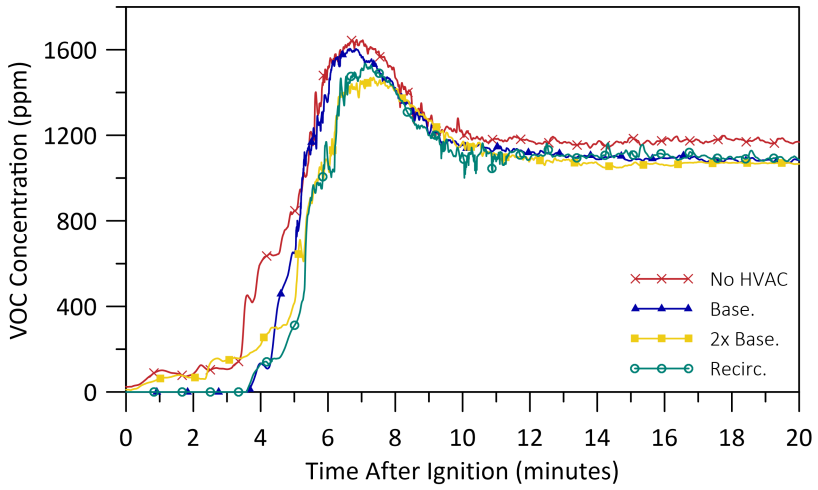

Figure 4.56: Plot comparing VOC measurements from the four tests at GIS 1 0.9 m in the fire room.

Concentrations measured at the 0.9 m height of GIS 1 in the fire room are most representative of the combustion products and therefore provides the best indication of combustion efficiency of the fire. Comparing peak concentrations of CO indicates that the combustion in the recirculation test is less efficient than in the no HVAC test. On the other hand, the peak concentrations of VOC suggest that more unburned fuel is entering the environment in the baseline HVAC test, suggesting that combustion may be less efficient in this test. Thus, it is difficult to conclude the relative combustion efficiency across all four tests. It is not sufficient to independently examine peak concentrations of each species, but instead they should be considered together when considering combustion efficiency of the fire. Generally, more CO than CO_2 will be produced in O_2 deprived (vitiated) environments, while more VOC will also be produced [79, 80]. In this light, the highest concentrations of both CO and VOC are measured in the no HVAC test, while the 2x baseline HVAC test has the lowest concentrations of both CO and VOC. This is consistent with the expectation that increasing the supply of OA to the fire room increases combustion efficiency and reduces the production of these toxic species.

Figure 4.53 shows a plot comparing the concentrations of VOC for all four tests at GIS

6 0.9 m in the small bedroom on the upper floor. The development of concentrations at this location are characterized by an initial growth from ambient to a peak VOC concentration, followed by a slow decrease in concentration until the end of the tests. The no HVAC test has a significantly higher peak concentrations, 1260 ppm, compared to the other tests. The baseline HVAC test has the second-highest peak concentration of 900 ppm, followed by the recirculation test with a concentration of 850 ppm, and the 2x baseline HVAC test with the lowest peak concentration of 800 ppm. In addition to the differences in peak concentrations, there are also significant differences in the slope of the increase in VOC concentrations, which are unique to the upper floor. The no HVAC test has the steepest slope (*i.e.* the fastest increase rate), the 2x baseline HVAC test has the shallowest slope, and the baseline HVAC and recirculation test have intermediate slopes. This shows a clear, and expected, trend of slower rates of increase in VOC concentration on the upper floor with increasing ventilation flow rate.

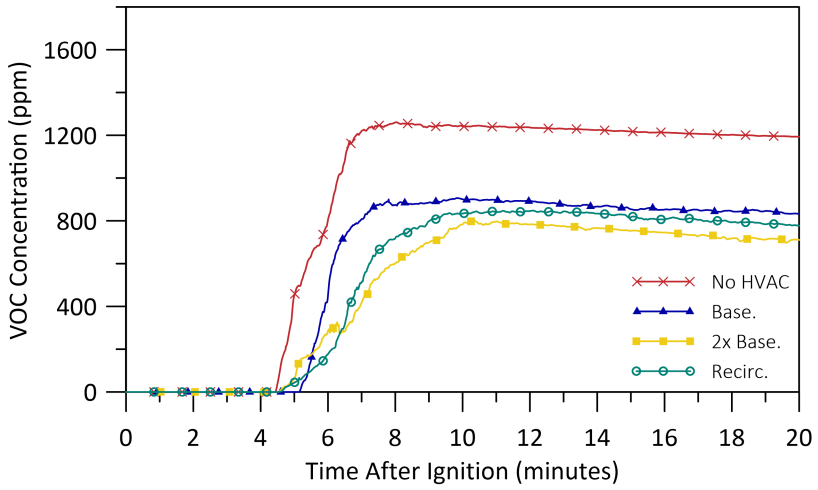

Figure 4.57: Plot comparing VOC measurements from the four tests at GIS 6 0.9 m in the small bedroom.

Overall, the production of VOC is highest in the tests that have the least amount of ventilation. In the 2x baseline HVAC test, which supplies the most OA to the fire room, the peak concentrations of VOC and steady state concentrations of VOC during later stages of the tests, are lowest. General trends in distribution of VOC concentration throughout the house match closely with patterns seen in the production of CO. The results agree that the no HVAC test, with the lowest amount of ventilation produces the highest levels of both species, while the 2x baseline HVAC test the lowest.

4.6 Relationship Between Factors

Previous sections have discussed the evolution of MLR, gaseous species concentrations, doorway smoke flows, as well as other factors throughout the duration of the tests and have compared the four tests against each other. This section focuses on the evolution of the environment in the fire room for each of the tests individually and discusses the link between the fire MLR, O_2 concentrations, and the doorway mass flow rates into and out of the fire room.

Figure 4.58 shows a plot of the fire MLR plotted with O_2 at GIS 1 0.9 m in the fire room and the mass flow rates into and out of the fire room for the no HVAC test. The mass flow rates are the sum of the flow rates through the fire room/kitchen door, the doorway at the bottom of the stairs, and the main floor corridor/kitchen doorway. In general, smoke flows out of the fire room and fresher air flows into the fire room. The plot shows that the O_2 concentration begins to decrease 17 seconds after the slope of the fire MLR increases from the initial slow fire growth to more rapid growth. Initially, O_2 concentration decreases at a slow rate, but this later transitions into a fast rate of decrease. The transition from the slow decrease of O_2 to the fast decrease of O_2 follows the increase of the slope of the fire MLR. As the fire grows it consumes additional oxygen, resulting in the measured decrease in O_2 concentration in the fire room. The peak fire MLR occurs 23 seconds after the fast decrease of O_2 concentration begins. After this, the O_2 concentration continues to decrease at a fast rate due to rapid consumption of O_2 from the environment after the time of peak fire MLR. As the fire begins to under ventilate, the sustained low O_2 concentrations restrict further development of the fire. The buildup of a denser layer of smoke in the fire room may also contribute to the fast rate of decrease in O_2; however, it is difficult to determine the smoke layer height or the density of smoke at the time when the decay in O_2 concentrations transition from slow to fast rates of decrease. If the buildup of a denser layer of smoke in the fire room is enough to affect measurements at GIS 1 0.9 m above the floor, then it is probable that the smoke is also being drawn in towards the flame, such that the fire is entraining vitiated air which would further limit ventilation and prevent the fire from continuing to grow.

Figure 4.58 also shows that the mass flow rate out of the fire room becomes greater than the mass flow rate into the fire room six seconds before the start of the rapid decrease in O_2 concentration. As this occurs, the flow of smoke out of the room increases relative to the flow of fresher air, with a higher O_2 concentration, into the room. The O_2 reaching the fire is therefore restricted. The minimum mass flow rate into the fire room occurs at approximately the same time as flame out, when the fire MLR reduces below 3 g/s. Two minutes later, the O_2 concentration begins to recover. This suggests that as the fire dies

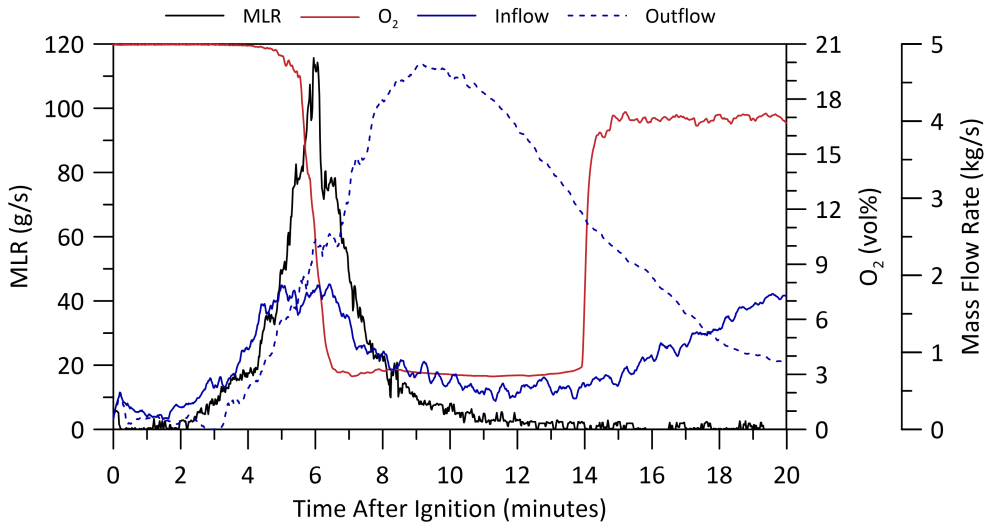

Figure 4.58: Plot comparing MLR with O_2 at GIS 1 0.9 m in the fire room and fire room doorway mass flow rates for the no HVAC test.

down and less smoke is produced, there is an increasing inflow of fresher air into the fire room from other compartments, which contributes to the recovery of O_2 in the fire room.

A similar plot showing the comparison of fire MLR, O_2, and the mass flow into and out of the fire room is shown in Fig. 4.59 for the baseline HVAC test. In this test, the concentration of O_2 begins to decrease 35 seconds after the slope of the fire MLR increases from its initial slower growth phase to the fast growth phase. Over this period, O_2 is slowly decreasing as well. The decrease in O_2 concentration becomes much more rapid three seconds before the peak fire MLR. While this transition is much closer to the time of peak MLR compared to the no HVAC test, it still occurs before the peak fire MLR is reached. Again, the growth of the fire drives the decrease in O_2 concentration up to the time when O_2 concentrations begin to decrease very quickly. After this point, the available O_2 appears to limit the size of the fire as the fire environment becomes under-ventilated.

The flow of smoke out of the fire room becomes greater than the flow of fresher air into the room four seconds after the peak MLR and seven seconds after the fast decrease of O_2 begins. This is not consistent with the no HVAC test, where the outflow becomes greater than the inflow prior to the fast decrease of O_2. In both tests though, the timing of the transitions are within a few seconds of one another. Therefore, the net flow through the doorways of the fire room is still linked to the very rapid decrease in available O_2. Recovery of the O_2 concentration in the baseline HVAC test begins approximately one minute after

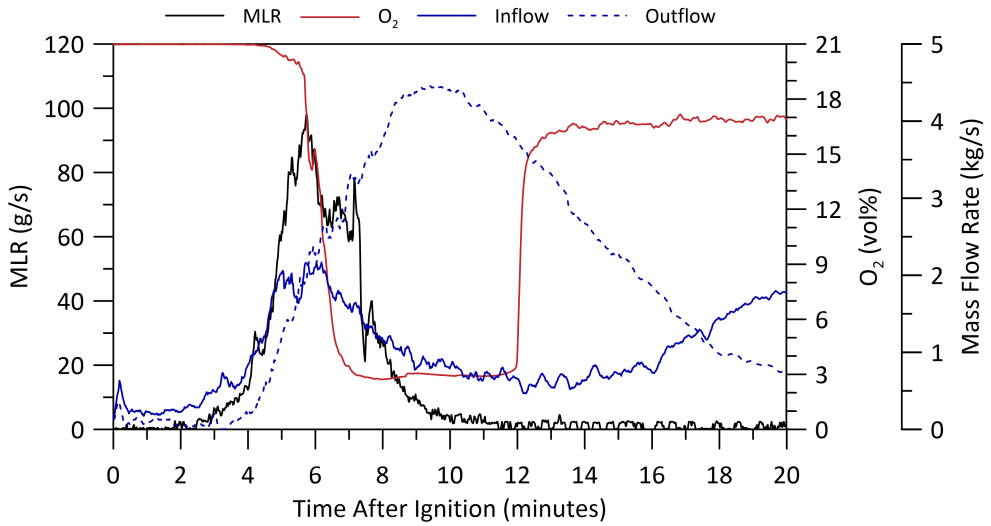

Figure 4.59: Plot comparing MLR with O_2 at GIS 1 0.9 m in the fire room and fire room doorway mass flow rates for the baseline HVAC test.

flame out and takes one minute to reach the steady state value. In contrast to the no HVAC test where minimum inflow of fresh air into the fire room occurs prior to recovery of O_2, the minimum inflow of fresher air into the fire room in the baseline HVAC test occurs 15 seconds after the recovery of O_2 in the fire compartment begins. While these differences make it difficult to ascertain if the inflow is the sole driver for recovery of O_2 in the fire compartment, there is clearly a strong correlation between the size of the fire, inflow rates and overall O_2 concentration in the fire compartment.

Figure 4.60 shows the comparison between fire MLR, O_2 concentration, and the mass flow into and out of the fire room for the 2x baseline HVAC test. In this test, the decrease in O_2 concentration begins eight seconds before the slope of the fire MLR profile increases, which is different from the previous tests. However, in this test, the fire MLR is also higher (fire is larger) at this time compared to the other tests supporting the notion that fire growth drives the overall trends in decreasing O_2 concentration within the compartment. The transition from the slow to the fast decrease in O_2 occurs 38 seconds before the peak fire MLR is reached, consistent with the timing seen in the previous two tests. Again, this suggests that as the fast decrease in O_2 begins, the fire becomes under-ventilated and further fire growth is limited. Minimum O_2 concentrations in the 2x baseline HVAC test are reached late in the decay phase of the fire, approximately two minutes before flame out, and the recovery of O_2 starts five minutes after flame out, which is much later than in the other tests. No apparent reason for this discrepancy has been found.

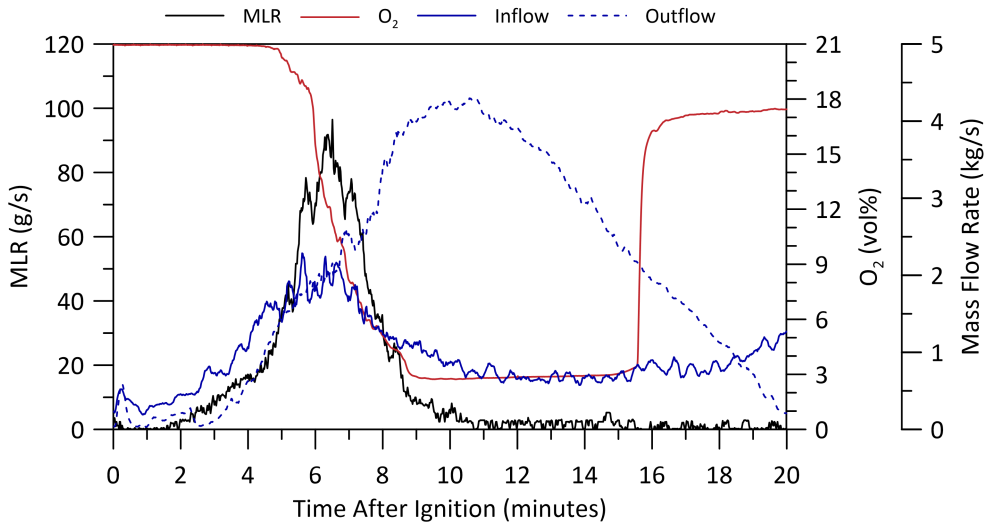

Figure 4.60: Plot comparing MLR with O_2 at GIS 1 0.9 m in the fire room and fire room doorway mass flow rates for the 2x baseline HVAC test.

The outflow of smoke from the fire room becomes greater than the inflow of fresher air into the fire room one minute after the fast decrease of O_2 concentration in the fire room, which is later compared to the previous tests. The two flow rates are approximately equal at the time when the fast decrease of O_2 begins, such that the outflow of smoke through the fire room doorways is still high enough to limit the intake of fresher air into the fire room accelerating the decrease in concentration of O_2. The inflow of fresher air into the fire room reaches its minimum one minute and 42 seconds before the O_2 concentration begins to recover, and continues to increase for the remainder of the test afterwards. This timing is consistent with the no HVAC test and further shows that the increasing inflow of fresher air into the fire room, coupled with the reduction of smoke production after flame out, is correlated with the rapid recovery of O_2 in the fire room.

Comparisons between the fire MLR, O_2 concentration, and the doorway mass flow rates into and out of the fire room are shown in Fig. 4.61 for the recirculation test. In this test, the decrease in O_2 concentration begins eight seconds after the fire MLR increases from the initial slower growth to a more rapid growth. This is consistent with timing of the no HVAC and baseline HVAC tests. The fast decrease in O_2 concentration begins at the time of the first peak in the MLR profile, which is well before the second peak that is considered to be more representative of the actual peak in fire growth. Due to the falling checker board next to GIS 1 in the fire room, trends in the profiles of peak fire MLR and O_2 concentrations with time are slightly different in this test. The falling checker board

causes enhanced mixing near GIS 1 which leads to a double peak in the fire MLR and a period of increasing O_2 concentration immediately prior to the fast decrease in O_2. Even with this anomaly, it is still clear that the initial decrease in O_2 is driven by growth of the fire until the time when the decrease in O_2 accelerates and the fire becomes limited by the low O_2 concentrations, resulting in the second peak and subsequent decay in fire MLR.

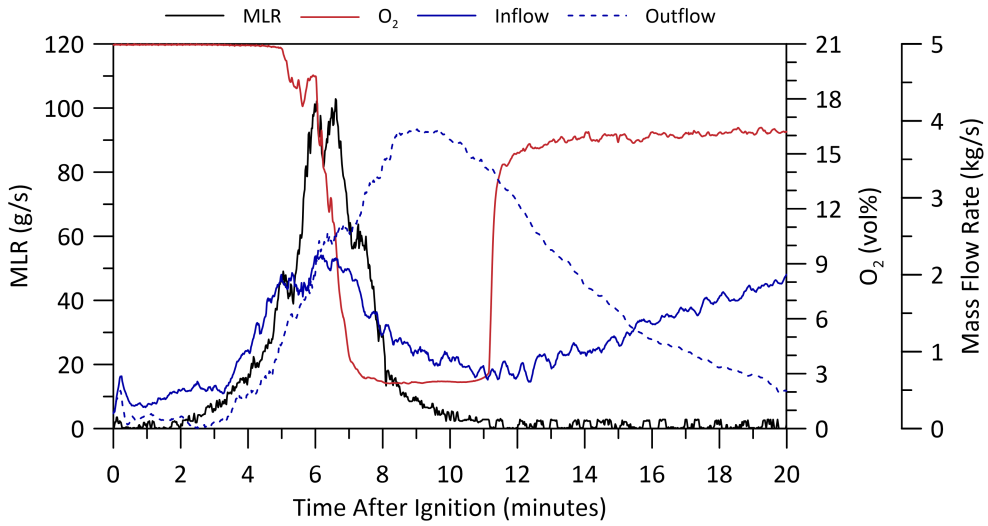

Figure 4.61: Plot comparing MLR with O_2 at GIS 1 0.9 m in the fire room and fire room doorway mass flow rates for the recirculation test.

The mass flow rate of smoke out of the fire room becomes greater than the mass flow rate of fresher air into the fire room three seconds after the fast decrease of O_2 begins. This is consistent with the timing of the baseline and 2x baseline HVAC tests, and the fast decrease of O_2 may even be delayed due to the falling of the checker board. Therefore, this provides further indication that the fast decrease of O_2 is related to the net flow of air through the doorways of the fire room. Recovery of O_2 in the recirculation test, begins 14 seconds after flame out, and takes two minutes to increase from the minimum concentration to the steady state concentration. This recovery period is comparably longer than for the other three tests, which all take around one minute to increase from the respective minimum concentrations up to the steady state concentrations. The mass flow rate of air into the fire room begins to increase one minute and 20 seconds after the O_2 concentration starts to recover, which is not consistent with the no HVAC and 2x baseline HVAC tests, where the mass inflow rate begins to increase before the O_2 concentration starts to recover. While there is a lag between mass inflow rate and O_2 recovery in the baseline HVAC test, it is much shorter, only 15 seconds. Nonetheless, due to the long recovery period in the

recirculation test, the increase of the mass flow rate of air into the fire compartment still occurs during the recovery period consistent with the clear link between fire size, recovery of O_2 and mass flow rate of air into the fire room.

In general, O_2 concentrations as measured at GIS 1 0.9 m above the floor begin to decrease near the time when the slope of the fire MLR with time profile increases. The initial slow rate of O_2 decrease at this position later transitions to a faster rate of decrease near the time when the mass flow rate of smoke leaving the fire room becomes greater than the mass flow rate of fresher air entering the fire room thus limiting the supply of air to the fire. In all four tests, the mass outflow from the fire room overtakes the mass inflow when the mass flows equal approximately 2 kg/s. This, along with the following development of the mass flow rates through the openings, suggests that the limit of the total flow rate through the fire room doorways is near 4 kg/s. To further explore this notion, the maximum mass flow rate available through an equivalent doorway representative of the combination of the three fire room doorways in the present test is computed using the equation $\dot{m}_g = 0.5 A_o \sqrt{H_o}$, where A_o is the total doorway opening area and H_o is the doorway height. This estimates a limiting value of mass flow of 4.2 kg/s, consistent with the observations from the experimental results [29].

Trends in data across all four tests suggests that fire growth coupled with smoke generation drives the reduction of the O_2 concentration in the fire room. Once the O_2 concentration is reduced significantly, the fire transitions into a ventilation limited burning regime, where additional fire growth is limited by the lack of O_2. The timing of the events after the fire is out further suggest that an increasing supply of fresher air into the fire room after flame out coupled with the reduced production of smoke leads to the rapid recovery of O_2 in the fire room.

4.7 Details of Extinction

As discussed in Sec. 2.4, extinction in ventilation limited compartment fires is typically governed by the concentration of O_2 available to the fire. The limiting oxygen concentration is not constant, but instead is dependent on many factors, including the ambient temperature in the compartment [87]. As the ambient temperature in the compartment increases, the heat feedback to the fuel surface also increases, which prolongs burning at reduced O_2 concentrations. At the same time, fires that produce higher compartment temperatures also consume more O_2, creating a feedback loop. To examine these relationships in the current tests, the details of fire room O_2 concentrations and temperatures during the decay phase of the fires are discussed, with a focus on extinction.

Figure 4.62 shows a plot of O_2 concentration measured at GIS 1 0.9 m in the fire room versus temperature measured at T5 0.93 m in the fire room for the no HVAC test. The plot depicts the O_2 in the upper layer of the fire room and the nearest measure of temperature throughout the test. At ignition, the O_2 concentration and temperature are both at ambient, with values of 20.95% and 25 °C, respectively. As the fire grows, the O_2 concentration decreases and the temperature increases. At approximately 100 °C, the slope of the O_2-temperature profile changes to become steeper. It is during this phase where the peak fire MLR occurs at an O_2 concentration of 11.3% and a temperature of 143 °C. The temperature begins to decrease shortly after the peak fire MLR when the O_2 concentration is around 10.5%. The O_2 concentration also continues to decrease until it reaches 8.5%, after which the temperature increases again until the peak temperature is reached. In this test, the minimum O_2 concentration and maximum temperature at the 0.93 m height occur nearly simultaneously. The minimum O_2 concentration is maintained as the temperature decreases until, at the time of flame out, the O_2 concentration and temperature are 3.0% and 69 °C, respectively. Shortly after flame out, the O_2 concentration recovers and temperatures continue to decrease back toward ambient. Recovery of O_2 from the minimum value to a final steady state concentration value occurs when the temperature is approximately 65 °C.

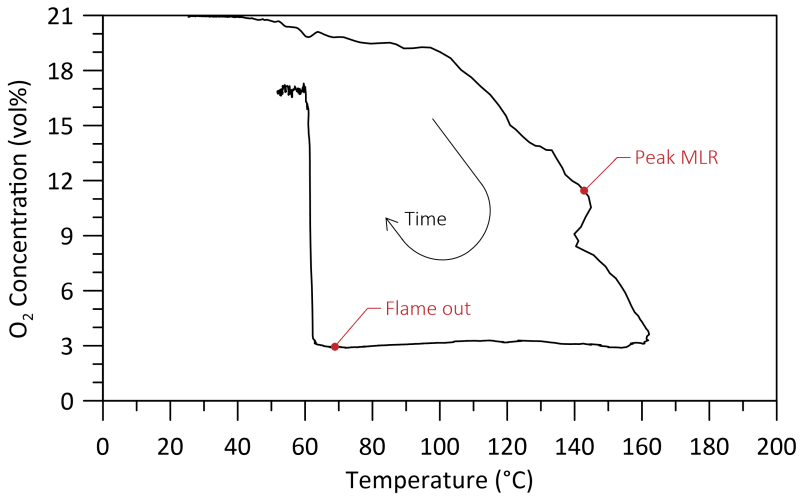

Figure 4.62: Plot of O_2 at GIS 1 0.9 m versus temperature measured at T5 0.9 m in the fire room for the no HVAC test.

A similar plot of the O_2 concentration measured at GIS 1 0.9 m in the fire room versus temperature measured at T5 0.93 m in the fire room for the baseline HVAC test is shown in Fig. 4.63. At ignition, the O_2 concentration and temperature are both at ambient.

As the fire grows, the temperature begins to increase and the O_2 concentration begins to decrease. Once the O_2 concentration reaches 19.3% and the temperature reaches 125 °C, the slope of the O_2-temperature profile becomes steeper. The peak MLR occurs during this steeper phase at an O_2 concentration of 16.2% and a temperature of 138 °C. The peak fire MLR in this test occurs at a slightly higher O_2 concentration and slightly cooler temperature compared to the no HVAC test. After the peak MLR, the slope of the O_2-temperature profile becomes more shallow. At approximately 150 °C, the O_2 concentration momentarily increases, and the temperature momentarily decreases. The cause of the momentary increase in O_2 and the decrease in temperature is unknown. After this, the O_2 concentration begins to rapidly decrease, while the peak temperature is reached. The minimum O_2 concentration in the baseline HVAC test is reached while the fire room is cooling. Flame out occurs during the cooling phase while the O_2 concentration is at the minimum value. The O_2 concentration and temperature at flame out is 2.9% and 75 °C, respectively. The O_2 concentration at the time of flame out is similar to that of the no HVAC test, while the temperature is slightly hotter in the baseline HVAC test. Finally, the recovery of O_2 occurs at a temperature of 70 °C, which is again a slightly hotter temperature than for the no HVAC test.

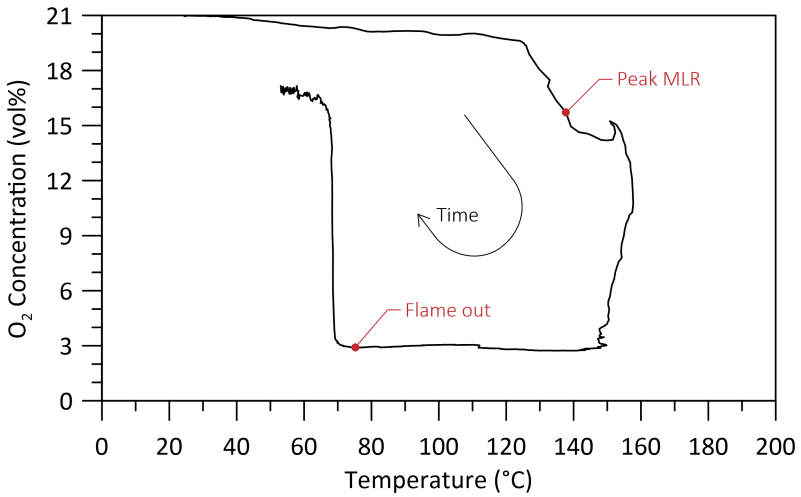

Figure 4.63: Plot of O_2 at GIS 1 0.9 m versus temperature measured at T5 0.9 m in the fire room for the baseline HVAC test.

Figure 4.64 shows a plot of O_2 concentration measured at GIS 1 0.9 m in the fire room versus temperature measured at T5 0.93 m in the fire room for the 2x baseline test. At ignition, the O_2 concentration and temperature are both at ambient and, as the fire grows, the temperature begins to increase and the O_2 concentration begins to decrease. In this

test, there is no distinct point where the slope of the O_2-temperature profile changes. The peak fire MLR in the 2x baseline HVAC test occurs at an O_2 concentration of 11.3% and a temperature of 124 °C, which is the same O_2 concentration as the no HVAC test with a cooler temperature compared to both the no HVAC and baseline HVAC tests. After the peak fire MLR, the temperature continues to increase, reaching a peak temperature, while the O_2 concentration continues to decrease. The minimum O_2 concentration in the 2x baseline HVAC test occurs while the fire room is cooling, and flame out occurs at the minimum O_2 concentration of 2.8% and a temperature of 80 °C, similar O_2 concentration with a hotter temperature compared to the previous two tests. Recovery of the O_2 concentration from the minimum value to the steady state value occurs at a temperature of 60 °C. The temperature during the O_2 recovery is slightly cooler than for the previous two tests, and there is a larger gap between the temperatures at flame out and at O_2 recovery. This may be explained by the enhanced cooling in later stages of the test due to the additional supply of OA into the fire room.

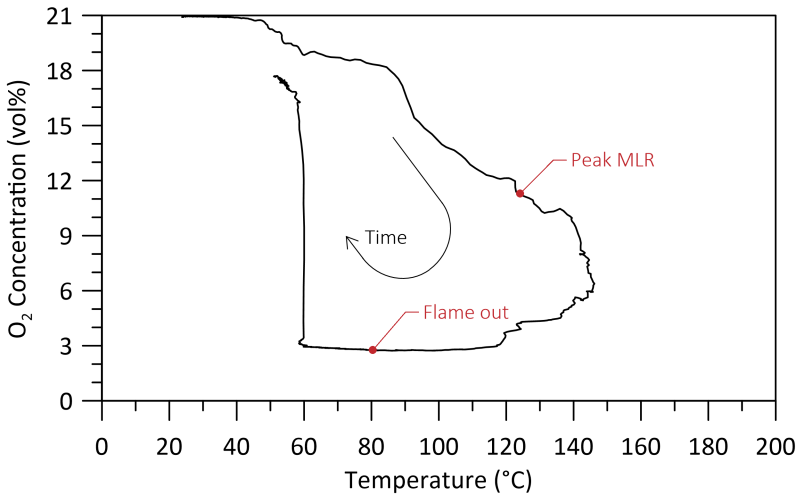

Figure 4.64: Plot of O_2 at GIS 1 0.9 m versus temperature measured at T5 0.9 m in the fire room for the 2x baseline HVAC test.

Figure 4.65 shows a plot of O_2 concentration measured at GIS 1 0.9 m in the fire room versus temperature measured at T5 0.93 m in the fire room for the recirculation test. At ignition, the O_2 concentration and temperature are both at ambient values. In this test, the O_2 concentration initially begins to decrease, but then increases slightly and reaches a constant value while the temperature in the fire room continues to increase. The first peak in the fire MLR is reached at the end of this period of constant O_2 concentration of 18.7% and a temperature of 135 °C. This O_2 concentration is higher, but the temperature

is similar in comparison to those corresponding to the peak fire MLR of the other tests. After the first peak in the fire MLR, the O_2 concentration begins to decrease again while the temperature continues to increase. The second peak in the fire MLR occurs at an O_2 concentration of 9.9% and a temperature of 180 °C. The O_2 concentration of the second fire MLR peak is significantly lower and the temperature is significantly hotter than the O_2 concentration and temperature at the peak fire MLR in the other tests. In the recirculation test, the second peak in the MLR occurs near the peak temperature in the fire room, and this temperature is maintained while the O_2 concentration decreases to the minimum concentration. While at the minimum concentration, the temperature in the fire room cools and flame out occurs at an O_2 concentration of 2.6% and a temperature of 92 °C. This O_2 concentration is comparable, although is slightly lower, than the other tests and the temperature is hotter than the other tests. Recovery of the O_2 concentration from the minimum concentration to the steady state value occurs at a temperature of 90 °C, which is at least 20 °C hotter than in any of the other tests.

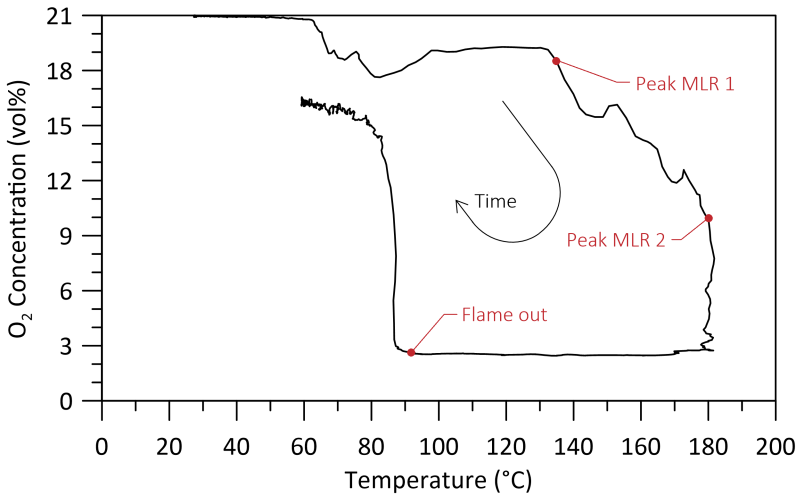

Figure 4.65: Plot of O_2 at GIS 1 0.9 m versus temperature measured at T5 0.9 m in the fire room for the recirculation test.

Measurements of O_2 concentration and temperature at the time of peak fire MLR and at flame out are listed in Table 4.4 for each of the four tests. Note that values listed for the recirculation test are from the second peak in fire MLR, which is more indicative of the conditions immediately prior to the decay of the fire. In general, the peak fire MLR is reached while the O_2 concentration is decreasing and before the temperatures in the fire room have peaked. As discussed previously, the decreasing O_2 concentration causes the fires to under-ventilate, which restricts fire growth. The fire room continues to

heat past the time of peak fire MLR as the fire is still producing heat in the early stages of decay. The values of O_2 concentration and temperature at the time of the peak fire MLR are indicative of conditions at the start of the decay phase. These values do not show a clear trend of higher temperatures with lower O_2 concentrations. At the time of flame out, there is a clear trend, where the tests with lower O_2 concentrations have higher temperatures. This is shown even though the tests all have similar O_2 concentrations at this time, varying by only 0.4% at most between the no HVAC test with the highest concentration and the recirculation test with the lowest. It is interesting that the tests show an increase in temperature and a lower O_2 concentration at flame out with increasing supply of OA into the fire room, which suggests the ventilation can enhance the feedback loop between limiting O_2 concentration and compartment temperature. Recovery of O_2 occurs between 60 °C to 70 °C in the no HVAC, baseline HVAC, and 2x baseline HVAC tests, but a significantly higher temperature of 90 °C is measured in the recirculation test at recovery. Therefore, the O_2 recovery cannot be linked to a specific temperature in the present tests.

Table 4.4: Summary of O_2 concentration and temperature at peak MLR and flame out for each test.

	Peak MLR		Flame out	
Test	O_2 (vol%)	Temp. (°C)	O_2 (vol%)	Temp. (°C)
No HVAC	11.3	143	3.0	69
Base. HVAC	16.2	138	2.9	75
2x Base. HVAC	11.3	124	2.8	80
Recirculation	9.9	180	2.6	92

The values at the peak fire MLRs listed in Table 4.4 are shown plotted on a scatter plot in Fig. 4.66 to further investigate any potential trends in the O_2-temperature relationship at the time of peak MLR of the fires. The plot also includes the first peak in fire MLR for the recirculation test and a line representing the flammability limit suggested by Utiskul *et al.* [88] and Mizukami *et al.* [89]. As suggested previously, there is no clear trend of lower O_2 concentration with higher temperatures when considering all four tests. However, the trend does exist when only considering the no HVAC, 2x baseline HVAC, and the second peak in fire MLR for the recirculation test[8]. The values of O_2 concentration and temperature at peak fire MLR for the no HVAC, 2x baseline HVAC, and the second peak

[8]The first peak in fire MLR in the recirculation test does not adhere to this trend further supporting use of the second peak in the discussions.

in the recirculation test are also very close to the flammability limit suggested by Utiskul. This further indicates that the fires in these three tests under-ventilate and extinguish due to lack of O_2 in a similar manner as predicted theoretically.

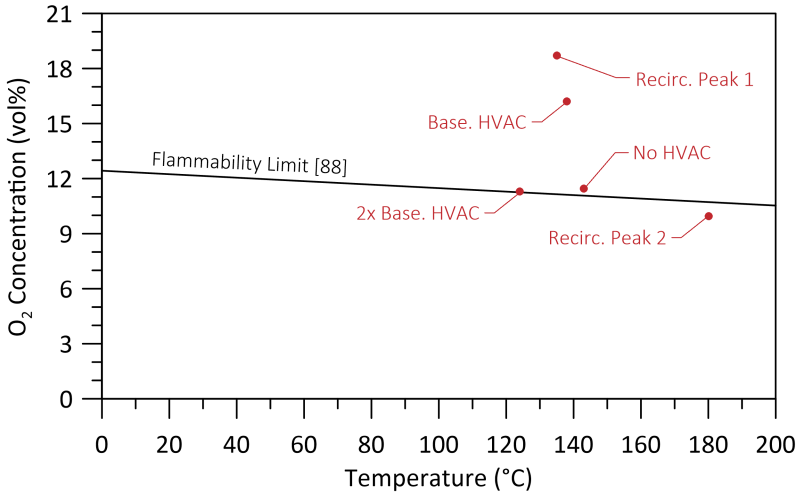

Figure 4.66: Plot comparing O_2 concentration versus temperature in the fire room at peak MLR to the Utiskul flammability limit.

Interestingly, the baseline HVAC test has a significantly higher O_2 concentration for the corresponding temperature at peak fire MLR compared to the other tests. This may be due to the different mode of flame spread in this test, where the fire preferentially spread vertically up the back couch cushion as opposed to horizontally across the seat cushion. Vertical flame spread up the back couch cushion may promote under-ventilation by restricting air entrainment into the burning area positioned in the corner of the couch between the first cushion and the arm rest. Measurements of O_2 and temperature more local to the fire, that would be more representative of the conditions of the air being entrained, would likely be more consistent with the theoretical estimates. Unfortunately, these measurements are not available for the present tests.

Experimental results from four ventilation-limited furniture fires, all burning identical fuel loads with varying mechanical ventilation configurations, have been presented and discussed in this chapter. The results are then used to characterize fire growth, environmental development, and smoke flow throughout the structure. In the next chapter, some of these results are used as input into existing engineering correlations to evaluate whether these correlations can be utilized to estimate heat flux, temperatures, and smoke flow in the present modern fire scenarios.

Chapter 5

Evaluation of Engineering Correlations

Engineering correlations are often used by fire protection engineers to verify the safety of building designs. Calculations include the estimation of heat flux to a target from a specified fire to evaluate the risk of igniting adjacent materials, the estimation of compartment temperatures, and the estimation of gas flow through a structure for occupant exposure and safety calculations. This chapter evaluates some of the most common engineering correlations for predicting these quantities using measured data from the current ventilation-limited fire scenarios.

5.1 Estimation of Heat Flux

Calculating the radiative heat flux emitted by a fire that is incident to a target is a common engineering design calculation. It is often carried out to determine if a target receives a high enough incident heat flux to incur damage, to ignite or to calculate a safe separation distance between the fire and target. This section focuses on estimating the incident radiative heat flux to the location of HFG 2 on the wall across from the couch (the target) during the baseline HVAC test. Calculated values are then compared to the measured heat flux at HFG 2. This test is chosen for the heat flux calculations because the environment in the fire room remains clearer during fire growth phase compared to any of the other tests. Since radiation is a line of sight process, clearer conditions, with increased visibility, are favourable for more accurate measurements of the flame size in images taken from video

recordings of the fire. In addition, any effects of smoke obscuring the line of sight between the HFG and the fire would be minimal in a clearer environment.

5.1.1 Heat Flux Calculation Methods

There are two common methods to estimate the heat flux to a target: the point source method and the area source method, both of which are applied and evaluated here. There are a number of other methods to estimate heat flux to a target in addition to the point or area source methods. These other methods are often applied to specific scenarios, such as when a flame is tilted by wind, and are not used in engineering design situations as often [77]. Thus, the two methods evaluated here are the most appropriate for the given fire scenario.

The point source method uses the simplest configuration of all radiation models, and is also considered to be the least accurate method [77], particularly for targets in the near field of a fire. It is recommended that the point source method be used only as an order of magnitude or first pass calculation for design scenarios. If the results of the point source method predict a heat flux close to a critical heat flux value for the scenario, then a more accurate approach would normally be applied. The point source method, assumes that the radiation from the fire is emitted from a single infinitesimally small point located at the mid-height of the flame, along the vertical centre line of the fire, as shown in Fig. 5.1. The flame has a height H (m), a width D (m), and the target is located at a distance R (m) from the centre line of the fire with a horizontal distance L (m).

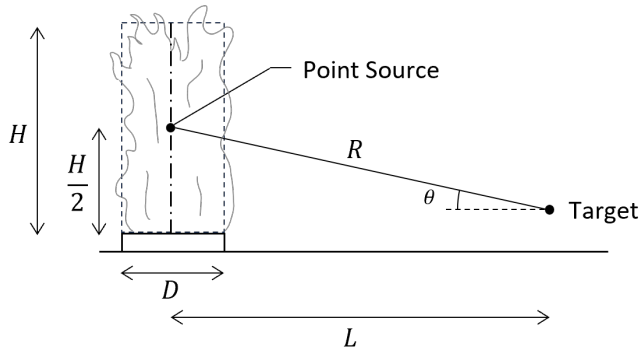

Figure 5.1: Configuration for the point source method.

Using this model, there is a simple relationship between the incident heat flux, the fire size, and the distance from the point source to the target, given by Eq. 5.1 [25], where

$\dot{q}''_r$ (kW/m^2) is the radiant heat flux incident to the target, χ_r is the radiative fraction, $\dot{Q}$ (kW) is the HRR of the fire, and θ (°) is the angle between the normal to the target and the centre line of the fire as shown in Fig. 5.1. The radiative fraction is the amount of the HRR which is emitted as radiation. It is a function of both fuel and fire size but is typically assumed to have a value of 0.3 [77, 25].

$$\dot{q}''_r = \frac{\chi_r \dot{Q} cos\theta}{4\pi R^2} \tag{5.1}$$

The point source method is most accurate at large distances from the fire, with estimates of heat flux known to be within 5% of the correct incident heat flux when L/D is greater than 2.5 [77]. The method is also known to underpredict the heat flux at closer locations, and it is recommended to use a factor of safety of two in these situations or when the calculated heat flux is less than 5 kW/m^2. The factor of safety is most appropriate for design applications when a conservative estimate is desired, not when an accurate/realistic result is needed.

The area source method is a more robust method which typically provides more accurate results than the point source method. In the area source method, the fire is approximated as a rectangle with a height equal to the flame height and a width equal to the diameter of the fire (assuming a fire with a circular base). The rectangle is assumed to have a uniform temperature representing an average flame temperature and therefore, the area has a uniform emissive power. The emissive power is estimated from the HRR of the fire with Eq. 5.2 [25], where E (kW/m^2) is the emissive power, H (m) is the flame height and D (m) is the flame width.

$$E = \frac{\chi_r \dot{Q} cos\theta}{2HD} \tag{5.2}$$

The incident heat flux to the target is then calculated using Eq. 5.3, where $F_{1\rightarrow 2}$ is the view factor between the fire (1) and the target (2) [25].

$$\dot{q}''_r = F_{1\rightarrow 2} E \tag{5.3}$$

The view factor is determined from the configuration of a rectangle (the flame) facing a differential area (the target), as shown in Fig. 5.2. The rectangle and the target must be configured so that the target is aligned with a corner of the rectangle. Tabulated view factors from Drysdale are used to evaluate the view factor for the present configuration [68].

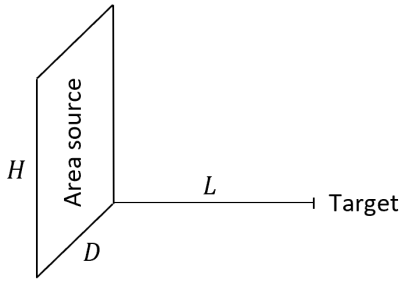

Figure 5.2: Configuration for the area source view factor.

The area source method is known to estimate the incident heat flux to a target to be approximately double that of the point source estimation due to the extended area used in the area source method [25]. In the area source method, it is recommended that the horizontal distance L between the fire and the target should be greater than two times the fire diameter D. Both the point source and area source methods for estimating incident heat flux from a fire to a target assume complete combustion and neglect the influence of smoke as a participating medium. The direct implementation of these methods also neglects any radiative heat flux from the hot gas layer that builds up within a fire compartment over time, or from any hot surfaces other than the flame. While these assumptions allow for simplification of the heat flux calculations, they introduce errors into heat flux estimations relative to values that actually occur or are measured during a fire.

Measurements from the experimental setup are used to create the geometrical configuration used in calculations per the correlations. Important positions include the location of the couch, the location of HFG 2, and the position of the flame on the couch. The location of the couch and the HFG are known from measurements taken prior to the test. The flame on the couch is assumed to be centred front-to-back on the couch cushions, and left-to-right positions are measured from images of the flame taken from camera 4 clipped at the time of the heat flux calculation. The HFG is positioned next to camera 4 and therefore, the images from camera 4 are a good representation of the view of the fire at the HFG as well.

The geometry used in the correlation, with dimensions locating the HFG relative to the fire, is shown in Fig. 5.3. The bottom of the flame is located on top of the couch cushion 0.6 m above the floor of the fire room, and the HFG is located on the wall across from the couch 0.79 m above the floor. The horizontal distance from the centre of the flame to the HFG is 2.27 m. The top view in Fig. 5.3 shows the HFG is approximately centred on the couch and is, therefore, offset one cushion width (0.74 m) from the centre of the first cushion. The outline of the flame shown is consistent with the position of the flame at the

time of ignition of the second cushion. As the fire grows the flame spreads, however, the centre of the flame shifts. Therefore, the position of the flame must be reevaluated using the images from camera 4 for the heat flux calculations performed at the time of peak fire MLR.

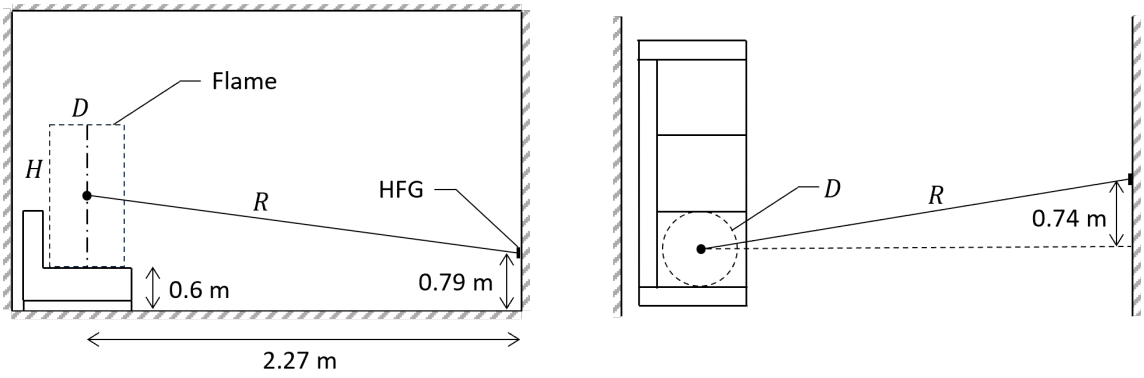

(a) Side view **(b)** Top view

Figure 5.3: Experimental configuration for the heat flux correlations.

The geometry described is the same between the point source and the area source calculations. In the point source calculation, the centre line position of the flame is the important factor, while the location of the edge of the rectangle approximating the flame is important in the area source calculation. Images of the flames at the time of ignition of the second cushion and at peak fire MLR are shown in Fig. 5.4 with the rectangular outline approximating the flame. It is clear that at ignition of the second cushion (Fig. 5.4a), the corner of the rectangle does not align with the HFG as required for determination of the view factor. Therefore, it is necessary to superimpose a second rectangle ('b' in Fig. 5.4a) with a corner that is aligned with the HFG. The view factor is calculated for this rectangle and for the rectangle encompassing the outer edges of both rectangles ('a plus b' in Fig. 5.4a). The final view factor used for the rectangle representing the flame is taken as the difference between the two view factors. At the time of peak fire MLR (Fig. 5.4b), the flame has progressed to the point where it is acceptable to assume that the bottom right corner of the fire is aligned with the HFG as required.

5.1.2 Heat Flux calculation Results

Inputs into the heat flux calculations from the baseline HVAC test including the HRR, flame width D, flame height H, and the view factor $F_{1\to 2}$ for both key times are listed in

(a) Ignition of second cushion **(b)** Peak MLR

Figure 5.4: Flame images showing representative areas for the heat flux correlations.

Table 5.1. The fire HRRs are calculated using the measured values of fire MLR at the time of the event using the effective heat of combustion of the couch materials using Eq. 3.1 as described in Sec. 3.2.2. The radiative fraction is assumed to be 0.3 as recommended in the literature.

Table 5.1: Summary of inputs in to the heat flux correlations for the baseline HVAC test.

Event	HRR (kW)	D (m)	H (m)	$F_{1\to2}$
Second cushion ignites	511	0.45	1.11	0.027
Peak MLR	1653	0.73	1.21	0.049

Results from the calculations, along with the values of measured heat flux, are shown in Table 5.2. The results show that at the time when the second cushion ignites, the measured heat flux is 3.2 $\mathrm{kW/m^2}$, while the heat flux estimated by the point source method is 2.2 $\mathrm{kW/m^2}$ and by the area source method is 4.0 $\mathrm{kW/m^2}$. In this case, the point source method underestimates the measured heat flux by 1.0 $\mathrm{kW/m^2}$, a 31% error, and the area source method overestimates the measured heat flux by 0.8 $\mathrm{kW/m^2}$, a 25% error. Similar trends are seen at the time of peak fire MLR. The measured heat flux at this time is 10.2 $\mathrm{kW/m^2}$, while the estimate by the point source method is 7.2 $\mathrm{kW/m^2}$ and the estimate by the area source method is 13.3 $\mathrm{kW/m^2}$. The point source method underestimates the measured heat flux by 3.0 $\mathrm{kW/m^2}$, a 29% error, and the area source method overestimates the measured heat flux by 3.1 $\mathrm{kW/m^2}$, a 30% error. In general, the values from the area source method are nearly double those of the point source method, which is consistent with the observations from Drysdale [25].

As expected, values of heat flux to the compartment wall at the position of HFG 2

Table 5.2: Summary of results from the heat flux correlations for the baseline HVAC test.

	Heat Flux (kW/m^2)		
Event	Measured	Point Source	Area Source
Second cushion ignites	3.2	2.2	4.0
Peak MLR	10.2	7.2	13.2

estimated using the point source method underestimate the measured heat flux, which is not a conservative result. However, when a factor of safety of two is applied to the point source method, as recommended for design calculations and when the heat flux is below $5\,kW/m^2$ as seen at the time when the second cushion ignites, the estimates of heat flux become greater than the measured values and are therefore conservative. At the same time, with the suggested factor of safety applied, estimated values severely overestimate the measurements, even more than the area source method. Estimations of heat flux made using the area source method are conservative, as this method consistently overestimates the measured heat flux. Interestingly, the errors seen with both the point source and area source methods are nearly the same magnitude but in opposite directions from the measured heat flux. Therefore, neither method can really be deemed more accurate than the other for the fire scenario at hand.

Previously mentioned sources of errors in the heat flux estimation methods include neglecting the effects of smoke as a participating medium and any incident radiation from the hot smoke layer or any other hot surfaces. Neglecting radiation from the hot layer or other hot surfaces that are in the line of sight of HFG 2 would introduce an underprediction in the estimations, since these additional sources of measured radiation are neglected in the calculations. However, neglecting the potential influence of smoke in the fire room would skew the correlations to overestimate the heat flux, as smoke is likely to absorb radiation emitted by the fire and obscure the view of the fire from the view point of HFG 2. Other sources of error that could result in overestimation include overestimating the size of the rectangle representing the fire and underestimating the separation distance between the fire and the HFG which could result from improper assumptions on the location of the fire. In addition, the HFG itself is subject to influence from convective heat transfer from the flow of air/smoke across the face of the gauge. This effect likely results in cooling of the gauge and would, therefore, result in the measured heat flux being less than the actual. Convective heat transfer across the gauge is more pronounced when the smoke layer descends past the gauge, which is consistent with the larger errors seen between the measured and area source estimated heat flux values at the time of peak fire MLR when

smoke has descended closer to the floor.

A combination of the various sources of error may well explain why the area source method overestimates the measured heat flux. The effects from the buildup of smoke in the fire room are likely more impactful in scenarios similar to the present experiments where the fire under-ventilates, increasing smoke production, and when the structure is sealed. It is difficult to further assess the reliability and comparability of the present results due to a lack of these types of experiments in the literature. On the other hand, the point source method is known to underpredict heat flux measurements due to the simplifications made in the configuration assumed in application of the method. Therefore, the results seen in the present experiments for the point source method are consistent with the literature.

5.2 Estimation of Compartment Temperature

Estimation of compartment temperatures is a common fire protection engineering calculation as compartment temperature is an essential parameter used to determine when a fire scenario may reach critical thresholds such as the onset of hazardous conditions, structural damage, ignition of objects, and the onset of flashover [29]. Obtaining an estimate of compartment temperature is often done through the use of an engineering correlation that is appropriate for the scenario at hand. There are numerous correlations which have been developed for use in either pre-flashover or post-flashover conditions.

This section focuses on applying compartment temperature correlations to estimate the temperature in the fire room throughout the duration of each of the four tests conducted in the present work. In total, three correlations are presented, each of which are developed for pre-flashover conditions. Correlations for the pre-flashover scenario are used because the four tests discussed in this work never reach flashover, as all four fires become ventilation limited and extinguish due to lack of O_2. Results from the calculations are compared to temperature measurements taken at the centre of the fire room. Errors between the calculated and measured values are discussed, with an emphasis on the estimation of peak temperature, since peak temperatures represent the most hazardous conditions in a fire scenario.

5.2.1 Temperature Correlations

Temperature correlations are typically semi-empirical correlations, meaning that they are developed from first principles of energy conservation and modified by fitting the result

to a set of experiments, which vary depending on the correlation. Energy conservation is commonly applied to the hot layer of a fire compartment, where energy added to the hot layer by the fire equals the energy lost from the hot layer through radiation and convection to the compartment surfaces plus the energy convected out of the compartment openings (enthalpy flow) [29]. Energy conservation must be applied as a function of time, because neither the HRR of the fire nor the volume of the upper hot gas layer is constant. For this reason and for simplicity, estimates of compartment temperature are typically calculated for a steady state fire situation.

The transport of energy in a compartment fire scenario is quite complex and, therefore, several simplifying assumptions are made to derive a correlation [29]. In addition, the set of experiments used for empirical fits of the constants in a given correlation vary between correlations and are by no means comprehensive across all possible fire scenarios. Some correlations also rely on additional correlations to estimate the mass flow rate of smoke through the compartment vents to evaluate the enthalpy flow term in the energy conservation model. For these reasons, each correlation has its own set of inherent assumptions and limitations that may make one more applicable than another to a given scenario.

Three engineering correlations are evaluated in this section, including the McCaffrey, Quintiere, and Harklroad (MQH) method [64], the Foote, Pagni, and Alvares (Foote, *et al.*) method [103], and the Beyler and Deal method [145]. All three of these correlations are semi-empirical and are developed for estimation of compartment temperature in pre-flashover scenarios. The correlations are used to predict spatially averaged upper layer temperatures and, therefore, cannot be used to calculate local temperatures, such as those needed to predict sprinkler or smoke detector activation [29]. Measurements from the present experiments show that the temperatures in the upper hot gas layer is not uniform, so the temperature from the thermocouple located 2.26 m above the floor at rake T3 in the centre of the fire room is selected as a representative upper layer temperature for comparison with the temperatures predicted using the correlations, as this location measures hot upper layer gas temperatures while avoiding ceiling jet flow. The comparison between measured and predicted temperatures is done throughout the test in a time resolved manner, with a focus on the prediction of peak temperature. This is done to evaluate the efficacy of the correlation during the transient stages of fire development and decay as well as in estimation of the peak temperature, which is the more commonly desired output of correlations for design calculations.

The MQH method is the most famous and commonly used method for estimating compartment temperatures. The upper layer gas temperature in a compartment is calculated by conservation of energy using correlations for ventilation flow rate and fits to experimental data from over 100 experiments [64]. The empirical fits include both transient and

steady state experiments using natural and synthetic polymer fuels, as well as hydrocarbon fuels [29]. This correlation does not incorporate the impacts of any flow due to forced ventilation, as it is developed for natural ventilation only.

The MQH method calculates the compartment temperature using the expression given by Eq. 5.4 [64], where $\Delta T_g = T_g - T_a$ (K) is the change in gas temperature (T_g) from ambient air temperature (T_a), $\dot{Q}$ (kW) is the HRR of the fire, A_o (m^2) is the compartment vent opening area, H_o (m) is the compartment vent opening height, h_k ($kW/m^2\,K$) is the conduction heat transfer coefficient, and A_T (m^2) is the total compartment wall surface area.

$$\Delta T_g = 6.85 \left(\frac{\dot{Q}^2}{A_o \sqrt{H_o} h_k A_T} \right) \tag{5.4}$$

The heat transfer coefficient is evaluated using either Eq. 5.5 or Eq. 5.6, depending on whether the exposure time (t) is greater or less than the thermal penetration time (t_p), where k_{wall} (kW/m K) is the thermal conductivity of the compartment wall, δ_{wall} (m) is the thickness of the compartment wall, ρ_{wall} (kg/m^3) is the density of the compartment wall, $c_{p,wall}$ (kJ/kg K) is the specific heat of the compartment wall, and t (seconds) is the elapsed exposure time.

$$h_k = \frac{k_{wall}}{\delta_{wall}} \text{ for } t > t_p \tag{5.5}$$

$$h_k = \left(\frac{k_{wall} \rho_{wall} c_{p,wall}}{t} \right) \text{ for } t < t_p \tag{5.6}$$

The thermal penetration time for the MQH method is evaluated using Eq. 5.7, where t_p is the thermal penetration time in seconds.

$$t_p = \left(\frac{\rho_{wall} c_{p,wall}}{k_{wall}} \right) \left(\frac{\delta_{wall}}{2} \right) \tag{5.7}$$

The MQH method is limited by the experimental data used for the empirical fits, where most of the tests have fires located at the centre of the compartment and there is a lack of data on ventilation limited fires [29]. This method applies to both transient and steady state fire situations, provided that the transient response can be captured by conduction through the compartment walls [64]. It is not applicable to rapidly developing fires in large

enclosures where there is significant fire growth before smoke can exit the compartment. McCaffrey *et al.* also report that the method is limited to hot gas layer temperatures below 600 °C, and attribute this limit to potential for flame extension into the upper layer, which is suggested to become significant above 600 °C [64]. In addition, the characteristic fire growth and thermal penetration time of compartment walls must be known in order to evaluate the heat transfer coefficient.

The method of Foote *et al.* [103] follows the same basic derivation as the MQH method. However, Foote *et al.* focuses this correlation on estimating upper layer temperatures in a compartment when there is forced ventilation, as opposed to the natural ventilation case targeted by the MQH correlation. The data used for the development of the Foote *et al.* correlation comes from a series of methane gas burner experiments conducted in a 6.0 m × 4.0 m × 4.5 m compartment with forced ventilation supplied near the floor at flow rates between 11 g/s to 325 g/s and exhausted near the ceiling [103]. These experiments have HRRs varying from 150 kW to 490 kW and are considered to be well ventilated. This correlation is limited by the relatively small input data set used in its derivation.

Estimates of compartment temperatures using the Foote *et al.* method are completed using the expression presented by Eq. 5.8 [103], where $\dot{m}_g$ (kg/s) is the mass flow rate of the forced ventilation, $c_{p,g}$ (kJ/kg K) is the specific heat of the upper layer gas (assumed air), and all other variables are the same as the MQH method. In addition, the heat transfer coefficient (h_k) is evaluated in the same way as for the MQH method.

$$\Delta T_g = 0.63 T_a \left(\frac{\dot{Q}^2}{\dot{m}_g c_{p,g} T_a} \right)^{0.72} \left(\frac{h_k A_T}{\dot{m}_g c_{p,g}} \right)^{-0.36} \tag{5.8}$$

A limitation of the Foote *et al.* correlation is that the mass flow rate of the forced ventilation must be known, and the correlation is not intended for compartments with natural vents such as open doorways or windows. Reference [29] does suggest an additional correlation, shown by Eq. 5.9, that can be used for natural ventilation cases, where $\dot{m}_{g,nat}$ (kg/s) is the mass flow rate through the natural vent, ρ_a (kg/m^3) is the air/gas density at ambient temperature, and $g = 9.81$ m/s^2 is the gravitational acceleration constant. In the present work, there is both natural ventilation, through the doorways adjacent to the fire room, and forced ventilation through the HVAC ductwork. Therefore, the total ventilation mass flow rate used in the present calculations is the sum of the natural flow rate given by Eq. 5.9 and the known forced ventilation flow rate into the fire room.

$$\dot{m}_{g,nat} = 0.1(\rho_a A_o \sqrt{g H_o}) \tag{5.9}$$

The Beyler and Deal method uses an improved correlation for compartments with forced ventilation that is suggested to be used as an alternative to Foote *et al.* [29]. This correlation is also derived from energy conservation in the upper layer in a fire compartment and improves the estimate of the heat transfer coefficient with its own correlation. Empirical data from over 250 compartment fire experiments with both natural ventilation and forced ventilation supply near the floor [145] are used in the correlation. Additional work also shows that the correlation has good prediction of compartment temperatures when forced ventilation is supplied near the ceiling as well [106]. In addition, this correlation is reported to be appropriate for both transient and steady state heat conduction through the compartment walls. However, the correlation is limited to provide results up until 2000 seconds (33 minutes) after ignition, as the heat transfer model breaks down after this [29].

The expression for compartment temperature using the Beyler and Deal method is shown in Eq. 5.10 [145], where all terms in the equation, except for the heat transfer coefficient (h_k), are the same as for the previous two correlations. The heat transfer coefficient is redefined in this correlation and is now given by Eq. 5.11. This expression for the heat transfer coefficient incorporates both transient and steady state conditions, and switches from transient to steady state at a thermal penetration time of $t_p = (\rho_{wall} c_{p,wall}/k_{wall})\delta_{wall}^2$, which is different from that used by the MQH and the Foote *et al.* methods.

$$\Delta T_g = \frac{\dot{Q}}{\dot{m}_g c_{p,g} + h_k A_T} \tag{5.10}$$

$$h_k = 0.4 \cdot \max\left(\frac{\sqrt{k_{wall}\rho_{wall}c_{p,wall}}}{t}, \frac{k_{wall}}{\delta_{wall}}\right) \tag{5.11}$$

Similar to the correlation by Foote *et al.*, the Beyler and Deal method does not prescribe a method to estimate the natural ventilation flow rate when it is unknown. There is only some general advice to use a conservative estimate for the natural vent mass flow rate when implementing the correlation [145]. Due to the lack of direction in the case of unknown flow rates, such as the natural flow rates through the fire room doorways, the independent correlation for $\dot{m}_{g,nat}$ given by Eq. 5.9 is used in applying this correlation to the present experiments, despite having no direct statement permitting this approach.

5.2.2 Implementation of Temperature Correlations

The engineering correlations to estimate compartment temperatures in the fire room for the present tests are implemented following the guidance and suggestions provided in the

literature, as described above. The details of each of the inputs into the calculations, for the fire scenario at hand, is provided here.

The primary, and perhaps most important, input parameter for the temperature correlations is the fire HRR. Measured values of HRR overtime from each of the tests is used. This HRR is calculated as the product of the measured MLRs (presented in Sec. 4.2.2) and the effective heat of combustion, as described in Sec. 3.2.2.

Another input is the thermal properties of the compartment walls, which is needed to account for heat losses to the walls. The walls of the fire room are modelled as an assembly of cement board, type-X fire rated gypsum board, and mineral wool batt insulation which closely resembles the construction of the walls. A schematic of the wall assembly model is shown in Fig. 5.5.

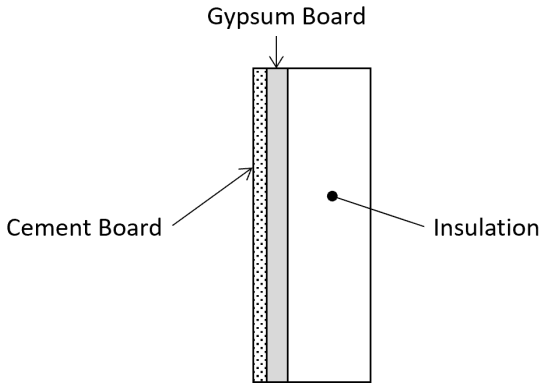

Figure 5.5: Cross-sectional schematic of the wall assembly model.

Thermal properties of each of the materials making up the wall assembly found in the literature and used in the present calculations are listed in Table 5.3. All of these properties are for the respective material at room temperature, and it is assumed that the properties remain constant under heating. The overall thermal properties of the wall assembly are calculated using Eqs. 5.12 - 5.14, where the subscript i represents the property corresponding to the individual components of the wall assembly. Properties for the overall wall assembly are also listed in Table 5.3.

$$k_{wall} = \frac{\delta_{wall}}{\sum \delta_i / k_i} \tag{5.12}$$

$$\rho_{wall} = \frac{\sum \delta_i / \rho_i}{\delta_{wall}} \tag{5.13}$$

Table 5.3: Summary of the thermal properties of the materials in the wall assembly.

Material	Ref.	k_i (kW/m K)	ρ_i (kg/m^3)	$c_{p,i}$ (kJ/kg K)	δ_i (m)
Cement Board	[146]	1.37×10^{-4}	1290	0.936	0.013
Gypsum Board (type-X)	[147]	2.58×10^{-4}	711	1.089	0.016
Insulation	[148]	2.00×10^{-4}	150	1.200	0.100
Wall Assembly		1.97×10^{-4}	331.9	1.160	0.129

$$c_{p,wall} = \frac{\sum \delta_i c_{p,i}}{\delta_{wall}} \tag{5.14}$$

The fire room itself is modelled as a 6.9 m × 3.2 m × 2.4 m compartment with three doorway openings. The size of each of the openings is listed in Table 5.4. However, the correlations require that the compartment have only a single vent opening. Therefore, it is necessary to calculate an effective opening that is equivalent to the combination of the three individual vents. The effective size of the equivalent single vent is calculated using Eq. 5.15 [29], where the subscript i is the index representing each doorway opening. The result is also listed in Table 5.4.

Table 5.4: Sizes of the three doorway openings in the fire room and the effective vent parameter.

Doorway	$A_{o,i}$ (m^2)	$H_{o,i}$ (m)
Fire room/kitchen	1.77	2.12
Fire room/staircase	2.09	2.11
Fire room/corridor	3.23	2.40
$\left(A_o\sqrt{H_o}\right)_{eff}$	10.61 m$^{5/2}$	

$$\left(A_o\sqrt{H_o}\right)_{eff} = \sum A_{o,i}\sqrt{H_{o,i}} \tag{5.15}$$

The final inputs needed for the temperature correlations are the properties of the upper layer gas or smoke. For simplicity, this gas is assumed to be air, which is a common assumption made when using correlations for engineering calculations. Properties of the air are assumed to be constant throughout the test and are evaluated at an ambient temperature of 295 K. The density of ambient air is taken as 1.2 kg/m^3, and the specific heat of ambient air is taken as 1.05 kJ/kg K. For the implementation of the forced ventilation

mass flow rate, the nominal volumetric flow rate specified for each test is converted to mass flow rate using this ambient air density.

5.2.3 Temperature Estimation Results

Figure 5.6 shows time resolved plots of the measured temperature from T3 2.26 m and estimated temperature results from the three correlations. It can be seen that the estimated temperature curves from all three correlations are essentially scaled HRR curves for each of the four tests, showing that the development of HRR drives the estimation of temperature which is entirely consistent with the derivation via an energy balance on the hot layer. Throughout the duration of each test, the MQH method consistently predicts the highest estimated temperature, the Beyler and Deal method predicts the lowest estimated temperature, and the Foote *et al.* method estimates a temperature between the two.

Results from all four tests show that each of the three correlations follow the slope/shape of the transient behaviour well, as temperatures increase during the growth phase of the fires. In the no HVAC and baseline HVAC tests, the Beyler and Deal method is clearly the best predictor of temperature during the transient phase. In the 2x baseline HVAC test and the recirculation test, the Foote *et al.* method provides the best predictions of temperature in the transient growth phase. The reasons that the higher temperature predictions of the Foote *et al.* method result in better prediction of the temperatures during fire growth for the 2x baseline and recirculation tests are as follows. In the 2x baseline HVAC test, the measured temperatures are similar to those in the no HVAC and baseline HVAC tests. However, the HRR is effectively lower due to the forced ventilation pushing the smoke layer over the flames. A lower HRR results in a lower estimated upper layer temperature and therefore, the correlation which previously overpredicted the temperature is now more effective. In the recirculation test, the measured temperature is greater than those of the previous three tests, and there is no similar increase in the HRR to match the increase in temperature. Therefore, the correlation that previously overpredicted temperatures is most appropriate in this test.

The plots also show that peak temperatures are estimated to occur prior to the measured peak temperature in each test. This is explained again by the relationship between HRR and temperature in the compartment. Temperatures continue to increase after the peak HRR since there is still significant heat released after the peak HRR and the gas in the compartment has a thermal capacity. However, this phenomenon is not captured by the correlations, causing the estimated peak temperature to occur earlier than measured. The estimated temperatures from each of the correlations continue to follow the profile

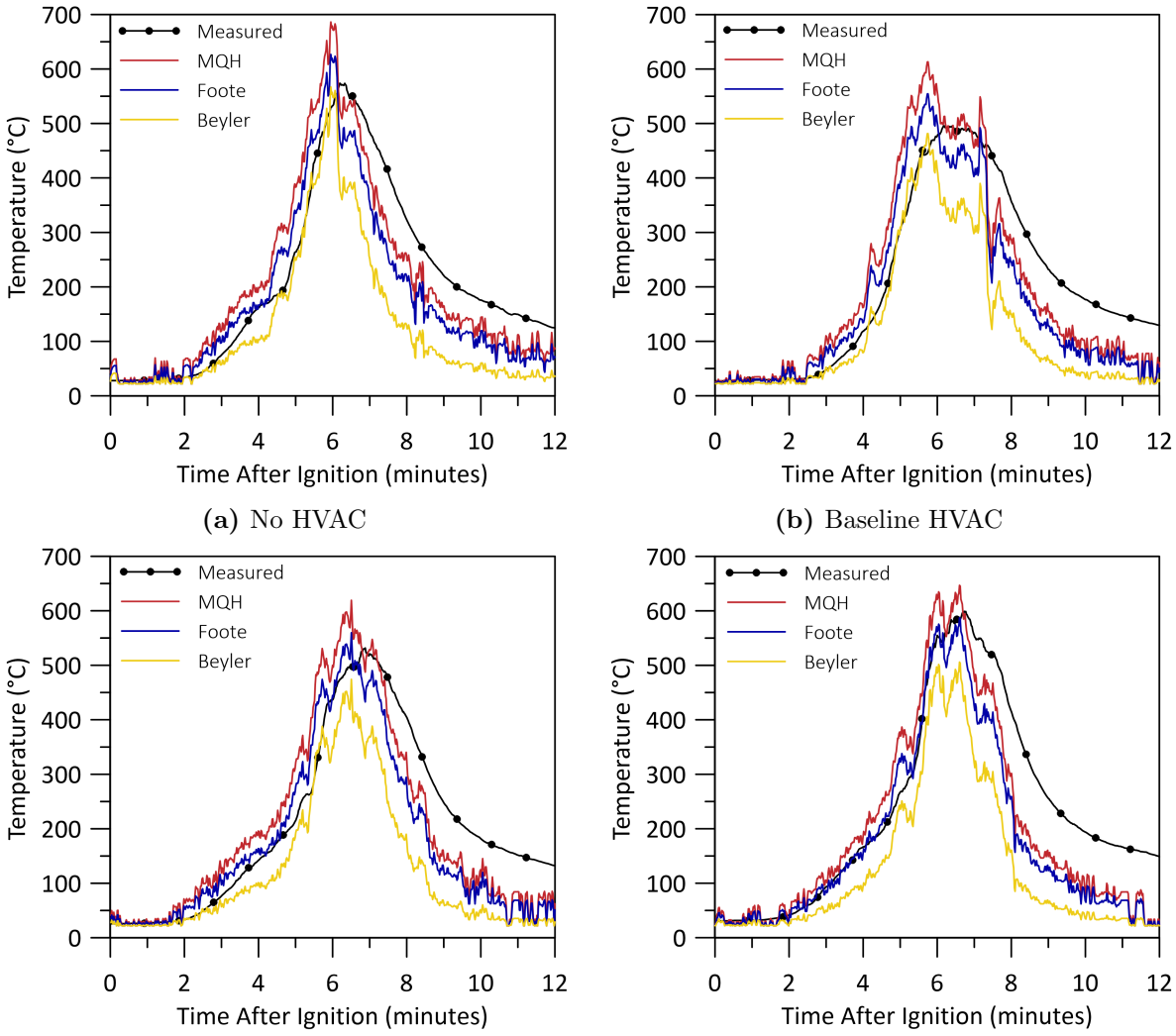

(a) No HVAC

(b) Baseline HVAC

(c) 2x Baseline HVAC

(d) Recirculation

Figure 5.6: Plots of measured and estimated temperatures versus time for each test.

of the HRRs after the peak. This causes the correlations to estimate that the fire room cools more quickly than is actually measured. As a result, each of the three correlations underestimate temperatures during the transient decay phase of the fires across all tests.

It is stated previously that the common desired output of engineering correlations is the peak temperature. Therefore, it is necessary to evaluate the correlations in terms of the accuracy of prediction of peak temperature. Table 5.5 lists the measured and estimated peak temperature from each correlation in each test, as well as the percent error of the estimation from the measured value. A positive percent error represents an overestimated temperature and a negative percent error represents an underestimated temperature. In engineering applications, it is desirable to have a conservative result, which in the case of temperature would mean a slightly overestimated value in many situations.

Table 5.5: Measured and estimated peak temperatures with percent error for each test.

		MQH		Foote *et al.*		Beyler and Deal	
Test	Measured (°C)	Estimated (°C)	Error (%)	Estimated (°C)	Error (%)	Estimated (°C)	Error (%)
No HVAC	574	686	20	627	9	567	-1
Base.	496	613	24	555	12	481	-3
2x Base.	532	619	16	560	5	474	-11
Recirc.	599	647	8	587	-2	506	-16

Considering only the value of absolute percent error, the Beyler and Deal method provides the most accurate estimates of peak temperature for the no HVAC and baseline HVAC tests, and the Foote *et al.* method is most accurate for the 2x baseline HVAC and recirculation tests. However, the Beyler and Deal method underpredicts peak temperature for every test and is therefore not conservative in predictions of damage and ignition thresholds for example. When considering only overestimated results (positive percent error), the Foote *et al.* method becomes the most accurate method for predicting peak temperature in the no HVAC, baseline HVAC, and 2x baseline HVAC tests, but underpredicts the peak temperature in the recirculation test. The MQH method provides the most accurate estimate for the recirculation test and is the only method to have a conservative result for all tests.

Figure 5.7 shows a bar chart of the average absolute percent error across all tests for each correlation. The MQH method has the highest average percent error of 16.9%, the Foote *et al.* method has the lowest average percent error of 6.1%, and the Beyler and

Deal method has an intermediate average percent error of 7.6%. In general, the MQH method is the least accurate at predicting peak temperatures in the present fire scenario. It is, however, the most conservative. The Foote *et al.* method is the most accurate for the present scenario and is also a conservative method as long as the HVAC system is not configured for recirculation. The Beyler and Deal method is only a few percent less accurate than the Foote *et al.* method, but in general is not conservative for damage predictions.

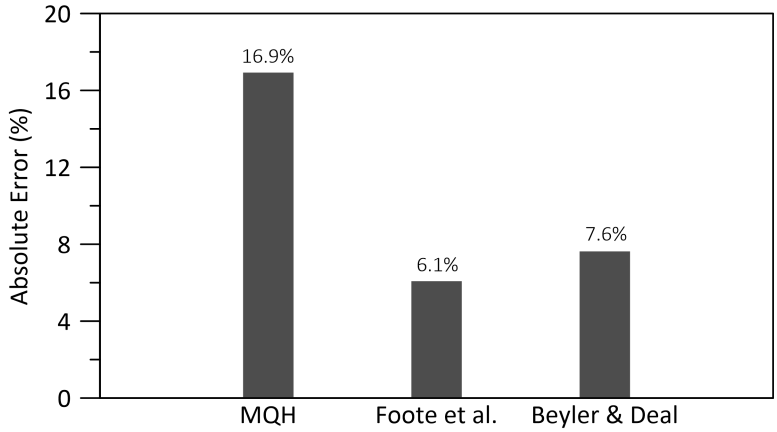

Figure 5.7: Plot of the average absolute error across all tests for each temperature correlation.

5.3 Estimating Doorway Mass Flow Rate

Obtaining an accurate estimate of fire induced flows through doorways, or other natural vents, is often desired in fire safety engineering design. Estimating mass flow rate into a fire compartment can provide details on the entrainment of fresher air into the compartment, which often dictates burning. At the same time estimates of the mass flow rate of smoke out of the compartment is important for characterizing the transport of heat and toxic gases to adjacent compartments, which dictates tenability and occupant safety. Similar to the temperature correlations, there are numerous flow rate correlations reported in the literature, which are typically developed for use in either stratified fire environments or in well-mixed situations [33]. In the stratified case, a compartment is assumed to consist of a hotter upper layer (smoke) and a cooler lower layer (air) with a distinct divide between the two, equivalent to a two-zone model of fire compartment development. In the well-mixed case, a compartment is assumed to have a uniform temperature throughout its

entire volume. Typically, the stratified case is applicable to pre-flashover conditions and the well-mixed case is more commonly applied to post-flashover conditions [33].

Doorway mass flow correlations are applied at the doorways to the fire room of the present tests to estimate the flow rates of smoke out of the fire room/staircase doorway and the flow of fresher air into the fire room through the same doorways. In total, four inflow correlations are implemented to estimate the flow of fresher air into the fire room and three outflow correlations are implemented to estimate the flow of smoke out of the fire room. All flow correlations in this section are derived for stratified fire compartments, which is most applicable to the scenario at hand because flashover is not reached. In addition, video observations, temperature and species concentration measurements show that the environment in the present fire room is not well-mixed. Estimated results from the correlations are compared to the measured flow rates discussed throughout Sec. 4.4.2 to evaluate their ability to predict both the development of the doorway flow rates during the transient growth and decay phases of the tests as well as the peak flow rates. Similar to the temperature correlations, an emphasis is placed on the ability of the correlations to conservatively predict peak flow rates which represent the most hazardous point in a fire scenario, when there is a maximum flow of air into the fire compartment and maximum flow of smoke to the other, adjacent compartments.

5.3.1 Doorway Mass Flow Rate Correlations

In the literature, there are a multitude of engineering correlations that have been developed to estimate the flow rate of gases through compartment vents. The majority of these correlations are semi-empirical, similar to the compartment temperature correlations. Flow correlations applicable to the stratified fire compartment situation are developed based upon a typical two zone compartment fire model, which is shown in Fig. 5.8. Applying first principles of fluid flow to this model allows for changes in pressure due to buoyancy caused by temperature differences and hydrostatic forces to be linked to velocity through the Bernoulli Equation. Refinement of the correlations is done through the use of empirical constants; often times, experimental observations are used to replace estimates of other input parameters as well to further improve the correspondence between predicted and measured flow rate estimates.

Figure 5.8 shows the two zones in the stratified fire compartment: the upper, uniformly mixed smoke layer with representative temperature T_g and density ρ_g, and the lower uniformly mixed air layer with representative temperature T_a and density ρ_a. The buoyancy forces caused by the differences in density cause a pressure gradient to form with respect

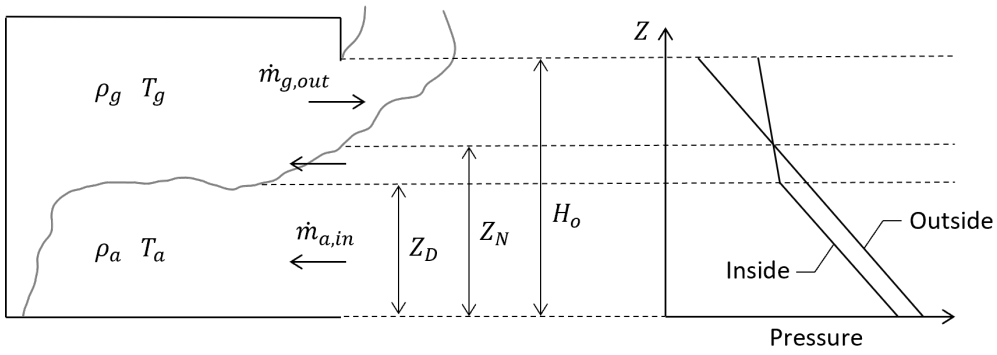

Figure 5.8: Schematic of the stratified flow model, showing example pressure gradients inside and outside the compartment.

to height above the compartment floor. This pressure gradient is different on the inside of the compartment than it is on the outside of the compartment, which creates a pressure difference and allows flow to establish through the compartment doorway. Above the neutral plane height (Z_N), the pressure inside the compartment is greater than the pressure outside, so smoke flows out of the compartment ($\dot{m}_{g,out}$). Below the neutral plane height, the pressure outside the compartment is greater than the pressure inside the compartment, causing air to flow into the compartment ($\dot{m}_{a,in}$). The discontinuity height (Z_D) represents the height of the interface between the two layers in the compartment. At this height, there is a sudden change in the pressure gradient inside the compartment caused by the sudden change in the gas temperature in the two-zone model.

The development of the flow correlations is done either by evaluating the flow of smoke out of the top section of the doorway above the neutral plane height or by evaluating the flow of air into the bottom section of the doorway below the neutral plane height. Often, the assumption is made that the inflow rate of air equals the outflow rate of smoke on the basis of mass conservation. This assumes that the only flow into and out of the fire compartment is through the doorway and neglects any introduction of air through a ventilation system, any leakage, or additional production of smoke by the fire. There are some correlations that take the mass production term into account, however, this introduces complexities into the correlations and is seldom used in practice as the added term typically only accounts for between 1% to 10% of the total mass flow rate [33].

Table 5.6 lists the doorway mass inflow correlations that are evaluated for the present fire scenarios. These four correlations, labelled IN1 to IN4, are all appropriate for stratified or two-zone doorway flows. In these correlations, $\dot{m}_{a,in}$ (kg/s) is the mass inflow rate, C_d

is an empirical flow coefficient, ρ_a (kg/m^3) is the density of the ambient air, w_o (m) is the width of the doorway opening, T_g (K) is the upper layer gas temperature, T_a (K) is the ambient air temperature, Z_N (m) is the neutral plane height, Z_D (m) is the discontinuity height, A_o (m^2) is the doorway opening area, and H_o (m) is the doorway opening height.

Table 5.6: Doorway mass inflow correlations.

Label	Correlation	Eq. #
IN1	$\dot{m}_{a,in} = \frac{1}{3} C_d \rho_a w_o \sqrt{2g\left(1 - \frac{T_a}{T_g}\right)(Z_n - Z_D)}\,(2Z_n + Z_D)$	(5.16)
IN2	$\dot{m}_{a,in} = \frac{2}{3} C_d \rho_a A_o \sqrt{2gH_o \frac{T_a}{T_g}\left(1 - \frac{T_a}{T_g}\right)\left(1 - \frac{Z_N}{H_o}\right)^3}$	(5.17)
IN3	$\dot{m}_{a,in} = 0.13 \rho_a A_o \sqrt{gH_o}$	(5.18)
IN4	$\dot{m}_{a,in} = 0.5 A_o \sqrt{H_o}$	(5.19)

Correlation IN1 (Eq. 5.16) is developed by Rockett [35]. It is derived for flow in the bottom section of the doorway and, therefore, directly calculates the inflow of ambient air into the fire compartment. This correlation assumes that the compartment has only a single vent/opening and is reported to potentially have significant errors when the upper layer temperature is relatively cool (below 150 °C) which may be the case for small fires [35]. Correlation IN2 (Eq. 5.17) is also developed by Rockett [35] and is derived for flow out the top section of the door. Therefore, this correlation calculates the outflow of smoke from the fire compartment and assumes that inflow in the lower portion of the opening is equal to the outflow in order to provide an estimate of the inflow rate. These correlations have been extensively used in the literature for the purposes of comparing to experimental fire data [37], verifying the correlation for various scenarios [149], and improving the correlations for more specific scenarios such as corridor flows [45]. Both IN1 and IN2 require the input of T_g, T_a, Z_N, and Z_D. These parameters must either be known, requiring data from experiments, or be estimated using other relations and simplifying assumptions. Since, this information is typically unknown for a given design scenario without experimental data, these correlations are often too complex to use in practice so further simplification is needed.

Correlations IN3 (Eq. 5.18) and IN4 (Eq. 5.19) are simplified versions of the previous

two inflow correlations. The derivation of these simplified correlations involves making assumptions about the value of the variables which are unknown. The complete simplification process to derive these correlations is outlined by Babrauskas [150] and by Karlsson and Quintiere [33]. In the simplification process, a value is assumed for the ratio of T_a to T_g based on experimental data, the neutral plane height is defined by Eq. 5.20 and depends on the ratio of the temperatures, and the discontinuity height is assumed to be zero [33]. Equation 5.20 is derived from the two-zone model under the assumption that inflow and outflow are equal, and that the nominal location for the neutral plane is in the mid-plane of the doorway ($H_o/2$). Assuming a discontinuity height of zero represents the maximum flow case, by creating the largest possible pressure difference between the inside and outside of the compartment in order to also provide a more conservative result [35]. Correlation IN3 still requires the input of the ambient air density, which can be calculated from ambient air temperatures and pressures using the ideal gas law. Correlation IN4 makes a further simplification, assuming a standard ambient temperature and atmospheric pressure and, therefore, substitutes a known value for the density of ambient air. With the simplifications made, these correlations are only meant to predict the peak/maximum flow through the doorway and are no longer capable of predicting the development of the flows during the transient phases of fire growth and decay.

$$Z_N = \frac{H_o}{1 + (\rho_a/\rho_g)^{1/3}} \tag{5.20}$$

Table 5.7 lists the doorway mass outflow correlations that are evaluated for the present tests. These three correlations, labelled OUT1 to OUT3, are developed in the same manner as the inflow correlations. In fact, since they are derived from the same model and also use the assumption that outflow is equal to inflow, correlation OUT1 (Eq. 5.21) from [35] is the same as correlation IN2 which directly calculates the mass outflow rate. In addition, OUT2 (Eq. 5.22) is the same as IN3, and OUT3 (Eq. 5.23) is the same as IN4. Therefore, the limitations and implementation of the outflow correlations are the same as for the inflow correlations discussed previously. The correlations are repeated and relabelled for clarity when comparing to the measured results.

5.3.2 Implementation of Flow Rate Correlations

The doorway mass flow correlations are implemented following the guidance provided in the literature, as described above. Details for each of the inputs into the correlations are described here for the fire scenarios in the present tests.

Table 5.7: Doorway mass outflow correlations.

Label	Correlation	Eq. #
OUT1	$\dot{m}_{g,out} = \frac{2}{3} C_d \rho_a A_o \sqrt{2 g H_o \frac{T_a}{T_g} \left(1 - \frac{T_a}{T_g}\right) \left(1 - \frac{Z_N}{H_o}\right)^3}$	(5.21)
OUT2	$\dot{m}_{g,out} = 0.13 \rho_a A_o \sqrt{g H_o}$	(5.22)
OUT3	$\dot{m}_{g,out} = 0.5 A_o \sqrt{H_o}$	(5.23)

The flow coefficient (C_d) is an empirical constant which can have a value ranging between 0.68 to 0.72, however, it well accepted to use a value of 0.70 for general application [40]. Thus, the value of 0.70 is used in these calculations. The constants needed for the calculation of density are the gas constant for air and the ambient pressure. The gas constant for air is taken as the standard value of 287.05 J/kg K. The ambient pressure is taken as the atmospheric pressure measured from a weather station located near the burn house. Values of atmospheric pressure are recorded each test day at the beginning of the test and are assumed to be constant throughout a test.

The doorway being evaluated in the present comparison is the fire room/staircase doorway. It has a width of 0.10 m, a height of 2.10 m, and an opening area of 2.09 m^2. The discontinuity height is assumed to be zero, similar to the assumption made during simplification of the more complex correlations. This is necessary since the literature lacks a method to estimate the discontinuity height, and there is no measurement in the present experiments that allows for a robust measure of the discontinuity height throughout the duration of the tests. Once again, this assumption corresponds to the maximum flow case, which provides the most conservative results.

The density of the inflowing air (ρ_a) and the out flowing gas (ρ_g) is calculated using the ideal gas law, using inputs of measured temperature, the standard gas constant for air and the atmospheric pressure observed on the day of the test. With this implementation, the densities are allowed to vary over the duration of the tests for correlations IN1, IN2, and OUT1. The remaining simplified correlations use a constant density evaluated at the beginning of the test at ambient conditions.

The temperatures used for input into the correlations are measured by the thermocouples located adjacent to the velocity probes at bottom and top of probe rake A4 located in the fire room/staircase doorway. These are positioned at 0.4 m and 2.0 m above the floor,

respectively. The temperature at the top probe location is taken as the upper layer/out flowing gas temperature (T_g) and the temperature at the bottom probe location is taken as the ambient/inflowing air temperature (T_a). Using the temperatures at the top and bottom probes ensures that the largest ratio of T_g to T_a is used, which again corresponds to the maximum flow case where the results are most conservative.

Prior to ignition, there is a discrepancy up to a few degrees Celsius between the temperature at the top probe and the temperature at the bottom probe, due to natural temperature gradients in the burn house. If this is implemented as is, the correlations would predict a flow prior to ignition when there should be no fire induced flow. Therefore, in order to compare only the estimated fire induced flows with the experimental data, the temperature at the top probe is corrected with a simple linear shift to match the temperature at the bottom probe based on the values of temperature measured during the baseline data collection prior to ignition. This removes any premature estimation of flow in the doorway.

In addition to evaluating the performance of each correlation, the influence of using a measured neutral plane height versus the estimated neutral plane height is also examined. The use of the estimated neutral plane height is done through direct application of Eq. 5.20. The measured neutral plane height is calculated from the velocity measurements using the method outlined in Sec. 3.2.4. For most of a given test, there is only a single neutral plane present in the doorway, as the direction of the flow only changes once over the height of the doorway opening. When this is the case, the measured neutral plane height is directly used. There are a few times when the velocity measurements suggest the presence of more than one neutral plane in the opening. When this is the case, the lowest neutral plane is selected to be used as input into the correlations. Selecting the lowest neutral plane height is most appropriate because analysis of the data shows that multiple neutral plane heights are typically detected when a phenomenon occurs near the top of the doorway, such as the recirculating flow discussed in Sec. 4.4.1. Such neutral planes near the top of the doorway are not appropriate to use as input values as they are not representative of the location separating the main inflow and outflow regions due to the fire.

Implementing the measured neutral plane height is not as simple as directly inputting the measured height into the correlations as Z_N in every correlation. Measurements of neutral plane height show that the neutral plane in the early stages of the tests is established near the top of the doorway and descends downwards as the fire develops and the volume of the upper layer increases. The way that the correlations are derived require that the cross-sectional area of the part of the doorway used for the derivation (the bottom of the doorway for IN1 and the top of the doorway for IN2 and OUT1) must initially be small. This ensures the flow rates in the early stages of the tests are small and progressively

increase as the fire develops, as required. There is no issue in directly using the measured neutral plane heights in correlations IN2 and OUT1, therefore, since the cross-sectional area of the flow is the top part of the doorway above the neutral plane. In this case, the cross-sectional area is initially small and becomes greater over time as required for the proper physical response. In contrast, in correlation IN1, the cross-sectional area of interest is the lower part of the doorway below the neutral plane. In this case, the cross-sectional area is initially large and diminishes as the neutral plane descends. Therefore, it is required to replace Z_N in correlation IN1 with $(H_o - Z_N)$ and then use the measured neutral plane as Z_N in this term to follow the physical development of a neutral plane during the test. If this correction is not made, the value of the inflow rate predicted by IN1 is severely overestimated in the early stages of a test and underestimated in the later stages of a test as the neutral plane reascends.

5.3.3 Inflow Rate Estimation Results

The results of the calculations of mass inflow rate using correlations IN1 to IN4 are discussed for each test separately. First, a detailed discussion is presented on the ability of the correlations to predict the measured transient development of the doorway flow rates. Then, each correlation is evaluated on its ability to conservatively estimate the measured peak flow rate. As mentioned previously, the influence of using the estimated versus measured neutral plane height is also evaluated. This is done by comparing the results of using the correlation IN1 with the measured neutral plane height (IN1m) to results of correlation IN1 using the estimated neutral plane height (IN1e). All other correlations use the measured neutral plane height, where applicable.

Figure 5.9 shows a plot comparing the measured and estimated mass flow rates from the staircase into the fire room for the no HVAC test, and a plot of the measured and estimated neutral plane heights. Comparing the estimated flow rates from the correlations requires discussion of the development of the neutral plane height, therefore, these two plots are paired together. In Fig. 5.9a inflows estimated using correlation IN1m begin to increase at 3:04 (m:ss) after ignition, and agree well with measured flow rates during the increasing phase until 5:07 after ignition. At this time, a sudden and rapid increase in the estimated flow rate occurs and results in significant overestimation of the measured flow rate until peak values are reached. The time of the peak flow rate is well predicted, but estimated flow rates continue to overestimate the measured values after the peak and through the decay phases of the fire. As discussed in Sec. 4.4.1, a flow reversal occurs in the structure in the later stages of the tests as the environment recovers and equilibrates through the structure. This results in an increase of the flow into the fire room at approximately 12

minutes after ignition in Fig. 5.9a. Due to the nature of this phenomenon, it is not captured by correlation IN1m, which instead estimates a continual decrease of flow rate until the end of the test. In Fig. 5.9b the measured neutral plane becomes established at 3:04 after ignition, the same time as when correlation IN1m begins to increase. At 5:07 after ignition, the neutral plane descends to a height where the correction term $(H_o - Z_N)$ approaches a value of one, thus, causing an amplification of the flow rate estimate. Coincidentally, this occurs near the time of peak flow in this test, resulting in the significant overestimate of the peak flow. Overestimation of flow rate through the remainder of the test is likely due to the relatively slow change in temperature in the fire room, since the neutral plane height is stable during this period. After the flow reversal, the neutral plane height rises again, which is captured in the correlation as a decrease in the correction term $(H_o - Z_N)$ which causes the flow rate predicted by correlation IN1m to decrease instead of increasing as measurements suggest during this period.

Correlation IN1e predicts an increase in flow rate through the doorway almost immediately after ignition (see Fig. 5.9a), resulting in significant overestimation of doorway flow development through the early transient stage of fire growth. This is because the cross-sectional area of the flow is too large in the early stages of the test, due to the assumption that the estimated neutral plane height is nominally at the mid-plane of the doorway opening (see Fig. 5.9b). This correlation does provide a good estimate of the peak flow rate, although the peak value is predicted to occur earlier than is measured. Similar to correlation IN1m, the flow rate during the decay of the fire is significantly overestimated, and again the flow reversal is not captured.

Correlation IN2 uses the measured neutral plane height. It predicts similar flow development to IN1m during the initial period (see Fig. 5.9a) with flow through the opening increasing at 3:04 after ignition, when the measured neutral plane is established. While the estimated flow rate continues to increase to a peak, the peak flow rate is underestimated and following the peak, the flow rate remains constant over the period that measured flow rates are decreases. As such, it again overpredicts the flow rate during this period until towards the end of the test. Again, there is no provision in the correlation to capture the measured flow reversal later in the test.

Correlations IN3 and IN4 estimate only peak flow rates in the opening and are therefore displayed as horizontal lines in Fig. 5.9a at values equal to the respective peak flow estimates. Correlation IN3 predicts a value of peak flow rate in very good agreement with the measured peak flow, albeit slightly on the conservative side. The predicted peak flow rate from correlation IN4 overestimates the measured value of peak flow, predicting a value between those of IN3 and IN1m. Values of the estimated peak flow rates from all inflow correlations for the no HVAC test, along with the percent error compared to the

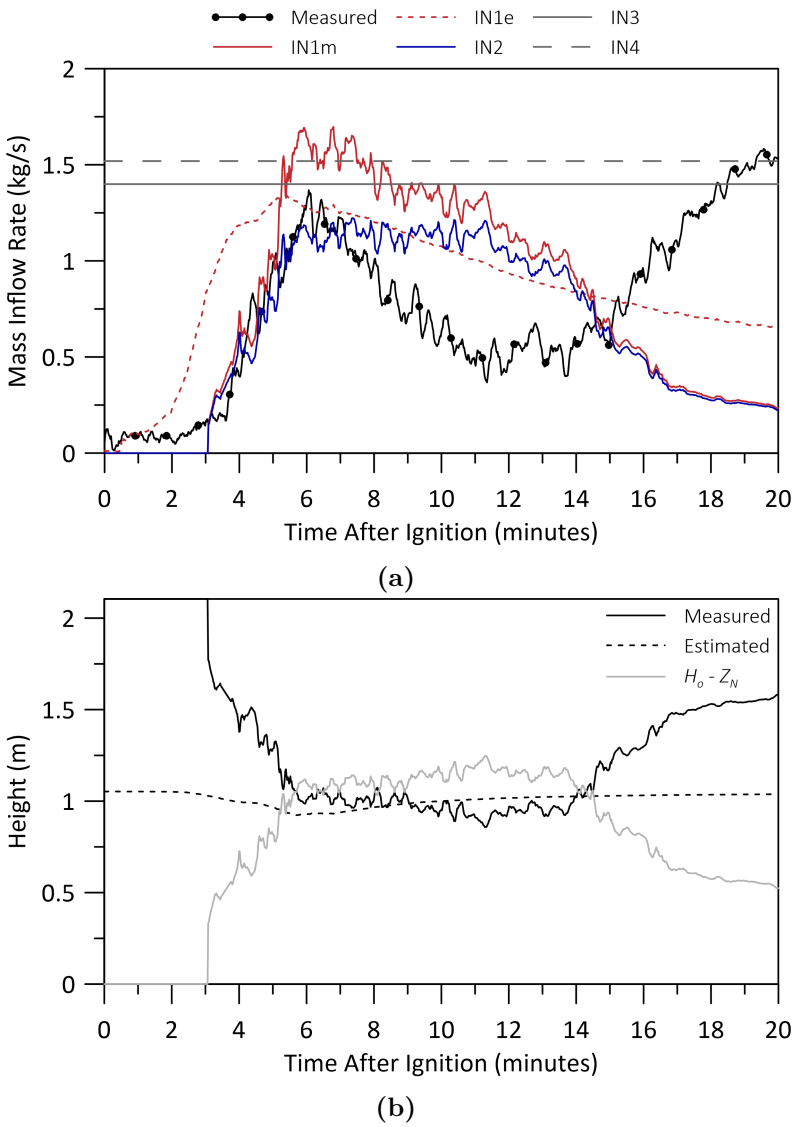

Figure 5.9: Plots of (a) measured and estimated mass inflow versus time and (b) measured and estimated neutral plane height versus time for the no HVAC test.

measured flow rate, are shown in Table 5.8. Positive values of percent error represent an overestimation or a conservative result, and a negative error represents an underestimate of the peak flow. In this test, correlations IN1e and IN3 provide the most accurate estimates of peak flow rate when considering only absolute error. However, IN3 provides a conservative estimate, while IN1e does not.

Table 5.8: Values of peak inflow and percent error for the no HVAC test.

Correlation	Peak Inflow (kg/s)	Error (%)
Measured	1.37	-
IN1m	1.70	24
IN1e	1.34	−2
IN2	1.22	−11
IN3	1.40	2
IN4	1.52	11

Figure 5.10 shows a plot comparing measured and estimated mass flow rate from the staircase into the fire room, and a plot of the measured and estimated neutral plane heights for the baseline HVAC test. In Figure 5.10a, flow rates predicted using the IN1m correlation begin to increase at 3:04 after ignition and show excellent agreement with the measured flow rate through fire growth, at the peak flow, and for the early part of the decreasing flow phase as well. After this, correlation IN1m overestimates measured flow rates for the remainder of fire decay and again cannot capture the increase in the measured flow rates after the flow reversal within the structure. Figure 5.10b shows that the measured neutral plane becomes established at 3:04 after ignition, the same time as when the flow rate estimated by correlation IN1m begins to increase, consistent with the previous test. At 6:10 after ignition, shortly after the time of peak flow, the correction factor $(H_o - Z_N)$ reaches a value near one and a sudden increase in flow rate is seen in the predicted values. This results in a sudden drop in flow rate though not as marked as in the no HVAC test. Thus, it does not affect the prediction of the peak flow in this case. As measured flow rate through the opening decreases, the neutral plane height is stable, similar to the no HVAC test, and the predicted flow rates do not decrease. Additionally, the rise in the neutral plane height after the flow reversal is not captured by the correlation, resulting in underestimation of the flow at the end of the test, again similar to in the no HVAC test.

The correlation IN1e predicts similar development of flow rates in this test as it has for the no HVAC test (see Fig. 5.10a). Estimated flow rates increase almost immediately after ignition, resulting in a significant over estimation of doorway flow rates during the initial

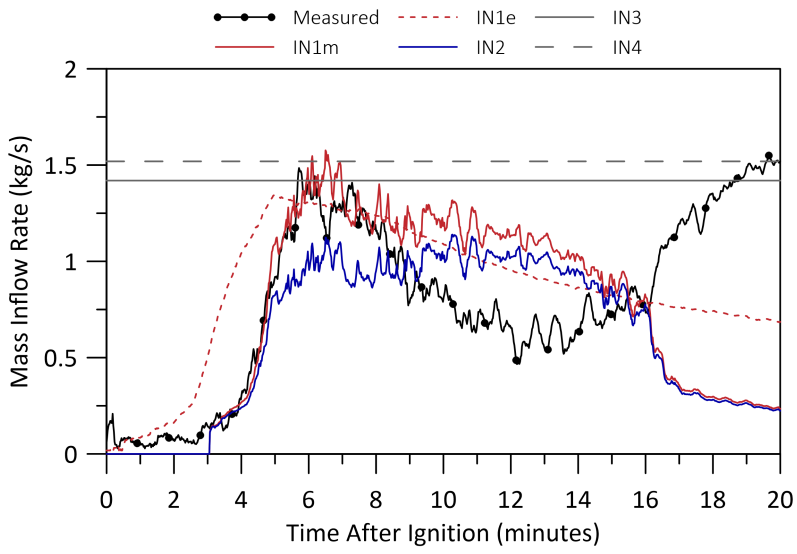

(a)

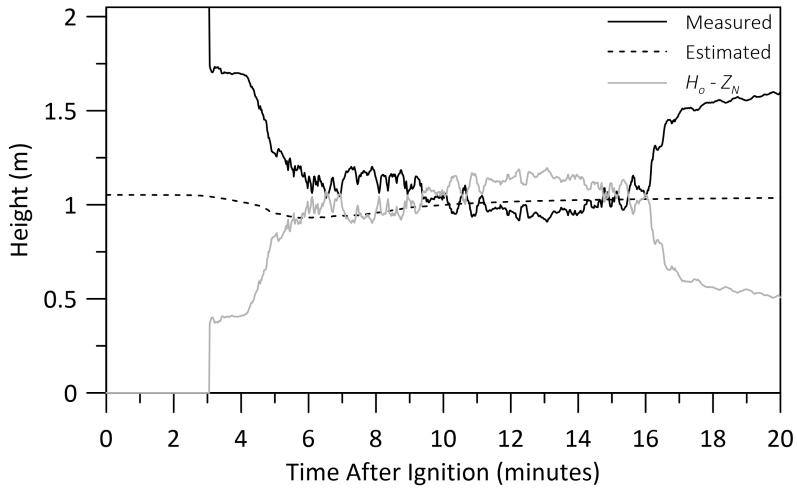

(b)

Figure 5.10: Plots of (a) measured and estimated mass inflow versus time and (b) measured and estimated neutral plane height versus time for the baseline HVAC test.

phase. The magnitude of peak flow rate is estimated well, but predicted to occur earlier than the measured peak flow. There is good agreement between flow rates estimated by the IN1e correlation and measured flow rate early in the decreasing phase of the fire; however, the correlation overestimates the flow rate in the later stages of the decay phase and flow reversal is not captured either.

Values of flow rate estimated by correlation IN2 are in very good agreement with the measured flow rates, and estimations by IN1m, during the early phase of the fire until 4:53 after ignition. After this time, predictions by the correlation deviate from measured flow rates and become nearly constant through the period of peak flow and subsequent decay. This results in the magnitude of the peak flow rate being significantly underestimated while flow rates during the decreasing phase are overestimated. Towards the end of the test, predictions from correlation IN2 once again match those of IN1m and the measured flow reversal is not captured.

The estimated peak flow rates from correlations IN3 and IN4 are again shown as horizontal lines on the plot in Fig. 5.10a. Both correlations predict peak flow rates in good agreement with the measured peak flow, with the IN3 correlation slightly underestimating the peak and IN4 slightly overestimating the peak. Correlation IN3 consistently predicts a lower value than IN4 because the ambient air density (measured on the day of the test) used in IN3 is lower than the standard air density used in IN4. Values of the estimated peak flow rates by all correlations for the baseline HVAC test along with percent error compared to the peak measured flow rate are shown in Table 5.9. In this test, correlation IN4 results in a conservative and the most accurate estimate of the peak flow.

Table 5.9: Values of peak inflow and percent error for the baseline HVAC test.

Correlation	Peak Inflow (kg/s)	Error (%)
Measured	1.48	-
IN1m	1.58	6
IN1e	1.34	−10
IN2	1.14	−23
IN3	1.42	−4
IN4	1.52	2

Figure 5.11 shows a plot comparing measured and estimated mass flow rates from the staircase into the fire room for the 2x baseline HVAC test, and the development of the measured and estimated neutral plane heights in that test. In Fig. 5.11a, flow rates predicted by correlation IN1m begin to increase at 2:42 after ignition agree well with

measured flow rates until 5:43 after ignition. At this point, prior to peak flow rate, a sudden increase in flow rate is predicted, similar to that seen in the no HVAC test. After the peak flow, the estimated flow rate does begin to decrease, however, it decreases much more slowly than the measured flow rates. This results in an overestimation of the flow rate for the duration of the decreasing flow phase and again, the correlation does not capture the flow reversal. In Fig. 5.11b, it is shown that the measured neutral plane height becomes established at 2:42 after ignition, at the same time as the estimated flow rate from correlation IN1m begins to increase. Similar to the no HVAC test, the sudden and rapid increase in the estimated flow rate near the time of peak flow can be explained by the factor $(H_o - Z_N)$ reaching a value of one. Interestingly, the estimated flow rate does not show the same accelerated decrease towards the end of the test as seen in the previous two tests. This is because the measured neutral plane height remains low for the remainder of the 2x baseline HVAC test, rather than recovering as seen in the previous tests. The cause of this difference in the neutral plane height is unknown. Finally, the correlation again does not capture the increase in the flow rate into the fire room after flow reversal within the structure.

Estimates of flow rate by the correlation IN1e (Fig. 5.11a) is similar as described for the previous two tests. The estimated inflow rate begins to increase almost immediately after ignition, leading to an overestimation of flow rate through the initial phase of the test. In this test, estimates of peak flow rate by the IN1e correlation are in good agreement with measured flow rates near the time of the peak flow, however, values of the peak flow rate are underestimated. Following this, the flow rates during the decreasing flow phase are overestimated that the flow reversal is not captured.

Estimates of flow rates using correlation IN2 are similar to seen in the no HVAC test. Values closely follow both measured flow rates and estimations from correlation IN1m during the increasing flow phase. Correlated values begin to deviate from those estimated by IN1m near the time of the measured peak flow. At this point, estimated flow rates using correlation IN2 become relatively constant until well into the decreasing flow phase. This results in an underestimation of the peak flow rate and an overestimation of the flow rate during the later phases of the test. In this test, predictions from correlation IN2 are also affected by the lack of recovery of the neutral plane height as seen in Fig. 5.11b. Again, flow reversal is not captured, consistent with other tests.

The estimated peak values from correlations IN3 and IN4 are shown for the 2x baseline HVAC test in Fig. 5.11a. For this test, both correlations provide fairly good estimates of the peak flow rate, although both underestimate the peak inflow rate values and are, therefore, not conservative results. Values of the estimated peak flow rate from all inflow correlations for the 2x baseline HVAC test along with percent error compared to the peak

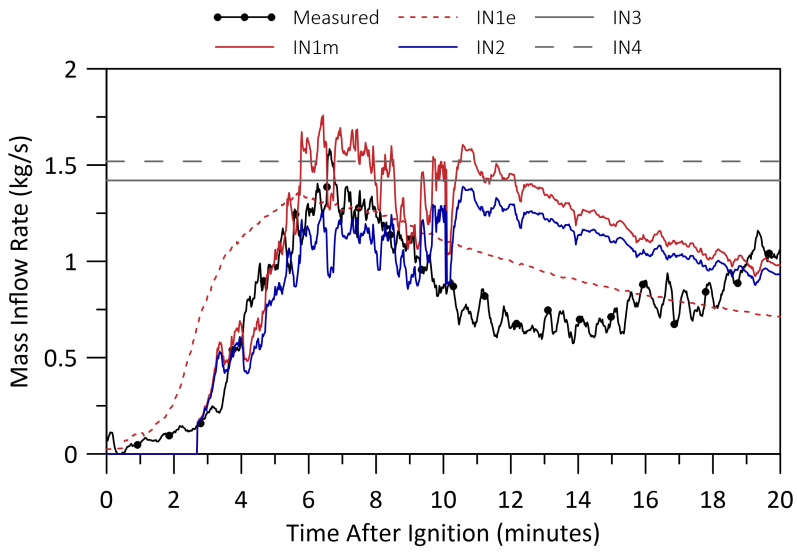

(a)

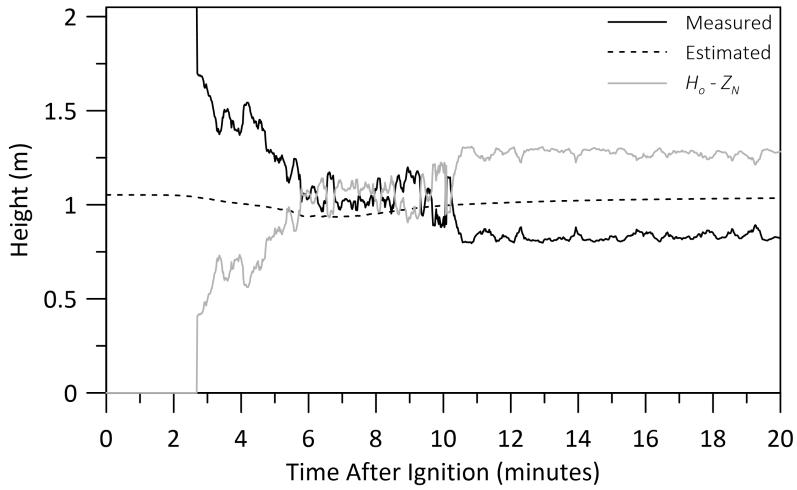

(b)

Figure 5.11: Plots of (a) measured and estimated mass inflow versus time and (b) measured and estimated neutral plane height versus time for the 2x baseline HVAC test.

measured flow rate are shown in Table 5.10. Correlation IN4 has the most accurate estimate in terms of absolute error, however, IN1m is the only correlation that overpredicts flow rate and leads to a conservative estimate.

Table 5.10: Values of peak inflow and percent error for the 2x baseline HVAC test.

Correlation	Peak Inflow (kg/s)	Error (%)
Measured	1.58	-
IN1m	1.76	11
IN1e	1.33	−16
IN2	1.39	−12
IN3	1.42	−10
IN4	1.52	−4

Figure 5.12 shows a plot comparing measured and estimated mass flow rate from the staircase into the fire room, and a second plot showing the development of the measured and estimated neutral plane height for the recirculation test. Figure 5.12a, shows that estimates of doorway flow rate from correlation IN1m begin to increase at 3:46 after ignition and agree well with measured inflow rates for the increasing flow phase of this test. The good agreement continues through the peak flow and into the decreasing flow phase. Similar to the previous tests, IN1m overpredicts the flow rate during later stages of the decreasing flow phase, likely due to the relatively slow decrease in temperature in the fire room. It also does not capture the flow reversal for the recirculation test, which is consistent with results from the previous tests. Figure 5.12b shows that the measured neutral plane becomes established in the doorway at the same time as when predicted flow rates from correlation IN1m begin to increase. The neutral plane height does lead to the correction factor $(H_o - Z_N)$ being near a value of one, shortly after the peak in flow. However, the effect of this is less severe in this test, compared to the no HVAC and 2x baseline HVAC tests because it occurs after the peak flow rate. After the flow reversal, the measured neutral plane height does increase, however, it does so slower than is seen in the no HVAC and baseline HVAC tests. Once again, the rise of the neutral plane after the flow reversal is not captured in flow rate estimates by the correlation, which results in underestimation of the flow rate during this period.

Correlation IN1e provides very similar predictions of mass flow rates as discussed for the previous tests (see Fig. 5.12a). The estimated inflow rate begins to increase almost immediately after ignition, resulting in an overestimation of the flow rate during the increasing flow phase of the test. In this test, IN1e underestimates the peak flow rate, overestimates

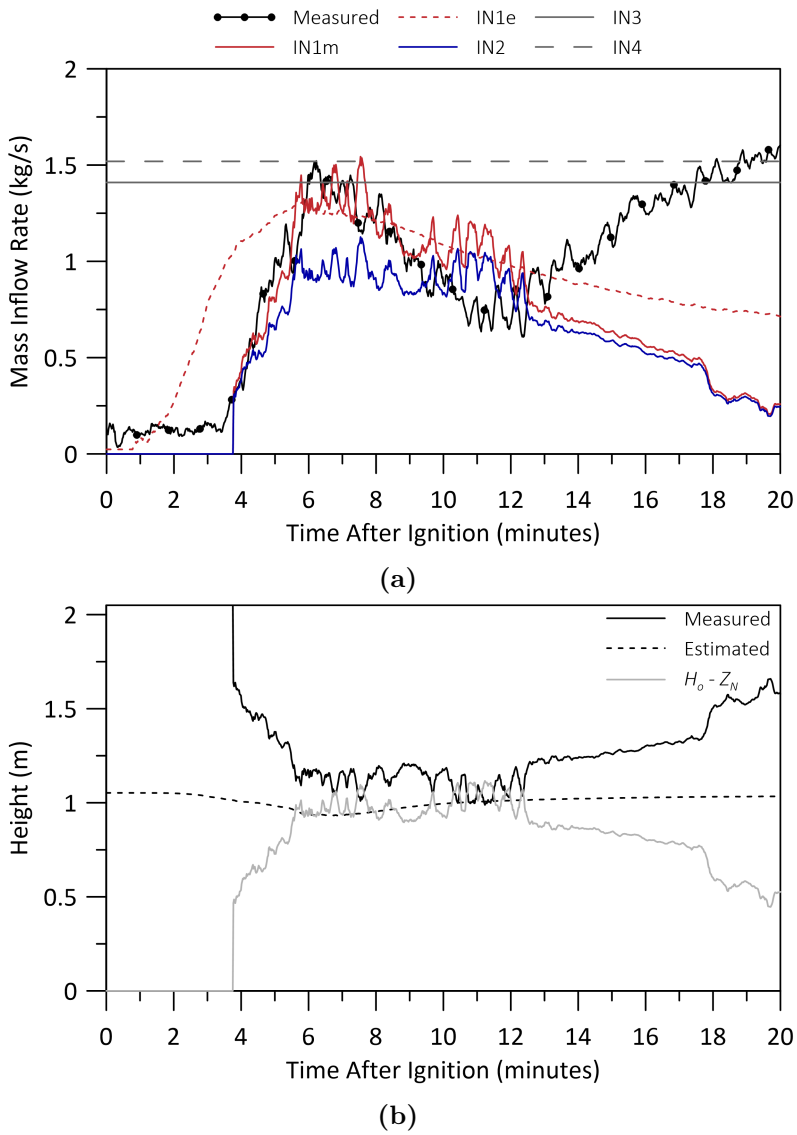

Figure 5.12: Plots of (a) measured and estimated mass inflow versus time and (b) measured and estimated neutral plane height versus time for the recirculation test.

the flow during the decreasing flow phase of the test, and does not capture the flow reversal.

Correlation IN2 provides good estimates of the measured inflow rate from the time when the neutral plane becomes established to 5:45 after ignition, with some periods of underestimation. After 5:45 into the test, estimated flow rate values by the correlation become relatively constant for the duration of the peak flow and well into the decreasing flow phase of the test. This is similar to the trends seen in the previous tests, where the peak flow rate is underestimated and the flow rate during the decreasing flow phase is overestimated. Correlation IN2 does not capture the flow reversal for this test, either.

Finally, peak flow rates estimated by correlations IN3 and IN4, are in good agreement with the measured peak flow rate in the recirculation test. Correlation IN3 slightly underpredicts the peak flow, while IN4 provides a higher estimate of the peak flow rate, matching the measured peak value. Values of the measured and estimated peak flow rate from all inflow correlations for the recirculation test along with percent error are shown in Table 5.11. In this test, IN4 provides the most accurate estimate and IN1m provides the second most accurate, and only conservative, estimate of the flow rate.

Table 5.11: Values of peak inflow and percent error for the recirculation test.

Correlation	Peak Inflow (kg/s)	Error (%)
Measured	1.52	-
IN1m	1.54	1
IN1e	1.31	−14
IN2	1.13	−26
IN3	1.41	−7
IN4	1.52	0

Figure 5.13 shows a plot comparing the average absolute error in estimated peak inflow rate across all four tests when compared to the measured peak value. Correlation IN2 is the least accurate correlation on average, while the simplified correlations IN3 and IN4 are the most accurate, and correlation IN1 has intermediate accuracy. Interestingly, using the estimated neutral plane height for IN1e leads to more accurate estimates of peak flow on average compared to when the measured neutral plane height is used for IN1m. This, however, does not translate to the performance of the correlations in the transient phases of the fires.

In general, the correlations respond similarly in each of the four tests. Correlation IN1m provides very good estimates of the measured inflow rate during the transient increasing

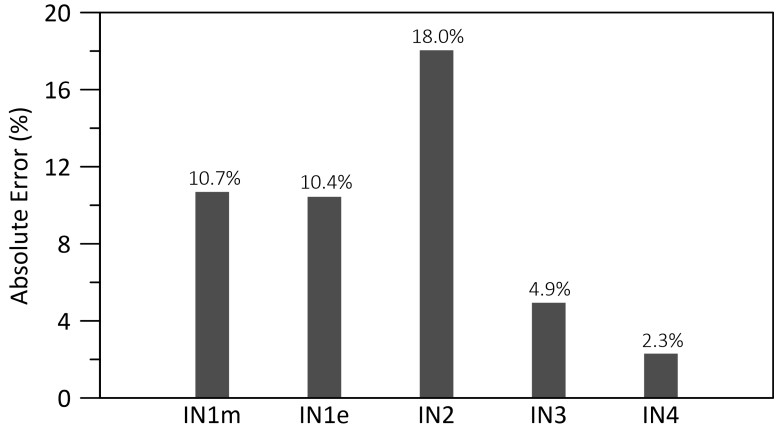

Figure 5.13: Plot of the average absolute error across all tests for each inflow correlation.

flow phase in the early stages of the tests. This correlation gives the most conservative estimates of peak flow rates, which sometimes result in significant overestimates of the values. Correlation IN1e generally overestimates measured flow rate values during the increasing flow phase of the tests because of the assumption that the estimated neutral plane height rests at the mid-plane of the doorway when there is no temperature gradient. This correlation usually provides reasonable estimates of the peak flow rate, however, the peak flow is predicted to occur earlier in the fire than is seen in the measured results. Correlation IN2 provides estimates similar to those from IN1m during the increasing flow phase of the tests. However, estimates using this correlation deviate and become relatively constant throughout the peak flow period and into the decreasing flow phase. This results in underestimations of the peak values of flow rate and over estimations of flow rates in the decreasing phase of the fire. Correlations IN3 and IN4, which only predict the peak flow rates, are, on average, the most accurate of all the correlations as seen in Fig. 5.13. Notably, IN4 always results in a higher estimate than IN3, making IN4 the more conservative of the two. All inflow correlations provide poor estimates of the inflow rates after the peak flow and during the decreasing flow phase of the tests. Similarly, none of the correlations capture the measured flow reversal in the tests.

Results show that the use of the estimated neutral plane height only provides reasonable estimates of flow rate during more steady state portions of the tests, such as during peak flow, when the actual neutral plane height is near the mid-height of the doorway. This is because the estimated neutral plane heights inherently relate to the assumption that the neutral plane naturally exists at the mid-height of the doorway when there is no flow, and is adjusted from there as a temperature gradient develops. The use of a measured

value of neutral plane height is more appropriate for the transient phases of the tests. However, the inherent definition of the neutral plane height can introduce significant errors into flow rate estimates if the neutral plane height lowers significantly prior to the peak flow rate. In addition, using measured values of neutral plane height still does not allow the correlations to capture the flow reversal phenomenon. This can be attributed to the recovery of the neutral plane, which rises towards the end of the test. Capturing the full rise in the neutral plane height is critical to ensure that the cross-sectional area of the flow increases sufficiently in the correlations to capture the flow rate increase, since the buoyant forces are decreasing as temperatures decrease. Further investigation into the definition and implementation of the neutral plane height into the correlations is needed to ensure correct response during the transient phases at both the beginning and the end of the fire tests.

5.3.4 Outflow Rate Estimation Results

The results of the calculation of mass outflow rate using correlations OUT1 to OUT3 are discussed for each test. First, a detailed discussion is presented on the ability of the correlations to predict the measured transients in doorway flow rate development. Then, each correlation is evaluated on its ability to conservatively estimate the measured peak flow rate. The influence of using the estimated versus measured neutral plane height is also evaluated. This is done by comparing the response of correlation OUT1 with the measured neutral plane height (OUT1m) to the response of correlation OUT1 with the estimated neutral plane height (OUT1e). The other two outflow correlations, OUT2 and OUT3, only provide estimates of the peak flow rate. In these calculations, the measured and estimated neutral plane heights are the same as presented in Figs. 5.9b, 5.10b, 5.11b, and 5.12b for the inflow correlations.

Figure 5.14 shows a plot comparing the measured and estimated mass flow rate out of the fire room into the staircase for the no HVAC test. The flow rate estimated by correlation OUT1m begins to increase at 3:04 after ignition, which is consistent with the time when the neutral plane is established in the doorway. Estimates of flow rate by this correlation show good agreement with measured flow rate through the increasing flow phase, with slight overestimates in some instances. At 5:55 after ignition, the measured and OUT1m estimated flow rates both become relatively constant and agree well until approximately 8:00 after ignition. At this time, the measured flow rate increases again, eventually reaching peak values prior to decreasing for the remainder of the test. Correlation OUT1m does not capture the second increase in flow rate, resulting in significant underestimation of the peak outflow rate. The estimated outflow rate does start to decrease at 11:40 after ignition;

however, it does so more slowly than the measured flow rate, resulting in an overestimation of the flow rate throughout most of the decreasing flow phase. This is likely due to the slow decrease in temperature, as discussed for the inflow correlations.

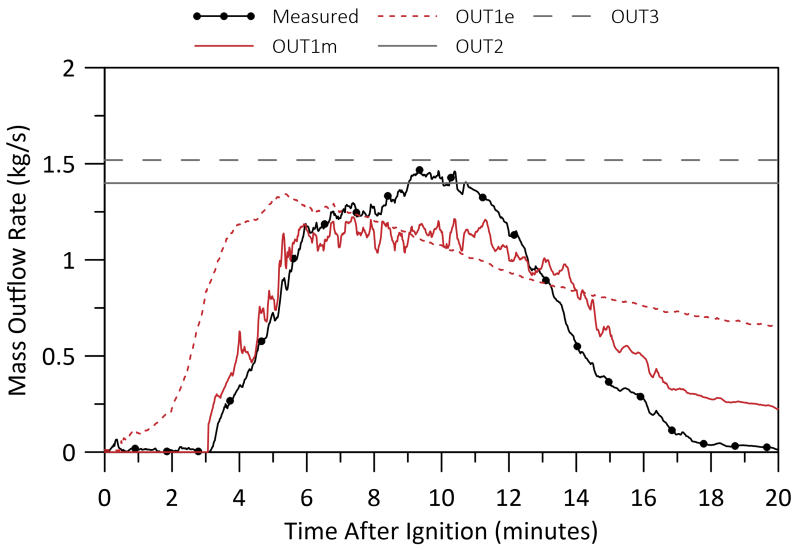

Figure 5.14: Plot of measured and estimated mass outflow versus time for the no HVAC test.

Correlation OUT1e, with the estimated neutral plane height, begins to increase almost immediately after ignition, similar to the response of IN1e. As a result, this correlation overestimates the flow during the increasing flow phase and predicts that the peak flow occurs much earlier than is measured. Correlation OUT1e overestimates flows until 6:40 after ignition and then underestimates them until into the decreasing flow phase of the test. Due to use of this correlation with the estimated neutral plane height, the estimated flow rate begins to decrease while the measured flow rate is still increasing. Unlike correlation OUT1m, the estimated neutral plane height does predict the second increase in the flow rate after a short period of relatively constant flow. However, this event is predicted to occur much too early. In addition, correlation OUT1e shows poor agreement with flow rates measured during the transient decreasing flow phase of the test, which is likely attributable to incorrect estimation of the neutral plane height.

The estimates of peak flow rate by correlation OUT2 and OUT3 are shown in Fig. 5.14 as horizontal lines, as these simplified correlations provide only a single peak value of flow. Correlation OUT2 slightly underestimates the peak value of outflow, while correlation OUT3 provides a higher estimate, which slightly overestimates the peak outflow. Table 5.12 lists values of the estimated peak flow rates by each outflow correlation, along with

the percent error compared to the measured flow rate for the no HVAC test. Once again, a negative error represents an underestimate, while a positive error represents an overestimate and a conservative result. In this test, correlation OUT3 provides the most accurate estimate of the peak outflow value and is the only correlation to provide a conservative estimate of the peak flow.

Table 5.12: Values of peak outflow and percent error for the no HVAC test.

Correlation	Peak Outflow (kg/s)	Error (%)
Measured	1.47	-
OUT1m	1.22	−17
OUT1e	1.34	−9
OUT2	1.40	−5
OUT3	1.52	4

Figure 5.15 shows a plot comparing the measured and estimated mass flow rates out of the fire room into the staircase for the baseline HVAC test. In this test, correlation OUT1m begins to increase at 3:04 after ignition, when the neutral plane is established, and the flow rate is slightly overestimated until 4:08 after ignition. After this, there is good agreement between measured and estimated flow rates by OUT1m through the rest of the increasing flow phase. Eventually, both the measured and estimated flow rates become relatively constant, with the time of this transition well predicted. The estimated flow rate remains constant until 12:15 after ignition, at which point the estimated flow rate begins to decrease. The measured flow rate is underestimated by OUT1m throughout the phase where the estimated flow rate is constant. There is also a slight increase in the measured flow rate at approximately 9:10 after ignition, which is not captured by OUT1m. Similar to the previous test, the flow rate through the decreasing flow phase is overestimated.

Correlation OUT1e follows very similar trends as described for the no HVAC test where the estimated flow rate begins to increase almost immediately after ignition, resulting in an overestimation of the flow rate through the increasing flow phase of the test. The value of peak flow rate is estimated well by OUT1e; however, it is predicted to occur earlier than measurements. In this test, OUT1e does not predict the slight increase in measured flow rate after the period of constant flow, which is different than for the no HVAC test. However, similar to the no HVAC test, estimates of flow by correlation OUT1e are in poor agreement with the measured outflow rate throughout the decreasing flow phase of the test.

Correlation OUT2 and OUT3 both overestimate the value of peak flow rate of the

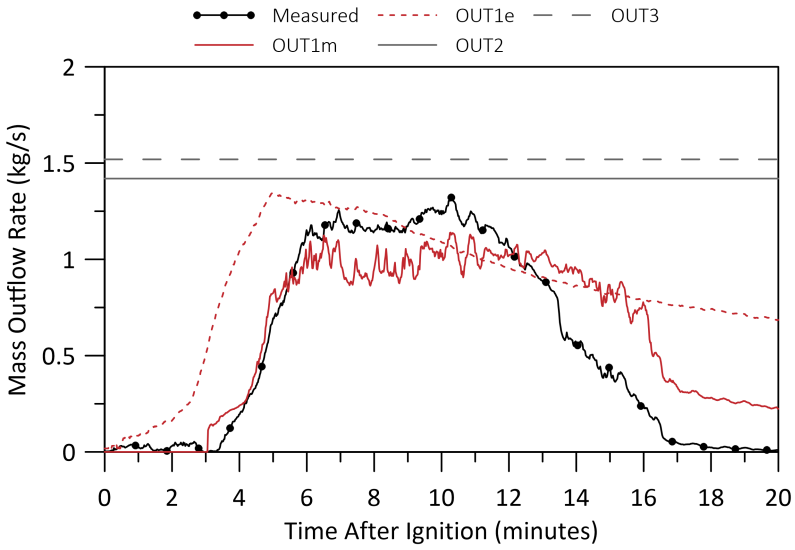

Figure 5.15: Plot of measured and estimated mass outflow versus time for the baseline HVAC test.

baseline HVAC test. Once again, OUT3 provides a higher estimated value because the standard air density used in this correlation is higher than the calculated air density from the day of the test used in correlation OUT2. Table 5.13 lists values of the estimated peak flow rates predicted by each outflow correlation, along with the percent error compared to the peak measured flow rate for the baseline HVAC test. Correlation OUT1e provides a conservative, and the most accurate, prediction of the peak flow, while correlation OUT1m is the only correlation that underestimates the peak outflow rate in this test.

Table 5.13: Values of peak outflow and percent error for the baseline HVAC test.

Correlation	Peak Outflow (kg/s)	Error (%)
Measured	1.33	-
OUT1m	1.14	−14
OUT1e	1.34	1
OUT2	1.42	7
OUT3	1.52	15

Figure 5.16 shows a plot comparing the measured and estimated mass flow rate out of the fire room into the staircase for the 2x baseline HVAC test. Correlated values of mass

flow rate from OUT1m begin to increase at 2:42 after ignition, when the neutral plane becomes established. Values are overestimated from this time until 4:10 after ignition. After this, flow rates through the remainder of the increasing flow phase and the peak flow rate are well predicted by OUT1m, including the slight increase in flow rate that occurs at 9:20 after ignition. In contrast, the decreasing flow rates that start at 11:00 after ignition and continue to the end of the test are poorly estimated by OUT1m. This can be attributed to the unusual response of the measured neutral plane height seen in the 2x baseline HVAC test.

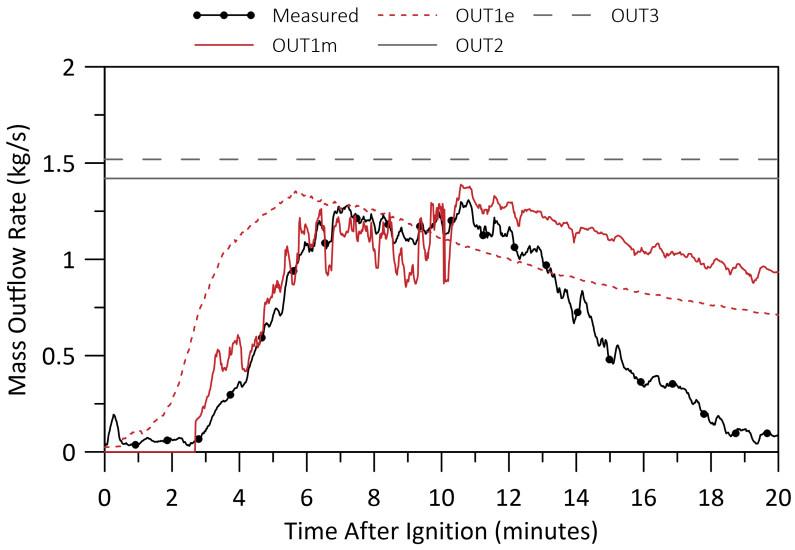

Figure 5.16: Plot of measured and estimated mass outflow versus time for the 2x baseline HVAC test.

Correlation OUT1e, once again, significantly overestimates the flow rate during the increasing flow phase of the test. There is good agreement between predicted peak flow by OUT1e and the measured peak flow. However, this correlation continues to provide poor predictions of flow rates in the decreasing flow phase of this test as well. In addition, the slight increase in flow rate measured at approximately 9:20 after ignition is not captured by OUT1e in the 2x baseline HVAC test.

Similar to the pattern seen in the baseline HVAC test, correlation OUT2 and OUT3 both overestimate the peak flow rates in the 2x baseline HVAC test as well. Values of the estimated peak flow rates by each outflow correlation, along with the percent error compared to the measured peak flow rate for the 2x baseline HVAC test, are listed in Table 5.14. In this test, all four outflow correlations provide conservative estimates of the

peak flow rate, with correlation OUT1e being the most accurate.

Table 5.14: Values of peak outflow and percent error for the 2x baseline HVAC test.

Correlation	Peak Outflow (kg/s)	Error (%)
Measured	1.31	-
OUT1m	1.39	6
OUT1e	1.35	4
OUT2	1.42	9
OUT3	1.52	16

Figure 5.17 shows a plot comparing measured and estimated mass flow rate out of the fire room into the staircase for the recirculation test. Estimations of flow rates using correlation OUT1m begin to increase at 3:46 after ignition when the neutral plane is established, and agree well with measured flow rates through the increasing flow phase of the test until approximately 5:55 after ignition. At this time, flow rates predicted by the correlation become relatively constant while measured flow rates continue to increase. Similar to the previous tests, OUT1m underpredicts the peak flow rate and overpredicts the flow rate later during the decreasing flow phase of the test.

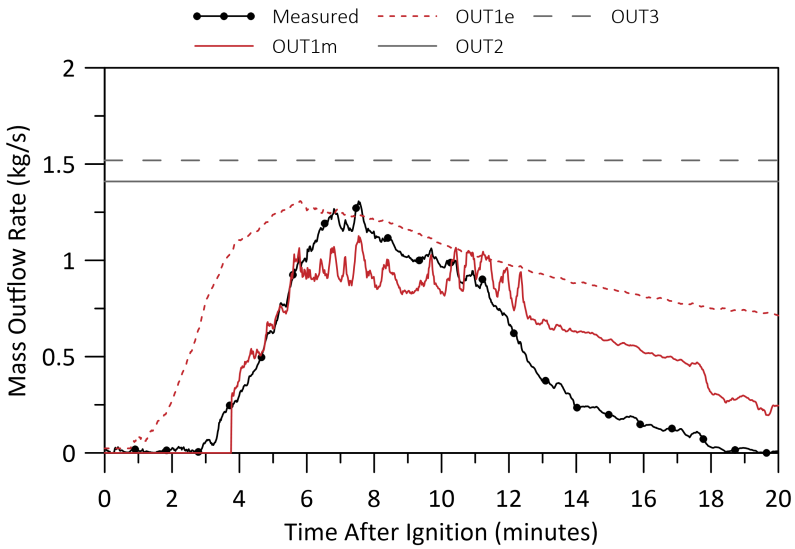

Figure 5.17: Plot of measured and estimated mass outflow versus time for the recirculation test.

Correlation OUT1e predicts flow rates that begin to increase almost immediately after ignition, again overpredicting the flow rate during the increasing flow phase of the test. This correlation provides an excellent estimate of the peak flow, although the peak flow is predicted to occur early in the test consistent with previous tests. Interestingly, flow rates in the first part of the decreasing flow phase, from shortly after peak flow to approximately 11:30 after ignition, are also well predicted by correlation OUT1e, although the accelerated decrease in measured flow rate that occurs after this time is not captured by the correlation.

Similar to the baseline and 2x baseline HVAC tests, correlations OUT2 and OUT3 both provide overestimates of peak flow rate for the recirculation test as well. Values of both the estimated peak flow rates by each outflow correlation, along with the percent error compared to the measured peak flow rate for this test, are listed in Table 5.15. In the recirculation test, correlation OUT1e provides the most accurate estimate of the measured peak flow rate. Correlation OUT2 provides the most accurate conservative estimate, while OUT1m is the only correlation to underestimate the values of peak flow in this test.

Table 5.15: Values of peak outflow and percent error for the recirculation test.

Correlation	Peak Outflow (kg/s)	Error (%)
Measured	1.31	-
OUT1m	1.13	−14
OUT1e	1.31	0
OUT2	1.41	8
OUT3	1.52	16

When implementing the measured neutral plane height in correlation OUT1m, predictions of the transient growth phase in the fire tests are generally good. The correlation consistently overestimates flow for a short period of time when the neutral plane first becomes established, but then quickly settles in to good agreement with the measured flow rates for the remainder of the increasing flow phase. Estimated values from this correlation then tend to flatten out and become constant through the peak flow and early stages of the decreasing flow phase. This results in underestimations of the peak flow rate and poor agreement with measured outflow rates throughout the decreasing flow phase. In addition, OUT1m does not capture secondary increases in outflow after a short period of relatively constant flow, seen most prominently in the no HVAC test.

Using the estimated neutral plane height in correlation OUT1e results in significant overestimation of the flow rate during the transient increasing flow phase of the tests. The decreasing flow phase of the tests is also poorly predicted by OUT1e, which predicts values

in even worse agreement than OUT1m in this phase. The correlation does, however, often predict values of peak flow that are in good agreement with peak measured flow rate values.

Figure 5.18 shows a plot comparing the absolute error of the estimated peak flow rate compared to that measured for each outflow correlation, averaged across all four tests. It can be seen that correlation OUT1e is, on average, the most accurate correlation, with an average error less than one percent. Correlation OUT2 has an average error of 4.7%, OUT1m has an average error of 9.6%, and correlation OUT3 is the least accurate, with an average error of 12.6%. With that said, OUT3 consistently provides the most conservative estimates of peak flow rate and values from OUT1m are consistently least conservative. In fact, OUT1m underestimates the peak flow in all tests except the 2x baseline HVAC test.

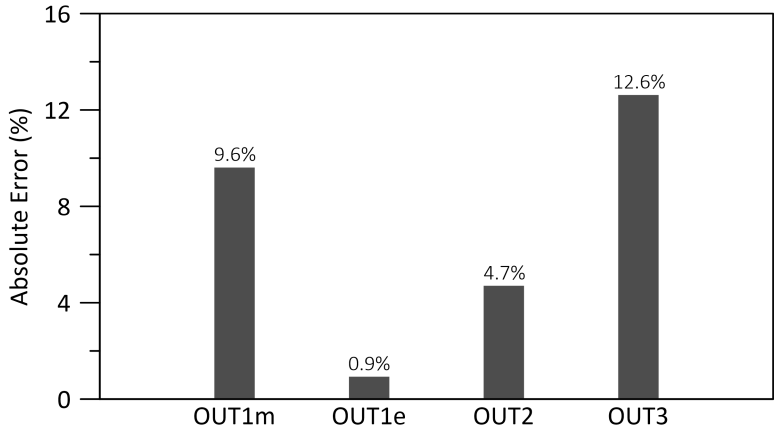

Figure 5.18: Plot of the average absolute error across all tests for each outflow correlation.

Overall, estimations of both the inflow and outflow rates through transient phases of the tests require use of complex correlations that require the input of many parameters and data from experiments. There are intricacies that affect the predicted values from these correlations, such as the definition of the neutral plane height. These intricacies must be understood in order to correctly use and interpret the output of the correlations. For estimation of peak flow rate, more simplified correlations are shown to provide comparable, if not superior, estimates of the measured peak flow rates.

This chapter has evaluated some common engineering correlations for predicting heat flux to a target based on fire size, fire room temperature development, smoke flow out of the fire room, and the flow of fresher air into the fire room. As closure to this thesis, the main conclusions from the experimental results discussed in the previous chapter, as well as from the implementation of correlations for the current fire tests, are presented next.

Chapter 6

Conclusions

Furniture fires in modern homes are likely to become ventilation limited, as fires involving modern furniture constructed of synthetic polymer materials grow very fast and airtight construction practices restrict the amount of ventilation air available to a fire. This scenario poses a significant risk to occupants as well as to responding firefighters. The previous chapters of this thesis discuss four full-scale furniture fire tests conducted in the University of Waterloo burn house. The experiments are aimed at studying the development of modern furniture fires with different mechanical ventilation configurations. The primary objectives of these experiments are to:

- Characterize the fire growth and overall development of the environment throughout the structure.
- Identify and discuss any differences between the tests which may be due to changes in the ventilation configuration.
- Evaluate the use of existing engineering correlations for prediction of key parameters using measurements from this set of experiments.
- Provide spatially and temporally resolved data and results that may be useful for future fire model validation and occupant egress research.

The following sections provide conclusions from the experimental and correlation aspects of the research as they pertain to these objectives. In closing, recommendations for future work are presented based on the results and conclusions.

6.1 Conclusions from the Experiments

Two of the main objectives of this work are to characterize the fire and the development of the environment inside the burn house for the mechanical ventilation test series, and to discuss the differences between these tests that may be a result of the different ventilation configurations. The following points present a summary of the findings related to these objectives.

1. Fires in all tests have comparable total fuel mass loss, indicating that the amount of air initially available in the structure plays a larger role than the amount of OA supplied into the structure in determining the duration of the tests. The position of the supply vents near the ceiling may also restrict additional incoming air flow from reaching the base of the fire and contributing to additional fuel mass loss.

2. Early fire growth is not affected by the HVAC configuration because there is enough O_2 initially available in the volume of the structure to sustain fire growth. The position of the supply vents, near the ceiling and away from the base of the fire, also likely reduce the impact of ventilation during this period.

3. Differences in fire development are noticeable after the second cushion of the couch ignites and the growth of the fire, as measured by fuel MLR, accelerates. At this point there is significant development of the smoke layer in the fire room, and values of peak MLR and time to peak MLR indicate that the ventilation supply forces the smoke layer down over the flames, which affects fire growth. Most notably, the 2x baseline HVAC test has the highest ventilation flow rates with the lowest peak MLR and the longest time to peak MLR.

4. The largest differences between tests are seen in the environment during the latter stages of the tests after peak fire MLR and as the environment recovers. For temperature specifically, supplying more OA results in cooler compartment temperature during this time and recirculation results in the hottest temperatures.

5. Differences are also seen in the O_2 concentrations between tests, specifically at the 0.9 m height in the fire room and at all heights in other compartments. There is a reduction in the rate of decrease on O_2 concentration with increasing supply of OA. There is no significant difference at the 0.3 m height in the fire room, which provides evidence that the overall supply of O_2 to the fire does not vary significantly between tests, as measured values at this location are most representative of the

combustion reactants. At all locations, minimum measured concentrations of O_2 are similar across all tests.

6. Differences in the peak and steady state concentrations of CO are also present at all locations. Higher concentrations are measured when less OA is supplied, consistent with low combustion efficiencies when there is reduced ventilation. However, the recirculation test has surprisingly low steady state CO concentrations, which may be due to increased oxidation in the hot gases as a result of the higher temperatures present in this test.

7. In agreement with trends seen in the concentrations of CO, peak VOC concentrations are also highest in the tests with the least amount of ventilation. The trends in production of these two compounds indicate that combustion efficiency is increased as the supply of OA into the fire room is increased.

8. Pressure buildup in the fire room due to smoke production and increases in temperature is enough to overcome the HVAC flow into the fire room in the baseline HVAC and recirculation tests (each with the baseline ventilation flow rate), causing backflow of smoke into the ductwork. This also occurs in the no HVAC test, however, it does not occur when the ventilation flow rate is doubled in the 2x baseline HVAC test. This has important implications in terms of possible smoke flow in ventilation ductwork which may occur throughout a scenario.

9. Doorway mass flow rates are not significantly impacted by the ventilation configuration. Analysis of the flow rates shows that the majority of the smoke flow out of the fire room is directed into the kitchen, while only approximately one quarter of the total smoke outflow is directed to the upper floor. At the same time, approximately half of the total air supply into the fire room is from the upper floor.

10. The staircase is shown to be a significant source of mixing, as the velocity fluctuation intensity is significantly greater at the top of the stairs than at the bottom. This is a key phenomenon that governs the development of a more uniform environment on the upper floor (in terms of both temperature and gas concentration), while the main floor remains stratified.

11. Some connections were identified when comparing the timing between the fire MLR, O_2 concentration in the fire room, and the doorway mass flow rates into and out of the fire room. Specifically, the timing between the decrease in O_2 and the peak in MLR indicates a transition from reduction in O_2 concentration as a consequence of fire growth to the limitation of the fire MLR due to low O_2 concentrations. Additionally,

the recovery of O_2 concentrations after flame out of the fire is linked to increased inflow of fresher air into the fire room as a result of a flow reversal that occurs as the fire compartment cools and smoke production, hence smoke flow out of the compartment, decreases.

12. Plotting fire room O_2 concentrations versus temperature at the time of peak MLR for all tests shows good agreement with the theoretical flammability limit suggested by Utiskul *et al.* [88] and Mizukami *et al.* [89]. The baseline HVAC test does not fit this trend, likely due to a significant difference in the mode of flame spread in this test as observed in the video recordings.

6.2 Conclusions from the Correlations

Another key objective for this research is evaluation of the use of engineering correlations to predict environmental parameters for the current fire scenarios. These include heat flux, compartment temperatures, and doorway mass flow rates. The following lists key conclusions from this evaluation of the engineering correlations.

1. Measured heat flux incident to the wall across from the couch was underestimated by the point source method and overestimated by the area source method. The area source estimates were nearly double those of the point source method, which is consistent with observations from the literature. Both methods can provide conservative estimates of fire heat flux exposure, with very conservative estimates arising when the recommended factor of safety of two is applied to the originally low estimates of the point source method.

2. In general, the three temperature correlations (MQH, Foote *et al.*, and Beyler and Deal) agree well with measured temperatures throughout the transient fire growth and at peak temperatures of all tests. The MQH correlation appears least accurate at estimating peak temperature on average across all tests, but is the most conservative. The Foote *et al.* correlation provides the most accurate peak temperature estimates with conservative results. The Beyler and Deal correlation appears to be the least accurate and consistently underestimates values of measured peak temperatures.

3. Results from the estimates of mass flow into the fire room show good agreement between correlations and measured flow rates during the transient fire growth period, provided that the neutral plane height is well predicted. Interestingly, the simplest

correlations provide the most accurate estimates of peak inflow rates on average across all tests and are generally conservative.

4. Estimates of mass flow out of the fire room show similar results as the mass inflow correlations during the transient growth phase of the fire, where the correlations agree well with measured flow rates provided that the neutral plane height is well predicted. However, in this case, the more complex correlation provides the most accurate prediction of the peak flow rate on average across all tests. The simplified correlations provide less accurate predictions of peak flow rates, but they are consistently the most conservative.

6.3 Recommendations for Future Work

The following are recommendations to improve the robustness of data collected in future experiments of the under-ventilated furniture fire project and suggestions for further work that is needed to improve engineering correlations for better estimates of environmental compartment fire parameters.

1. Small differences seen in the measurements between tests should be further investigated to separate those differences caused by changes in the ventilation configuration between tests or those caused by other anomalies, such as the differences in fire spread observed in the baseline HVAC test and the double peak in MLR seen in the recirculation test. This should be done by conducting repeats of the four tests discussed in this thesis. Repeat tests will also improve the robustness of the data for use in correlations, as well as for future model validation purposes.

2. Further investigation is needed into the exchange of gases between the fire room and the kitchen/corridor to verify the observations of one-way flows of smoke from the fire room into these compartments as the fires grow. This has key implications into the supply of fresher air into the fire room to the fire. It is recommended to increase the resolution of velocity measurements in these doorways by adding additional probes in the fire room/kitchen door and by adding probes at the threshold between the fire room and main floor corridor.

3. Improved measurements of CO_2 concentration are needed to facilitate further characterization of the fire induced environment, analysis of combustion efficiency, and

to investigate the potential oxidation of CO to CO_2 in, for example, tests with recirculation. Identification and installation of a sensor with increased upper limit of CO_2 measurement capability is a critical step in improving these measurements.

4. Smoke layer height or smoke density measurements should be included in an extended analysis of the relationship between fire MLR, fire room O_2 concentrations, and doorway flows. The objective of this would be to determine if the decrease of O_2 is closely related to the buildup of smoke at the gas sensor location. In this respect, it is recommended to develop a method to provide time resolved smoke density measurements near all of the gas sensor locations in future tests.

5. Measurements of O_2 and other gaseous species concentrations near the base of the fire are needed. This will not only provide measurements of concentration necessary for improved analysis of fire extinction processes, but will also provide measures of combustion reactants local to the fire for in-depth combustion analysis. It is recommended to implement a system capable of sampling gases close to the fire for use with the existing gas sensor boxes.

6. Mass flow correlations should be improved to provide better estimates of mass flow rate during the transient phases of the fire. This is key for accurate estimation of the transport of smoke in fires that are not characterized by a prolonged steady state phase, such as those in the present scenarios. Specifically, the estimation of neutral plane height should be improved to align more closely with measurements of neutral plane heights during transient phases and then integrated into advanced correlations for estimation of doorway flows.

In closure, the data and results presented throughout this thesis improve current understanding of how modern furniture burns in ventilation-limited multi-compartment structures and how the fire induced environment develops in a typical two-storey home. The listed recommendations for future work will improve the robustness of the data and provide further insights into phenomenon that remain under investigation.

References

[1] CBC News, "Modern homes burn 8 times faster than 50 years ago," Sept. 2013. [Online]. Available: https://www.cbc.ca/news/canada/windsor/modern-homes-burn-8-times-faster-than-50-years-ago-1.1700063.

[2] S. Beattie, "Fires are burning hotter and faster, firefighters say. that means residents have only minutes to escape," Feb. 2023. [Online]. Available: https://www.cbc.ca/news/canada/hamilton/ontario-fatal-fires-1.6734900.

[3] UL Fire Safety Research Institute, "New comparison of natural and synthetic home furnishings." [Online]. Available: https://fsri.org/research/new-comparison-natural-and-synthetic-home-furnishings.

[4] Statistics Canada, "Circumstances surrounding unintentional fire-related deaths, 2011 to 2020." [Online]. Available: https://www150.statcan.gc.ca/n1/daily-quotidien/220616/dq220616b-eng.htm.

[5] Statistics Canada, "Fire-related deaths and persons injured, by type of structure." [Online]. Available: https://www150.statcan.gc.ca/t1/tbl1/en/tv.action?pid=3510019501.

[6] B. Lattimer and D. Gottuk, "Effect of combustion conditions on species production," in Hurley *et al.* [151], ch. 16, pp. 486–528.

[7] C. M. Fleischmann, "Backdraft phenomena," tech. rep., National Institute of Standards and Technology, June 1994.

[8] B. Forrest, E. Weckman, M. DiDomizio, P. Senez, and N. Ryder, "Smoke development and movement during ventilation-limited fires in a multi-storey house," *Fire and Materials*, 2020.

[9] B. Forrest, *Heat Release Rate in Ventilation-Limited Furniture Fires*. MASc Thesis, University of Waterloo, 2020.

[10] P. Senez, P. Mulherin, and E. Weckman, "Repeatability of underventilated compartment fire testing with complex fuel packages," in *15th International Conference and Exhibition on Fire and Materials*, Interscience Communications Ltd, Jan. 2017.

[11] V. Babrauskas and R. D. Peacock, "Heat release rate: The single most important variable in fire hazard," *Fire Safety Journal*, vol. 18, pp. 255–272, Jan. 1992.

[12] A. Tewarson, "Heat release rate in fires," *Fire and Materials*, vol. 4, no. 4, pp. 185–191, 1980.

[13] B. Karlsson and J. G. Quintiere, "Energy release rates," in *Enclosure Fire Dynamics* [152], ch. 3, pp. 37–58.

[14] M. Janssens, "Calorimetry," in Hurley *et al.* [151], ch. 27, pp. 905–951.

[15] W. Thornton, "XV. The relation of oxygen to the heat of combustion of organic compounds," *The London, Edinburgh, and Dublin Philosophical Magazine and Journal of Science*, vol. 33, no. 194, pp. 196–203, 1917.

[16] V. Babrauskas, "Heat release rates," in Hurley *et al.* [151], ch. 26, pp. 799–904.

[17] D. Drysdale, "The pre-flashover compartment fire," in *An Introduction to Fire Dynamics* [153], ch. 9, pp. 349–386.

[18] J. G. Quintiere, "Compartment fires," in *Fundamentals of Fire Phenomena*, ch. 11, pp. 339–376, West Sussex, England: John Wiley and Sons LTD, 2006.

[19] D. Drysdale, "The post-flashover compartment fire," in *An Introduction to Fire Dynamics* [153], ch. 10, pp. 387–440.

[20] C. Huggett, "Estimation of rate of heat release by means of oxygen consumption measurements," *Fire and Materials*, vol. 4, no. 2, pp. 61–65, 1980.

[21] V. Babrauskas, "Development of the cone calorimeter—A bench-scale heat release rate apparatus based on oxygen consumption," *Fire and Materials*, vol. 8, no. 2, pp. 81–95, 1984.

[22] "Standard for smoke control systems." NFPA 92, National Fire Protection Association, 2021.

[23] D. Drysdale, "Smoke: Its formation, composition and movement," in *An Introduction to Fire Dynamics* [153], ch. 11, pp. 441–474.

[24] B. Karlsson and J. G. Quintiere, "Fire plumes and flame heights," in *Enclosure Fire Dynamics* [152], ch. 4, pp. 59–92.

[25] D. Drysdale, "Diffusion flames and fire plumes," in *An Introduction to Fire Dynamics* [153], ch. 4, pp. 121–179.

[26] R. Alpert, "Ceiling jet flows," in Hurley *et al.* [151], ch. 14, pp. 429–454.

[27] G. Mulholland, T. Handa, O. Sugawa, and H. Yamamoto, "Smoke filling in an enclosure," *Fire Science and Technology*, vol. 1, no. 1, pp. 1–31, 1981.

[28] G. Heskestad, "Fire plumes, flame height, and air entrainment," in Hurley *et al.* [151], ch. 13, pp. 396–428.

[29] W. Walton, P. Thomas, and Y. Ohmiya, "Estimating temperatures in compartment fires," in Hurley *et al.* [151], ch. 30, pp. 996–1023.

[30] R. D. Peacock, K. B. McGrattan, G. P. Forney, and P. A. Reneke, "CFAST–consolidated fire and smoke transport (version 7) volume 1: Technical reference guide," *NIST Technical Note 1889v1*, 2015.

[31] V. Babrauskas and R. B. Williamson, "Post-flashover compartment fires: Basis of a theoretical model," *Fire and Materials*, vol. 2, no. 2, pp. 39–53, 1978.

[32] T. Tanaka, "Vent flows," in Hurley *et al.* [151], ch. 15, pp. 455–485.

[33] B. Karlsson and J. G. Quintiere, "Pressure profiles and vent flows for well-ventilated enclosures," in *Enclosure Fire Dynamics* [152], ch. 5, pp. 93–126.

[34] J. Prahl and H. W. Emmons, "Fire induced flow through an opening," *Combustion and Flame*, vol. 25, pp. 369–385, Aug. 1975.

[35] J. A. Rockett, "Fire induced gas flow in an enclosure," *Combustion Science and Technology*, vol. 12, pp. 165–175, Apr. 1976.

[36] I. Nakaya, T. Tanaka, M. Yoshida, and K. Stechler, "Doorway flow induced by a propane fire," *Fire Safety Journal*, vol. 10, pp. 185–195, May 1986.

[37] K. D. Steckler, "Flow induced by fire in a compartment," in *Proceedings of the Combustion Institute*, pp. 913–920, The Combustion Institute, 1982.

[38] E. Zukoski, "Fluid dynamic aspects of room fires," *Fire Safety Science*, vol. 1, pp. 1–30, 1986.

[39] K. D. Steckler, J. G. Quintiere, and R. W. J., "Flow induced by fire in a compartment," tech. rep., National Bureau of Standards, Sept. 1982.

[40] K. D. Steckler, H. R. Baum, and J. G. Quintiere, "Fire induced flows through room openings-flow coefficients," *Symposium (International) on Combustion*, vol. 20, pp. 1591–1600, Jan. 1985.

[41] S. B. Dalziel and G. F. Lane-Serff, "The hydraulics of doorway exchange flows," *Building and Environment*, vol. 26, pp. 121–135, Jan. 1991.

[42] L. Wang and J. G. Quintiere, "An analysis of compartment fire doorway flows," *Fire Safety Journal*, vol. 44, pp. 718–731, July 2009.

[43] J. G. Quintiere and L. Wang, "A general formula for the prediction of vent flows," *Fire Safety Journal*, vol. 44, pp. 789–792, July 2009.

[44] C. Lim, *I. Mixing in Doorway Flows. II. Entrainment in Fire Plumes.* PhD Thesis, California Institute of Technology, 1984.

[45] J. G. Quintiere, B. J. McCaffrey, and W. Rinkinen, "Visualization of room fire induced smoke movement and flow in a corridor," *Fire and Materials*, vol. 2, pp. 18–24, Jan. 1978.

[46] S. N. Pope, *Turbulent Flows.* Cambridge University Press, 2012.

[47] M. Lesieur, *Turbulence in Fluids.* Dordrecht, The Netherlands: Springer, 2008.

[48] K. B. McGrattan, H. R. Baum, and R. G. Rehm, "Large eddy simulations of smoke movement," *Fire safety journal*, vol. 30, no. 2, pp. 161–178, 1998.

[49] K. McGrattan, S. Hostikka, R. McDermott, J. Floyd, C. Weinschenk, and K. Overholt, "Fire dynamics simulator user's guide," *NIST special publication*, vol. 1019, no. 6, 2021.

[50] Y. Wang, P. Chatterjee, and J. L. de Ris, "Large eddy simulation of fire plumes," *Proceedings of the Combustion Institute*, vol. 33, no. 2, pp. 2473–2480, 2011.

[51] W. Zhang, A. Hamer, M. Klassen, D. Carpenter, and R. Roby, "Turbulence statistics in a fire room model by large eddy simulation," *Fire Safety Journal*, vol. 37, no. 8, pp. 721–752, 2002.

[52] B. McCaffrey and G. Heskestad, "A robust bidirectional low-velocity probe for flame and fire application," *Combustion and Flame*, vol. 26, pp. 125–127, Feb. 1976.

[53] S. C. Kim and J. Y. Kim, "The effect of flow approaching angle on the velocity measurement using bi-directional velocity probe," *Procedia Engineering*, vol. 62, pp. 797–803, Jan. 2013.

[54] L. A. Kent and M. E. Schneider, "The design and application of bi-directional velocity probes for measurements in large pool fires," *ISA Transactions*, vol. 26, no. 4, pp. 25–32, 1987.

[55] R. A. Bryant, "A comparison of gas velocity measurements in a full-scale enclosure fire," *Fire Safety Journal*, vol. 44, pp. 793–800, July 2009.

[56] B. C. Hogan, H. Bocanegra, R. C. Alarcon, N. Yilmaz, A. B. Donaldson, and W. Gill, "Examination of the bi-directional velocity probe used in flames," in *Volume 2: Fora*, pp. 49–56, ASMEDC, Jan. 2009.

[57] B. J. G. Sette, "Critical considerations on the use of a bi-directional probe in heat release measurements," *Fire and Materials*, vol. 29, pp. 335–349, Sept. 2005.

[58] J. Weisinger, *Characterization of the University of Waterloo Live Fire Research Facility Wind Generation System*. MASc Thesis, University of Waterloo, 2004.

[59] A. Hamins, E. Johnsson, M. Donnelly, and A. Maranghides, "Energy balance in a large compartment fire," *Fire Safety Journal*, vol. 43, pp. 180–188, Apr. 2008.

[60] R. A. Bryant, "The application of stereoscopic PIV to measure the flow of air into an enclosure containing a fire," *Experiments in Fluids*, vol. 47, pp. 295–308, Aug. 2009.

[61] B. Betting, E. Varea, C. Gobin, G. Godard, B. Lecordier, and B. Patte-Rouland, "Experimental and numerical studies of smoke dynamics in a compartment fire," *Fire Safety Journal*, vol. 108, 2019.

[62] R. A. Bryant, "A new approach to ventilation measurements in enclosure fires," in *Proceedings of the 11th international conference on fire science and engineering*, (London, England), pp. 453–463, Sept. 2007.

[63] B. Karlsson and J. G. Quintiere, "Gas temperatures in ventilated enclosure fires," in *Enclosure Fire Dynamics* [152], ch. 6, pp. 127–152.

[64] B. J. McCaffrey, J. G. Quintiere, and M. F. Harkleroad, "Estimating room temperatures and the likelihood of flashover using fire test data correlations," *Fire Technology*, vol. 17, pp. 98–119, May 1981.

[65] Y. He, A. Fernando, and M. Luo, "Determination of interface height from measured parameter profile in enclosure fire experiment," *Fire Safety Journal*, vol. 31, pp. 19–38, July 1998.

[66] J. Wu, "A basic guide to thermocouple measurements," application note, Texas Instruments, 2018.

[67] W. M. Pitts, E. Braun, R. D. Peacock, H. E. Mitler, E. L. Johnsson, P. A. Reneke, and L. G. Blevins, "Temperature uncertainties for bare-bead and aspirated thermocouple measurements in fire environments," *National Institute of Standards and Technology*, Oct. 1998.

[68] D. Drysdale, "Heat transfer," in *An Introduction to Fire Dynamics* [153], ch. 2, pp. 37–82.

[69] B. Karlsson and J. G. Quintiere, "Heat transfer in compartment fires," in *Enclosure Fire Dynamics* [152], ch. 7, pp. 153–192.

[70] A. T. Modak, "Thermal radiation from pool fires," *Combustion and Flame*, vol. 29, pp. 177–192, Jan. 1977.

[71] J. De Ris, "A scientific approach to flame radiation and material flammability," *Fire Safety Science*, vol. 2, pp. 29–46, 1989.

[72] G. H. Markstein, "Relationship between smoke point and radiant emission from buoyant turbulent and laminar diffusion flames," *Symposium (International) on Combustion*, vol. 20, pp. 1055–1061, Jan. 1985.

[73] G. H. Markstein, "Radiative energy transfer from gaseous diffusion flames," *Symposium (International) on Combustion*, vol. 15, pp. 1285–1294, Jan. 1975.

[74] A. Nasr, S. Suard, H. El-Rabii, J. Garo, L. Gay, and L. Rigollet, "Heat feedback to the fuel surface of a pool fire in an enclosure," *Fire Safety Journal*, vol. 60, pp. 56–63, Aug. 2013.

[75] G. Santo and F. Tamanini, "Influence of oxygen depletion on the radiative properties of PMMA flames," *Eighteenth Symposium (International) on Combustion*, vol. 18, pp. 619–631, Jan. 1981.

[76] C. Lautenberger, C. Tien, K. Lee, and A. Stretton, "Radiation heat transfer," in Hurley *et al.* [151], ch. 4, pp. 102–137.

[77] C. Beyler, "Fire hazard calculations for large, open hydrocarbon fires," in Hurley *et al.* [151], ch. 66, pp. 2591–2663.

[78] K. S. Mudan, "Geometric view factors for thermal radiation hazard assessment," *Fire Safety Journal*, vol. 12, pp. 89–96, Oct. 1987.

[79] B. Karlsson and J. G. Quintiere, "Combustion products," in *Enclosure Fire Dynamics* [152], ch. 9, pp. 238–265.

[80] P. Blomqvist and A. Lönnermark, "Characterization of the combustion products in large-scale fire tests: comparison of three experimental configurations," *Fire and Materials*, vol. 25, pp. 71–81, Mar. 2001.

[81] C. Wong, C. Fleischmann, and M. Spearpoint, "Contribution of upholstered furniture to residential fire fatalities in new zealand," tech. rep., University of Canterbury, 2001.

[82] J. C. Wakefield, "A toxicological review of the products of combustion," Technical Report HPA-CHaPD-004, Health Protection Angency Centre for Radiation, Chemical and Enviornmental Hazards, 2010.

[83] W. M. Pitts, "The global equivalence ratio concept and the prediction of carbon monoxide formation in enclosure fires," tech. rep., National Institute of Standards and Technology, Gaithersburg, MD, 1994.

[84] S. Ukleja, M. Delichatsios, J. Zhang, and M. Suzanne, "Carbon monoxide production during underventilated fires in corridors," *Fire Safety Science*, vol. 11, pp. 316–330, 2014.

[85] C. Beyler, "Flammability limits of premixed and diffusion flames," in Hurley *et al.* [151], ch. 17, pp. 529–553.

[86] A. Macek, "Flammability limits: thermodynamics and kinetics. final report," tech. rep., National Bureau of Standards, Washington, DC (USA). Center for Fire Research, 1976.

[87] J. G. Quintiere and A. S. Rangwala, "A theory for flame extinction based on flame temperature," *Fire and Materials*, vol. 28, pp. 387–402, Sept. 2004.

[88] Y. Utiskul, J. G. Quintiere, A. S. Rangwala, B. A. Ringwelski, K. Wakatsuki, and T. Naruse, "Compartment fire phenomena under limited ventilation," *Fire Safety Journal*, vol. 40, pp. 367–390, June 2005.

[89] T. Mizukami, Y. Utiskul, and J. G. Quintiere, "Application of zone models for under-ventilated compartment fires," in *Heat Transfer, Volume 2*, pp. 69–77, ASMEDC, Jan. 2006.

[90] K. Mizuno, S. Tanaka, and Y. Hasemi, "Study of force - ventilated fires in closed space," *Fire Science and Technology*, vol. 13, no. Suppl, pp. S_63–S_82, 1993.

[91] W. Chow and S. Tsui, "Temperature distribution induced by fires in a small chamber with forced ventilation," *Journal of Fire Sciences*, vol. 16, pp. 125–145, Mar. 1998.

[92] Y. Hayashi, Y. Hasemi, and A. Ptchelintsev, "Smoke layer formation by fires in forced ventilation enclosure," *Fire Safety Science*, vol. 6, pp. 805–816, 2000.

[93] B. Zhang, J. Zhang, X. Wang, S. Lu, C. Li, and R. Chen, "Effects of air inlet configuration on forced-ventilation enclosure fires on a naval ship," *Fire Technology*, vol. 52, pp. 547–562, Mar. 2016.

[94] J. Backovsky, K. Foote, and N. Alvares, "Temperature profiles in forced-ventilation enclosure fires," *Fire Safety Science*, vol. 2, pp. 315–324, 1989.

[95] S. Melis and L. Audouin, "Effects of vitiation on the heat release rate in mechanically-ventilated compartment fires," *Fire Safety Science*, vol. 9, pp. 931–942, 2008.

[96] H. Prétrel, L. Bouaza, and S. Suard, "Multi-scale analysis of the under-ventilated combustion regime for the case of a fire event in a confined and mechanically ventilated compartment," *Fire Safety Journal*, vol. 120, Mar. 2021.

[97] H. Pretrel, P. Querre, and M. Forestier, "Experimental study of burning rate behaviour in confined and ventilated fire compartments," *Fire Safety Science*, vol. 8, pp. 1217–1228, 2005.

[98] O. Aljumaiah, G. Andrews, B. Mustafa, H. Al-qattan, V. Shah, and H. Phylaktou, "Air starved wood crib compartment fire heat release and toxic gas yields," *Fire Safety Science*, vol. 10, pp. 1263–1276, 2011.

[99] W. K. Chow and W. L. Chan, "Experimental studies on forced-ventilated fires," *Fire Science and Technology*, vol. 13, no. 1 & 2, pp. 71–87, 1993.

[100] W. K. Chow, "Modelling of forced-ventilation fires," *Mathematical and Computer Modelling*, vol. 18, pp. 63–66, Sept. 1993.

[101] W. K. Chow, "Use of zone models on simulating compartmental fires with forced ventilation," *Fire and Materials*, vol. 19, no. 3, pp. 101–108, 1995.

[102] M. Peatross and C. Beyler, "Ventilation effects on compartment fire characterization," *Fire Safety Science*, vol. 5, pp. 403–414, 1997.

[103] K. Foote, P. Pagni, and N. Alvares, "Temperature correlations for forced-ventilated compartment fires," *Fire Safety Science*, vol. 1, pp. 139–148, 1986.

[104] N. J. Alvares, K. L. Foote, and P. J. Pagni, "Forced ventilated enclosure fires," *Combustion Science and Technology*, vol. 39, pp. 55–81, Aug. 1984.

[105] H. Prétrel and J. Such, "Effect of ventilation procedures on the behaviour of a fire compartment scenario," *Nuclear Engineering and Design*, vol. 235, pp. 2155–2169, Sept. 2005.

[106] C. Beyler, "Analysis of compartment fires with overhead forced ventilation," *Fire Safety Science*, vol. 3, pp. 291–300, Jan. 1991.

[107] W. Le Saux, H. Pretrel, C. Lucchesi, and P. Guillou, "Experimental study of the fire mass loss rate in confined and mechanically ventilated multi-room scenarios," *Fire Safety Science*, vol. 9, pp. 943–954, 2008.

[108] L. Audouin, L. Rigollet, H. Prétrel, W. Le Saux, and M. Röwekamp, "OECD PRISME project: Fires in confined and ventilated nuclear-type multi-compartments - overview and main experimental results," *Fire Safety Journal*, vol. 62, pp. 80–101, Nov. 2013.

[109] H. Pretrel and L. Audouin, "Doorway flows induced by the combined effects of natural and forced ventilation in a three compartment assembly," *Fire Safety Science*, vol. 10, pp. 1015–1027, 2011.

[110] H. Prétrel, W. Le Saux, and L. Audouin, "Pressure variations induced by a pool fire in a well-confined and force-ventilated compartment," *Fire Safety Journal*, vol. 52, pp. 11–24, Aug. 2012.

[111] F. Bonte, N. Noterman, and B. Merci, "Computer simulations to study interaction between burning rates and pressure variations in confined enclosure fires," *Fire Safety Journal*, vol. 62, pp. 125–143, Nov. 2013.

[112] S. Vaux and H. Prétrel, "Relative effects of inertia and buoyancy on smoke propagation in confined and forced ventilated enclosure fire scenarios," *Fire Safety Journal*, vol. 62, pp. 206–220, Nov. 2013.

[113] S. Ghanekar, C. Weinschenk, G. P. Horn, K. Stakes, R. M. Kesler, and T. Lee, "Effects of HVAC on combustion-gas transport in residential structures," *Fire Safety Journal*, vol. 128, p. 103534, Mar. 2022.

[114] J. G. Quintiere, "Fire behavior in building compartments," *Proceedings of the Combustion Institute*, vol. 29, pp. 181–193, Jan. 2002.

[115] A. J. Wolfe, C. L. Mealy, and D. T. Gottuk, "Fire dynamics and forensic analysis of limited ventilation compartment fires volume 1: Experimental," tech. rep., US Department of Justice, Oct. 2009.

[116] C. Weinschenk and J. Regan, "Analysis of search and rescue tactics in single story single-family homes part II: Kitchen and living room fires," tech. rep., UL's Fire Safety Research Institute, May 2022.

[117] R. Zevotek, K. Stakes, and J. Willi, "Impact of fire attack utilizing interior and exterior streams on firefighter safety and occupant survival: Full-scale experiments," tech. rep., UL Firefighter Safety Research Institute, Jan. 2018.

[118] R. Zevotek and S. Kerber, "Study of the effectiveness of fire service positive pressure ventilation during fire attack in single family homes incorporating modern construction practices," tech. rep., UL Firefighter Safety Research Institute, May 2016.

[119] P. Reszka, C. Abecassis Empis, H. Biteau, A. Cowlard, T. Steinhaus, I. A. Fletcher, A. Fuentes, M. Gillie, and S. Welch, "Experimental layout and description of the building," in *The Dalmarnock Fire Tests: Experiments and Modelling*, The University of Edinburgh, Nov. 2007.

[120] C. Abecassis Empis, A. Cowlard, S. Welch, and J. L. Torero, "Test one: The 'uncontrolled' fire," in *The Dalmarnock Fire Tests: Experiments and Modelling*, The University of Edinburgh, Nov. 2007.

[121] A. Cowlard, T. Steinhaus, C. Abecassis Empis, and J. L. Torero, "Test two: The 'controlled fire'," in *The Dalmarnock Fire Tests: Experiments and Modelling*, The University of Edinburgh, Nov. 2007.

[122] A. C. Bwalya, E. Gibbs, G. D. Lougheed, and A. Kashef, "Characterization of fires in multi-suite residential dwellings: Phase 1 - room fire experiments with individual furnishings," tech. rep., National Research Council Canada, Sept. 2010.

[123] D. Madrzykowski and C. Weinschenk, "Understanding and fighting basement fires," tech. rep., UL Firefighter Safety Research Institute, Aug. 2018.

[124] S. Kerber, "Impact of ventilation on fire behavior in legacy and contemporary residential construction," tech. rep., UL Firefighter Safety Research Institute, Dec. 2010.

[125] S. Kerber, "Study of the effectiveness of fire service vertical ventilation and suppression tactics in single family homes," tech. rep., UL Firefighter Safety Research Institute, June 2013.

[126] S. Kerber, "Analysis of one and two-story single family home fire dynamics and the impact of firefighter horizontal ventilation," *Fire Technology*, vol. 49, pp. 857–889, Oct. 2013.

[127] D. Madrzykowski and C. Weinschenk, "Impact of fixed ventilation on fire damage patterns in full-scale structures," tech. rep., UL Firefighter Safety Research Institute, Apr. 2019.

[128] K. Stakes, K. Stakes, J. Bryant, N. Dow, J. Regan, and C. Weinschenk, "Analysis of the coordination of suppression and ventilation in multi-family dwellings," tech. rep., UL Firefighter Safety Research Institute, June 2020.

[129] J. Su, N. Benichou, A. Bwalya, G. Lougheed, B. Taber, P. Leroux, G. Proulx, A. Kashef, C. McCartney, and J. Thomas, "Fire performance of houses. phase I. study of unprotected floor assemblies in basement fire scenarios. summary report," tech. rep., National Research Council Canada, Dec. 2008.

[130] C. Lin, S. Wang, C. Hung, and J. Hsu, "Ventilation effect on fire smoke transport in a townhouse building," *Heat Transfer—Asian Research*, vol. 35, no. 6, pp. 387–401, 2006.

[131] Y. He and V. Beck, "Smoke spread experiment in a multi-storey building and computer modelling," *Fire Safety Journal*, vol. 28, pp. 139–164, Mar. 1997.

[132] C. Weinschenk, "Analysis of search and rescue tactics in single-story single-family homes part I: Bedroom fires," tech. rep., UL's Fire Safety Research Institute, May 2022.

[133] B. Taylor and C. Kuyatt, "Guidelines for evaluating and expressing the uncertainty of NIST measurement results," tech. rep., National Institute of Standards and Technology, 1994.

[134] T. Melcher, R. Zinke, M. Trott, and U. Krause, "Experimental investigations on the repeatability of real scale fire tests," *Fire Safety Journal*, vol. 82, pp. 101–114, May 2016.

[135] J. Fang, "Repeatability of large-scale room fire tests," *Fire Technology*, vol. 17, pp. 5–16, Feb. 1981.

[136] "Requirement, test procedure and apparatus for testing the smolder resistance of materials used in upholstered furniture." TB 117-2013, Bureau of Electronic and Appliance Repair Home Furnishings and Thermal Insulation, State of California Department of Consumer Affairs, 2013.

[137] Omega, "What is a type K thermocouple." Available: `www.omega.ca/en/resources/k-type-thermocouples`. Accessed 13-01-2023.

[138] Vatell Corporation, "Thermogauge." Available: `www.vatell.com/index.php/thermogage`. Accessed 13-01-2023.

[139] MARS Scale Corp, "Load cells." Available: `www.marsscale.com/load_cells.html`. Accessed 7-6-2022.

[140] Fire & Risk Alliance, "Calibration certificates - university of waterloo gas sensing units." calibration report, Issued: Aug. 13, 2020.

[141] "Novatech P-695 operating manual," 2007.

[142] "Methods of test for assessment of the ignitability of upholstered seating by smouldering and flaming ignition sources." BS 5852, British Standards Institute, 2006.

[143] "Reaction to fire tests - heat release, smoke production and mass loss rate - part 1: Heat release rate (cone calorimeter method) and smoke production rate (dynamic measurement)." ISO 5660-1:2015, International Standards Organization, 2015.

[144] R. J. Crewe, A. A. Stec, R. G. Walker, J. E. A. Shaw, T. R. Hull, J. Rhodes, and T. Garcia-Sorribes, "Experimental results of a residential house fire test on tenability: Temperature, smoke, and gas analyses," *Journal of Forensic Sciences*, vol. 59, no. 1, pp. 139–154, 2014.

[145] S. Deal and C. Beyler, "Correlating preflashover room fire temperatures," *Journal of Fire Protection Engineering*, vol. 2, pp. 33–48, May 1990.

[146] Fire Safety Research Institute, "Materials database - fiber cement board." Available: `www.materials.fsri.org/materialdetail/fiber-cement-board`. Accessed 18-07-2023.

[147] S. Manzello, S.-H. Park, T. Mizukami, and D. Bentz, "Measurement of thermal properties of gypsum board at elevated temperatures," in *Proceedings of the Fifth International Conference on Structures in Fire*, 2008.

[148] V. Kodur and T. Harmathy, "Properties of building materials," in Hurley *et al.* [151], ch. 9, pp. 277–324.

[149] A. Tewarson, "Fully developed enclosure fires of wood cribs," *Symposium (International) on Combustion*, vol. 20, pp. 1555–1566, Jan. 1984.

[150] V. Babrauskas, "Estimating room flashover potential," *Fire Technology*, vol. 16, pp. 94–103, May 1980.

[151] M. J. Hurley, D. Gottuk, J. R. Hall, K. Harada, E. Kuligowski, M. Puchovsky, J. Torero, J. M. Watts, and C. Wieczorek, eds., *SFPE Handbook of Fire Protection Engineering*. New York, NY, USA: Springer New York, 2016.

[152] B. Karlsson and J. G. Quintiere, *Enclosure fire dynamics*. Boca Raton, FL, USA: CRC Press, 2000.

[153] D. Drysdale, *An Introduction to Fire Dynamics*. Chichester, West Sussex: Wiley, 3rd ed ed., 2011.